BROWN BOVERI REVIEW

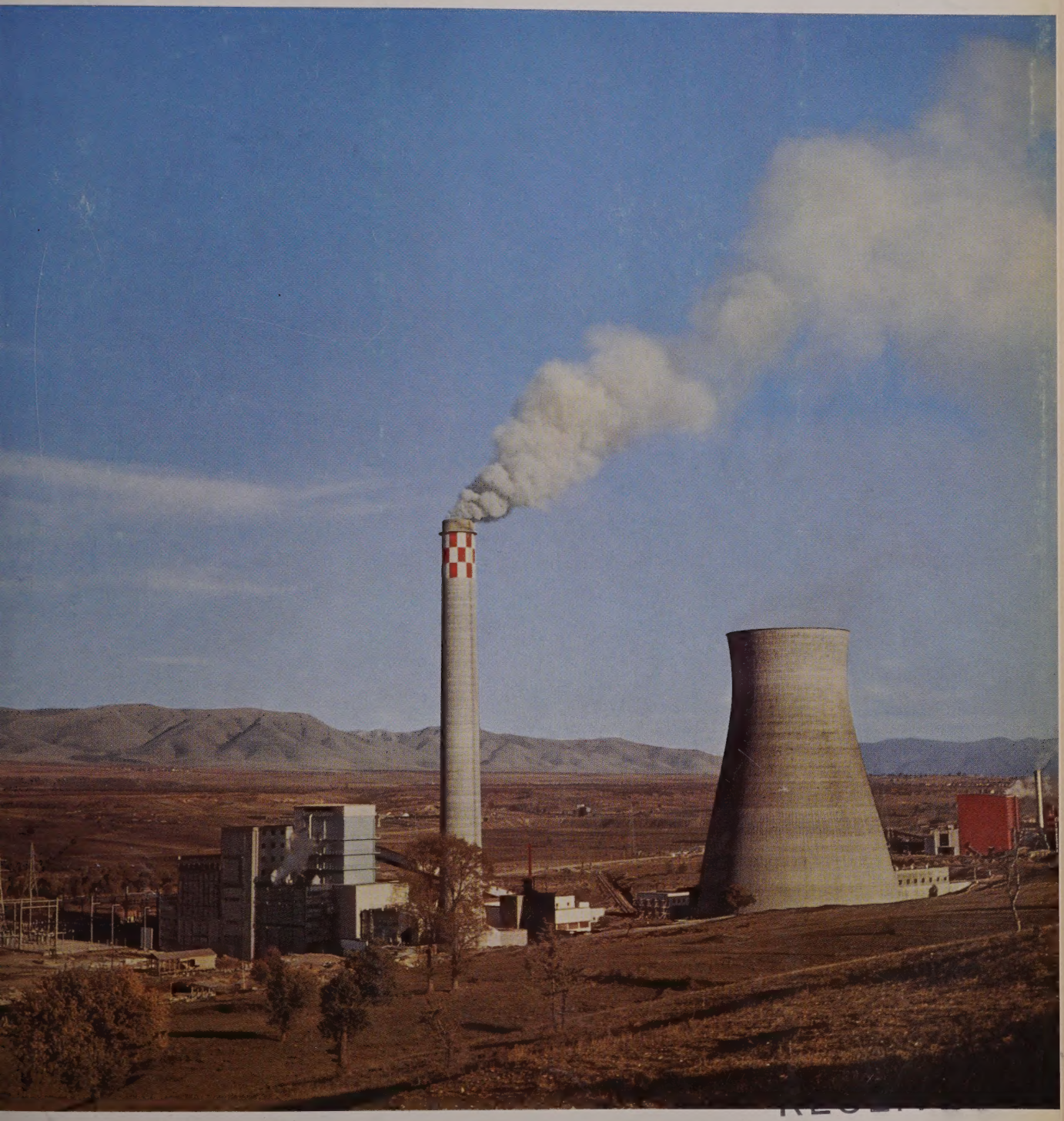

The 70-MW steam power station at Ptolemais in Greece

(At the time the electrostatic precipitators were not in operation)

WN BOVERI REV. VOL. 47 No. 12 p. 781–904 BADEN, DECEMBER 1960

Printed in Switzerland

THE BROWN BOVERI REVIEW

ISSUED BY BROWN, BOVERI & COMPANY, LIMITED, BADEN (SWITZERLAND)

VOL. 47 DECEMBER 1960 No. 12

CONTENTS:

THE THEORY OF COMBINED STEAM AND GAS TURBINE INSTALLATIONS

621.165:621.438
621.438:621.165

Steam and gas turbines can be combined to produce mechanical power in such a way that the combined installation achieves a higher efficiency than the steam or gas turbine running alone. Several different arrangements are feasible, the best overall arrangement being dependent upon the given data and the desired performance. For example, it is possible to incorporate a gas-turbine cycle in the combustion circuit of the boiler of a steam system; alternatively a waste-heat boiler and steam turbine can be made to follow a gas turbine. In the first arrangement the main stress is laid on the steam turbine, in the second on the gas turbine.

This article gives a comprehensive and unbiassed survey of the combinations worth considering and derives the basic thermo-dynamic relationships, which determine their mode of operation. These relationships, though quite simple, have not always been correctly analysed.

The primary goal is the attainment of the highest possible thermal efficiency, although this is not solely decisive for the choice of a particular system. The initial outlay and other factors, such as safety, ease of control, fuel properties, number of running hours, and so on, are also quite important. To make any general statements about such factors is, of course, impossible. In the present article the economics of a typical example will be investigated. The remarks apply to installations intended to produce only electricity. The discussion of the special advantages of installations for the simultaneous generation of electricity and process heat was deliberately omitted for the sake of simplicity.

I. Review of Combined Gas and Steam Turbine Plants

FIG. 1 and the enclosed loose leaf show a number of layouts, with the aid of which the various possible combinations of gas and steam turbines can be surveyed.

To begin with, diagram A represents a straightforward steam plant. It has been simplified as far as can be permitted for the illustration, but it may be stressed at this point that subsequent considerations will be devoted to all kinds of steam plants, from the simplest to the most complicated. The parts of the steam plant which are of interest here are: The boiler *a*, the boiler fans *b*, the air heater *c*, the combustion chamber with at least one burner *d*, the steam section of the boiler—comprising economizer, evaporator, superheater and possibly a reheater—these are indicated in the diagram as a simple through system *e*. Belonging to the turboset are the steam turbine *f*, the generator *g*, the condenser *h*, the feedwater pump *i*, an arbitrary number of feedwater heaters and de-aerating heaters *k*.

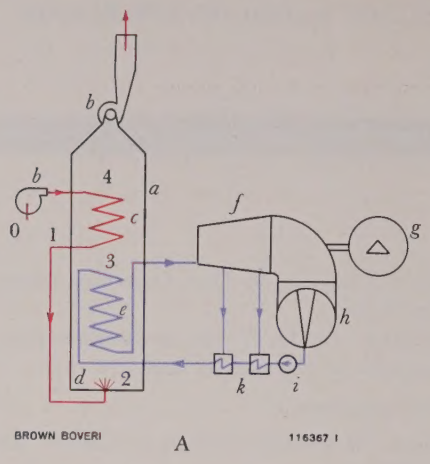

A

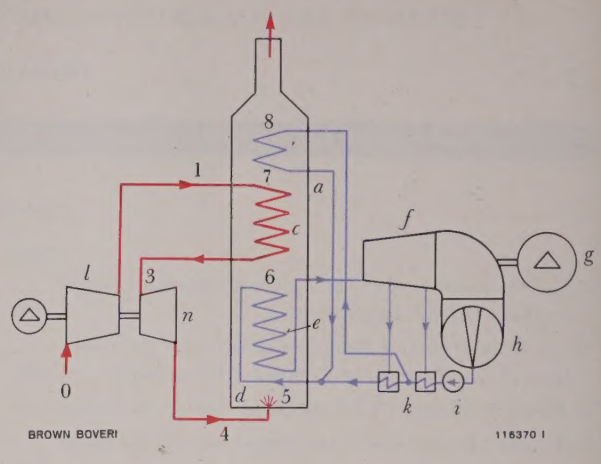

D

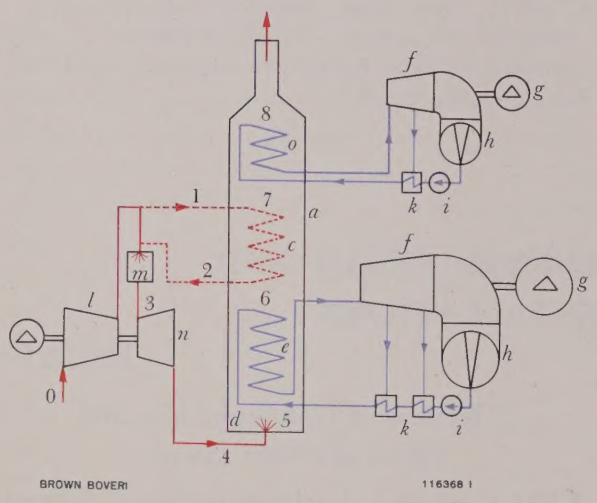

B

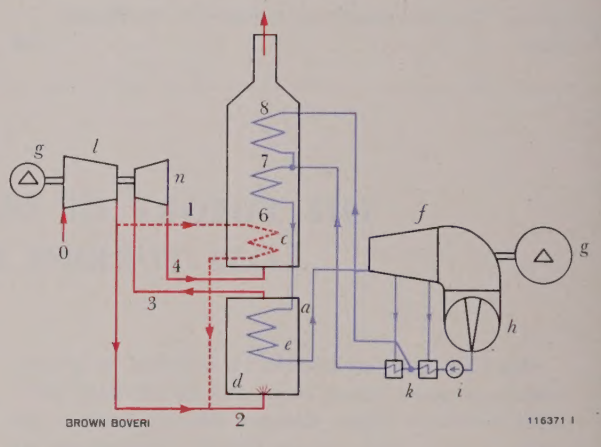

E

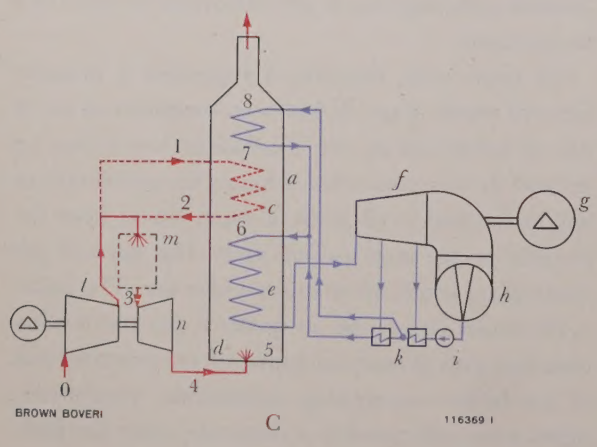

C

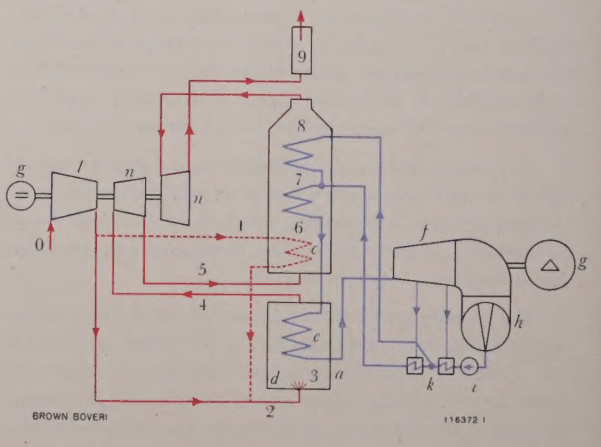

F

In the diagrams B, C and D the boiler is preceded by a gas-turbine set, the exhaust heat of which is utilized in the fire-box of the boiler.

In B and C air is compressed in a compressor *l* and is heated in a special combustion and swirl chamber *m* to the desired input temperature of the

Supplement to the article by C. Seippel and R. Bereuter:
The Theory of Combined Steam and Gas Turbine Installations

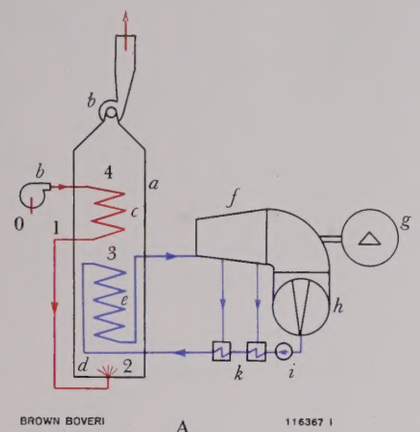

A

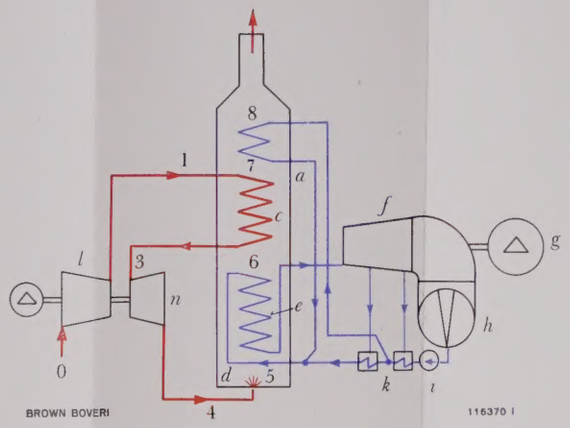

D

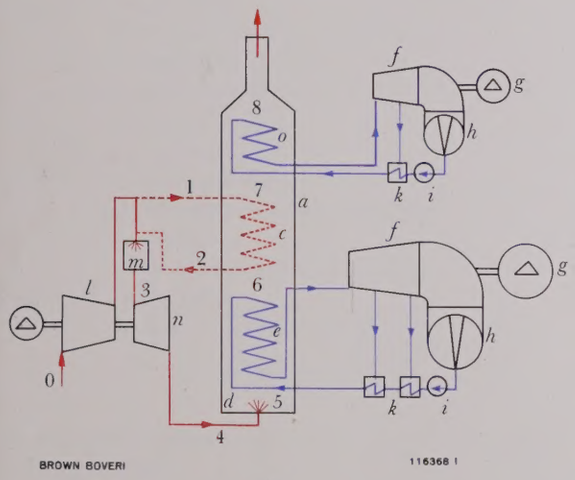

B

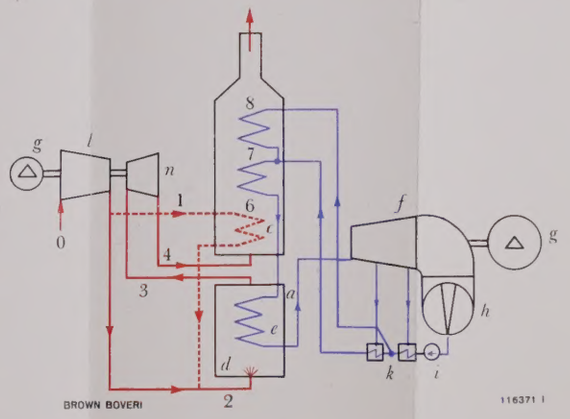

E

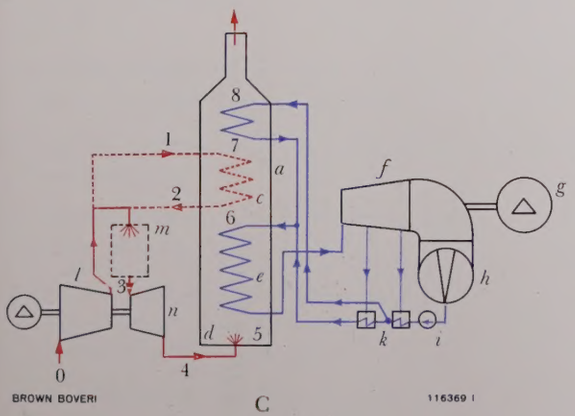

C

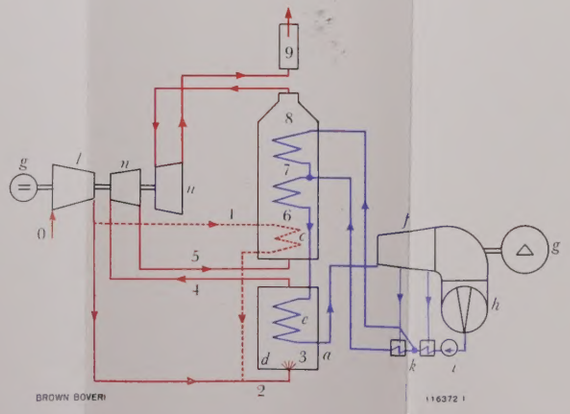

F

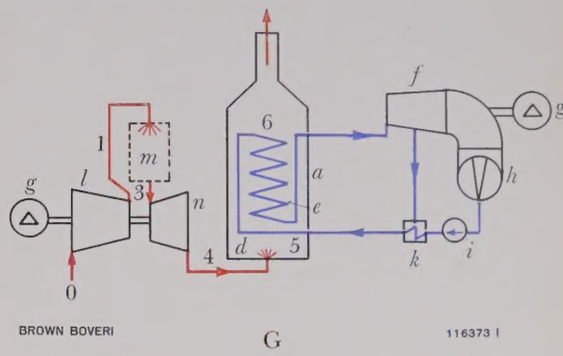

G

Circuit diagrams of combined steam and gas turbine installations

Red: Open combustion circuit
Blue: Closed water-steam circuit

a = Boiler
b = Boiler fans
c = Air heater
d = Combustion chamber with burner
e = Steam part of boiler
f = Steam turbine
g = Generator
h = Condenser
i = Feedwater pump
k = Feedwater heater and de-aerator
l = Compressor
m = Combustion and swirl chamber
n = Gas turbine
o = Autonomous heat-recovery steam circuit

A: *Plain steam installation* with air heater and bled-steam feed-water heating

B: *Combined installation* with combustion turbine preceding boiler. Heat recovery by autonomous recuperation steam circuit

C: *Combined installation* with preceding combustion turbine. Heat recovery by transfer to part of feedwater

D: *Combined installation* as C, but with air indirectly heated before expansion

E: *Combined installation* with pressure-charged boiler firing (Velox principle)

F: *Combined installation* with pressure-fired boiler, expansion being divided between a hot and a cold stage to reduce the temperature of the exhaust gases

G: *Gas turbine* without preceding steam cycle, but followed by a heat-recovery steam system

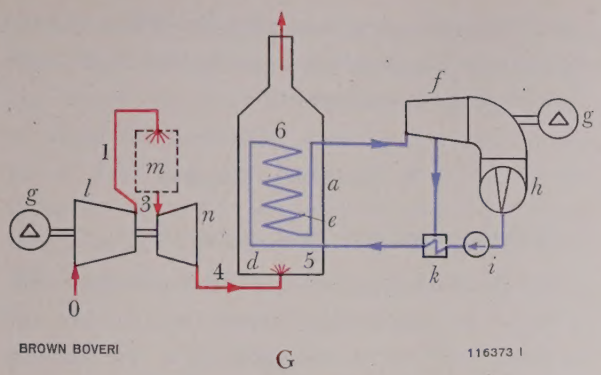

Fig. 1. – Circuit diagrams of combined steam and gas turbine installations

Red: Open combustion circuit

Blue: Closed water-steam circuit

a = Boiler
b = Boiler fans
c = Air heater
d = Combustion chamber with burner
e = Steam part of boiler
f = Steam turbine
g = Generator
h = Condenser
i = Feedwater pump
k = Feedwater heater and de-aerator
l = Compressor
m = Combustion and swirl chamber
n = Gas turbine
o = Autonomous heat-recovery steam circuit

0–9 (see Tables I and II)

A: *Plain steam installation* with air heater and bled-steam feedwater heating

B: *Combined installation* with combustion turbine preceding boiler. Heat recovery by autonomous recuperation steam circuit

C: *Combined installation* with preceding combustion turbine. Heat recovery by transfer to part of feedwater

D: *Combined installation* as C, but with air indirectly heated before expansion

E: *Combined installation* with pressure-charged boiler firing (Velox principle)

F: *Combined installation* with pressure-fired boiler, expansion being divided between a hot and a cold stage to reduce the temperature of the exhaust gases

G: *Gas turbine* without preceding steam cycle, but followed by a heat-recovery steam system

expansion turbine. The air can be heated in an air heater before it flows into the combustion chamber. In the turbine *n*, which drives the compressor, the hot gas gives up power and an appreciable useful output in addition. This gas then enters the fire-box of the boiler and still contains an ample amount of oxygen for combustion. By compression the air is heated by more than 100 °C. Therefore in the air heater it cannot reduce the temperature of the exhaust gases to the extent possible in A. But since the exhaust gases still ought to be cooled to the limit imposed by the dew-point and corrosion, diagram B contains an autonomous steam circuit *o* utilizing the waste heat. Instead of this, diagram C shows the waste heat being transferred to a leg of the feedwater system, which in many cases renders the air heater superfluous.

In D the air is not raised to the temperature required by the expansion turbine by *internal combustion*, but by being heated *externally* in the boiler. However, this necessitates a costly heat exchanger; on the other hand, the expansion turbine operates with clean air. This, so far, is the only possible solution for combined installations in which the fuel has a high ash content, particularly with coal.

Diagram E shows a pressure-fired boiler, for instance of the well-known "Velox" type. The Velox boiler belongs to the combined installations as soon as its charging set delivers excess power, which was already the case with early designs of Velox units. The main part of the boiler precedes the gas turbine and operates under pressure. The other part, usually only the economizer, follows the gas turbine.

In diagram F the gases are expanded in two stages: a high-pressure stage with high temperatures, and a low-pressure stage with lower temperatures, the object of which is to reduce the temperature of the exhaust gas more than can be done by a heat exchanger. The walls of the latter must be colder than the gases, which is unnecessary in the l.p. turbine.

Finally, diagram G shows the important case of a gas turbine with a waste-heat boiler.

The systems illustrated in the diagrams permit of certain variants. In B, C, E and F the air heater can be left out, which may affect the efficiency, under certain conditions. Moreover, it is permissible to dispense with recuperation in B, provided one is

willing to accept a drop in efficiency. The air can also be compressed in several stages with intercoolers and the gas expanded in several stages with reheating.

At this point one problem warrants special attention. Combined installations, such as in B and C for instance, have a pair of combustion chambers in series. The second operates with air containing a reduced amount of oxygen, but at a high temperature, so that combustion does not present any difficulties. On the other hand, with gas or oil firing, it is possible, in the event of a misfire in one of the combustion chambers, for the flame to flash over explosively from the other. The installation must consequently be built in such a way that this cannot cause any damage.

Two-stage combustion has been thoroughly tested with gas turbines and has proved reliable. Both combustion chambers are explosion-proof.

The idea of harnessing gas and steam turbines together is by no means new. Stodola [1][1] discussed utilization of waste heat in a steam circuit in 1922, while in 1936 Schröder [2] drew up the main boiler connections with gas turbines. Numerous patents, many of which would not stand up to a novelty search, though, describe different variants. It is therefore logical to ask why more combined plants have not been built, if this is the case. Doubtless this is partly due to a dislike of complication in operation. It was feared that new sources of trouble could be introduced into the installation. It is considered right to think of a combined gas and steam plant when this does not involve any more complications, either as regards operation or maintenance, than the boiler fans which it replaces. By adhering to the wealth of experience gained with gas turbines and charging sets, it may be claimed that this goal has been attained.

II. Thermodynamics of Combined Steam and Gas Turbine Plants

A. Steam Plant with a Gas Turbine in the Combustion Circuit

Starting with a steam plant as in diagram A, the first question to be investigated was, under what circumstances and by how much the efficiency could be improved by inserting a gas turbine in the combustion circuit, as shown in B.

1. The Energy Balances

a. *Straightforward steam plant, diagram A*

For the combustion air and combustion gases Fig. 2 shows the relationship between temperature and enthalpy, referred to the enthalpy at the ambient temperature. Plotted in this curve are the successive states in the combustion circuit.

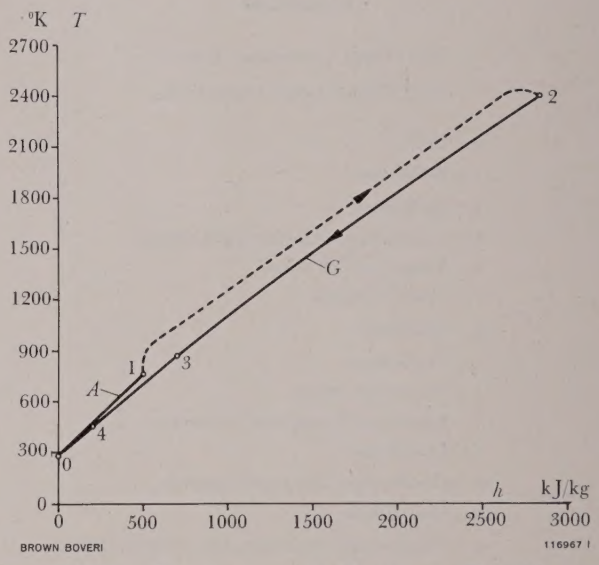

Fig. 2. – Temperature – enthalpy diagram $T = f(h)$

A = Air G = Combustion gas

(See diagram A and Table I)

TABLE I

		Enthalpy flow referred to 1 kg air per second
0–1	Air heating	Q_0 (+)
1–2	Combustion Introduced as fuel which calorific value H_0 Remaining after subtraction of losses due to radiation and unburnt fuel	$\eta_H H_0$ (+)
2–3	Heat given up to steam circuit	V_0 (—)
3–4	Heat given up to air heater	Q_0 (—)
4–0	Heat lost up the chimney	Z_0 (—)

[1] The figures in brackets refer to the bibliography on p. 799.

In view of the complicated diagrams which follow, Fig. 2 has been unfolded and a method of representation chosen, by which the changes in energy in the combustion circuit can be placed successively, regardless of their sign. The latter can be seen from the droop or rise of the temperature curve, as well as from a special portion of the curve below the axis. (Fig. 3 which, in contrast to Fig. 2, is not to scale.)

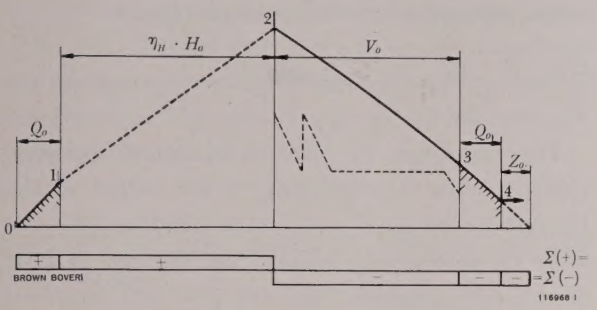

Fig. 3. – Unfolded temperature – enthalpy diagram $T = f(h)$ for air and combustion gas according to system A

Dotted below V_0: Steam states in the boiler

TABLE II

		Enthalpy flow referred to 1 kg air per second
0–1	Compression	C (+)
1–2	Air heating	Q (+)
2–3	First combustion stage	$\eta_H H_1$ (+)
3–4	Expansion	E (—)
4–5	Second combustion stage	$\eta_H H_2$ (+)
5–6	Heat given up to steam circuit	V (—)
6–7	Heat transferred to air	Q (—)
7–8	Heat-recovery stage (recuperation)	R (—)
8–0	Heat lost up the chimney	Z (—)

b. *Combined plant, diagram B*

Fig. 4 shows the successive states in the combustion circuit. From the Tables I and II above, the following energy balances are obtained:

a: Steam plant (suffix "$_0$")

$$Q_0 + \eta_H H_0 - V_0 - Q_0 - Z_0 = 0$$

or, solved for the heat absorbed by the steam

$$V_0 = \eta_H H_0 - Z_0 \qquad (1)$$

b: Combined plant (without suffix)

$$C + Q + \eta_H H_1 - E + \eta_H H_2 - V - Q - R - Z = 0$$

or, solved for the heat absorbed by the steam

$$V = \eta_H (H_1 + H_2) - Z - (E - C) - R \qquad (2)$$

The outputs of the two plants are

a: $$P_0 = \eta_{th} V_0 - P_{0,\,aux} \qquad (3)$$

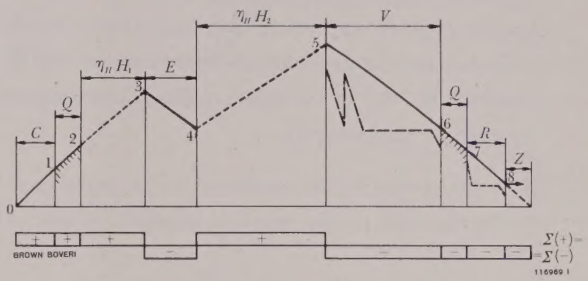

Fig. 4. – Temperature – enthalpy diagram $T = f(h)$ for air and combustion gas according to system B

Dotted below V: High-pressure steam states in boiler
Dotted below R: Low-pressure steam states in heat-recovery circuit

in which

η_{th} = the thermal efficiency of the steam turbine, referred to the terminal output, less the power consumed by the drives of the feedwater and cooling-water pumps, and the heat V_0 absorbed by the steam.

$P_{0,\,aux}$ = the power consumed by the auxiliaries, excepting the feedwater and cooling-water pumps.[2]

b: $$P = \eta_{el}(E - C) + \eta_{th} V + \eta_R R - P_{aux} \qquad (4)$$

in which

η_{el} = the efficiency of the generator of the gas-turbine set

η_R = the thermal efficiency of the utilization of the waste heat (recuperation efficiency)

[2] Strictly speaking, it should be borne in mind that some of the heat coming from the auxiliaries is utilized by the boiler and must therefore be taken into account in the heat and energy balances. For the sake of simplicity the recovered heat is subtracted from the power of the auxiliaries, so that P_{aux} denotes the net amount.

Let us now compare the two plants, assuming an air throughput of 1 kg/s and the following conditions:

(i) The pressure and temperature of the live steam —and if necessary of the reheated steam—and the vacuum and feedwater temperatures are equal in both cases. The internal efficiency of the steam turbine, the feedwater and cooling-water pumps, and the quality of the feed-heaters and generator are also equal in both cases, and hence the thermal efficiency of the steam turbine. This most important, and also logical, assumption naturally only applies to the h. p. steam circuit in B, but not for any recuperation circuit (top of diagram B), the steam data in which are limited by the gas temperature.

(ii) The fuel input is also assumed to be equal and to correspond to the smallest possible excess of air

$$H_1 + H_2 = H_0$$

On page 793 the conditions are shown under which this assumption is justified.

(iii) The exhaust-gas temperature is assumed to be equal in both cases, and thus the exhaust gas loss too.

$$Z = Z_0$$

(iv) Power of the auxiliaries: The power for the auxiliary pumps of the steam turbine, especially the feedwater and cooling-water pumps, was taken into account in η_{th} and was thus made proportional to the output of the steam turbine, which is reasonably accurate. The remaining auxiliary power is mainly consumed by the boiler fans in A, which are omitted in B. Instead the gas turbine operates with a back pressure which overcomes the boiler resistance, thereby reducing the gas turbine output. In the calculation we omit these two approximately equal terms, so that the auxiliary power can be expressed as $P_{aux} = P_{0,\,aux}$.

Under these assumptions the equation for the flow of energy (2) may be written

$$V = \eta H_0 - Z_0 - (E - C) - R$$

or, allowing for (1),

$$V = V_0 - (E - C) - R \qquad (2a)$$

and the power equation (4)

$$P = \eta_{el}(E - C) + \eta_{th}[V_0 - (E - C) - R] + \\ + \eta_R R - P_{aux} \qquad (4a)$$

If we now subtract equation (3) from this, the gain in output per kg/s of air becomes

$$P - P_0 = (\eta_{el} - \eta_{th})(E - C) - (\eta_{th} - \eta_R) R \qquad (5)$$

Since equal heat input was assumed, the percentage improvement in the thermal efficiency of the installation, referred to that of the steam plant is

$$\frac{\Delta\eta}{\eta_0} = \frac{P - P_0}{P_0} = (\eta_{el} - \eta_{th}) \frac{E - C}{P_0} - (\eta_{th} - \eta_R) \frac{R}{P_0} \qquad (6)$$

The expression (5) consists of a first, positive, additive term corresponding to the output of the gas-turbine set $\eta_{el}(E - C)$ from which $\eta_{th}(E - C)$ must be subtracted, because the amount of heat $(E - C)$ is obtained from the gas, and thus not available for the steam cycle. It contains a second, negative term, namely $-(\eta_{th} - \eta_R)\ R$, originating from the residual heat R which performs work with a poorer recuperation efficiency η_R than if it had been utilized in the h.p. steam circuit with η_{th} via the air heater.

With the aid of equation (6) it is possible to calculate the improvement effected by combining a gas turbine with a steam plant. First the recuperation power R and the efficiency of recuperation η_R must be studied more closely; later the expressions for E and C, and their optimization are dealt with.

2. *The Recuperation Power R*

In the straightforward steam plant the exhaust gases at the air inlet to the preheater are considerably hotter than the incoming air. The enthalpy of the exhaust gases, referred to the ambient temperature (Fig. 5a) is higher by the amount of the exhaust-gas losses Z_0. In the combined installation the air is already heated to a temperature T_1 by compression before it enters the heater. It is often warmer than the exhaust gas leaving the steam plant. Consequently the gas temperature at the outlet from the air heater has to be increased, in order that the heat may be transferred with a sufficient temperature difference. An obvious solution is to dispense with the part of the heater in which the air is heated to T_1 in the ordinary steam plant, and to retain the

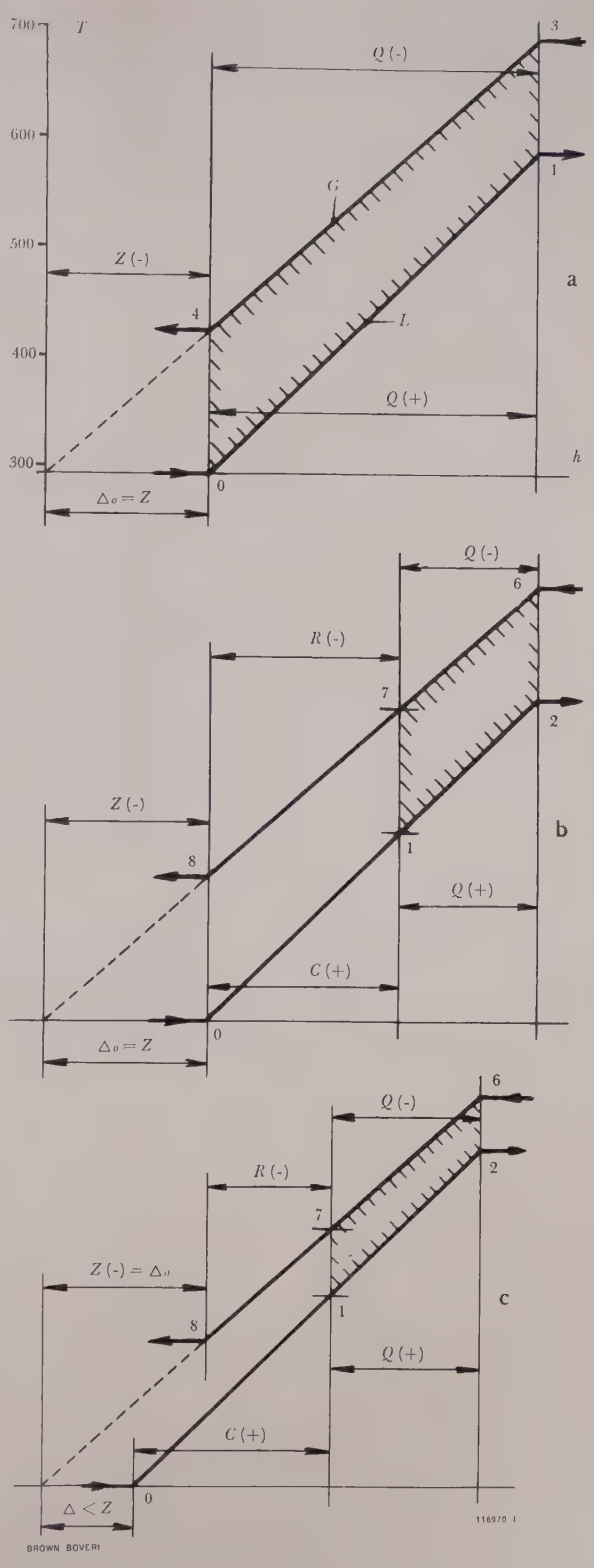

Fig. 5. – Temperature – enthalpy diagram $T = f(h)$ for the air heater

a: Recuperation $R = 0$ (System A)
b: Recuperation $R = C$ (System B)
c: Recuperation $R = C - (Z - \Delta)$ (System B)

rest of the heater unchanged. It heats the air with the same temperature difference between gas and air, and attains the same final temperature as before (Fig. 5b). In this case the loss of the transferred amount of heat corresponds exactly to the work of compression. This heat is supplied by the recuperator and is given by

$$R = C \tag{7}$$

But there are often reasons for deviating from this law, as follows:

a. Reduction of the temperature difference between air and gas in the air heater. In the steam plant this is defined, on the one hand by the atmospheric temperature and, on the other, by the lowest temperature to which the exhaust gases may be cooled without moisture condensing and giving rise to such difficulties as corrosion. In the combined plant the temperature difference may be lowered so long as this is advantageous for the efficiency, which should be rated higher than the extra costs for the heat exchanger. The enthalpy difference per second between gas and air is then, as may be seen from Fig. 5c, no longer Z_0 but Δ, which is $< Z_0$. In this case the recuperation power is

$$R = C - (Z - \Delta) \tag{8}$$

b. Here a remark concerning the ordinary steam plant is called for. Also, with such installations, the temperature difference in the air heater, which is indeed the cause of thermodynamic losses, can be reduced by pre-heating the air by low-pressure bled steam before it is conveyed to the flue-gas heat exchanger. The thermal efficiency can thus be improved.

c. Sometimes the recuperation power is increased above the value C, in order to dispense completely with the air heater (1–2 in diagram B).

d. Instead of utilizing the heat in a waste-heat boiler with a special turbine, as in B, it can be used to heat the feedwater for the main turbine, as in C. Then it is advantageous for the feedwater flow to be divided after it passes the lower feed-heating

stages. One part flows through the upper feed-heating stages, the rest through the waste-heat boiler. This is feasible since the "hydraulic coefficient" of the current of water—the product of the specific heat and the mass flow—is greater than that of the gas current. Diagram C shows this variant. Here the air heater is shown dotted because in most cases it may well be dispensed with.

Fig. 6 shows the temperatures in the recuperation system. The gas current is cooled from T_7 to T_8, while the portion of the feedwater current is heated from T'_8 to T'_7. The slope of the line $T'_7 - T'_8$ depends on the ratio in which the feedwater current is divided. It could be made parallel to the gas line $T_7 - T_8$. It is still better to make T'' proportional to T, which is not only simple as regards calculation, but gives an optimum thermodynamic result.[3]

When an air heater is provided (diagrams C and D), T_7 is determined, as before, by the compression temperature and the temperature difference in the air heater. In this case

$$R = C - (Z - \Delta)$$

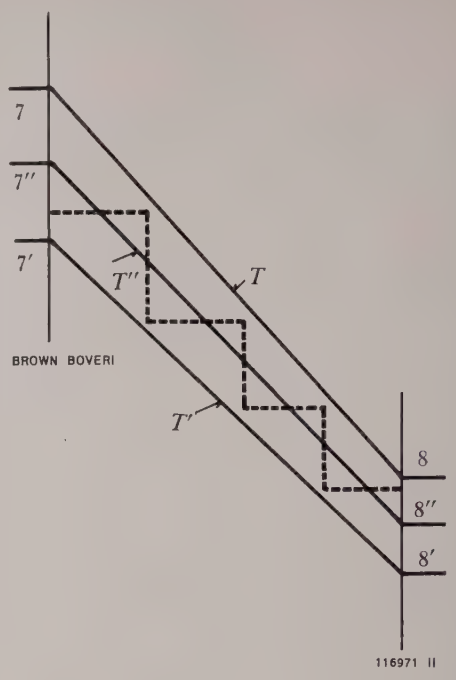

Fig. 6. – Temperature – enthalpy diagram $T = f(h)$ in the recuperator and bled-steam feedwater heaters

T = Temperature of exhaust gases
T' = Temperature of feedwater
T'' = Temperature of bled steam

Care must be taken to ensure that the feedwater temperature T'_7 agrees with the final temperature of the bled-steam heating—or of any intermediate stage—and if it does not, the ratio in which the water is divided must be changed, dispensing with the exact proportionality of T and T'.

If the flue-gas is not used to preheat the air, T_7 is determined by the final temperature T'_7 of the feedwater and the temperature difference of the heat transfer from flue-gas to feedwater. In this case

$$R = (h_7 - h_8)\, \dot{m}_E \qquad (9)$$

in which $h_{7,\,8}$ are the enthalpies and $\dot{m}_E$ the mass flow of the flue-gases.

3. The Recuperation Efficiency

Of the heat to be recuperated R, only the portion η_c is available to do work, according to Carnot's law, i.e.

$$\eta_c = \frac{1}{R}\int_{T_8}^{T_7}\left(1 - \frac{T_0}{T}\right) dR = 1 - \frac{\log_e T_7/T_8}{T_7 - T_8} \cdot T_0 \qquad (10)$$

[3] Proof of this statement:

A quantity of heat Q is to be transferred from a medium with a given temperature distribution T to another medium with a temperature T' which can be chosen freely. T' must be such that, for a given transfer area and overall heat transmission coefficient k, the increase in entropy is a minimum.

The heat transfer area is

$$A = \frac{1}{k}\int_0^Q \frac{dQ}{T - T'}$$

and the increase in entropy

$$s = \int_0^Q \left(\frac{1}{T'} - \frac{1}{T}\right) dQ$$

We now have to find the function (T') which minimizes the integral

$$I = \int_0^Q \left[\left(\frac{1}{T'} - \frac{1}{T}\right) + \lambda \cdot \frac{1}{T - T'}\right] \cdot dQ = \int_0^Q F(T')\, dQ$$

λ being an arbitrary multiplier. The Euler equation of the variation calculus in this case is

$$\frac{\partial F}{\partial T'} = 0 \text{ and gives } -\frac{1}{T'^2} + \frac{\lambda}{(T - T')^2} = 0$$

or $\dfrac{T - T'}{T'} = \sqrt{\lambda}$, i.e. T' is proportional to T.

owing to the linear relationship between R and T,

in which T = gas temperature

T_0 = ambient temperature (i.e. of cooling water).

The heat must be transferred to a working medium such as a steam circuit, as indicated in Fig. 4 by the dotted lines. The three sections of the line represent feed-heating, evaporation and superheating. The useful part of the heat contained in the steam, i.e. the "cycle efficiency", is given by

$$\eta_{Pr} = \frac{\Delta h - T_0 \cdot \Delta s}{\Delta h} \qquad (11)$$

where Δh and Δs represent the enthalpy $\int dQ$ and entropy $\int dQ/T'$ absorbed by the steam generator. Since the temperature T' in the steam circuit is lower than T in the gas,

$$\eta_{Pr} < \eta_c$$

The useable energy in the steam is utilized at the "thermodynamic" efficiency of the turbine η_{td}, which takes into account the losses in the turbine and generator, the power used to drive the feed pump and irreversibility of the feed-heating system and condenser.

Hence $$\eta_R = \eta_{Pr} \cdot \eta_{td} \qquad (12)$$

Winning energy from heat carriers at not unduly high temperatures was comprehensively studied for atomic power plants. Reference may be made to article [3] in the bibliography, which gives the fundamental theory for the design of a recuperation system. The recuperation efficiency η_R can be read directly off Fig. 6 of that article.

When the recuperated heat is transferred to the feedwater as in C and D, the output of the turbine can be equated to the two amounts of heat applied to the circuit per second, namely $V = V' + V''$ and R:

$$P = \eta_{th}(V' + V'') + \eta_R R$$

where R = recuperated power from the exhaust-gas temperature to the temperature corresponding to the highest bleed point,

V'' = power recuperated above the temperature determined by the highest bleed point. Hence V'' is applied to the whole of the feedwater and can thus be added to the boiler.

$\eta_R R$ can be determined as follows: T_7, T_8, T'_7 and T'_8 (Fig. 6) are stipulated, T_8 being the given final temperature of the gas, T'_7 the given final temperature of the feedwater; T_7 and T'_8 are given by the selected temperature differences of the preheater. Then R and the ratio of the division of the feedwater have to be determined, and the bleeding quantities taken from the thermal diagram of the turbine, in particular those quantities which would have been required to heat the diverted feedwater. The gain in output resulting from its remaining in the turbine can also be determined from the thermal diagram.

For general investigations, in which the flow diagram of the plant is not exactly stipulated, the following procedure may be adopted: the stepped curve for the temperature of the bled steam (Fig. 6) is replaced by a straight line T''_7 and T''_8. The available percentage of the enthalpy of the bled steam is then

$$\eta''_c = 1 - \frac{\log_e T''_7/T''_8}{T''_7 - T''_8} \cdot T_0$$

This is converted at the "hydraulic efficiency" of the turbine, and therefore

$$\eta_R = \left(1 - \frac{\log_e T''_7/T''_8}{T''_7 - T''_8} \cdot T_0\right) \eta_{hydr}$$

If proportional temperatures are also chosen, substituting

$$T' = (1 - \delta')\ T$$
$$T'' = (1 + \delta'')\ T' \qquad (13)$$

we obtain

$$\eta_R = \left[1 - \frac{1}{(1-\delta')(1+\delta'')} \cdot \frac{\log_e T_7/T_8}{T_7 - T_8} \cdot T_0\right] \eta_{hydr} \qquad (14)$$

in which η_R, as desired, is expressed in terms of T_7 and T_8.

4. The Output of the Gas-Turbine Set and the Choice of its Working Pressure

The compression and expansion powers C and E per kg/s of air are calculated with the aid of the following equations, the suffixes 0 and 1 referring to the stagnation conditions before and after the compressor blading, 3 and 4 before and after the turbine blading (diagrams C and D).

$$C = c_{pc} \cdot (T_1 - T_0) \qquad (15)$$

$$T_1 = T_0 \pi^{a_c} \qquad (15a)$$

where $\pi = \frac{p_1}{p_0}$ compression ratio

$$a_c = \left[\frac{R}{c_p}\right]_c \cdot \frac{1}{\eta_c}$$ polytropic exponent of the compression (15b)

η_c = polytropic efficiency of the compressor blading

R = gas constant

$$E = \frac{\dot{m}_E}{\dot{m}_c} \cdot c_{pE} \cdot (T_3 - T_4) \quad (16)$$

$$T_4 = T_3 (\varepsilon\pi)^{-a_E} \quad (16a)$$

where $\varepsilon\pi = p_3/p_4$, the pressure ratio on expansion

$$\varepsilon = \Pi\left(1 - \frac{\delta p}{p}\right)$$

or $\log_e \varepsilon = -\sum \frac{\delta p}{p}$, in which $\sum \frac{\delta p}{p}$ is the sum of all pressure drop ratios in the inlet and outlet pipes of the machines, piping, combustion chambers, heat exchangers —and, under the appropriate conditions, less the resistance on the gas side of the boiler (as a result of assumption (iv) on page 788)

$$a_E = \left[\frac{R}{c_p}\right]_E \cdot \eta_E$$ polytropic exponent of expansion (16b)

η_E = polytropic efficiency of the turbine blading

$\dot{m}_c$, $\dot{m}_E$ = mass flow through compressor and turbine, respectively. The mass flow of the gas is greater than that of the air by the fuel input, and less than it by the leakage.[4]

With the aid of equation (5) an attempt will now be made to obtain the compression ratio π which yields the maximum power gain and, in consequence of the constant heat input, the maximum efficiency.

The equation (5) has to be differentiated and equated to zero.

$$d(P - P_0) = d[(\eta_{el} - \eta_{th}) \cdot (E - C) - (\eta_{th} - \eta_R) \cdot R] = 0$$

In this we must distinguish between the variation and non-variation of the recuperation energy R with changes in π. This is so when this energy is fed into an autonomous steam circuit, likewise when the gas temperature at the inlet to the recuperator is governed by a preceding flue-gas air heater, and the latter influences the choice of the bleed points. In contrast R is invariable when the gas temperature is only prescribed by the final temperature of the feedwater (E and F on page 784). This simple case is hereby assumed. From the above equation there remains

$$d(E - C) = 0$$

The most favourable gas turbine is the one with the maximum output per kg air per second, and not the one with the maximum efficiency.

With the aid of equations (15) and (16) we obtain

$$d(E - C) = -c_{pc} \cdot dT_1 - \frac{\dot{m}_E}{\dot{m}_c} \cdot c_{pE} \cdot dT_4 =$$

$$= -c_{pc} \cdot a_c \cdot T_1 \cdot \frac{d\pi}{\pi} + \frac{\dot{m}_E}{\dot{m}_c} \cdot c_{pE} \cdot a_E \cdot T_4 \cdot \frac{d\pi}{\pi} = 0$$

or with

$$\eta_G = \frac{\dot{m}_E}{\dot{m}_c} \cdot \frac{c_{pE}}{c_{pc}} \cdot \frac{a_E}{a_c} = \frac{\dot{m}_E}{\dot{m}_c} \cdot \frac{R_E}{R_c} \cdot \eta_c \cdot \eta_E$$

$$T_1 = \eta_G \cdot T_4 \quad (17)$$

Since the inlet temperatures T_0, T_3 are generally given, we may substitute

$$\pi^{(a_c + a_E)} = \frac{\eta_G}{\varepsilon^{a_E}} \cdot \frac{T_3}{T_0} \quad (18)$$

with the aid of (15a) and (16a). If, on the other hand, R is variable, then η_R will also be variable. It is convenient to introduce the marginal value $\eta_{R,mg}$ of η_R, which originates from the degree of utilization of the last element of input heat dR. This occurs at the highest temperature T_7. Hence its Carnot fraction is $1 - T_0/T_7$ instead of

$$1 - \frac{\log_e T_7/T_8}{T_7 - T_8} \cdot T_0$$

so that, to a first approximation, $\eta_{R,mg}$ and η_R may be substituted in this proportion. According to the definition of the marginal efficiency

$$d(\eta_R R) \equiv \eta_{R,mg} \cdot dR$$

From (7) or (8) we obtain $dR = dC$; while, according to (17) and (18)

$$T_1 = \left(\frac{\eta_{el} - \eta_{th}}{\eta_{el} - \eta_{R,mg}}\right) \cdot \eta_G \cdot T_4 \quad (17a)$$

[4] The above equations apply for constant specific heat during compression and expansion. For general considerations this may be held to be admissible. For binding guarantee calculations it is essential to work with exact gas tables.

$$\pi^{(a_c+a_E)} = \left(\frac{\eta_{el}-\eta_{th}}{\eta_{el}-\eta_{R,mg}}\right) \cdot \frac{\eta_G}{\varepsilon^{a_E}} \cdot \frac{T_3}{T_0} \qquad (18a)$$

When evaluating this equation it must be borne in mind that π is implicitly included in $\eta_{R,mg}$.

In the realization of an installation it is, of course, not necessary to adhere strictly to the optimum working pressure. The price and controllability of the machines may give rise to modifications which, provided they are not unduly large, only cause quite small drops in the efficiency, which can be tolerated as such. However, the efficiency at optimum pressure should always be regarded as a measure of what can be attained.

B. Gas Turbines with Heat Recovery

1. First let us consider a gas turbine without any subsequent combustion, i.e. a straightforward gas turbine with heat recovery (diagram G). The stipulation of constant fuel input, as laid down on page 788, is dispensed with in this case.

In the heat balance (2) we assume $V = 0$ and $H_2 = 0$.

$$\eta_H H_1 - Z - (E-C) - R = 0$$

or, with equation (8): $R = C - (Z-\Delta)$

$$\eta_H H_1 = E + \Delta$$

The output is

$$P_1 = \eta_{el}\,(E-C) + \eta_R R - P_{aux}$$

and the efficiency

$$\eta_{GT} \equiv \frac{P_1}{H_1} = \frac{\eta_{el}\,(E-C) + \eta_R R - P_{aux}}{\frac{1}{\eta_H}\,(E+\Delta)} \qquad (19)$$

2. In the second combustion chamber (diagram B) the fuel energy H_2 which can be increased from 0 to $H_0 - H_1$, is added. In the steam turbine the amount $\eta_{th}\eta_H H_2$ is produced in addition.[5]

[5] Simultaneously the final air heating temperature can be changed and the ratio of the first to the second fuel input shifted, without changing the efficiency of the installation. This might be necessary if the gas temperature in the h.p. boiler were not sufficiently high to realize the desired steam cycle. It must then be remembered that, in subsequent equations, H_1 and H_2 are no longer the fuel heat inputs to the combustion chambers, but that H_1 is the heat needed by the gas-turbine cycle alone, and H_2 the surplus above it.

The efficiency of the combined installation—with variable amount of excess air—is given by

$$\eta = \frac{P_1 + \eta_{th}\,\eta_H H_2}{H_1 + H_2} = \frac{\eta_{GT} H_1 + \eta_{th}\,\eta_H H_2}{H}$$

or

$$\eta - \eta_{GT} = (\eta_{th}\,\eta_H - \eta_{GT})\,\frac{H_2}{H} \qquad (20)$$

The H_2 part of the steam plant is only advantageous when

$$\eta_{th}\eta_H > \eta_{GT}$$

Equation (20) shows that H_2 must be made as large as possible, provided $\eta_{th}\,\eta_H$ is greater than η_{GT}. This implies that, as for the plain steam cycle, an effort should be made to execute combustion with the smallest possible amount of excess air. The stipulation $H_1 + H_2 = H_0$ on page 788 is thus justified. If, on the other hand, $\eta_{th}\eta_H$ is smaller than η_{GT}, it is preferable to substitute $H_2 = 0$, i.e. the second combustion stage is dispensed with altogether. A solution between these extremes, i.e. where only part of the available oxygen is utilized in the second combustion chamber, never brings any advantage, as far as the efficiency is concerned. It is nevertheless selected sometimes, when the relationship of the gas turbine output to that of the steam turbine has to be shifted, either for economic reasons or to obtain full benefit from an existing gas or steam turbine.

The results of investigations which have been carried out may be summarized as follows:

a. The superiority of a *combined installation over a plain steam plant* is given by equations (5) and (6). Let us introduce the term

$$\eta_{GT}^{*} = \frac{\eta_{el}\,(E-C) + \eta_R R}{E} \qquad (21)$$

In the numerator is the output of a gas turbine with heat recovery, in the denominator the work of expansion, which would be equal to the heat input to a gas turbine with a perfect heat exchanger and without any losses in the combustion chamber. If this ideal gas turbine efficiency were substituted in (5), the gain in efficiency could be expressed in the following simple form:

$$\eta - \eta_0 = (\eta_{GT}^{*} - \eta_{th})\,\frac{E}{H} \qquad (22)$$

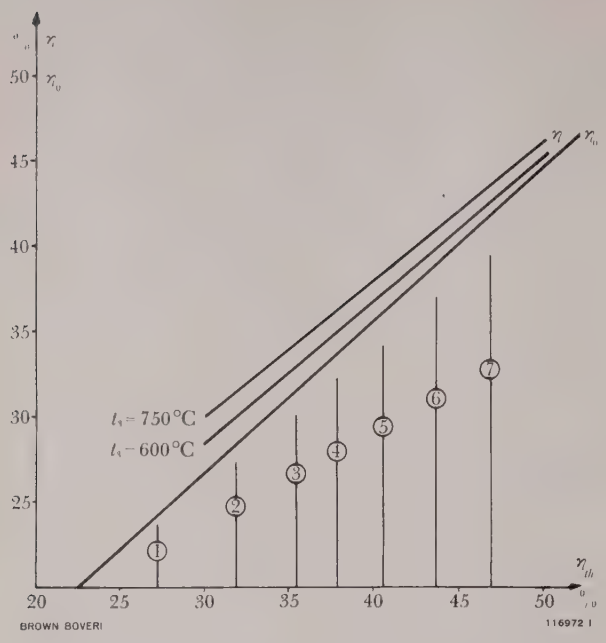

Fig. 7. – Efficiency of a steam plant η_0 and combined steam-gas turbine installation η according to system D, in terms of the thermal efficiency η_{th} of the steam turbine at two values of t_3, the inlet temperature for the gas turbine

① St. Andrä, Austria
② Tuncbilek, Turkey
③ Donington, Great Britain
④ Fortuna III, Germany
⑤ Philip Sporn, USA
⑥ River Rouge, USA
⑦ Eddystone, USA

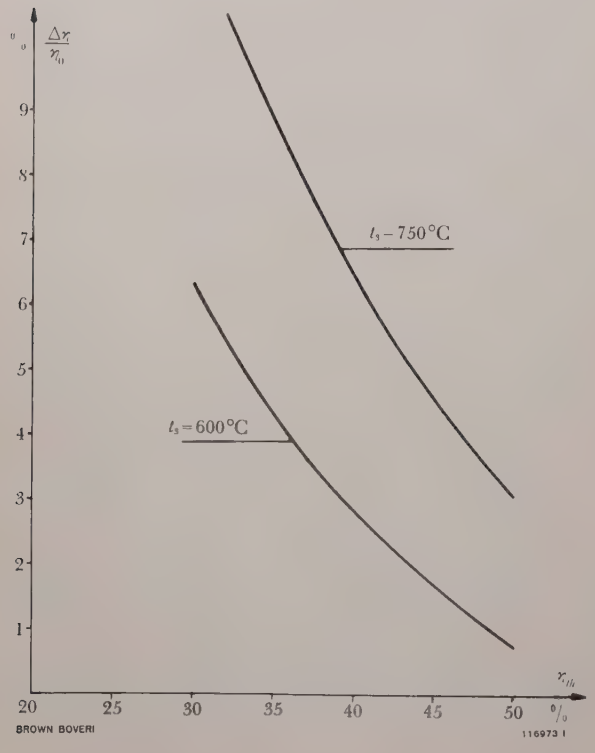

Fig. 8. – Multiplicative improvement in efficiency $\Delta\eta/\eta_0$ as a function of the thermal efficiency of the steam turbine η_{th} for combined steam-gas turbine installations in accordance with system D, at two values of t_3, the inlet temperature to the gas turbine

b. The superiority of a *combined plant over a plain gas turbine with heat recovery* may be expressed equally simply if we introduce a further "ideal" gas turbine efficiency, defined by

$$\eta_{GT}^{**} = \eta_{GT} / \eta_H$$

This corresponds to the efficiency of the gas turbine with heat recovery, referred to the actual heat input to the gas, i.e. without combustion chamber losses.

$$\eta - \eta_{GT} = (\eta_{th} - \eta_{GT}^{**}) \frac{\eta_H H_2}{H} \qquad (23)$$

c. From the last two equations we may derive the following criteria for the installation with the best efficiency.

$\eta_{th} > \eta_{GT}^{*}$ plain steam plant

$\eta_{GT}^{*} > \eta_{th} > \eta_{GT}^{**}$ combined plant with additional combustion

$\eta_{GT}^{**} > \eta_{th}$ gas turbine with heat recovery, but without additional combustion

The combined installation with additional heating is thus only advantageous when the thermal efficiency of the steam cycle η_{th} is between the limits η_{GT}^{*} and η_{GT}^{**}.

C. Results, Other Circuit Arrangements and Control Systems

Fig. 7 shows the efficiency of a straightforward steam installation η_0 and that of a combined steam and gas plant η for a temperature of 600 °C and 750 °C before the gas turbine in terms of thermal efficiency η_{th} of the steam turbine. The η_{th} values of a number of existing steam plants are also plotted [4]. From this illustration it can be seen that an improvement of $\Delta\eta = \eta - \eta_0$ can always be achieved with the combined installation. The multiplicative improvement $\Delta\eta/\eta_0$ decreases with increasing η_{th}, as may be seen in Fig. 8, drawn to an enlarged scale. With higher temperatures at the inlet to the gas turbine the improvement is correspondingly greater.

If, in a gas-turbine set, the air is compressed in several, say n stages with intercooling, and expansion takes place in m stages with reheating, it is no longer permissible to use the equations (18) and (18a) for π. But for such cases it is possible to derive appropriate equations.

Since numerical investigations of systems including intercooling, even with recovery of the dissipated heat in a partial feedwater current, so far resulted in deterioration of the efficiency and since, on the other hand, the gain with reheating was very modest and only obtainable under definite conditions, we believe that such combinations are not interesting for the conventional gas turbine inlet temperatures. Present remarks are therefore confined to giving three more, simple equations which can be used in such cases, without going into their complicated derivation and application. The optimum total compression ratio for variable R and η_R is given by

$$\pi^{\left(\frac{a_c}{n}+\frac{a_E}{m}\right)} = \frac{(\eta_{el}-\eta_{th})\ \eta_G\ [T_{3j}]_j}{\varepsilon^{a_E/m}\ [(\eta_{el}-\eta_{R,mgi})\ T_{0i}]_i} \qquad (24)$$

where $i = 1, 2 \ldots n$

$j = 1, 2 \ldots m$

and $[\ ]_i$ or $[\ ]_j$ denote the geometric mean, for example for i the n-th root of the product of n quantities.

The individual optimum compression and expansion ratios are

$$\frac{\pi_i}{\pi^{1/n}} = \left\{ \frac{[(\eta_{el}-\eta_{th})\ T_{0i}]_i}{(\eta_{el}-\eta_{R,mgi})\ T_{0i}} \right\}^{1/a_c} \qquad (25)$$

$$\frac{\pi_j}{(\varepsilon\pi)^{1/m}} = \left\{ \frac{T_{3j}}{[T_3]} \right\}^{1/a_E} \qquad (26)$$

If, however, R and η_R are constant, the terms $(\eta_{el}-\eta_{th})$ and $(\eta_{el}-\eta_{R,mgi})$ in (24) and (25) become equal to 1. Equation (26), however, remains unchanged.

The typical example given below deals with the behaviour of the set at full load. Should there be any importance attached to partial load, this demands exhaustive investigation, which can only be outlined here. For variable load the following alternatives would, for instance, have to be considered:

1. Bypass combustion chamber,
2. Split-shaft gas turbine,
3. Gas-turbine set designed for the principal load point, and generation of overload output by supplementary fans for the boiler.

III. Example of a Typical Economic Investigation

Primarily we are interested in learning which of the systems A to G is the most economical. In this case one variant, namely B, can be eliminated straight away; it was merely introduced for fundamental reasons but is obviously a good deal more expensive than C, besides having a poorer efficiency.

System F can only be recommended in preference to E in special cases. Admittedly it offers a proved thermodynamic advantage, but this is quite insignificant. If a plant is only intended to supply heat and no electricity, or if, for any reasons, e.g. for control purposes, as much as possible of the power gain is to be obtained from the steam turbine and as little as possible from the gas turbine, system F will be adopted. Moreover, this system shows that, owing to the heat pump effect of the gas turbine, it should be possible in principle to attain a thermal efficiency of a boiler of over 100%, a statement which some years ago was, quite wrongly, received with grave disapproval in the technical press.

Compared with C (without air heater), system G is rather at a disadvantage from the efficiency aspect with the chosen steam cycle, but nevertheless very interesting in situations where, for other reasons, a gas turbine is employed as the main machine.

In the following remarks only the systems A, C, D and E without air heater will be compared with one another. The installations were first calculated thermodynamically with oil as the fuel and the prices estimated as accurately as possible in the limited amount of time available for this investigation. In order to obtain approximate prices without too much work, the following assumptions were made, which, to a certain extent, were due to the fact that the investigation uses data of for a project ready for execution.

1. For all four systems the same total steam-turbine output is assumed, including the auxiliaries and generator. This yields constant costs for the steam turbine and boiler, and thus for the entire steam plant.

2. Consequent upon the choice of fuel, the mixing temperature before the gas turbine for systems C to E was fixed at 600 °C. The pressure ratio was made optimum for each cycle.
3. Atmospheric temperature assumed to be 15 °C.
4. Stipulated cooling-water temperature 10 °C.
5. Temperature of the exhaust gases 150 °C.
6. For A, C and D the efficiency allowing for boiler radiation and unburnt fuel was assumed to be 97 %, but in E was made 98 %, because in that case the boiler is much smaller.
7. Electrical efficiency of the generator driven by the gas turbine 98 %.
8. In accordance with the theory developed, combustion is as complete as possible in all cases, assuming an air surplus of 20 %.
9. The installations were all based on the following steam-turbine data:

Live-steam pressure	130 kg/cm² abs
Live-steam temperature	530 °C
Reheating temperature	525 °C
Pressure in condenser	0·0265 kg/cm²
7-stage bleeding for feedwater heating	
Thermal efficiency of the steam turbine	42·2 %

TABLE III

Scheme			A	C	D	E without air heater
Heat input per s from fuel	H	kW	179 000	189 000	186 000	188 000
Efficiency after radiation, including incomplete combustion	η_H		0·97	0·97	0·97	0·98
Heat transferred per s to steam	$\eta_H H$	kW	173 000	183 000	181 000	184 000
Absorbed by the steam circuit	$V' + V''$	kW	162 000	153 000	156 000	155 000
Absorbed by recuperation	R	kW	—	11 600	8 000	8 800
Output of steam turbine with V''	$\eta_{th}(V' + V'')$	kW	68 300	64 700	65 800	65 600
Power gained by recuperation	$\eta_R R$	kW	—	3 630	2 470	2 720
Total steam turbine output	P_{ST}	kW	68 300	68 300	68 300	68 300
Gas turbine output	$\eta_{el}(E - C)$	kW	—	6 800	6 100	8 400
Loss due to boiler fans, less gain in steam cycle	ΔP_{fan}	kW	380	—	—	—
Reduction in gas turbine output due to expansion to boiler or recuperator inlet pressure, less gain in steam cycle	ΔP_{GT}	kW	—	450	960	340
Gas turbine auxiliaries	P_{aux}	kW	—	200	200	200
Net output of the whole plant	P	kW	67 900	74 500	73 200	76 200
Quantity of live steam		kg/s	54·6	51·9	52·4	52·2
Feedwater temperature before boiler		°C	212	212	238	246
Optimum compression ratio		π_{opt}	—	~5·2	5·5	6·0
Efficiencies and improvements in %						
Efficiency of the plain steam plant		η_0	38·1	38·1	38·1	38·5
Improvement in efficiency		$\Delta\eta$	—	1·14	0·87	1·92
Percentage improvement on η_0		$\Delta\eta/\eta_0$	—	3·0	2·3	5·0
Overall efficiency of the combined installation		η	38·1	39·2	39·0	40·4

TABLE IV

Scheme		A	C	D		E without air heater
Air temperature before heater	°C	17	214	211		—
Air temperature after heater	°C	248	300	600		
Gas temperature before air heater	°C	350	350	650		—
Gas temperature after air heater	°C	150	275	315		—
Air mass flow in air heater	kg/s	76·2	80·6	79·4		—
Gas mass flow in air heater	kg/s	80·5	85·2	84·0		—
Specific heat of air in air heater	kJ/kg °C	1·014	1·036	1·071		—
Specific heat of gas in air heater	kJ/kg °C	1·106	1·125	1·176		—
Heat transferred per unit time P_{AH}	kW	17 800	7 220	33 100		—
				Ferritic	Austenitic	
Mean temperature difference gas-air Δt_m	°C	119	55	83	56	—
$k F = P_{AH}/\Delta t_m$	kW/°C	150	130	305	145	—
Total pressure drop in air heater	%	3·6	3·6	3·6	11·9	—
Price ratio air heater/steam plant	%	1·5	1·3	3·0	10·8	—
Overall price ratio air heater/steam plant	%	1·5	1·3	13·8		

TABLE V

Scheme		A	C	D		E Without air heater	
				R	*V″*	*R*	*V″*
Water temperature before recuperator	°C	—	123	123	212	123	212
Water temperature after recuperator	°C	—	212	212	238	212	246
Gas temperature before recuperator	°C	—	275	244	315	244	334
Gas temperature after recuperator	°C	—	150	150	244	150	244
Water mass flow in recuperator	kg/s	—	29·6	20·5	52·4	22·2	52·2
Gas mass flow in recuperator	kg/s	—	85·2	84·0	84·0	84·7	84·7
Water mass flow heated by bled steam	kg/s	54·6	22·3	31·9	—	30·0	—
Total water mass flow	kg/s	54·6	51·9	52·4	52·4	52·2	52·2
Heat transferred per unit time P_{rec}	kW	—	11 600	8 010	6 300	8 800	8 400
Mean temperature difference Δt_m	°C	—	41·7	29·4	51·2	29·4	55·4
$k F = P_{rec}/\Delta t_m$	kW/°C	—	278	272	123	300	152
Pressure drop on air side of recuperator	%	—	3·9	2·2	1·7	2·0	1·9
Price ratio recuperator/steam plant	%	—	3·2	3·1	1·4	3·5	1·7
Overall price ratio recuperator/steam plant	%	—	3·2	4·5		5·2	

The price differences C–A, D–A and E–A were worked out. They are due to the gas-turbine set, the changed air heaters and feedwater heaters, the extra recuperators and, particularly in E, to the pressure-charged boiler. From the constant price of the steam plant, as per assumption 1, and the price differences, we can obtain the total price for the installation by summation. At the same time the net output of the complete installation was worked out for the various alternatives, and of course is not the same for all systems. But this fact is reflected in the cost of the installation per kW output. For the individual systems the following flows of energy per s are obtained in kW (Table III, page 796).

Table IV (page 797) shows the data of the air heater with approximate prices referred to the price of the entire steam plant (less building and erection), which was made 100%.

In the above it is striking that in system D, the air heater has to have a ferritic and an austenitic section, owing to the high temperature, and this naturally increases its price.

Table V (page 797) shows the data of the recuperators with price estimates, again referred to the price of the entire steam plant, less building and erection.

Thus all the information has been tabulated, from which the total prices of the installations and the cost of the installation per kW net output can be calculated.

Discussion of the results can be kept quite brief. *From the Tables it follows that system E without air heater is by far the most favourable variant.* Not only is the improvement in efficiency of this installation highest (Table III), but the specific price per kW is also most favourable. The latter is mainly due to the

TABLE VI

Scheme		A	C	D	E without air heater
Complete steam turboset	%	38·5			
Boiler	%	30·8			
Piping, feedwater pumps, water treatment plant, cooling plant	%	9·6	as A	as A	as A
Electrical auxiliaries, switchgear	%	17·3			
Miscellaneous	%	3·8			
Complete steam plant, excluding building and erection work	%	100·0	100·0	100·0	100·0
Price differences compared with A					
Gas turboset	%	—	+ 11·3	+ 11·3	+ 11·4
Air heater	%	—	— 0·2	+ 12·3	— 1·5
Recuperator	%	—	+ 3·2	+ 4·6	+ 5·2
Bled-steam feed-heating	%	—	— 0·6	— 0·4	— 0·4
Boiler	%	—	—	—	— 11·9
Electrical equipment and piping	%	—	+ 3·7	+ 3·5	+ 3·8
Total price difference	%	—	+ 17·4	+ 31·3	+ 6·5
Total price of whole installation excluding building and erection work	%	100·0	117·4	131·3	106·5
Installation price per kW net output	%	100·0	107·0	122·0	95·0

boiler being pressure-charged which, according to latest investigations, implies that appreciable savings in weight and price may be anticipated.

Without mentioning particularly any of the data in this article, the following results may be gained from the investigations. Comparison of the four systems also works out in favour of E for other fuels, such as natural gas or blast-furnace gas. This conclusion ought also to apply for coke-oven gas, although this has not been investigated in detail. For systems burning only coal it is only feasible to employ system A or D, the former being obviously preferable from the price aspect.

If several fuels have to be used, the installations naturally become more complicated, although liquid and gaseous fuels can both be burned in plants of system E. If coal is added to these, it will be better to adopt system A and connect it in parallel with E on the steam side.

The article which follows describes four installations which are in service or under construction, all of which employ heat recovery with combined systems, illustrated by photographs and diagrams.

In conclusion, the Company would like to express their conviction in the promising future which lies ahead of combined installations with pressure-charged boilers followed by gas turbines. It is firmly believed that, in the long run, these installations will conquer the field in which liquid and gaseous fuels are employed.

C. SEIPPEL
R. BEREUTER

(KME)

Bibliography

[1] A. STODOLA: Dampf- und Gasturbinen. 5th edition 1922, pp. 984 and 995. Springer-Verlag, Berlin.

[2] K. SCHRÖDER: Der innere Ausbau von Kraftwerken. Die Wärme. 1936, Vol. 59, No. 9, p. 158-61.

[3] C. E. LUNDGREN, C. SEIPPEL: Thermal Problems of Atomic Power Stations (II). Brown Boveri Rev. 1956, Vol. 43, No. 12, p. 515–24.

[4] K. SCHRÖDER: Grosse Dampfkraftwerke. Vol. 1: Kraftwerksatlas (1959), Springer-Verlag, Berlin.

Bibliography relevant to the subject but not cited in the article:

[5] H. MELAN: Zukünftige Entwicklung der thermischen Energieerzeugung. Öst. Z. Elektrizitätswirtsch. 1954, Vol. 7, No. 4, p. 106–13.

[6] H. MELAN: Series of articles on Korneuburg power station in Energiewirtschaft, Vienna, 1960, Vol. 1, No. 4, p. 9–33.

[7] K. H. SCHÜLLER: Kombinierte Dampf-Gas-Prozesse. BBC Nachr. 1959, Vol. 41, No. 10/11, p. 404–37.

[8] MONTPROFIT: L'installation combinée gaz/vapeur en service à l'Usine Génératrice de Bône II d'Electricité et Gaz d'Algérie. Report 164 G1/22, World Power Conference, Vienna 1956.

[9] P. F. MARTINUZZI: Gas-Steam Power Generation. ASME Paper No. 60—GTP-6 (1960).

[10] W. KARRER: Die seriegeschaltete Gasturbine im Heizkraftwerk. Diss. ETH, Zurich 1950.

[11] W. KARRER: Dampf-Luftanlagen für gleichzeitige Erzeugung von mechanischer Energie und Wärme. Schweiz. Bauztg. Vol. 126 (1945), No. 12, p. 133–136.

[12] W. KARRER: Die Ausnützung der Abwärme von Gasturbinen in Dampfanlagen. Motortech Z. Vol. 18 (1957), No. 6, p. 187–189.

Relevant Patents

[13] Swiss patents 246084 and 287354 (Brown Boveri).

[14] Maschinenfabrik Oerlikon: Swiss patents 245488, 275575 and 336648.
Brown Boveri has acquired these patents.

[15] US Patent 1978837, General Electric Co.

PRACTICAL EXAMPLES OF UTILIZING THE WASTE HEAT OF GAS TURBINES IN COMBINED INSTALLATIONS

621.438:662.99

To supplement the theoretical considerations in the foregoing article, the present contribution deals with four installations, partly in service and partly being erected, in which interesting improvements in the thermal efficiency have been effected by combining gas turbines with various steam and industrial heat cycles. The layouts selected are explained and the attained results listed. Special attention is paid to Korneuburg thermal power station in Austria, the first plant to be completed with a typical combined cycle.

OWING to its simple design, the low initial and running costs, the easy supervision and maintenance, the small amount of water required, and other favourable properties, the open-cycle gas turbine has already won a prominent position in the sphere of power generation. As the preceding article proves, the combination of a gas turbine with a steam turbine allows an overall thermal efficiency to be attained which is considerably higher than the individual efficiencies of the component parts.

Due to the better economic performance which is attainable the combination of a gas turbine with a steam turbine continues to gain in importance. Admittedly most of the installations employing this combination were not originally planned as such. Either an existing gas turbine was augmented by a waste-heat boiler and steam turbine, or a new steam plant combined with an existing gas turbine; alternatively, when a power station was extended to increase its electrical output, existing steam systems were utilized to exploit the waste heat of new gas turbines, in order to improve the thermal efficiency of the latter in an inexpensive way. Since most of them have grown up gradually, many of the well-known combined plants do not fit in with the standard diagrams. This is also true of the subsequently described examples of combined gas and steam turbines. Interesting results have nevertheless been obtained, which justify mentioning these installations and describing some of their features.

The economic performance of a gas turbine can, however, be improved by utilizing the waste heat for heating purposes. Many cases of this application are known. But now, as the first known example of its kind, there is a station in which the heat is not merely a by-product, but where the gas turbine with a waste-heat boiler proves to be the most favourable method of simultaneously generating electricity and heat. This installation is described as the fourth example dealt with below.

Korneuburg Power Station near Vienna, Austria (Fig. 1)

The Austrian capital is a typical load centre with a very heavy demand. It is normally supplied with electricity from the Austrian grid system, the power for which is generated in the hydro-electric plants in the west of the country. Owing to this dependence upon distant supply stations, there has long been a desire for the energy to be generated nearer home, firstly to achieve greater reliability and secondly to avoid costly transmission lines used only during the periods of peak demand, and their associated losses. With the increasing consumption and growth of the peaks, the existing 160-MW station in Simmering was no longer able to cope with the demand and the need for an additional thermal station became obvious. This scheme was also favoured by the supplies of natural gas just north of Vienna.

The new generating station had to satisfy widely differing requirements, which it is almost impossible to bring over a common denominator. These are:

Fig. 1. – Korneuburg thermal power station near Vienna, Austria, seen from the south

Behind the building, from left to right: Waste-heat boiler and chimney of the first gas turbine, chimney of the second gas turbine, boiler of the 70/77-MW steam turboset being erected; in front of the building are the transformers and outdoor substation.

The supply of electricity in the peak periods

Emergency operation in the event of a breakdown on the lines from the west

Base-load operation over long periods, e.g. when there is a shortage of power from hydro-electric sources.

For base-load operation a 70/77-MW steam turboset will be provided, for live steam conditions of 126 kg/cm² and 525 °C, with reheat to 520 °C. The three-cylinder turbine and generator are at present under construction by Brown Boveri. Since this part of the station is not very interesting for the particular considerations of this article, it is mentioned in passing (Fig. 2), merely for the sake of completeness.

The other stipulations, including rapid availability, low capital outlay, personnel costs and maintenance charges for peak-load generation, were best fulfilled by the gas turbine. Hence two of the well-known twin-shaft turbines (Fig. 3) were ordered with a maximum output of 30 MW each at the terminals. With two-stage compression and intercoolers and, likewise, two-stage expansion with reheat, these turbines already exhibit quite a creditable efficiency. During the planning stage it proved advisable to combine with a steam cycle in order to improve the economic performance of the installation still further. The gas turbines are followed by waste-heat boilers and a 25-MW steam turbine.

The choice of location for the new station fell on Korneuburg, just above Vienna, on the left bank of the Danube, where ample water is available for cooling all through the year (Fig. 4). Thus the station is close to the Bisamberg transformer substation, and therefore to the 110-kV ring round Vienna. It is

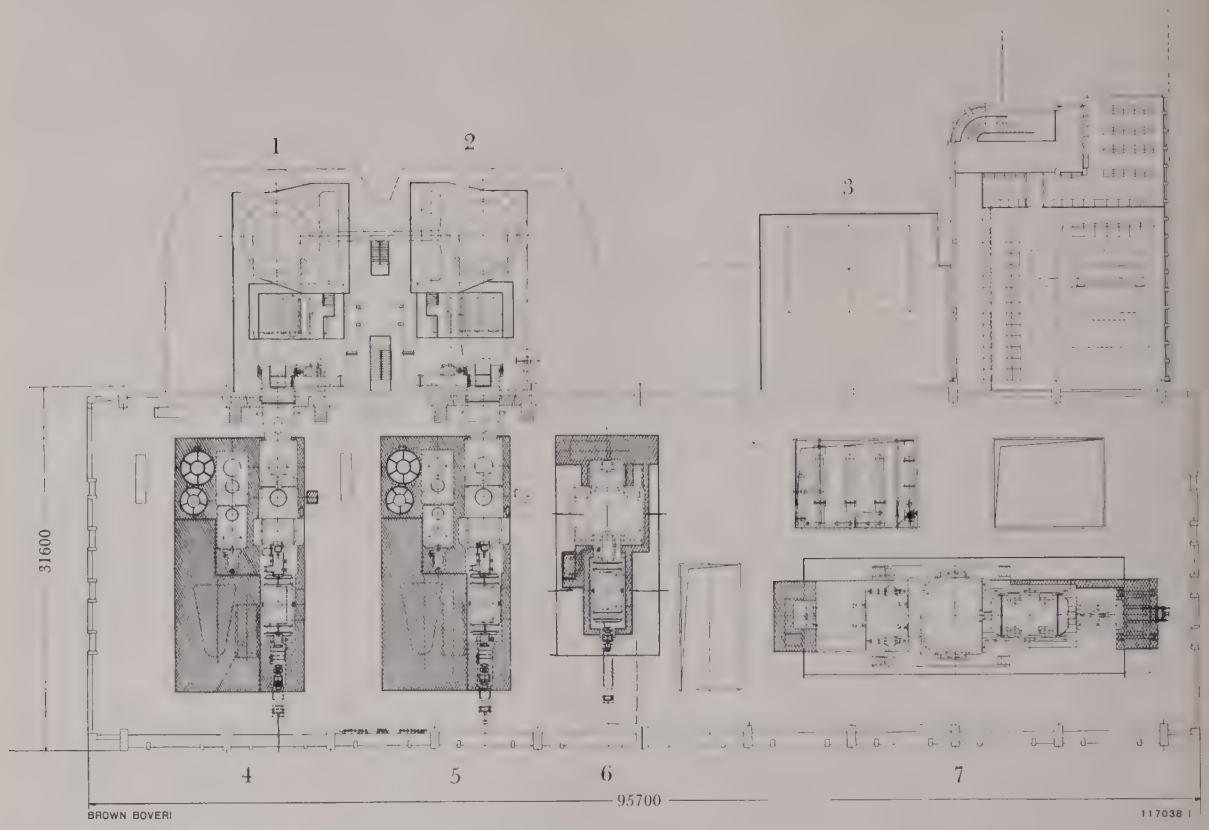

Fig. 2. – Plan of the machine house at Korneuburg

1 = Boiler 1 (waste-heat) for 50 t/h
2 = Boiler 2 (waste-heat) for 50 t/h
3 = Boiler 3 (Benson) for 240 t/h
4 = Machine 1, gas-turbine set 25 MW
5 = Machine 2, gas-turbine set 25 MW
6 = Machine 3, heat-recovery turbine 25 MW
7 = Machine 4, steam turboset 77 MW

also near the western leg of the Niogas natural-gas pipeline, while the fuel oil used to augment the supply of gas can be delivered cheaply by waterway.

The thermal power station at Korneuburg is operated jointly by the Niederösterreichische Elektrizitätswerke AG., and the Österreichische Elektrizitätswirtschaft AG. (Verbundgesellschaft) who founded the company known as Dampfkraftwerk Korneuburg GmbH. specially for the purpose.

The Combined Gas and Steam Cycles of Korneuburg Station

Each of the 25/30-MW gas-turbine sets is connected on the unit principle with a waste-heat boiler. The steam raised in these boilers drives a 25-MW condensing turboset (Fig. 5). Each boiler is connected to the steam turbine by a separate pipe, the steam impinging on a separate set of live-steam nozzles, so that the heat-recovery turbine (as the steam turbine is subsequently named) can be run with only one gas turbine and waste-heat boiler. This arrangement of the combined installation at Korneuburg resulted as the solution to the problem of improving the efficiency of the gas turbine, chosen for its special properties as a peak-load machine, by utilizing the heat contained in the exhaust gases. The most suitable scheme proved to be the conversion of this heat into electricity by means of a subsequent steam cycle. Since the main stress was on the recovery of the heat, rather than the generation of supplementary electricity, this steam cycle was, in principle, merely intended to generate electricity corresponding to the amount of heat received. This arrangement conforms to diagram G in the preceding article.

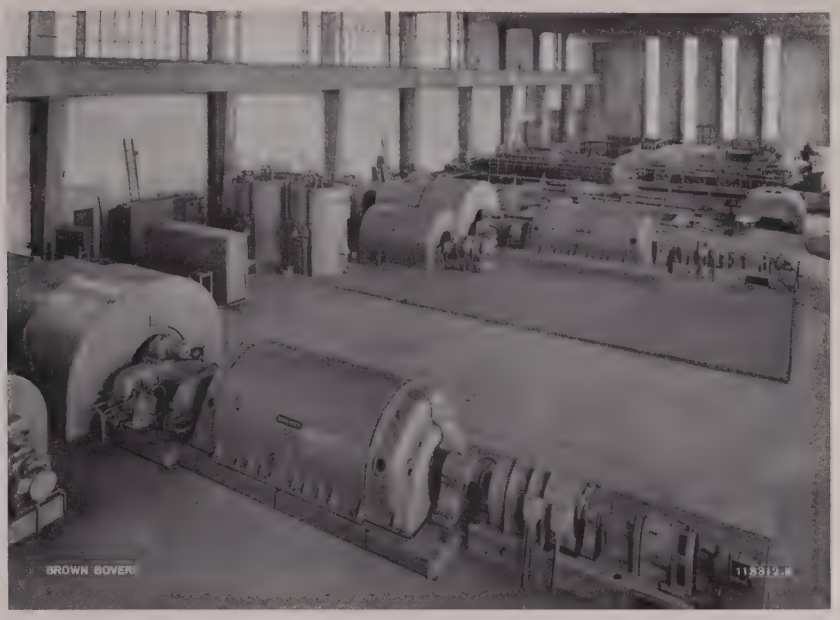

Fig. 3. – View inside Korneuburg power station

In the foreground are the two twin-shaft gas turbines, behind them the prepared foundations for the 25-MW heat-recovery steam turbine, and in the background the foundations for the 70/77-MW steam turboset.

As detailed investigations proved, the steam cycle would have been unsatisfactory if the heat recovery had not been supplemented by an additional heat input. Otherwise the low live-steam conditions, with a relatively low heat drop, and the resultant low efficiency of the steam cycle, would have necessitated a large and proportionately expensive turbine, for which, moreover, no suitable designs would have been available. Unfavourable conditions would also have arisen from the fact that the majority of the expansion would have taken place in the wet-steam region. It was therefore decided that the live-steam data would be raised by supplementary firing, thereby permitting the use of a standard type of turbine with the highest possible heat drop in the thermal cycle.

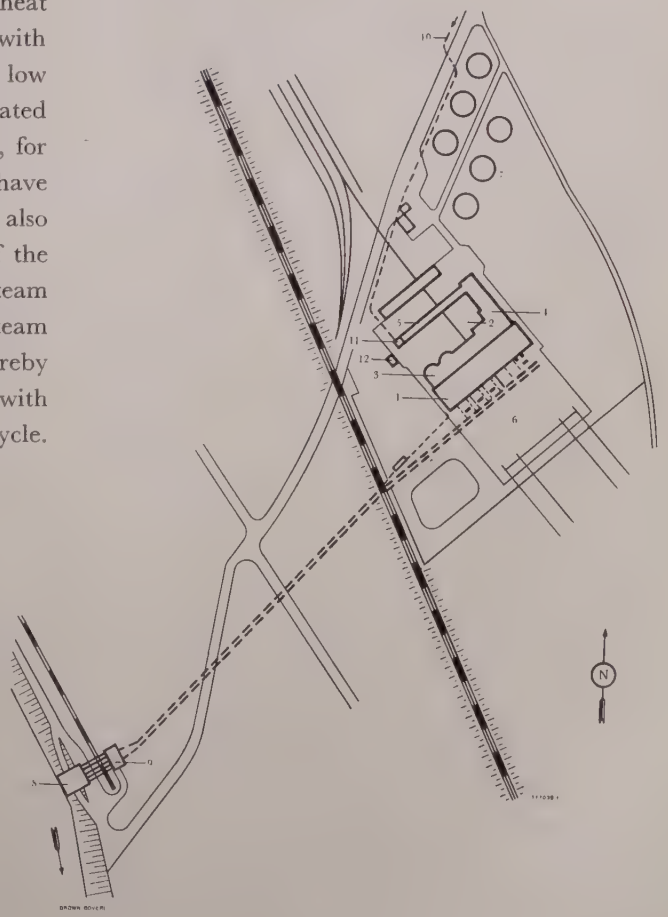

Fig. 4. – Layout of Korneuburg power station

1 = Turbine house
2 = Boiler of 70/77-MW unit
3 = Air intake with waste-heat boiler above
4 = Control room and offices
5 = Store
6 = Outdoor switchgear
7 = Fuel tanks
8 = Cooling-water intake and pump house
9 = Filter-house for cooling water
10 = Fuel-gas inlet pipe
11 = Measurement and control of fuel gas
12 = Fuel-gas compressor house

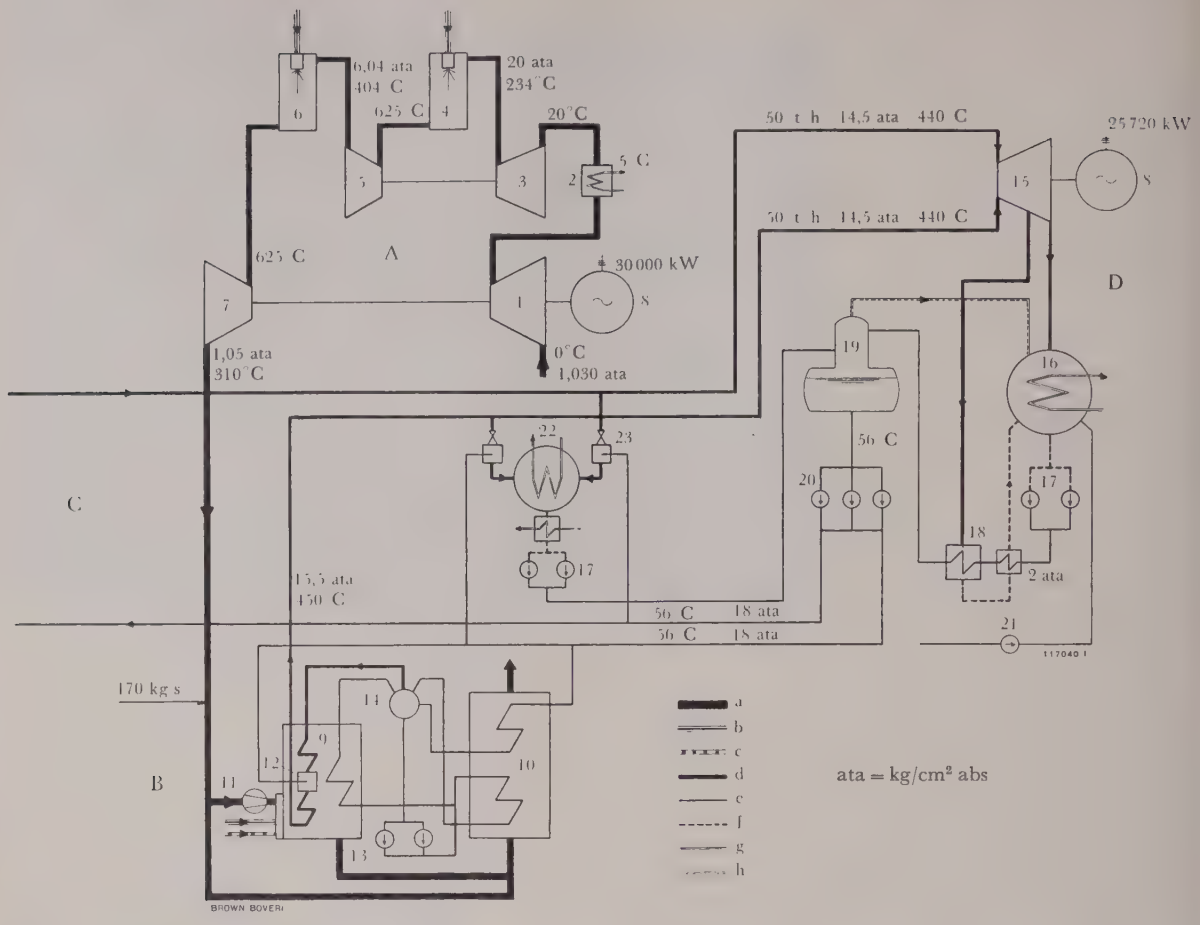

Fig. 5. – Thermal diagram of the combined gas and steam-turbine installation at Korneuburg. (Values shown are approximate and correspond to the machines as built)

A = Gas-turbine set II
B = Waste-heat boiler belonging to *A*
C = From and to waste-heat boiler of set I
D = Heat-recovery steam turbine

a = Working cycle of the gas turbine (air/exhaust gas)
b = Fuel gas (natural gas)
c = Fuel oil
d = Steam
e = Feedwater
f = Condensate
g = Cooling water
h = Air

1 = Low-pressure compressor
2 = Intercooler
3 = High-pressure compressor
4 = High-pressure combustion chamber
5 = High-pressure turbine
6 = Low-pressure combustion chamber
7 = Low-pressure turbine
8 = Generator 35 MVA, 6300 V, 50 c/s
9 = Waste-heat boiler with economizer and evaporator sections
10 = Superheater boiler with supplementary firing

11 = Gas blower for superheater
12 = Injection cooler for controlling temperature
13 = Boiler recirculation pump
14 = Steam separator drum
15 = Heat-recovery steam turbine
16 = Condenser
17 = Condensate pump
18 = Bled-steam feed-heater with condensate cooler
19 = De-aerator and feedwater tank
20 = Feedwater pumps
21 = Make-up water pump
22 = Starting condenser
23 = Steam pressure reducing and cooling station

Since heating the whole of the exhaust gas up to the necessary temperature would have been thermodynamically unfavourable, a separately heated superheater was provided, into which only part of the exhaust gas enters.

In order to achieve an optimum overall efficiency, the gases in the waste-heat boiler must be cooled as far as possible, without running the risk of condensation of moisture and the accompanying corrosion. This is most conveniently achieved in a com-

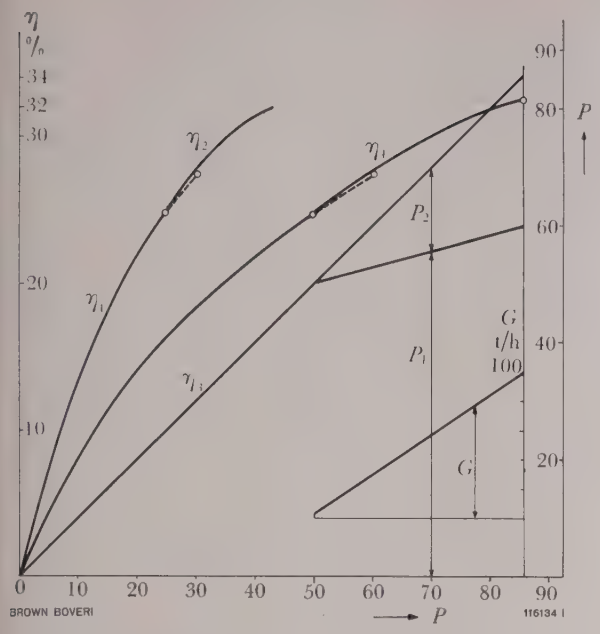

Fig. 6. – Efficiency diagram of the combined gas turbine and steam plant at Korneuburg power station

The diagram is plotted for the most economical operation of the waste-heat boiler. It contains approximate values and is based on an atmospheric temperature of 0 °C and on the effective operating conditions of the combined cycle, to be expected from measurements taken on gas-turbine set II.

P = Output at generator terminals
P_1 = Output of gas turbine
P_2 = Output of heat-recovery steam turbine
η_1 = Efficiency of a single gas turbine
η_2 = Efficiency of one gas turbine and heat-recovery steam turbine
η_3 = Efficiency of two gas turbines equally loaded
η_4 = Efficiency of two gas turbines with heat-recovery steam turbine
G = Quantity of live steam generated in the waste-heat boilers, with both gas turbines in operation

bination of a gas turbine with a steam cycle by partly or completely heating the feedwater in the waste-heat boiler instead of with bled steam. At Korneuburg the available heat is adequate for heating all the feedwater, thus rendering unnecessary the divided-flow arrangement (C in the preceding article) described as the most advantageous method.

By combining the gas turbine with a steam cycle, the thermal efficiency of the installation can be improved from 27·5 % (the effective efficiency of the gas turbine alone at an outdoor air temperature of 0 °C and at full load) to 32·6 % (Fig. 6). This improvement is particularly remarkable when compared with the values attained with standard machines of the same size; the overall efficiency of the previously mentioned 70/77-MW unit (boiler and turboset), also supplied for Korneuburg, is about 36 % at its optimum point, by way of comparison. To achieve this, none of the special properties of the gas turbine had to be sacrificed. The machines can be started at any time and be fully loaded in 15–20 minutes. The steam cycle operates with low live-steam data, thereby not imposing unduly severe conditions regarding treatment of the water or upkeep. Furthermore, since the waste-heat boiler and steam turbine are almost self-regulating in normal operation, the addition of the steam cycle does not complicate supervision of the gas turbine, or involve any extra personnel.

Components of the Combined Installation at Korneuburg

Gas turbines

The gas turbines are of the established Brown Boveri twin-shaft design (Fig. 7); they are designed to employ natural gas as fuel. A detailed description can be dispensed with here, as this type of unit has been the subject of numerous articles in the past [1, 2].[1]

Waste-heat boiler

As part of the "unit" to which each gas turbine belongs, there is a waste-heat boiler (this term, though accepted nowadays in engineering practice, is strictly a misnomer, and ought to be replaced by heat-recovery boiler), designed as a forced-circulation boiler, operating on the La Mont process.[2] Each boiler consists of two parts, the true waste-heat boiler in the form of a chimney, which, besides containing all the feedheating surface, contains about 82 % of the evaporator surface (Fig. 5, 8 and 9), and the separate superheater, which also contains the remaining 18 % of the evaporator surface. Some of the exhaust gases from the gas turbine, tapped off the gas outlet pipe, are forced into the superheater by a blower. The gas input to the superheater can be controlled in terms of the quantity of

[1] The figures in square brackets refer to the bibliography at the end of the article.

[2] Supplied by Wagner-Biró AG., Graz.

TABLE I

Main data of the gas-turbine sets

		Guaranteed values
Operating conditions:		
Barometric pressure	kg/cm²abs	1·033
Air inlet temperature	°C	0
Temperature of cooling water	°C	5
Pressure drop at inlet and exhaust	mm w.g.	max. 50
Terminal output under the above conditions and at a power factor of 0·8	kW	25 000
Thermal efficiency under the above conditions and at the effective maximum output measured under the same conditions	%	26
Quantity of combustion air under the above conditions	kg/s	appr. 165
Temperature of exhaust gases	°C	appr. 310

additional fuel, in such a manner that there is an air excess of 5 to 10 % in the superheater.

The waste-heat boilers were equipped with a system of temperature control for the live steam emerging from the superheater, employing injection coolers between the superheater elements. The pressure is controlled by the control elements of the subsequent heat-recovery turbine.

TABLE II

Technical data of the boilers

Quantity of exhaust gas	Nm³/h	475 000
Temperature of turbine exhaust	°C	max. 325
Steam generation	t/h	50
Steam pressure after superheater	kg/cm² abs	15·5
Steam temperature after superheater	°C	450
Feedwater temperature	°C	56
Supplementary fuel		natural gas (normal) and fuel oil

Heat-recovery steam turbine

This is a normal Brown Boveri reaction turbine built for the following data:

The turbine is of single-cylinder design with double-flow l.p. section (Fig. 10). It possesses two separate steam inlet pipes, each with a main stop valve and a pair of regulating valves (Fig. 11). These two independent sets of controls maintain the live-steam pressure of the two waste-heat boilers.

TABLE III

		Half load	Full load
Live-steam pressure	kg/cm² abs	14·5	14·5
Live-steam temperature	°C	440	440
Temperature of cooling water	°C	5·5	5·5
Live-steam quantity	t/h	50	100
Output at generator terminals	kW	12 510	25 720
Back pressure	kg/cm² abs		0·021
Final feedwater temperature	°C	45	max. 56
Heat rate	kcal/kWh	3009	2883
Speed	rev/min	3000	

The feedwater is heated to 56 °C by single-stage bleeding. The rest of the heat is supplied by the exhaust gases in the waste-heat boiler.

The steam turbine and the two gas turbines are all equipped with identical generators, rated 35 MVA, 6·3 kV, 50 c/s at a power factor of 0·8.

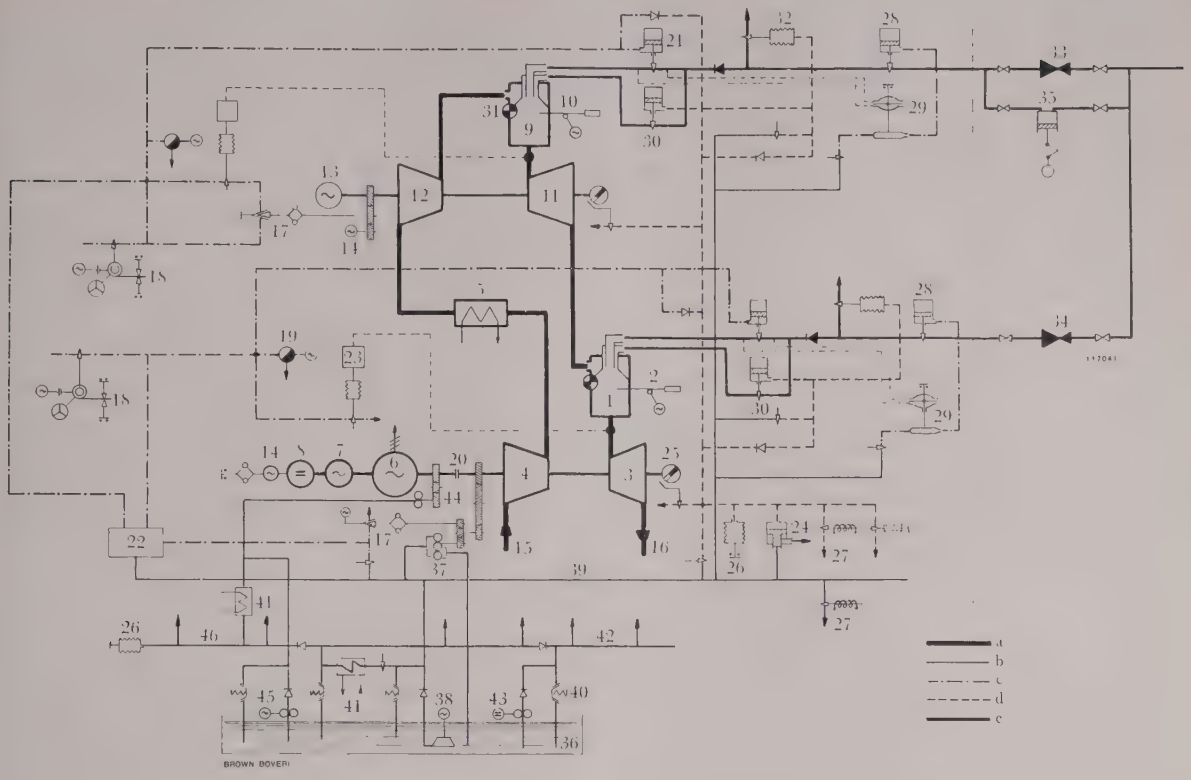

Fig. 7. – Schematic diagram of the two-stage gas-turbine sets at Korneuburg

a = Working cycle of the gas turbine
b = Hydraulic and lubricating oil system
c = Control oil system
d = Emergency stop and safety oil system
e = Fuel gas

1 = Low-pressure combustion chamber
2 = Low-pressure ignition rod
3 = Low-pressure turbine
4 = Low-pressure axial compressor
5 = Intercooler
6 = Generator
7 = Starting motor of l.p. turbine
8 = Exciter
9 = High-pressure combustion chamber
10 = High-pressure ignition rod
11 = High-pressure turbine
12 = High-pressure axial compressor
13 = Starting motor for h.p. turbine
14 = Rev-counter
15 = Fresh-air intake
16 = Exhaust to chimney

Speed control

17 = Governor
18 = Starting valve
19 = Pulsators
20 = Gear coupling
21 = Gas regulating valve
22 = Control relays

Safety devices

23 = Temperature regulator with compressed-air control
24 = Safety relay
25 = Overspeed governor
26 = Pressure switch
27 = Solenoid valve

Fuel supply system

28 = Reducing valve
29 = Pressure-difference regulator
30 = Gas valve for ignition
31 = Flame monitor
32 = Gas vent valve
33 = Gas reducing station, h.p. side
34 = Gas reducing station, l.p. side
35 = Gas compressor

Control and lubricating oil system

36 = Oil tank
37 = Main oil pump (gear pump)
38 = Auxiliary oil pump for the complete set
39 = Pressure oil header
40 = Valve maintaining pressure
41 = Oil cooler
42 = Cooling-oil system for turbine bearings
43 = Cooling-oil pump for the turbines 3 and 11
44 = Gear oil pump of generator
45 = Auxiliary oil pump of generator
46 = Generator lubricating system

Operation of the Combined Installation

Operation of one or both gas turbines for any length of time without the steam turbine is not intended, hence it was considered unnecessary for a tank to be provided for storing the large quantity of treated boiler feedwater. The boilers therefore remain full all the time. But in the event of the gas turbine having to be started up alone to cater for

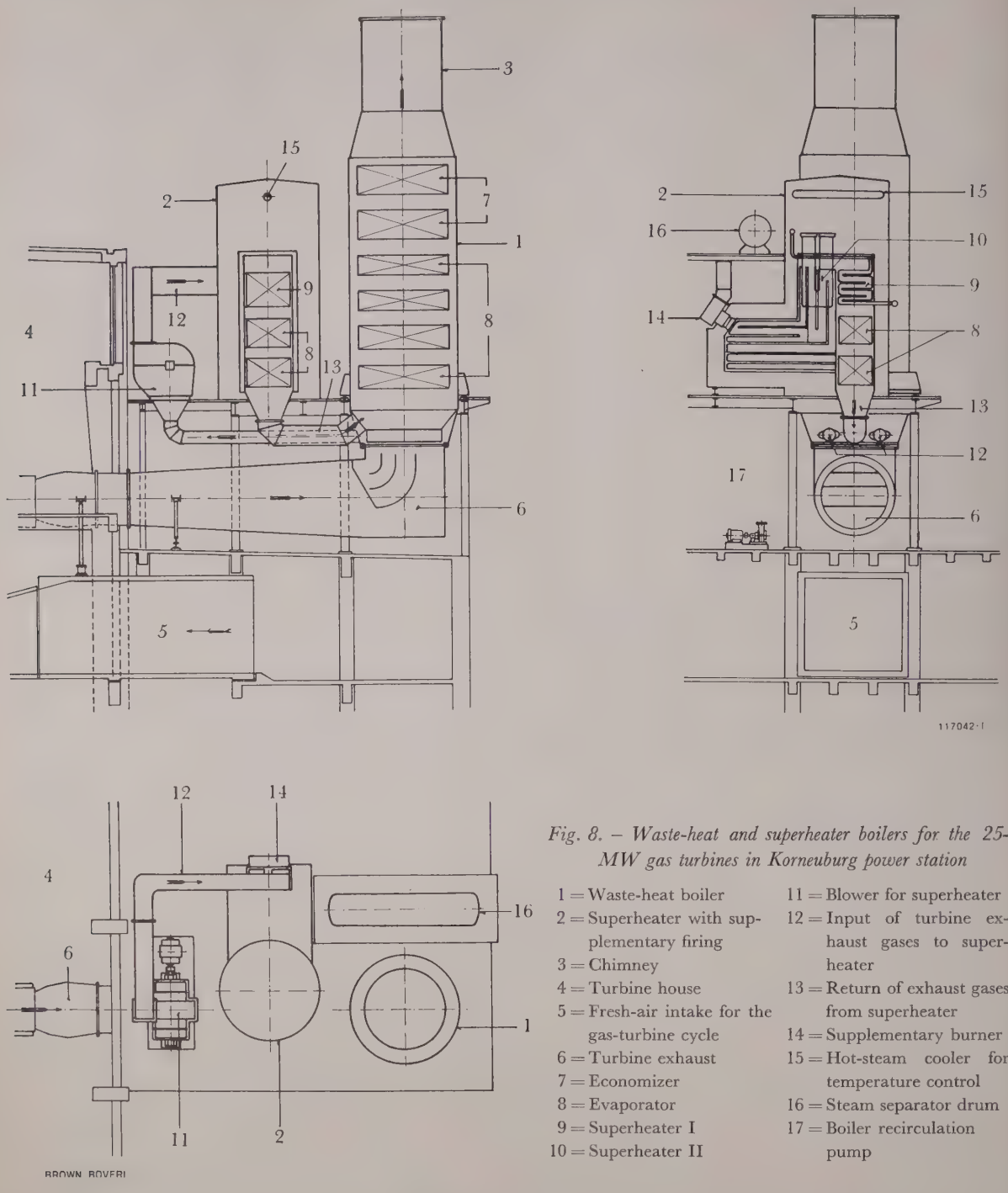

Fig. 8. – Waste-heat and superheater boilers for the 25-MW gas turbines in Korneuburg power station

1 = Waste-heat boiler
2 = Superheater with supplementary firing
3 = Chimney
4 = Turbine house
5 = Fresh-air intake for the gas-turbine cycle
6 = Turbine exhaust
7 = Economizer
8 = Evaporator
9 = Superheater I
10 = Superheater II
11 = Blower for superheater
12 = Input of turbine exhaust gases to superheater
13 = Return of exhaust gases from superheater
14 = Supplementary burner
15 = Hot-steam cooler for temperature control
16 = Steam separator drum
17 = Boiler recirculation pump

peak demand or in an emergency during the summer, there is an auxiliary condenser with reduction and injection (Fig. 5) which dissipates the heat produced in the waste-heat boiler when the steam turbine is idle. This condenser is also used for starting the steam turbine. When the combined plant is started up, the gas turbine is first put on-load and the mixture of steam and water produced in the waste-heat boiler condensed in the auxiliary condenser. As soon as superheated steam is available, this is switched over from the auxiliary condenser to the steam turbine, which is then run up. The turbine control system attends to the control of the pressure from this point onward, as mentioned

Fig. 9. – Korneuburg thermal power station seen from the west, with the waste-heat boilers of the gas-turbine sets (right) and the partly completed boiler of the 70/77-MW steam turboset (left)

In the foreground the economizer and evaporator sections of the waste-heat boilers can be seen, with chimney on top, and at the rear the separate superheater.

before, while the boiler controls keep the steam temperature constant; the two boilers operating quite independently.

Operational Results

The two gas turbines came into regular service in November 1959 and January 1960, respectively. Since the waste-heat boilers were erected in the course of 1960, and the steam turbine during the winter of 1960/61, the gas turbines have so far been running alone. The exhaust gases are already passed through the completed evaporator section of the boilers which are not yet filled with water, and so into the air. Up to October 25th 1960, the following results had been recorded:

TABLE IV

		Set I	Set II
Number of hours run		5 446	3 912
Number of starts		200	321
Electricity produced	MWh	146 908	105 173

In February 1960 acceptance measurements were taken on gas-turbine set II by the Vienna College of Technology. The maximum admissible output of 30 MW was then achieved with an air temperature slightly above 0 °C, without the combustion gas temperature at the inlet to the l.p. turbine even reaching the value permitted for normal con-

tinuous operation. Thus, according to these measurements, the guaranteed output was exceeded by about 20%; in other words the two gas turbines have a large reserve capacity.

The 16-MW Gas-Turbine Set of the Cornigliano Steelworks, Italy

During the last few years Brown Boveri have delivered a number of gas turbines burning blast-furnace gas to steelworks [3]. To improve their efficiency these are all equipped with air heaters (unfortunately these are commonly referred to as recuperators, though this does not agree with the terminology of the preceding, theoretical article).

Encouraged by the good results obtained with these machines in service, particularly in steelworks, for whose special conditions they are ideally suited, Cosider S.p.A., Genoa, entrusted Brown Boveri with the order for a single-shaft unit, burning blast-furnace gas; this order was placed early in 1960, for completion by the end of 1961. The installation is designed for the following performance figures.

TABLE V

Barometric pressure	kg/cm² abs	1·033
Air inlet temperature	°C	15
Normal terminal output under the above conditions	kW	16 000
Thermal efficiency under the above conditions and at max. output	%	18·6
Quantity of combustion air	kg/s	appr. 130
Quantity of exhaust gas	kg/s	appr. 164
Gas temperature at turbine inlet	°C	max. 750
Exhaust-gas temperature	°C	appr. 420
Speed of turbine	rev/min	3000
Speed of blast-furnace gas compressor	rev/min	5939

In the Cornigliano steelworks a large amount of process heat is required. It also has an existing steam system from which turbine-driven compressors, etc., are fed. Therefore, in order to attain as high an overall efficiency as possible, an obvious solution was to utilize the possibilities of combining the new gas turbine with these heat consumers.

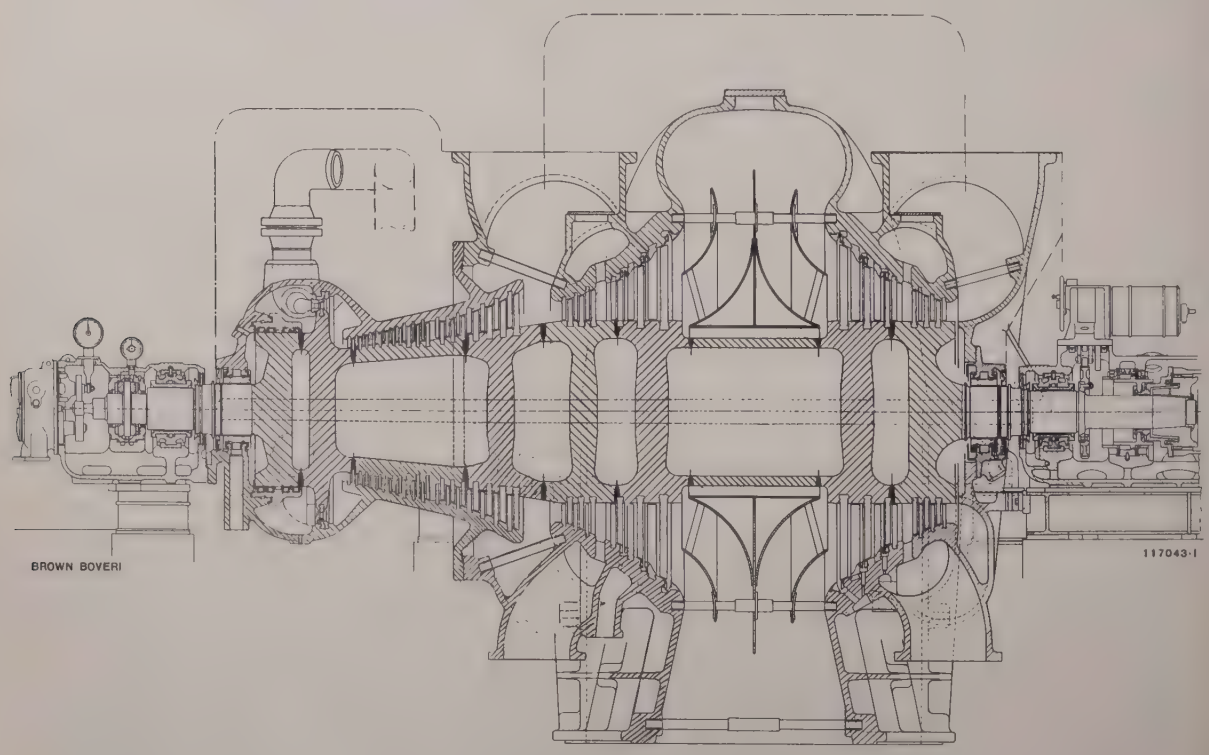

Fig. 10. – Section through the 25-MW heat-recovery steam turbine for Korneuburg

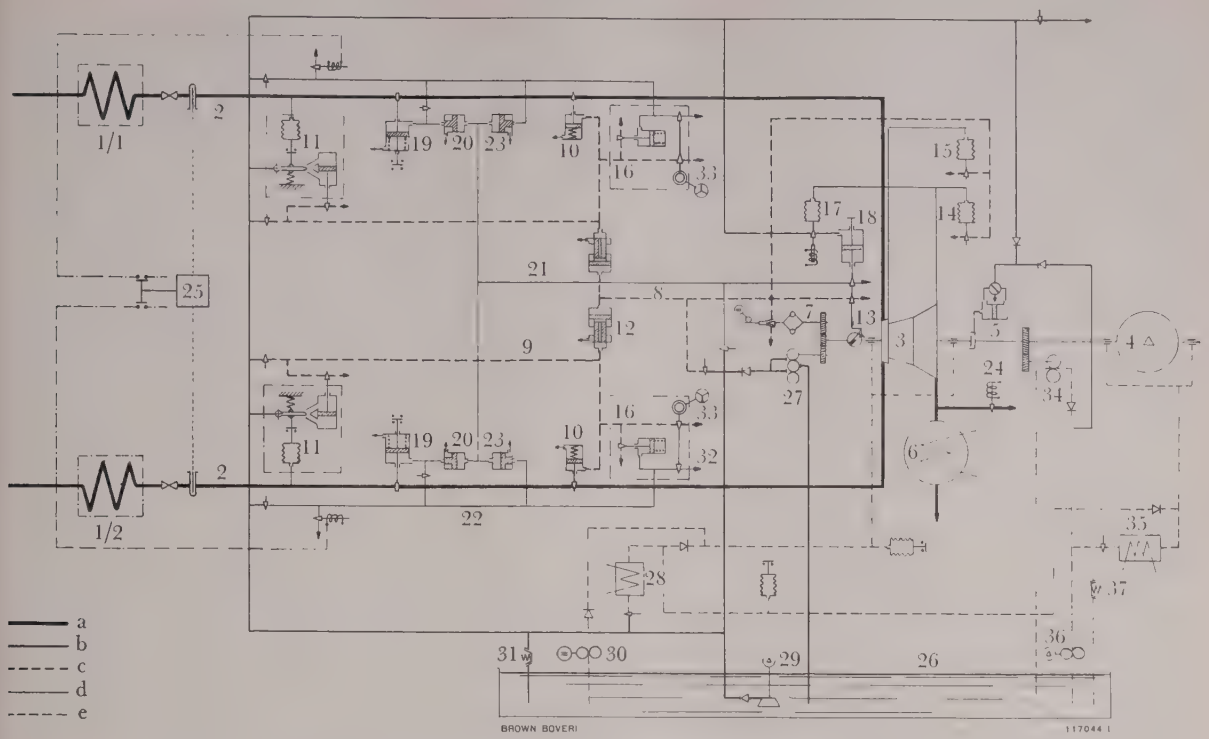

Fig. 11. – Simplified control diagram for the 25-MW heat-recovery steam turbine for Korneuburg

a = Steam
b = Pressure oil system
c = Control-oil system
d = Emergency stop and safety oil system
e = Lubricating system

Parts of the steam turboset
1/1 = Waste-heat boiler of gas-turbine set I
1/2 = Waste-heat boiler of gas-turbine set II
2 = Live-steam pipe
3 = Steam turbine
4 = Generator 35 MVA, 6300 V, 50 c/s
5 = Hydraulically operated clutch
6 = Condenser

Control system
7 = Governor
8 = Governor system
9 = Secondary control system of inlet valves
10 = Regulating inlet valves
11 = Live-steam pressure regulator
12 = Static relay of secondary control system

Safety devices
13 = Overspeed governor
14 = Vacuum limiter
15 = Impulse chamber pressure limiter
16 = Starting gear
17 = Vacuum breaker
18 = Starting and tripping device
19 = Main stop valves
20 = Safety relay of main stop valves 19
21 = Emergency stop oil system
22 = Secondary emergency stop oil system
23 = Safety relay
24 = Vacuum breaking valve
25 = Temperature difference regulator

Oil supply system
26 = Oil tank
27 = Main oil pump of turbine
28 = Oil cooler
29 = Motor-driven auxiliary oil pump
30 = Emergency auxiliary oil pump
31 = Pressure-holding valve
32 = Pressure-holding valve of secondary emergency stop oil system 22
33 = Pressure valve of secondary control system
34 = Main oil pump of generator
35 = Oil cooler
36 = Motor-driven auxiliary oil pump
37 = Pressure-holding valve

The exhaust gases pass into a waste-heat boiler[3] (Fig. 12) the operating conditions of which are dictated by the existing distribution system. At a final feed-heating temperature of 110 °C, live steam is produced at 18 kg/cm² and 350 °C; the boiler also supplies warm water heated from 20 to 80 °C. The feedwater heater, evaporator and superheater are all incorporated in the boiler. Hence, as regards the steam cycle, the chosen arrangement conforms to diagram G in the preceding article. The live-

[3] Supplied by Morteo, Società per Azioni, Genoa.

steam temperature is relatively low; but a thermodynamic improvement of the overall cycle was not feasible, owing to the existence of the steam distribution system mentioned above.

The given temperature conditions would in fact not have made it necessary to provide additional heating. The reason for slightly increasing the temperature by additional firing in the exhaust-gas pipe is that, by so doing, the heating surface in the boiler can thereby be reduced, thus lowering the installation costs.

The temperature of the feedwater returning from the steam system is too high for the exhaust gases to be cooled in an economizer to the lowest temperature possible with respect to corrosion. Hence a hot-water heater connected through a heat exchanger with an existing system is provided in the boiler (Fig. 12).

The generated steam is converted into useful power in the existing steam turbines, with a specific consumption of 4·75 kg/kWh. This gives the following energy balance for the plant as a whole (see Table VI):

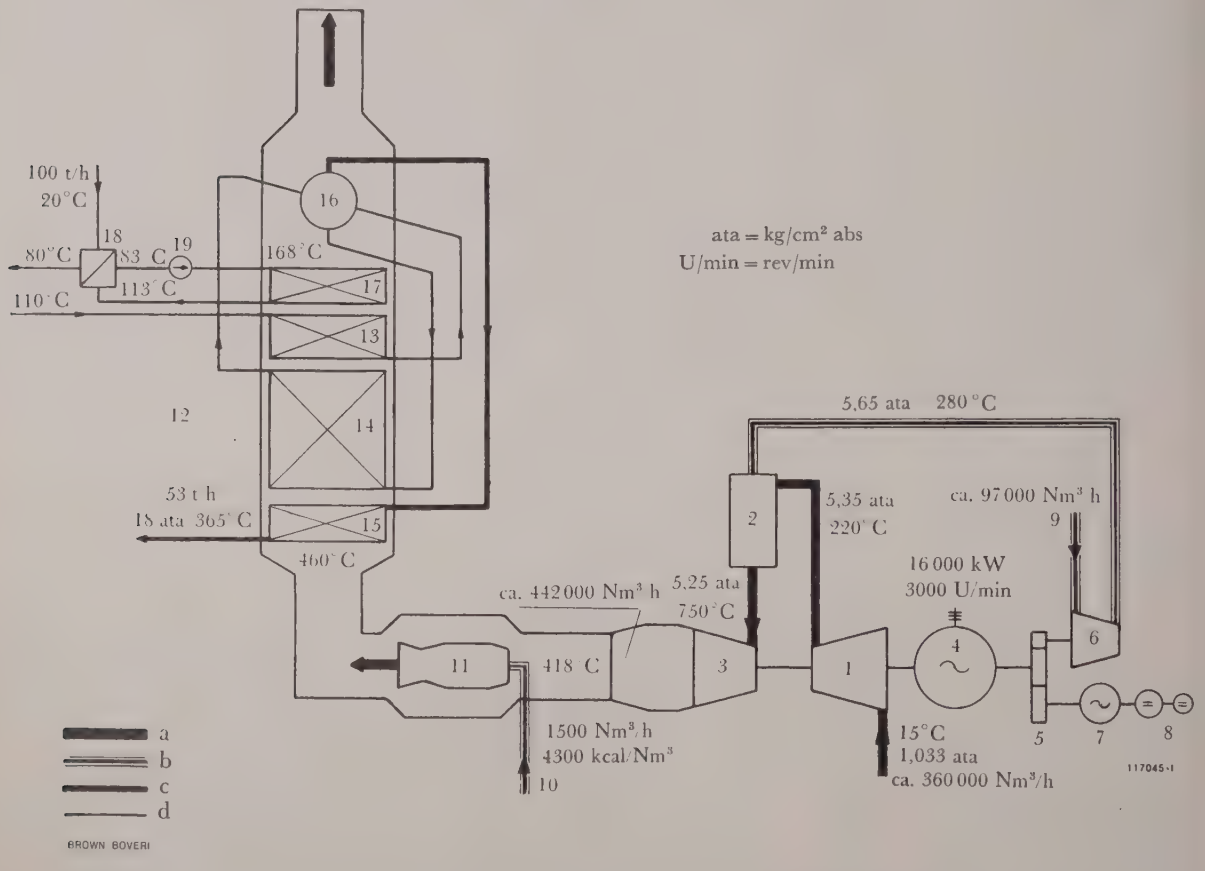

Fig. 12. – Gas-turbine set at Cornigliano, Italy. Thermal cycle diagram of the turbine with heat recovery

a = Working cycle of the gas turbine (air/exhaust gas)
b = Fuel gas
c = Steam
d = Water
1 = Combustion-air compressor
2 = Combustion chamber
3 = Turbine
4 = Generator 22 500 kVA, 12 kV, 50 c/s
5 = Gear driving the blast-furnace gas compressor, starting motor and exciters
6 = Blast-furnace gas compressor
7 = Starting motor
8 = Main and pilot exciters
9 = Blast-furnace gas
10 = Coke gas
11 = Supplementary combustion chamber
12 = Waste-heat boiler, designed on the natural-circulation principle
13 = Feedwater heater
14 = Evaporator
15 = Superheater
16 = Waste-steam drum
17 = Economizer
18 = Heat exchanger
19 = Circulating pump of closed economizer system

TABLE VI

Useful energy		
Electrical output of the gas turbine	16 000 kW	$13{\cdot}73 \times 10^6$ kcal/h
Steam generated in waste-heat boiler	53·0 t/h	
Specific consumption of the steam turbines	4·75 kg/kWh	
Resultant power which can be generated with steam obtained by heat recovery	11 150 kW	$9{\cdot}58 \times 10^6$ kcal/h
Quantity of hot water	100 t/h	
Temperature increase in water	60 °C	
Resultant heat delivery to hot water		6×10^6 kcal/h
Added energy		
Heat added by fuel, at the gas turbine efficiency of 18·6 %		$73{\cdot}9 \times 10^6$ kcal/h
Supplementary firing of waste-heat boiler		
Quantity of gas	1 500 Nm^3/h	
Calorific value	4 300 kcal/Nm^3	
Corresponding amount of heat added to waste-heat boiler		$6{\cdot}45 \times 10^6$ kcal/h

The new gas turbine will be erected in an existing building (Fig. 13), the waste-heat boiler outdoors.

Although this is the first case of a gas turbine of this type being installed without a heat air heater the main parts, such as the turbine, compressor, combustion chamber, blast-furnace gas blower, etc., are exactly the same as have been used for numerous similar installations. A machine of the same kind is the 14-MW gas turbine running at the Österreichische Alpine Montangesellschaft steelworks at Donawitz. A photograph of the latter installation therefore gives a good idea of the ultimate appearance of the Cornigliano machine, at present under construction (Fig. 14). The only difference between the two is that the blast-furnace gas blower for Cornigliano is turned through 180 ° and on the side of the gearing opposite the generator. Adjacent to the gas blower, connected to the turboset through a separate gear train, are the starting motor and the main and pilot exciters (Fig. 13).

Combined Gas-Turbine Installation at Dudelange Steelworks, Luxembourg

Since 1951 there has been a 5400-kW gas-turbine set fired with blast-furnace gas, running in the ARBED steelworks at Dudelange (Fig. 15) [4]. It is performing extremely well and, with a total of 63 000 hours' service, has the longest service record of all Brown Boveri gas turbines.

When the steelworks had to increase their electric generating capacity, they were confronted with the problem of which system—steam or gas—was preferable. Despite the excellent performance of the gas turbine, a steam installation was chosen, for the following main reasons:

A large additional demand had arisen for steam, which could not have been economically handled by a gas turbine and waste-heat boiler alone. This demand was increased by having to shut down some old boilers.

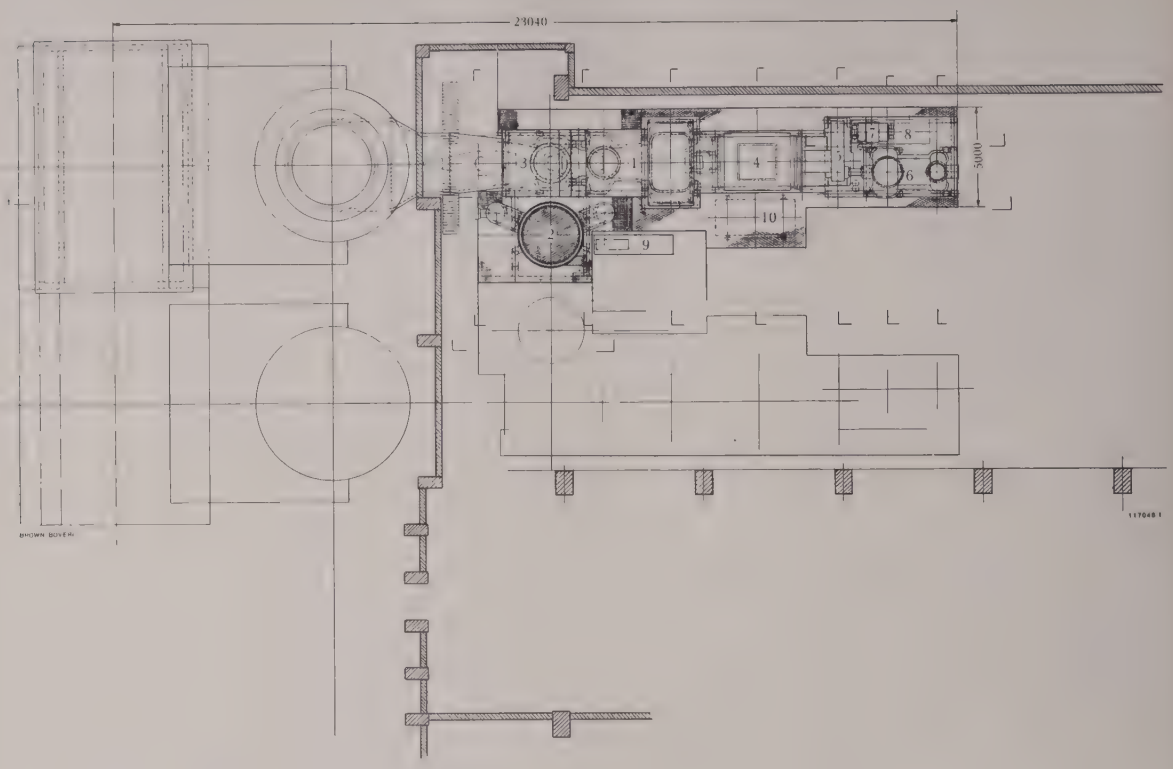

Fig. 13. – Plan view of the gas-turbine set at Cornigliano

1 = Combustion air compressor
2 = Combustion chamber
3 = Turbine
4 = Generator
5 = Gear for driving the gas compressor, starting motor and exciters
6 = Blast-furnace gas compressor
7 = Starting motor
8 = Main and pilot exciters
9 = Supervisory panels
10 = Lubricating oil tank

The transmission of load surges in the electricity system to the gas network could be diminished by employing the obsolete boilers as steam reservoirs, and by designing the steam turbine as a dual-pressure machine.

Frequent operation at partial load, at which the efficiency of the steam turbine is better than that of a gas turbine.

The extension to the power station involves the following main elements:

A 65-t/h boiler, designed for live steam at 55 kg/cm², 480 °C, with feedwater at 164 °C.[4]

A Brown Boveri two-cylinder steam turbine with ACEC generator, rated 13 300 kW, 15 700 kVA; live-steam pressure 55 kg/cm² abs, controlled extraction (up to a maximum of 40 t/h) or addition of steam (from the reservoir) at 8·5 kg/cm² abs, with three uncontrolled bleed points for heating the feedwater (Fig. 16).

An air-cooled condenser for 50 t/h.[5]

The possibility of combining the new steam installation with the existing gas turbine was closely studied by the client, with the object of attaining as high an overall efficiency as possible [5], the following solution finally being adopted (Fig. 17).

To begin with, all the combustion air needed by the new boiler will be provided by the exhaust gases from the gas turbine. The consumption of the boiler is about 17 % of the gas leaving the air heater at a temperature of roughly 220 °C; by using this mixture instead of fresh air, a corresponding saving is effected in the fuel for the boiler. The exhaust gases leave the boiler at a temperature of about

[4] Supplied by S.A. Babcock-Smulders, Brussels, Belgium.

[5] Supplied by Gesellschaft für Luftkondensation mbH., Bochum, Germany.

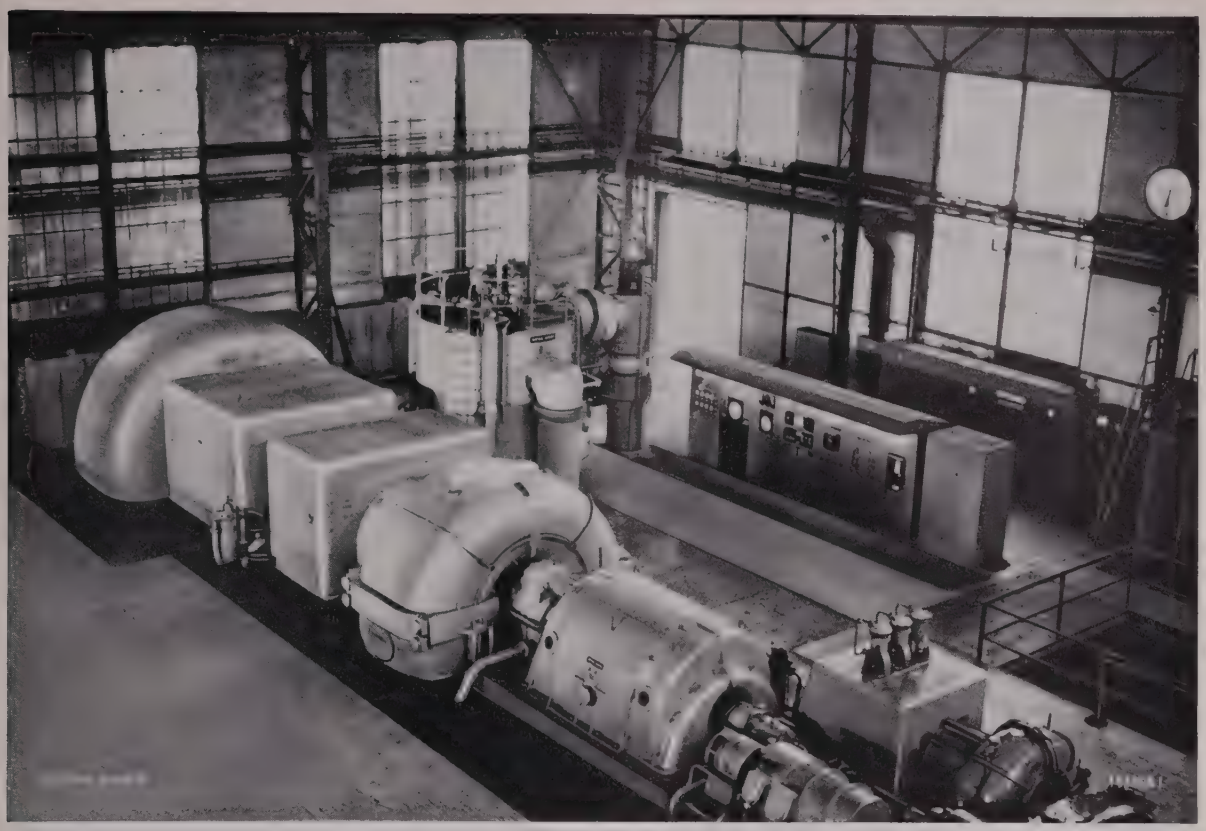

Fig. 14. – 14-MW gas-turbine set burning blast-furnace gas, in the Donawitz steelworks of the Österreichische Alpine Montangesellschaft

From left to right: gas turbine, air compressor, generator, gear with gas compressor; at the rear is the combustion chamber and switchboard.

160 °C. The arrangement visualized is similar to that in diagram C of the preceding article, with the following modifications. The boiler exhaust gases are cooled to the final temperature in a heat exchanger where they are used to heat the blast-furnace gas employed as fuel by the boiler. This dispenses with an economizer in the boiler. On the other hand, owing to the available excess of exhaust gas resulting from the disproportionality between the output of the gas turbine and that of the steam plant, a use must be found for these gases. The most economical solution to this question proved to be their use for feedwater heating in the steam cycle, thus saving bled steam and increasing the output of the steam turbine. This arrangement improves the thermal efficiency of the combined installation, the gain in the gas turbine cycle more than offsetting a slight reduction in the steam cycle. The greater part of the exhaust gases not needed for the boiler consequently flows through a feed-heater incorporated in the chimney, heating the feedwater of the new steam turbine from about 60 to 164 °C. This temperature is higher than the saturated-steam temperature corresponding to the bleeding pressure of the feed-heater through which the feedwater subsequently flows. There is therefore no condensation in the latter and, when the gas turbine is running, no heating steam is extracted from the two upper bleed points of the turbine. In this installation too, since the heat contained in the exhaust gases is sufficient for heating the feedwater to the desired temperature, there is no need to divide the flow of feedwater between heaters using bled steam and exhaust gases.

The combination of the new steam plant with the existing gas-turbine set is interesting and rewarding, even when the resultant improvement is not very high, owing to the rather low temperature

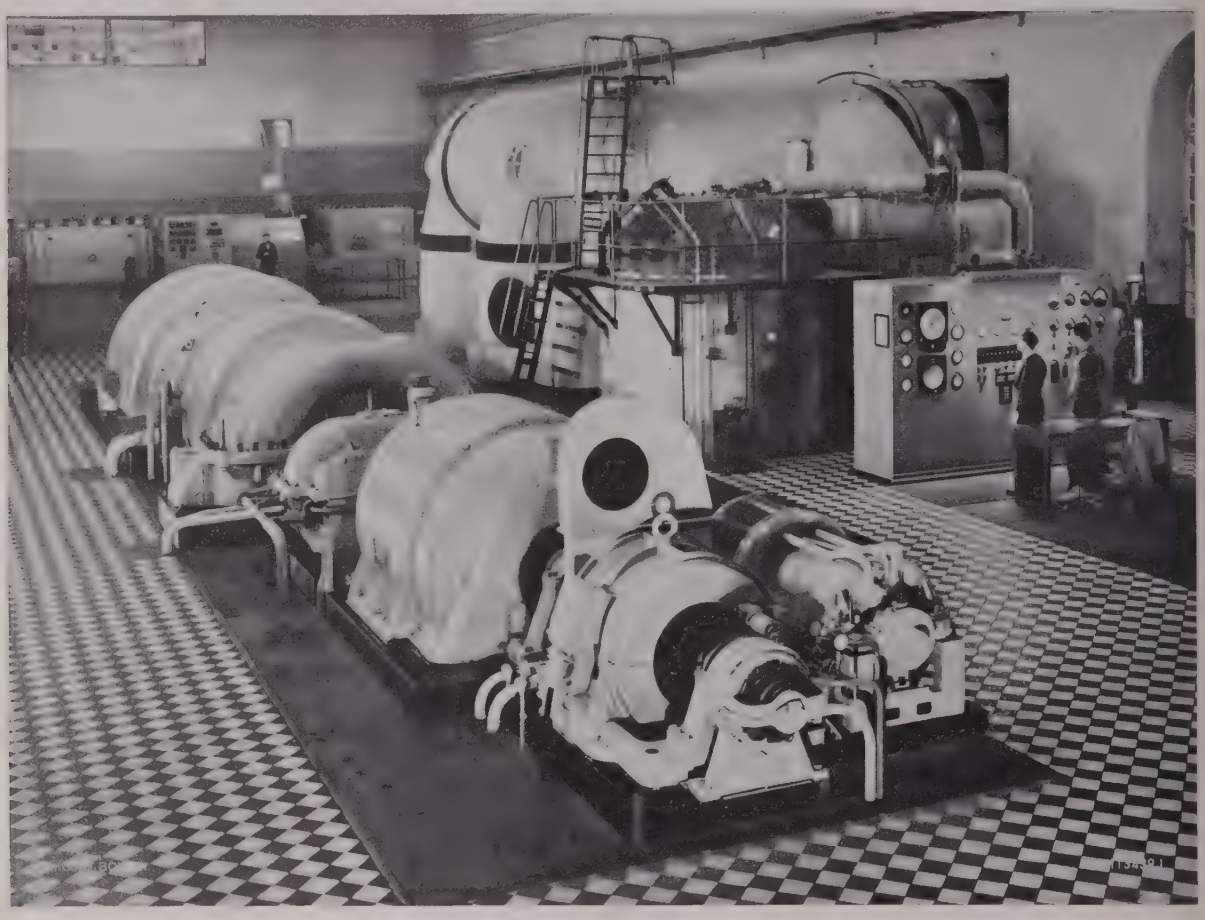

Fig. 15. – 5400-kW gas-turbine set in the Dudelange steelworks of ARBED, Luxembourg

In the foreground is the gas-turbine set; behind it the combustion chamber, air heater and switchboard. In the background the 13 300-kW dual-pressure steam turboset.

of the gas turbine exhaust gases after the heat recuperator, and owing to the use of a large proportion of the heat contained in the exhaust gases at a low temperature—for feedwater heating. Naturally the efficiency of the combined installation is largely dependent on the quantity of steam extracted for use in the heating network, and on the value of this heat. At zero extraction and full load on the turbine, according to the management's calculations, the total thermal efficiency of the combined installation increases from 20 % (effective mean efficiency of the gas turbine alone), or 24 % (steam plant alone), to 27·4 % [5].

The new steam section was commissioned in July 1956. Since then it has been operating without giving the least trouble, and attains the values calculated in the planning stage.

Vahr District-Heating Station near Bremen

A further example of the combination of gas turbines with heat cycles deserves mentioning although, strictly speaking, it does not belong in the group with which this number is mainly concerned. This installation (Fig. 18), believed to be the first of its kind, is situated at Vahr, near Bremen, and is noteworthy for a number of reasons.

This is the first example of a complete suburb with 40 000 inhabitants being supplied with heat by gas turbines.

During the planning there was no need to allow for any existing facilities; it was thus possible to select the optimum solution in every respect.

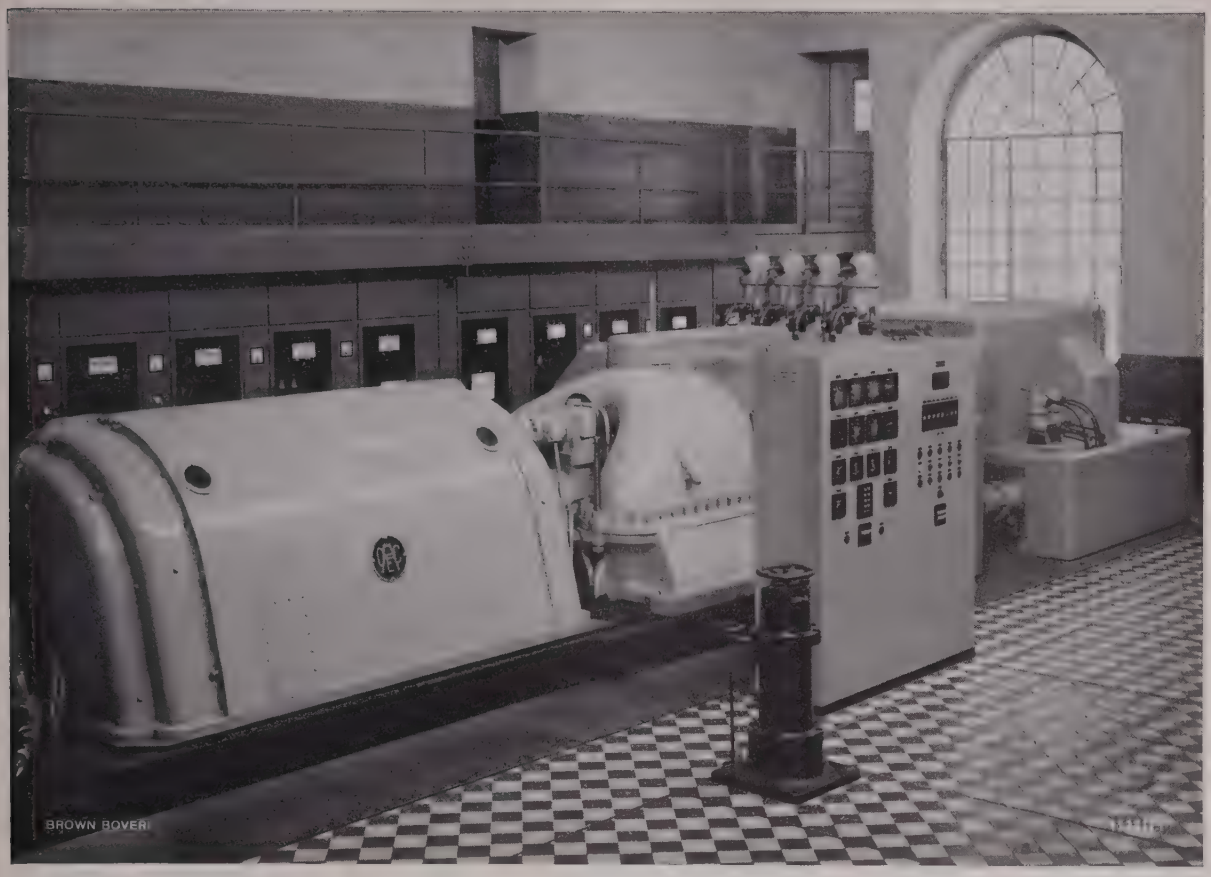

Fig. 16. – 13 300-kW dual-pressure steam turbine in the Dudelange steelworks of ARBED in Luxembourg

To achieve optimum conditions, not only were new methods adopted in the choice of the machine type, but an interconnected thermal system was created, which permitted the combined operation of different heat producers to achieve the most favourable effect.

All dwellings and other properties in this new suburb—the maximum heat consumption of which, when completed, will work out to about 88 million kcal/h—are to be supplied from the new district-heating plant being erected by the Public Utilities of the City of Bremen, the heat being carried by hot water at an outgoing temperature of 110–130 °C. In addition to supplying heat, the new station has to generate electricity for the new suburb and to supplement the city supply network.

The question of whether a steam or gas-turbine power station should be erected was given careful study. The machines provided had to comply with the following requirements, among other things.

The initial outlay should be as low as possible, in order that the cost of generating heat and electricity should not be weighted too heavily with interest and amortization, particularly in view of the small number of running hours per year.

Starting, loading and shutting down should be rapid, with easy control and low losses, in order that the sets may be taken into and out of service several times a day, to cope with peak load demand.

The electrical output should be high in relation to the heat output because, apart from catering for the power consumption of the all-electric suburb, the station has to make quite a large contribution to the general supply system; a large, immediately available stand-by capacity is to be provided even when the heating is shut off.

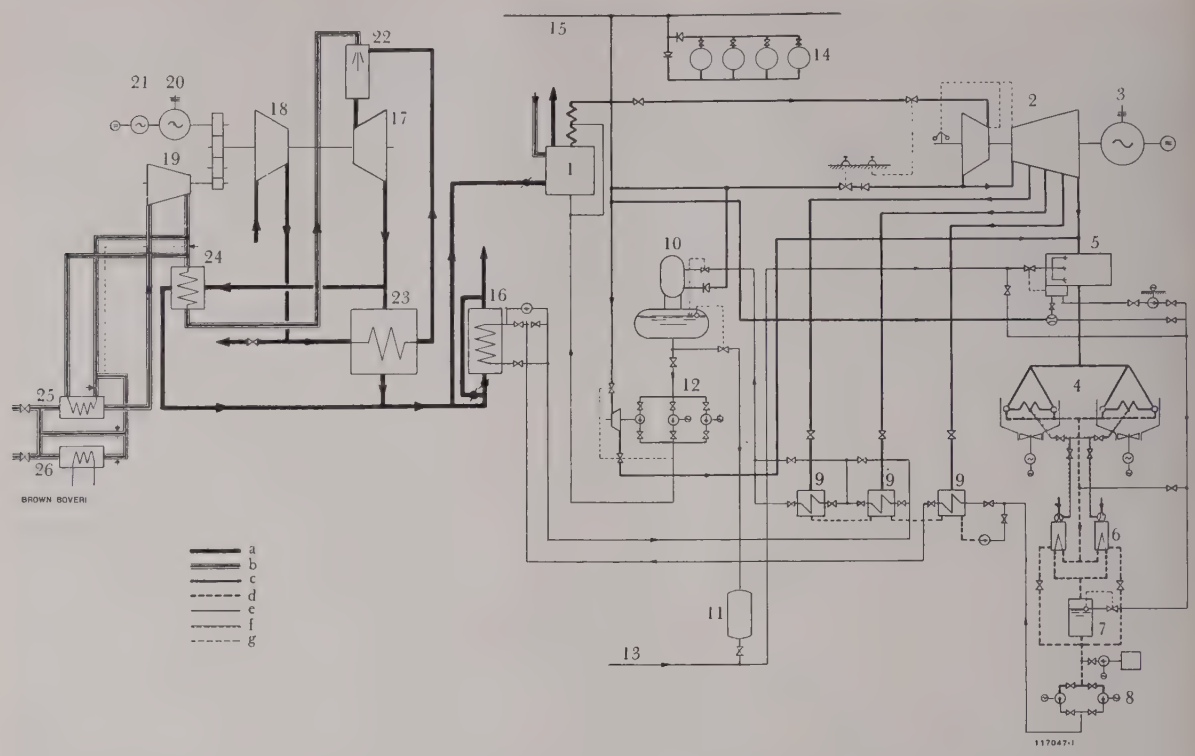

Fig. 17. – Thermal diagram of the combined gas and steam turbine installation at Dudelange, Luxembourg

1 = Boiler
2 = Steam turbine
3 = Generator
4 = Air-cooled condenser
5 = Steam cooler
6 = Steam-jet ejector
7 = Raw-water degasifier
8 = Condensate pumps
9 = Feedwater heater
10 = Feedwater tank
11 = Spare tank
12 = Feedwater pumps
13 = Raw-water treatment
14 = Steam accumulators
15 = Heating network
16 = Waste-heat boiler
17 = Gas turbine
18 = Air compressor
19 = Blast-furnace gas compressor
20 = Generator
21 = Starting motor
22 = Combustion chamber
23 = Recuperator (air heater)
24 = Gas heater
25 = Gas drier
26 = Gas cooler
a = Working cycle of gas turboset (air/exhaust gas)
b = Fuel gas (blast-furnace gas)
c = Steam
d = Condensate
e = Feedwater
f = Air
g = Impulse line

The amount of cooling water required must be small because the only supply available is an artificial pond holding 50 000 m³, and because the risk of creating mist ruled out the erection of a cooling tower in a residential area.

Since the gas turbine meets these requirements in an ideal manner, the municipal authorities decided on this type of machine and entrusted Brown Boveri, Mannheim, with the task of planning what, to all accounts, is the first gas-turbine district-heating station in the world [6, 7, 8, 9].

In addition to the above conditions being stipulated, it was laid down that, owing to the location of the station in a residential area, precautions had to be taken to avoid disturbing the residents by noise and exhaust fumes. Both requirements have been satisfied. By sound-proofing the machine house and fitting silencers in the air intake ducts and exhaust-gas piping, the noise level of the plant was reduced to such an extent that it is less than 50 phon at all points on the boundary of the station site, the noise of the turbines being almost completely drowned by the sound from the nearby main road. In order to avoid all risk of ash or other products of combustion producing an annoying deposit, and particularly to ensure that the SO_2 content of the atmosphere in

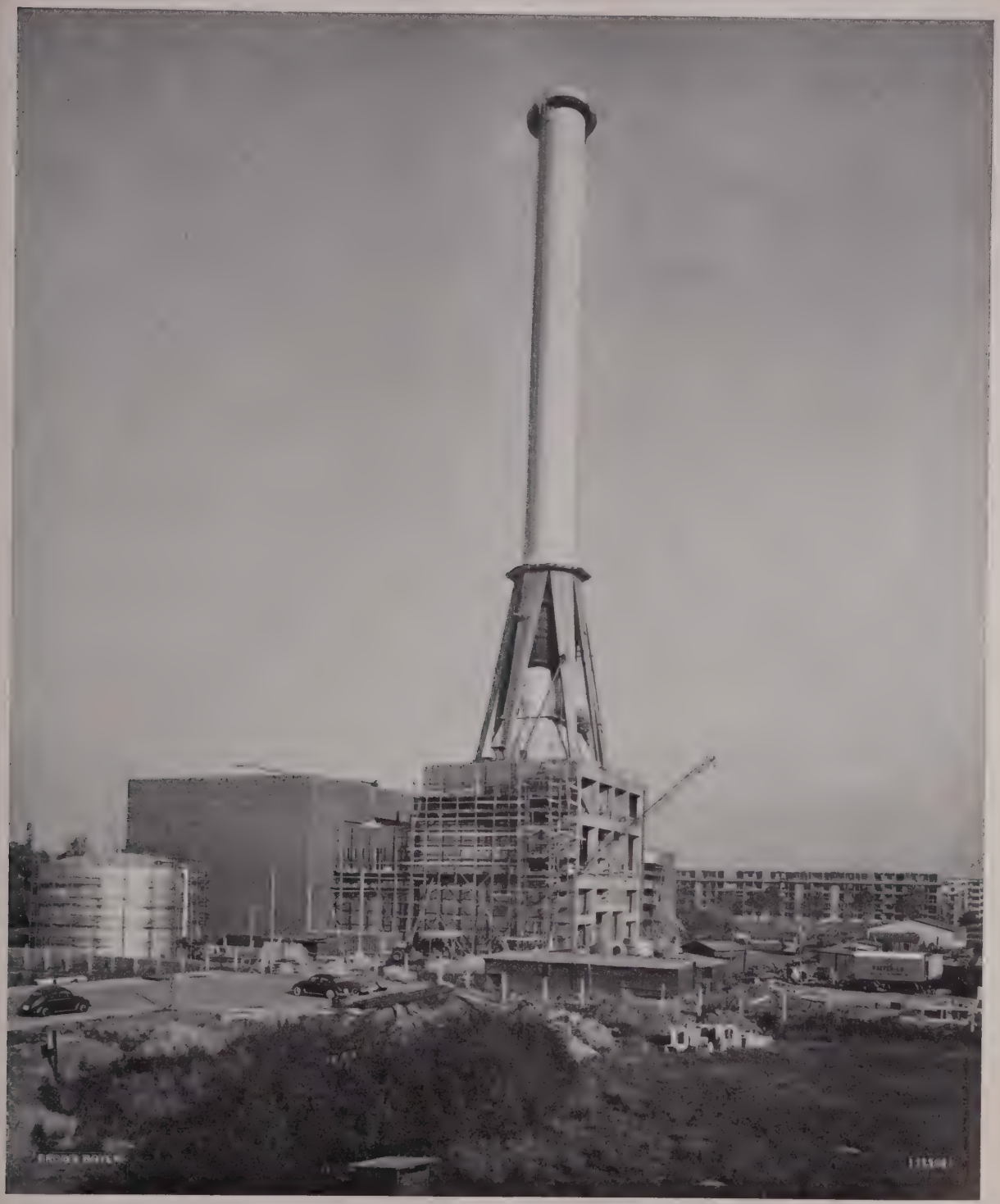

Fig. 18. – Vahr district-heating station of the Bremen Municipal Utilities
The building has since been completed.

the residential area does not exceed the permitted maximum of 0·5 mg/m³ when both turbines are in operation, and under unfavourable weather conditions, a very high chimney was erected, rising to a height of 107 m above ground level (Fig. 18).

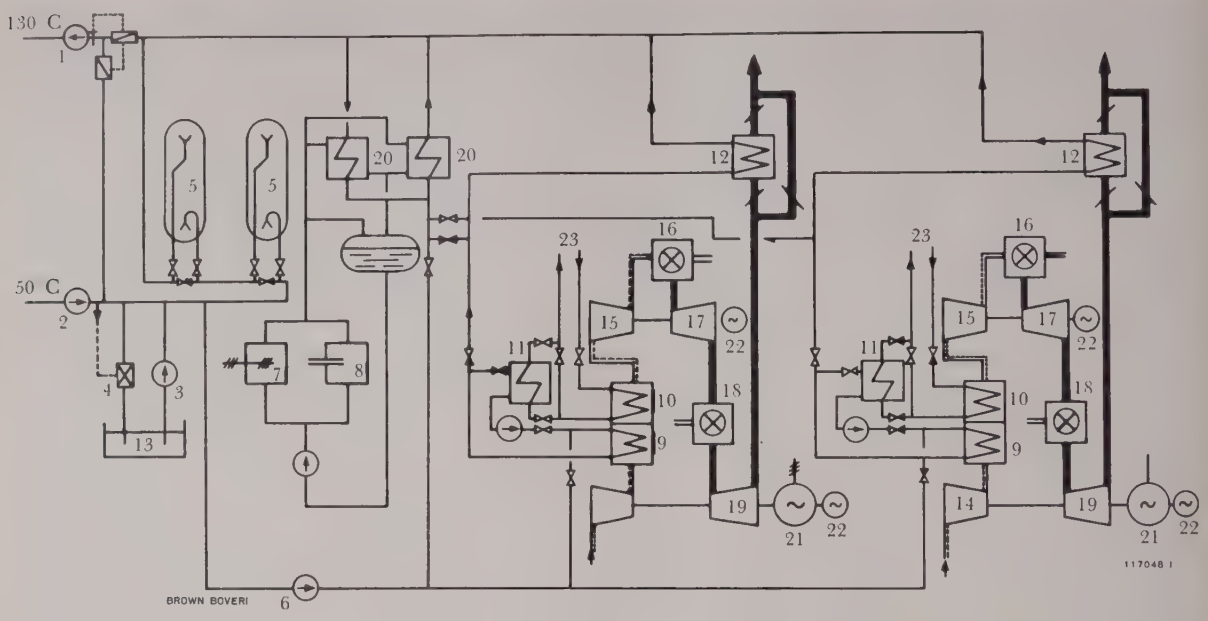

Fig. 19. – Schematic diagram of Vahr power station

1 = Circulating pump (hot water flow)
2 = Circulating pump (hot water return)
3 = Pressure-holding pumps
4 = Pressure regulator for heating system
5 = Hot-water storage tank
6 = Storage pumps
7 = Electric boiler
8 = Triple-draught boiler, oil-fired
9 = Intercooler II
10 = Intercooler I
11 = Aftercooler
12 = Waste-heat boiler
13 = Expansion tank
14 = Low-pressure compressor
15 = High-pressure compressor
16 = High-pressure combustion chamber
17 = High-pressure turbine
18 = Low-pressure combustion chamber
19 = Low-pressure turbine
20 = Heat exchanger
21 = 33-MVA generator
22 = Starting motor
23 = Cooling water

Thermal Diagram of Vahr Power Station

As much as possible of the heat output has to be produced by the gas turbines. To achieve this, heat is not only taken from the exhaust gases, but the intercoolers are also used as sources of useful heat. The water returning from the heating network first flows through the intercoolers of the twin-shaft gas-turbine sets (Fig. 19), absorbing 12 $\times$ 10^6 kcal per hour per set. By utilizing the hot water in the high-temperature part of the intercoolers, thus dissipating about 60% of the heat to be extracted from the combustion air, it is not only possible to gain useful heat, but also to save valuable cooling water. Fresh-water cooling is then only required for the second part of the intercooler, in order to cool the combustion air as much as possible before it enters the h.p. compressor. These advantages more than offset the extra cost of the two-part intercooler.

The preheated water which is heated in the intercooler next flows through the waste-heat boiler allocated to each gas turbine, which imparts a further 18 $\times$ 10^6 kcal/h to the water, enabling it to re-enter the heating network at a temperature of 110–130 °C. This flow temperature is controlled within the above limits according to the demand for heat, by adaptation to the atmospheric temperature.

If, in exceptional circumstances, the gas turbines have to run without generating any heat, special after-coolers cooled by fresh water and connected in series with the fresh-water section of the intercoolers absorb the incoming heat, while the waste-heat boilers are bypassed.

The heating system contains two hot-water storage tanks, each holding 300 m^3, which permit the full amount of heat to be taken from the gas turbines and the maximum efficiency of the installation maintained, even when the heat extracted by the heating network is less. In these tanks and the piping about 55×10^6 kcal can be stored. As soon as the storage tanks are full, the turbines are shut off and the heating network fed from the storage tanks.

Apart from the waste-heat boilers the installation has four oil-fired boilers, each with a capacity of $6{\cdot}1 \times 10^6$ kcal/h. These were employed for supplying heat to the houses in the area before the first gas turbine was commissioned. They will continue to be used when the station is completed, to cater for extraordinary heat requirements in cold weather, or when only a small amount of heat is required and it would be uneconomical to run a gas turbine. The plant also contains four electric boilers, each producing $2{\cdot}6 \times 10^6$ kcal/h, used to absorb excess electrical energy of the hydro-electric plant of the municipal authority, and of turbosets which have to be kept running round the clock for safety reasons. The oil-fired and electric boilers are not connected direct to the heating network, but generate steam which transfers its heat to the heating water in special heat-exchangers. These different heat generators bring up the total heat-generating capacity of the station to $94{\cdot}8 \times 10^6$ kcal/h.

Layout of Vahr Power Station

The two gas-turbine sets installed in the machine house (Fig. 20) were built by Brown Boveri, Mannheim; they are of the well-known twin-shaft type and, in principle, exactly like the sets in Korneuburg. The sole difference is in the intercoolers and the fuel. As mentioned, the former is in two parts while the fuel at Vahr is normally heavy oil. The two sets are started with diesel oil, controlled from a central control room, from which they can be supervised. The two gas-turbine sets are designed for the following conditions:

TABLE VII

Barometric pressure	kg/cm^2 abs	1·033
Air inlet temperature	°C	1·5
Temperature of cooling water	°C	10
Rated output at generator terminals under the above conditions	MW	25
Thermal efficiency under above conditions and at maximum effective output	%	24·5
Temperature at gas turbine inlet	°C	max. 630

The waste-heat boilers[6] allocated to the turbines are housed in a special building. In them the temperature of the exhaust gases is reduced from 320 to 180 °C. In order to diminish the risk of corrosion on the gas side, due to the temperature possibly dropping below the dew-point of the acid, the boilers are of cast-iron finned tubes which, with their cast skin and thick walls, are more resistant to attack than steel tubes.

Other separate buildings, adjoining one another to form a complex, contain the oil-fired and electric boilers, the intake air filters and electrical switchgear.

Operation of the Power Station

The removal of heat from the intercoolers and the utilization of the heat contained in the exhaust gases greatly increases the economic performance of the gas turbines. The attainable efficiency cannot be defined unambiguously, since it is governed by commercial considerations determining the value of the heat. The heat balance of a unit comprising gas turbine and waste-heat boiler is then as follows:

TABLE VIII

Heat added with the fuel		$87{\cdot}7 \times 10^6$ kcal/h
Useful electrical output	25 MW	$21{\cdot}5 \times 10^6$ kcal/h
Heat generated for heating		30×10^6 kcal/h

[6] Supplied by Deutsche Babcock & Wilcox-Dampfkesselwerke AG., Oberhausen, Germany.

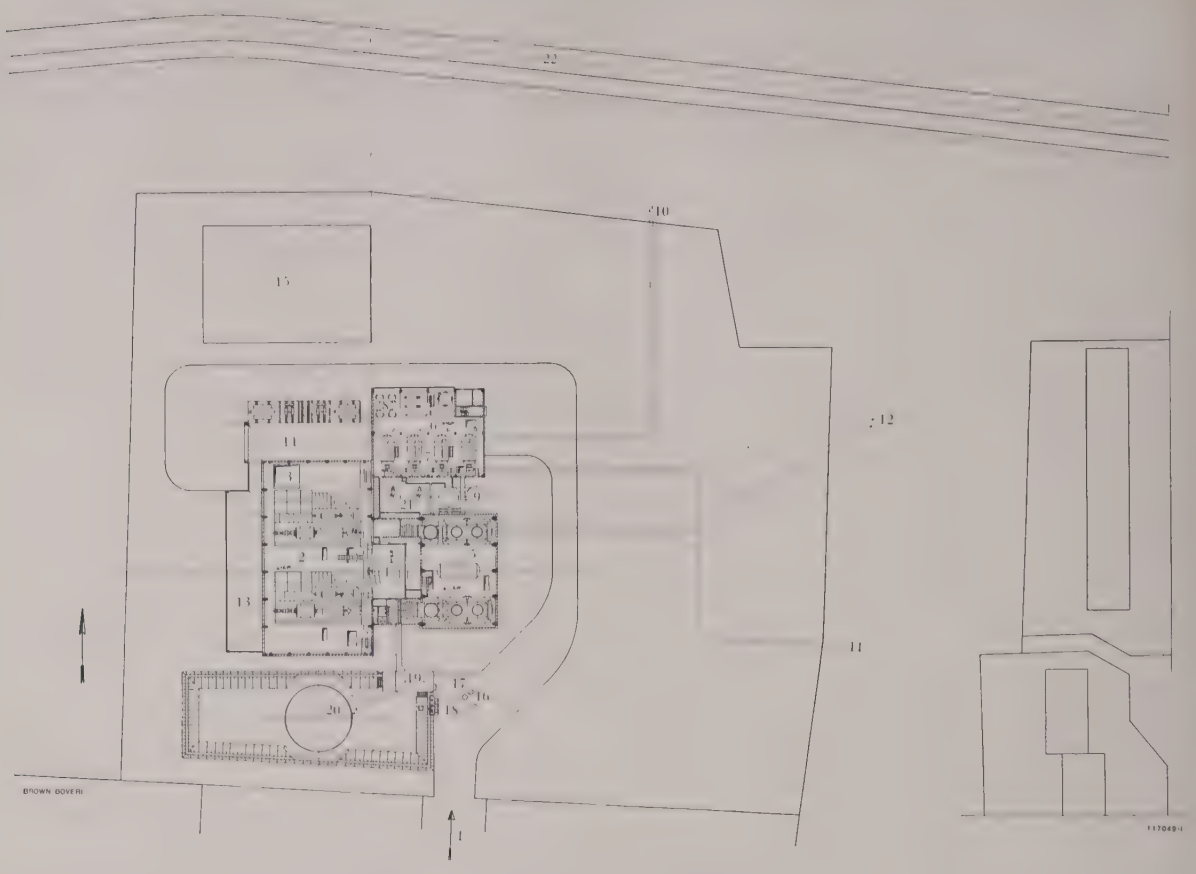

Fig. 20. – Layout of Vahr district-heating station

1 = Approach road
2 = Machine house
3 = Erection opening
4 = Control room building
5 = Waste-heat boiler building
6 = Boiler-house
7 = Oil-fired boilers
8 = Electric boilers
9 = Hot-water storage tank
10 = Heating system, northern leg
11 = Heating system, southern leg
12 = Cooling-water inlet and outlet
13 = Filter building
14 = Switchgear 10/6 kV, indoors
15 = 110-kV switchyard
16 = Oil tanker-wagon discharge point
17 = Light oil
18 = Heavy oil
19 = Fuel pump-house
20 = Heavy-oil tank, containing 2000 m^3
21 = Light and heavy oil service tanks
22 = Main road

As stated before, the various heat generators are supposed to be employed in such a manner that the maximum overall performance of the station can be attained by operating the gas turbines at optimum efficiency. The operating diagrams were worked out by the municipal authority in this manner [10] and may be explained by considering the theoretical programmes for two days during the winter, with different atmospheric temperatures (Fig. 21 and 22). These diagrams illustrate the alternating operation of gas turbines, oil-fired and electric boilers, the two gas turbines being switched on or off, not only according to the demands of the heating system, but also according to the peak loads of the electricity system. In the winter of 1959/60, after the first gas turbine had been commissioned, the amount of heat dissipated by the heating system, and the electrical output were measured (Fig. 23 and 24). These readings proved the correctness of the theoretical diagrams, since both the heat dissipation and power output conformed to the expected curves and, as anticipated, the heat and power peaks coincided, thus facilitating economical operation. The measured values are merely somewhat

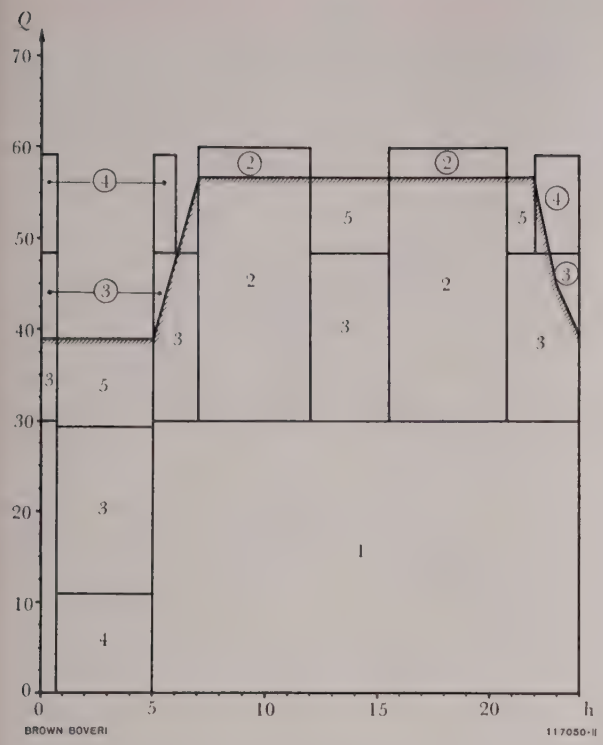

Fig. 21. – Theoretical running programme of the various heat generators in Vahr power station on a cold winter day

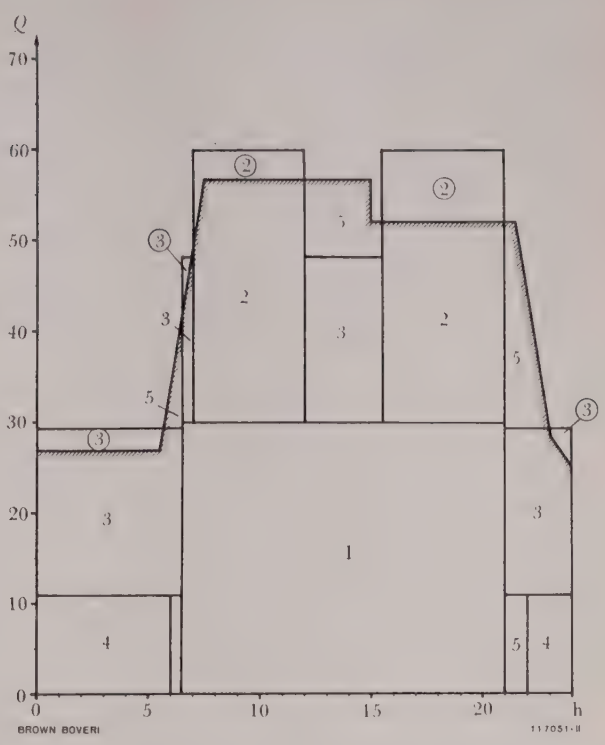

Fig. 22. – Theoretical running programme of the various heat generators on a mild winter day

1 = Gas turbine I running
2 = Gas turbine II running
3 = Oil-fired boilers running
4 = Electric boilers running
5 = Discharging the storage tanks
○ Charging up the storage tanks

Abscissae: Time t in hours Ordinates: Quantity of heat Q in Gcal/h

lower than the theoretical figures because the suburb is not completely built yet.

According to the visualized operating programme, the various heat generators will be run for the following periods every year:

Gas turbine I	3000 h
Gas turbine II	1000 h
Electric boilers	2000 h
Oil-fired boilers	1500 h

The first of the gas-turbine sets commenced regular service in December 1959, the second being due for commissioning at the end of 1960. Acceptance measurements which have been taken show the output to be about 7 % higher than the guaranteed figure, while the efficiency is about 1 % better than the guaranteed value.

Conclusions

In all four of the installations described the efficiency was improved by combining a gas turbine with a steam or industrial heating cycle. The extent of the improvement when a steam cycle follows the gas turbine depends on the design of the steam system, which, in the installations described, could not be freely selected with a view to optimum economic performance in every case. Nevertheless the achieved gains were quite appreciable and prove that the right policy was adopted in going over to combined installations.

In the case in which the energy contained in the exhaust gases of the turbine is utilized for heating, the attainable result is largely dependent on the value placed on the heat. In general though it may be established that as soon as there are consumers

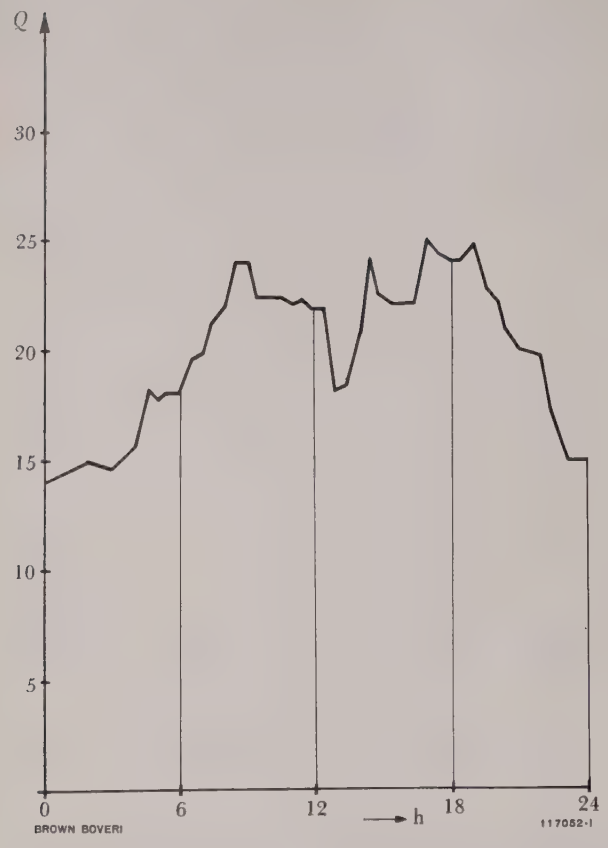

Fig. 23. – Effective heat output of Vahr power station on a cold winter day with a mean temperature of —7 °C

The suburb is not completely built

Abscissae: Time t in hours

Ordinates: Quantity of heat Q in Gcal/h

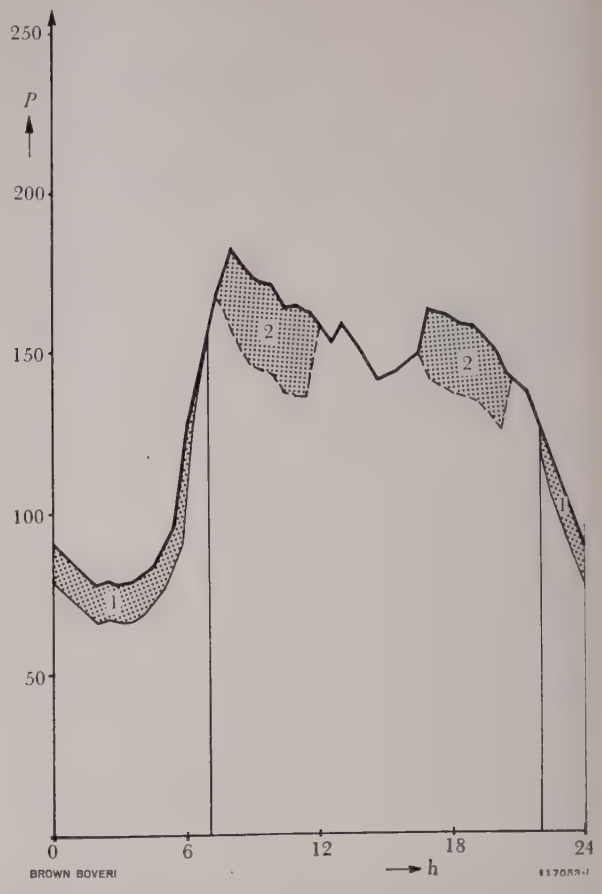

Fig. 24. – Electrical load on the Bremen municipal network on a cold winter day with a mean temperature of —7 °C

Note the operation of the gas turbines during the periods of peak demand.

Abscissae: Time t in hours

Ordinates: Output P in MW

1 = Input to electric boilers

2 = Power generated by gas turbines

prepared to accept this heat, the expense involved in its utilization is always worth while.

All four installations utilize not only the energy contained in the exhaust gases, but add supplementary heat to the subsequent cycle. At Korneuburg, Cornigliano and Vahr the gas turbines, however, provide the majority of the heat. At Vahr the supply of heat must be assured when the gas turbines are switched off. Normally this problem is solved most advantageously by equipping the waste-heat boiler with a supplementary blower and firing system. At Vahr, however, this method was impracticable because the heating system had to function before the gas turbines were commissioned. Consequently, as explained, oil-fired boilers were also installed.

At Korneuburg and Cornigliano the extra heat is applied in the waste-heat boiler itself. As described, this takes place in a separate superheater at Korneuburg, in which merely a small portion of the exhaust gases are heated further. Thus, with only a small amount of additional fuel, it is possible to arrive at a high inlet temperature for the subsequent steam cycle, thereby improving the latter accordingly and so obtaining a high overall efficiency for the combined installation.

The same method was not convenient at Cornigliano, as the temperature difference between the turbine exhaust and the steam system necessitated

little additional temperature rise, if any. The provision of a separate combustion chamber with superheater would therefore not have been worth while; hence the method chosen was to incorporate the burner in the exhaust-gas pipe.

All four installations represent interesting solutions to similar problems. For the short time during which they have been running, they have given good results and fulfilled the hopes placed in them. It is to be hoped that they will become the start of a broad development in the sphere of combined installations.

(KME) W. P. AUER

Bibliography

[1] H. PFENNINGER: Die Gasturbinenkraftwerke Livorno und Fiumicino, Italien. Motortech. Z. 1957, Vol. 18, No. 6, p. 189–93.

[2] W. P. AUER: Gasturbinen im Kraftwerk Luigi Orlando in Livorno. Schweiz. Bauztg. 1957, Vol. 75, No. 24, p. 390–2.

[3] H. PFENNINGER: Brown Boveri Gas Turbines for an Inlet Temperature of 750 °C. Brown Boveri Rev. 1960, No. 1/2, Vol. 47, p. 35–64.

[4] H. PFENNINGER: Operating Experience with Brown Boveri Gas-Turbine Installations. Brown Boveri Rev. 1953, Vol. 40, No. 5/6, p. 144–66.

[5] C. PESCHON: Un exemple de turbo-machine en sidérurgie. Rev. Tech. Luxemb. 1947, Vol. 49, p. 147–69.

[6] R. ZINKL: Heizkraftwerk Vahr der Stadtwerke Bremen. Brennstoff, Wärme, Kraft 1957, Vol. 9, No. 12, p. 575–8.

[7] H. STORCH: Das Gasturbinenkraftwerk Vahr. BBC Nachr. 1959, Vol. 41, No. 10/11, p. 512–4.

[8] H. MAYER: Dampf- und Gasturbinen in der öffentlichen Elektrizitätswirtschaft. BBC Nachr. 1960, Vol. 42, No. 6/7, p. 273–9.

[9] R. ZINKL: Das Gasturbinen-Heizkraftwerk Bremen-Vahr. Motortech. Z. 1960, Vol. 21, No. 9, p. 382–5.

[10] K. KASTROLL: Das Kraftwerk Vahr. Paper presented to the Congress of the Union Internationale des Distributeurs de Chaleur, Utrecht, April 25/27th, 1960.

PTOLEMAIS POWER STATION IN GREECE

621.311.22 (495)

The Greek national electricity undertaking decided to build a power station to utilize the large lignite deposits in northern Greece. For this project Brown Boveri were nominated as general contractors in charge of all work. The contract covered the planning and delivery of the mechanical and electrical equipment, the preparation of all building plans and the responsibility for supervision of the building work. This article shows how the duties involved were organized. The mechanical equipment and some of the features of the electrical installation are described. The concluding chapter deals with the erection, transport, installation and commissioning.

GREECE has drawn up a programme of electrification, closely related to the enormous progress being made in agriculture. Combined with this is a project to create a new industrial centre in West Macedonia, in the northern part of the country. The considerable lignite deposits in the area have already led to a briquette factory being built; a fertilizer plant is also in the course of erection. To provide the electric power needed locally and to

Fig. 1. – Aerial view of the 70-MW power station at Ptolemais in Greece

The electrostatic precipitators were not in operation at the time.

Fig. 2. – The 150-kV supply network in Greece

▨ = Hydro-electric stations
□ = Steam power stations
△ = Substations
——— = Existing transmission lines
– – – = Proposed extension to the network

help cope with the steadily rising demand of the city of Athens, plans were prepared for Ptolemais power station, burning the local lignite, and have since been put into effect.

Advised by previous investigations into the lignite deposits, the national electricity authority—the Public Power Corporation, Athens (PPC)—decided on the location of the generating station, which was to be beside the Soulu, a stream running close to the lignite mines. An existing 150-kV line to Athens, 450 km distant, finally clinched the choice of site, in open fields beside the road between the village of Ptolemais and nearest town Kozani.

Fig. 2 shows how Ptolemais fits into the general power supply organization for the whole country. Electricity is mainly transported to the south, through Larissa substation. The line to the north connects Ptolemais with the hydraulic station Agra. A second line to the north is planned, with the destination of Bitolj substation, for power exchange with Yugoslavia.

In the spring of 1956 the PPC called for tenders for a complete 70-MW lignite-fired power station, with the possibility of future extension to 340 MW. In September of the same year an "all-in" contract was awarded to Brown Boveri, Baden, under the terms of which the Company was nominated as general contractor, with full responsibility for planning, erection and commissioning the thermal and electrical equipment, including the planning, calculation and supervision of all building work.

The Power Station

This 70-MW power station is connected on the unit principle and contains the largest steam turbine in Greece at present. It is intended to act as a base-load station, because the lignite is available in large quantities at a favourable price.

The power-house and ancillary buildings are mainly built of reinforced concrete; the steel for reinforcement and the small amount of constructional

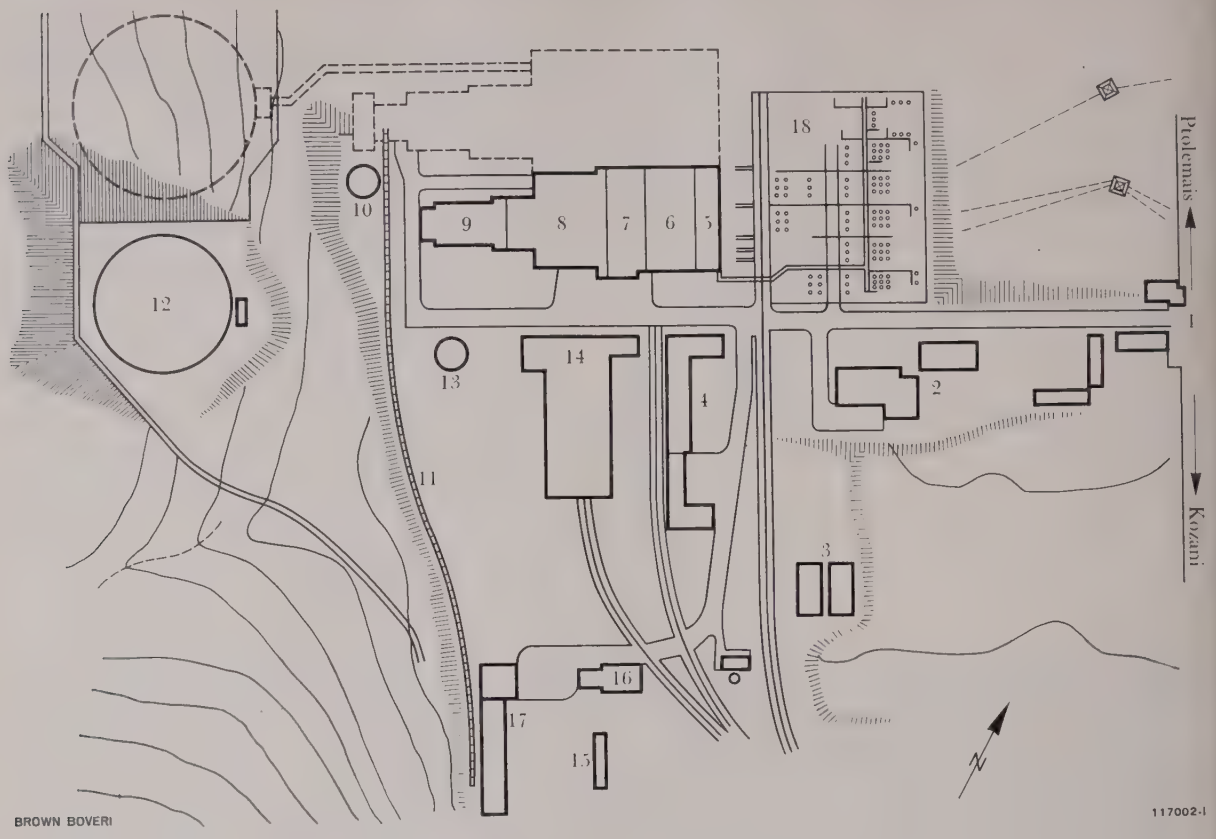

Fig. 3. – General layout of buildings on the station site

1 = Road Ptolemais Kozani
2 = Canteen and accommodation
3 = Settling basin
4 = Office and garages
5 = Indoor switchgear
6 = Machine house
7 = Bunker house
8 = Boiler-house
9 = Electrostatic precipitator
10 = Chimney
11 = Ash disposal
12 = Cooling tower
13 = Basin of high-speed clarifier
14 = Workshop and water purifier
15 = Coal stockyard
16 = Coal pulverizer house
17 = Coal storage bunker
18 = Switchyard

steelwork needed was imported into Greece. The building work was carried out by Greek firms; only for building the cooling tower and the dam was an Italian firm engaged.

The power-station buildings stand on concrete rafts because the building site only permits a relatively low specific loading, so that the pressure had to be kept as small as possible. A pile foundation was out of the question, as there were apparently no solid strata even deeper into the soil. The heaviest part of the building, i.e. the lignite bunkers, stands on lignite; the remaining sections, such as machine house and boiler-house are on clay or clayey gravel.

The groundwater level is about 1·5 m below the surface of the soil, consequently it had to be constantly lowered by pumping while building was in progress. Pile shuttering of the excavated area was not necessary because the flow of groundwater was quite small. The foundation rafts and cellar walls had to be thoroughly waterproofed, to prevent the entry of groundwater into the cellars. For this reason all building joints below the datum line had to be sealed with flexible rubber strips. All buildings were calculated according to German and American earthquake regulations, because Ptolemais is situated in an area where earthquakes of medium severity may be experienced.

Fig. 3 shows the general layout of the power station relative to the site; Fig. 4 a sectional elevation through the station.

The Table below gives the characteristic data of the station.

The plan for this power station was based on the principle of not choosing any extreme data, in order to keep operation simple and safe. This was mainly governed by such factors as the low quality of the fuel—unusually low calorific value, appreciable moisture content, high ash content—the geographical remoteness of the site, and the difficulty of obtaining suitable personnel. Therefore standard equipment was employed for the power station; moreover, the equipment had to be as self-supporting as possible, particularly in operation.

From the start the workshop was dimensioned for the final size of the station, and contains machine tools capable of carrying out repair work to all the power plant. Laboratories were also provided for examination of the lignite, water and oil. Since the procurement of hydrogen for cooling the generators depends on importation into Greece, an electrolysis plant for generation of the hydrogen also had to be supplied.

TABLE I

Principal data of Ptolemais power station

		Supplier
General contractors		Brown, Boveri & Co., Ltd., Baden, Switzerland
Planning, supervision of building and erection work		Brown, Boveri & Cie. AG., Mannheim, Germany
Boiler		
Single-drum, natural circulation		Kohlenscheidungsgesellschaft mbH., Stuttgart, Germany
Max. capacity	285 t/h	
Live steam at	92 kg/cm², 513 °C	
2 boiler feed-pumps driven by electric motors	each 356 t/h	Klein, Schanzlin & Becker AG., Frankenthal
Electrostatic precipitators		Lurgi Apparatebau-Gesellschaft mbH., Frankfurt/Main, Germany
Steam turbine and hydrogen-cooled generator		Brown Boveri & Co., Ltd., Baden, Switzerland
Maximum output	70 MW at p.f. 0·85	
Live steam	85 kg/cm², 510 °C	
Feedwater heating	to 210 °C	
Vacuum	0·064 kg/cm²	
Cooling-water temperature	24 °C	
Switchgear 150/15/6/0·4 kV		Brown, Boveri & Co., Ltd., Baden, Switzerland
Transformers		Brown, Boveri & Co., Ltd., Baden, Switzerland
2 main transformers	each 42 MVA	
Ratio	15·75/150 kV	
1 station service transformer	15 MVA	
Ratio	150/15·75 kV	
Cooling tower internals		Balcke, Maschinenbau-AG., Bochum, Germany
Self-ventilating, water throughput	12 000 m³/h	
Fuel handling		J. Pohlig AG., Cologne
Capacity of conveyors	2 × 450 t/h	
Treatment of cooling and drinking water		Permutit AG., Berlin
120-t machine-house crane		De Roll's Ironworks, Berne, Switzerland

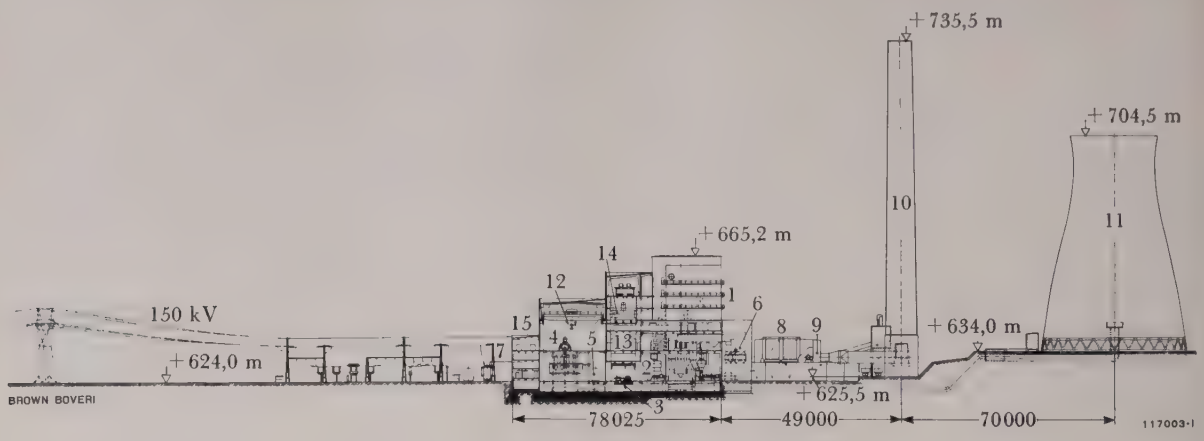

Fig. 4. – Longitudinal section through the power station

1 = Boiler-house
2 = Coal mills
3 = Boiler feed-pumps
4 = Turboset
5 = Condenser
6 = Air heater (Ljungström)
7 = Transformers
8 = Electrostatic precipitators
9 = ID fan
10 = Chimney
11 = Cooling tower
12 = Machine-house crane
13 = Thermal and electrical control rooms
14 = Boiler, bunker
15 = Switchgear

Organization of Responsibilities

The client expressly stipulated that, in matters of a technical or administrative nature, he would only deal with the firm bearing the main responsibility, or their appointed officers. In Baden the Sales Department for thermal power stations was available for this task. In order to simplify these dealings with the client, in the spirit of the contract, a mechanical engineer and a civil engineer were delegated to Athens as the official representatives of the general contractors.

When work commenced at the site, the client delegated an engineer to Ptolemais for liaison with our clerk-of-works and chief erector.

Brown Boveri, Mannheim, undertook the technical and civil planning, their work being governed by the principles employed in Baden, and by the material supplied by the latter works. To facilitate the execution of a homogeneous overall and detailed plan, a team of engineers was built up in Baden, Mannheim, Athens and on site, who assured uniform, correlated leadership as a result of their continuous consultation with one another.

For the procurement of such mechanical or electrical equipment which could not be made in the Baden or Mannheim factories, orders were placed with 42 sub-contractors. As the firm responsible for the preparation of the lignite, the Kohlenscheidungsgesellschaft mbH., Stuttgart, collaborated with Brown Boveri, but in some cases dealt with the client direct.

Building Organization

The overall contract placed with the Company included the erection of quite a number of buildings, the planning, calculation and preparation of the civil engineering drawings for which were performed by the Building Dept. of Brown Boveri, Mannheim. Owing to the fact that the planning and execution, with regard to arrangement and connection of all electrical equipment, whether of Brown Boveri or outside make, was in the hands of the Company, it was possible to co-ordinate the various parts of the installation in accordance with the economically and technically most favourable aspects. All told, the following buildings were erected by Brown Boveri:

Power-house and switchyard

Building for the fuel supply—coal bunkers, crushing plant, bridges, etc.

Fly-ash bunker

Hyperbolic cooling tower of reinforced concrete

Reinforced concrete chimney, lined with acid-resistant brick

Workshop, laboratory and water treatment plant

Hydrogen generation plant

Canteen and staff accommodation

Office building with garages

Porter's lodge

A village with 28 houses of six different types for the staff, with central heating and drinking-water supply from the power station.

Other civil engineering works were the roads, paths and railway lines within the station area, roads in the village; the main and side dams, with a total length of 2000 m and a maximum height of 12 m, with bottom outlet, automatic overflow control, pump-house, a complete drainage system with clarification plant.

A provisional hutted camp with canteen was also built for the labourers.

The main dam is 100 m long, the middle 50 m being of reinforced concrete, while the remainder is of 500 l/s, but the spillway had to be designed to handle the maximum flood capacity of 900 m^3/s, or 1800 times the normal amount.

The total volume of concrete for the entire building site amounted to about 65000 m^3, with roughly 5500 t of reinforcing steel.

The Company's responsibilities on site covered supervision of the building work, to ensure the draw-

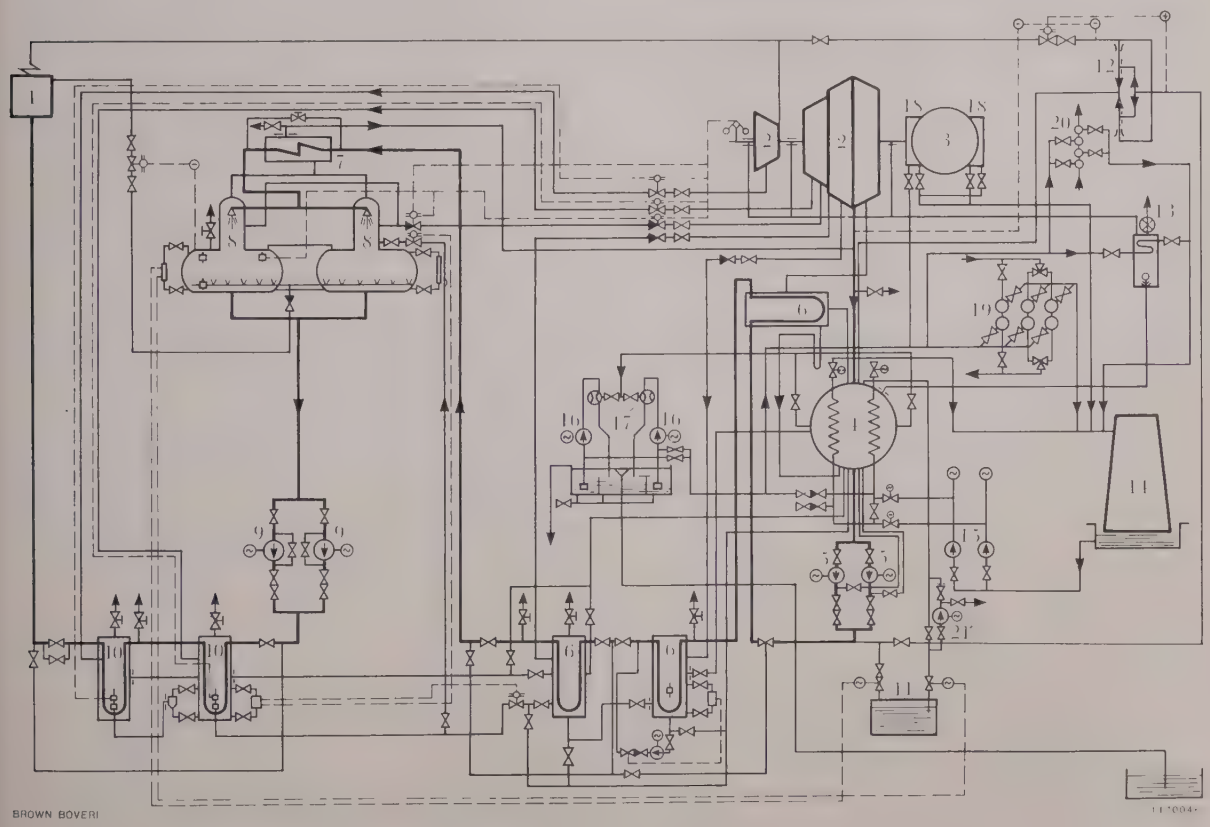

Fig. 5. – Thermal diagram

1 = Boiler
2 = Turbine
3 = Generator
4 = Condenser
5 = Condensate pumps
6 = Low-pressure feed heaters
7 = Waste-steam condenser
8 = De-aerator, feedwater tank
9 = Boiler feed-pumps
10 = High-pressure feed heaters
11 = Cold condensate tank
12 = Condensate injector
13 = Condenser for gland steam
14 = Cooling tower
15 = Cooling-water pumps
16 = Spray pumps
17 = Water-jet air ejector
18 = Hydrogen cooler
19 = Oil cooler
20 = Oil cooler for hydrogen glands
21 = Cold condensate pump

ings were strictly adhered to, and that the scheduled promises were kept. Finally the completed building lots had to be handed over to the client. Among other duties, the Chief Clerk of Works delegated by Brown Boveri also had to carry out regular checks on the building soil and on the quality of the concrete. The Company's office on site also kept all the accounts.

Boiler and Steam Turbine

(Fig. 5)

The 41 m high double-draught boiler stands in a boiler-house up to 20 m above datum, the upper part being surrounded by corrugated asbestos sheeting. The combustion chamber is square in plan view, the four lignite-dust burners being arranged at the corners.

A diesel-oil firing system, which can be used up to 12% of the boiler capacity, is employed for starting the boiler. Three hammer mills, each with a capacity of 50 t/h, are used for pulverizing the lignite, a fourth being held in reserve. Hot gas is extracted from the combustion chamber to dry the lignite in the mills. Two pairs of radial f.d. and i.d. fans attend to the throughput of air and flue-gas, the actual exchange of heat taking place in two Ljungström heaters. After passing through a pair of electrostatic precipitators, the flue-gas, cleaned of all fly-ash, is expelled through the 105 m high chimney.

The slag from the combustion chamber is removed by a wet deslagger and belt conveyor, the ash from the second boiler draught and from the precipitators being removed pneumatically. Slag and ash are collected in a common bunker, from where they are conveyed by rail to the lignite mine.

The two-cylinder steam turbine, without reheat, provides the bled steam for a three-stage low-pressure and a two-stage high-pressure feed-heat system. Feedwater heater No. 4 is designed as a mixer with de-aerator and feedwater tank. The hydrogen-cooled generator, the main and pilot exciters are rigidly coupled to one another. The turboset is mounted on concrete foundations with a very low resonance frequency. An evaporator was dispensed with because a demineralization plant (capacity $2 \times 7{\cdot}5$ m³/h) was provided to prepare the boiler feedwater. A starting bypass for a maximum of 90 t/h allows the live steam to be conveyed direct into the condenser, bypassing the turbine, condensate being injected for cooling.

Fuel Supply

The specification laid down the following conditions for the fuel supply.

The fuel from the mine is to be carried into the power-station area, and the ash and slag disposed of in special railway wagons, each holding 40 t and with a gauge of 1 m. From the wagon the lignite

TABLE II

Quality of the fuel		A	B	C
Proportions delivered	%	40–50	40–50	5–10
Upper calorific value	kcal/kg	1850–2150	1500–1800	1000–1500
Moisture content	%	55–60	55–60	55–60
Ash content	%	5–8	8–12	12–24

Minimum stipulations: Upper calorific value not less than 1500 kcal/kg
Ash content not more than 13 %
Moisture not more than 55 %

proceeds to a closed bunker, where it is stored. The bunker can hold 3500 t, corresponding to the consumption over a period of 24 hours at 70 MW output, and, assisted by two ejector trucks, can deliver 450 t over each of a pair of belt conveyors. These two transport systems convey the lignite over magnetic separators, automatic scales and shaking grids into the four hoppers of the boiler bunker. A branch before the shaking grids allows the fuel to be taken to an outdoor stockyard with a capacity of 300 000 t, instead of to the boiler. From there bulldozers push the fuel into the storage bunker. Apron feeders carry the lignite from the hoppers to the four hammer mills, in which the fuel is pulverized.

Water Supply

(Fig. 6)

As regards the water supply for the operation of the power station, the contract refers to the Soulu, a stream flowing close by the site, with a minimum flow of 500 m^3/h and a few artesian wells within a radius of about 2 km, having a depth of 200 m and yielding different, but quite small volumes of water. In order to ensure an adequate supply of water, a comprehensive study of the surrounding area had to be made, with the assistance of Greek experts. Since no reliable flow measurements were available for the stream, a measuring

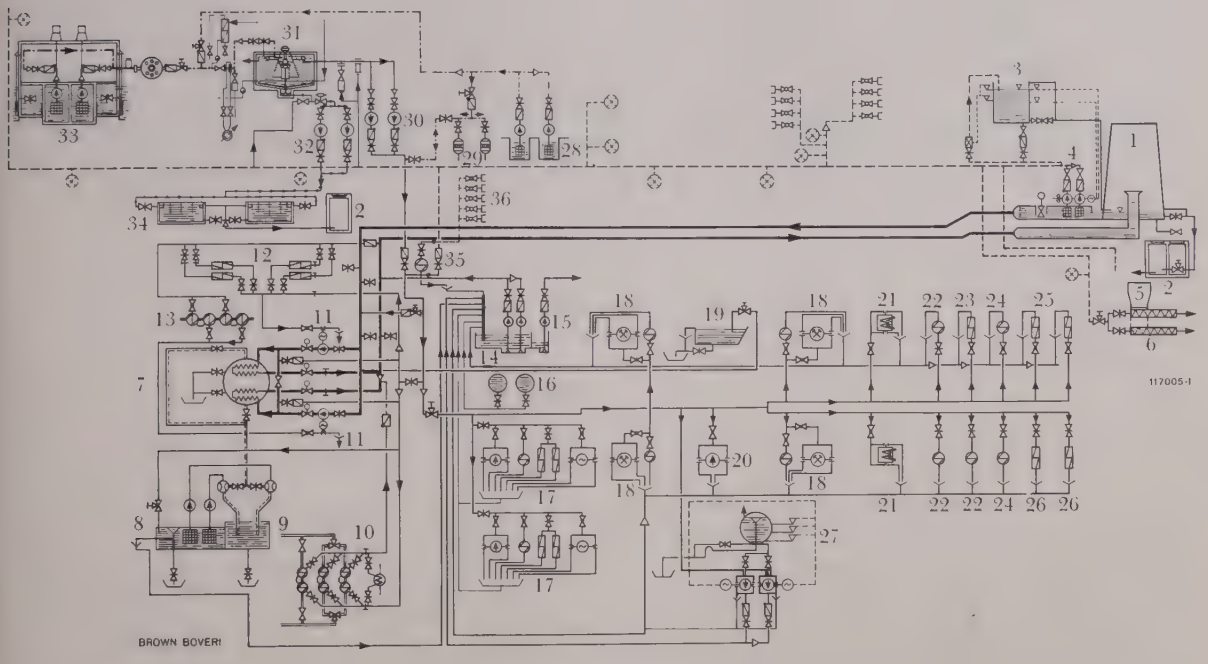

Fig. 6. – Cooling-water system of Ptolemais power station

1 = Cooling tower
2 = Drainage sump
3 = Cooling-water reservoir
4 = Fire extinguisher pumps
5 = Ash pumps
6 = Wetting conveyor
7 = Condenser
8 = Spray-water basin
9 = Main oil cooler
10 = Gland-steam condenser
11 = Main cooling-water pump
12 = Hydrogen cooler
13 = Sealing-oil cooler
14 = Water recirculating pump
15 = Sludge pump
16 = Condensate tank
17 = Boiler feed-pump
18 = Coal mills
19 = Wet-ash conveyor
20 = Starting pump
21 = Air heater
22 = After-cooler
23, 25 = Ash removal compressors
24 = ID fan
26 = General compressor
27 = Reservoir for water drained from boiler and condenser
28 = Well pumps
29 = Cooling filter
30 = Clean-water pumps
31 = Water-softening plant
32 = Sludge pumps
33 = Raw-water pumps
34 = Settling basin
35 = Air-conditioning plant
36 = Bunker house

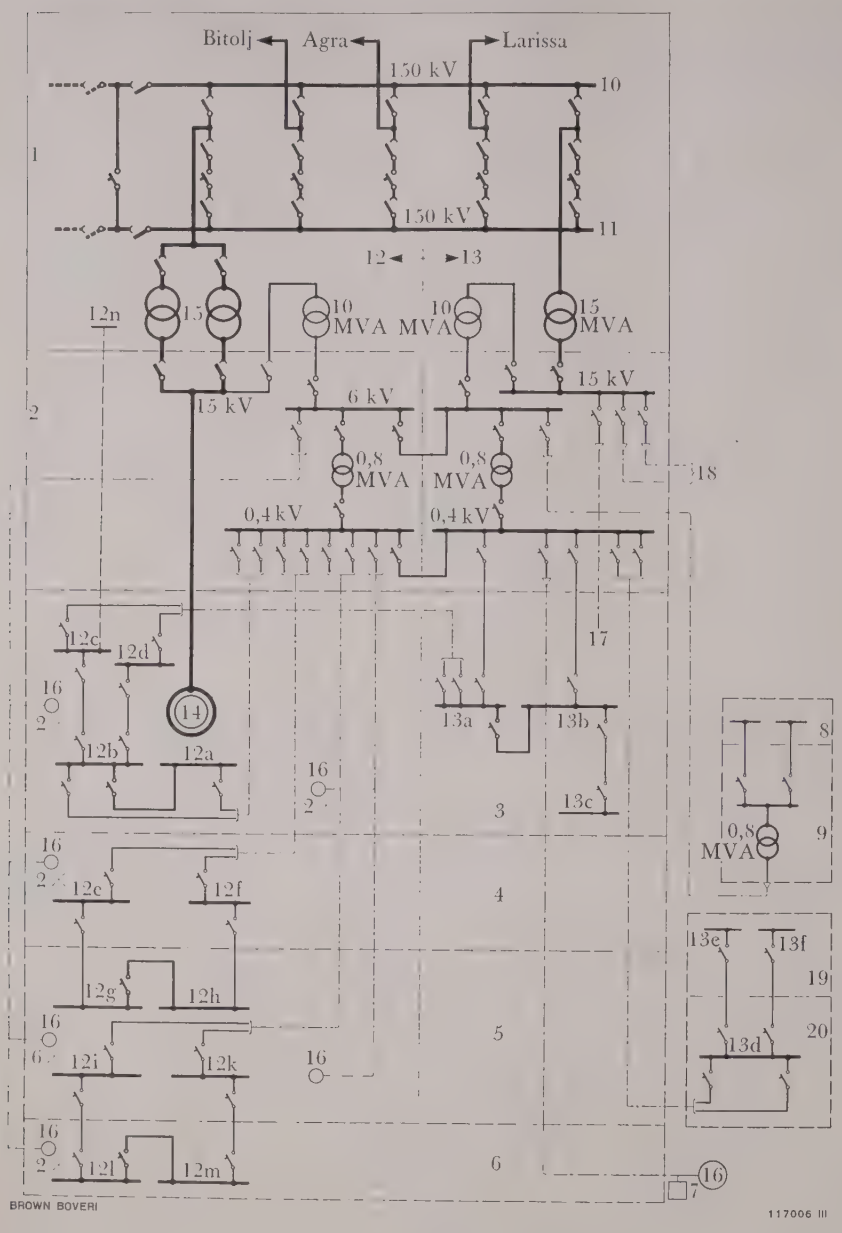

Fig. 7. – Electrical diagram of Ptolemais power station

1 = Switchyard
2 = Indoor switchgear
3 = Machine house
4 = Bunker house
5 = Boiler-house
6 = Precipitator
7 = Cooling tower
8 = Coal pulverizers
9 = Coal transfer point
10 = Auxiliary busbars
11 = Main busbars
12a–n = Unit auxiliaries
13a–f = General auxiliaries
14 = Generator 82 MVA
15 = Main transformers 2×42 MVA
16 = Motors (see Table III, page 839)
17 = Electric boiler
18 = Local supply system
19 = Workshop
20 = Water treatment

point was set up and a daily record of the flow made. The results obtained in the course of a year exhibit the remarkable fluctuation of 480–2000 m³/h.

In order to assure a steady flow of water, the client had specified the erection of a dam across the Soulu. On the basis of the continuous water measurements and the soil soundings performed by local and foreign experts, the dam project gradually matured to the client's satisfaction. The reservoir, with a total capacity of about 300 000 m³ affords adequate storage capacity, as well as ensuring uniform flow. When producing the full output of 70 MW, the station requires about 200 m³/h of water, so that the full reservoir contains enough water for about a month. The building work on the dam, including excavation of the basin, lasted just over a year.

In view of the limited water supply, a cooling tower was provided, in order to minimize the quantity of sludge. For the make-up water a mechanical filter and de-mineralization plant were supplied.

Fig. 8. – View of the switchyard at Ptolemais

Portal frames of hot-galvanized rolled-steel sections.

From left to right: Sections 1 and 3 for the outgoing feeders to Larissa and Agra. Section 6 for the future line to Bitolj.

The intention was for the reservoir to supply all the make-up water; but since it is generally so turbid, due to the mud and stones carried down by the water, the make-up and drinking water (maximum demand 7·5 m^3/h) is normally drawn from two groundwater wells, each capable of yielding 100 m^3/h.

This over-dimensioning of the water supply is justified, since it must be possible to draw on the wells for make-up water in the event of the Soulu carrying insufficient water. Owing to the fact that, when the wells were being sunk (60 cm diameter), one of them could not be taken more than half the desired depth, but it was nevertheless productive, there are now the following wells available: two with a depth of 210 m, each producing 100 m^3/h and one 100 m deep, producing 50 m^3/h.

Electrical Equipment

(Fig. 7, 8 and 9)

For the connection of the 150 and 15-kV equipment the client's specification had to be observed, while the rest of the switchgear, for the station supply service, could be freely chosen to suit the operating conditions of the mechanical equipment, and to comply with the stipulation of maximum reliability.

The connection of the 150-kV switchgear with main and auxiliary busbars allows the transfer breaker to be kept as a reserve for any other breaker. Moreover, by suitably connecting the longitudinal isolators, the transfer breaker can be used as reserve for the present, first busbar section, and also for a second, future set of busbars. To counteract the

Fig. 9. – Outdoor switchgear

Left: Airblast breakers for 150 kV, 3500 MVA, with combined control unit for breaker and isolator

Right: Isolators

difficulty in switching over the protective and metering circuits when the transfer breaker is employed as an emergency breaker, the instrument transformers for each bay are connected in the line section outside the portion disconnected by the isolators.

The airblast breakers supplied have a breaking capacity of 3500 MVA and are equipped with carrier transfer for single and triple-pole rapid reclosure. This reclosure facility, however, cannot be taken into service until the existing breakers in the substations at Agra and Larissa have been modified. The circuit-breakers and the pneumatically operated isolators can be locally controlled from the cabinets, or remote controlled from the central control room.

The 15-kV switchgear is for three feeders for the supply into the local network, for a fourth connecting with the nearby Liptol briquette factory's power station, and a fifth supplying the electric boiler used for the general heating when the station is idle. The metalclad switchgear contains airblast breakers for a rated voltage of 20 kV, with a breaking capacity of 400 MVA, enclosed in drawout units. These are housed in the switchgear building with the 6-kV equipment.

A voltage of 6 kV was chosen for the larger motors of the auxiliaries, and 400 V for the remaining services. The 6-kV switchgear is also metalclad, like the 15-kV gear, and contains airblast breakers for a rated voltage of 10 kV with a breaking capacity of 400 MVA. It is subdivided into a unit for the

turboset and a general service unit, interconnected by means of a transfer breaker. For the low-voltage supply ironclad distribution gear is employed which, for the main circuits, is also divided into two groups, e.g. 12a and 12b, interconnected by a transfer breaker. Each group is separately fed from the main supply centre, thereby assuring maximum possible reliability. Appropriate steps have already been taken to enable the system to be extended in the future, by the provision of additional feeders. The supply to the auxiliaries in accordance with the disposition of the distribution gear is illustrated in Fig. 7.

The lighting scheme covers the supply to the interior lighting in the building, the exterior lighting in the power station area and for the coal stockyard, and floodlighting of the walls for special occasions. The layout of the lighting distribution gear, which was supplied by Brown Boveri, Mannheim, is shown in Fig. 10.

In order to keep the short-circuit power as low as possible, the Brown Boveri electronic phase-comparison unit is used to switch over the auxiliaries. This task can be performed with a very short dead period and a correspondingly low run-up current for the motors. In oscillogram a in Fig. 11 can be seen the trace of a slow switchover, while b shows a rapid changeover from "General" to "Unit" and c the reverse. A noteworthy feature is the much smaller and shorter duration of the run-up currents of the motors. Thus the change from one auxiliary supply to another involves much smaller current surges and consequently reduces the stresses on the transformers, thereby enhancing the reliability of the installation.

The motors for the auxiliaries are all of the squirrel-cage type for direct-on-line start, and are mostly totally enclosed. Tables III and IV list the various motors employed.

By far the greater part of the consumption of the auxiliaries is shared between twelve high-voltage motors, which consume about 75 % of the auxiliary power.

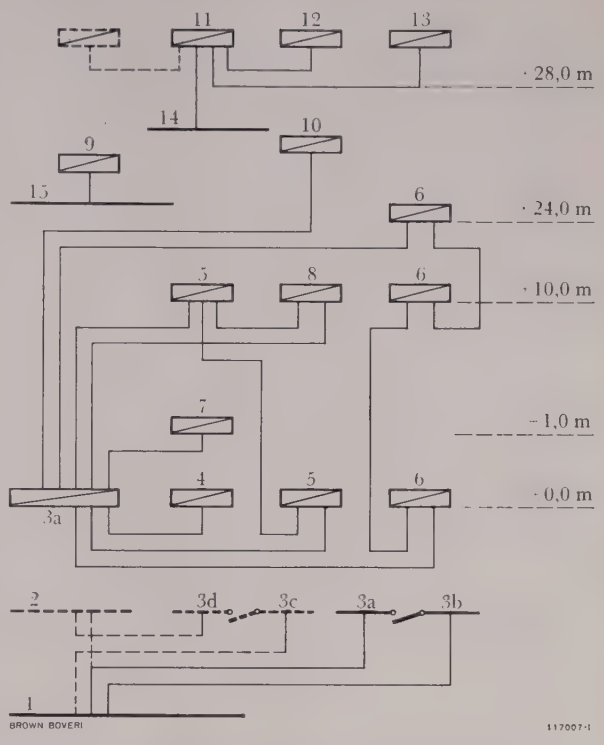

Fig. 10. – Lighting distribution scheme for Ptolemais power station

1 = General distribution, first phase
2 = General distribution, future extension
3a–d = Main lighting distribution for units 1–4
4 = Switchyard
5 = Machine house
6 = Boiler-house
7 = Switchgear bay
8 = Control room
9 = Coal handling plant
10 = Fuel conveyor bridge
11 = Workshop
12 = Water treatment plant
13 = Laboratory
14 = Supply taken from water treatment plant (corresponding to 13d in Fig. 7)
15 = Supply taken from fuel handling station (corresponding to 9 in Fig. 7)

Particular care was devoted to the choice of cables and laying them. The various kinds of cable used are listed in Table V.

The routing of the cables was settled in the preliminary planning and needed very little correction during erection. The cables are supported on prefabricated, galvanized trays with an overall length of 400 m, which could be assembled on site without any welding and with the minimum of adaptation.

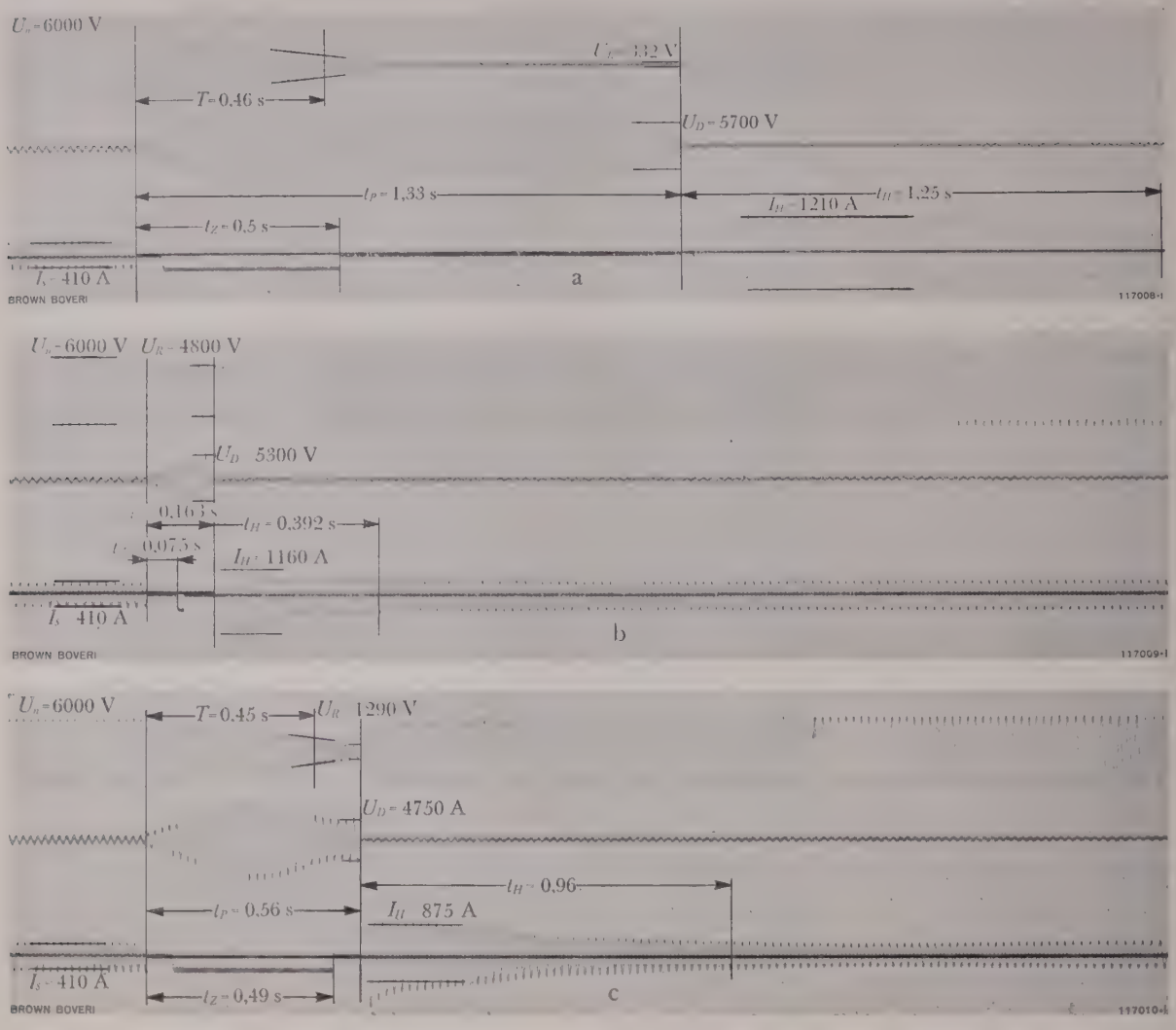

Fig. 11. – Switching over the auxiliaries with the electronic phase-comparison relay

a: Slow switchover
b: Fast switchover from general to unit distribution system
c: Fast switchover from unit to general distribution system
U_n = Rated voltage of 6-kV busbars
U_R = Residual voltage immediately before switching over
U_D = Voltage difference at the instant of reclosure
I_s = Steady-state service current
I_H = Starting current
T = Time taken by the residual motor voltage to reach 37% of rated value
t_H = Starting time
t_P = Dead time
t_Z = Time, measured from the start of the dead time until the thyratron fires

In this way it was possible to considerably reduce the erection time. Fig. 12 shows part of the main cabling between the switchgear bay and the storage bunker. The wiring for lighting, telephone, loudspeaker system and clocks was laid in steel conduit and soft-metal conduit.

The electrical control room (Fig. 13) is immediately adjacent to the thermal control room, separated only by a glazed partition. This arrangement was specified by the client with the object of promoting close collaboration between the two control points and, if necessary, allowing savings to be made in the control centre. In order to obtain the shortest possible leads between the machine room and the boiler-house, the control room was located between these two, in the bunker building.

TABLE III

Summary of the auxiliaries

Distribution system (see Fig. 7)	Number of motors	Total power kW	Mean load factor	Purpose	Location
Station service: Unit					
6 kV	12	8350	0·6	Boiler feed-pump, ID and FD fans, mills, cooling-water pumps	Machine and boiler-house
0·4 kV (Main)	5	663	0·45	Compressor for pneumatic ash disposal	Machine and boiler-house
12a and 12b	9	158	0·25	Cooling-water pumps and accessories	Machine house
12e and 12f	12	105	0·35	Apron feeders and accessories, starting pump	Bunker house
12g and 12h	16	94	0·3	Pneumatic conveyors, ash-removal conveyors, oil-firing pumps, etc.	Boiler-house
12i and 12k	12	65	0·6	Aux. boiler pumps, air heater, etc.	Boiler-house
12l and 12m	11	15	0·6	Fans, aux. pumps, dust knockers, etc.	Precipitator
12a and 12b 12g and 12h 12i and 13b	19	9	—	Air heaters for central heating	Machine and boiler-house, workshop
12c	7	45	0·6	Turbine auxiliaries	Machine house
12n	36	5	—	Fans for cooling transformers	Switchyard
Station service: General					
0·4 kV (Main)	3	219	—	Compressors, fire pump	Precipitator, cooling tower
13d	20	132	0·7	Water pumps	Water treatment
13e, 13f	22	90	—	Machine tools	Workshop
13a, 13b	16	252	—	Switchgear, compressors, cranes, lifts, well pumps, etc.	Miscellaneous
13c	3	17	—	Electric boiler, auxiliary drive	Machine house
Lighting (main dist.)	7	23	—	Hydrogen electrolyser, air-conditioning plant	Electrolysis plant, machine house
Local network substation	8	151	—	Raw-water pumps, winches	Intake
Fuel handling	30	707	0·55	Conveyors, crushers, etc.	Bunkers, crusher house

The electrical control room contains all control, protective and signalling elements concerned with the output of energy, from the generator terminals to the outgoing overhead lines for 150 and 15 kV. Also included are the controls for the input to the station service system. The thermal control room, on the other hand, contains the electrical controls for the auxiliaries belonging to the turbine and boiler.

The desk in the control room contains the central station of a loudspeaker system and two-way telephone sets for communication between the carrier networks erected by Brown Boveri and Siemens, or the public telephone system and the house system.

TABLE IV

Summary of the total power of the auxiliaries

Motors	Number	Total rating kW	Mean load factor
6 kV (unit)	12	8 350	0·6
0·4 kV (unit)	108	1 150	0·4
6 + 0·4 kV (unit)	120	9 500	—
Total general	128	1 600	—
Total all motors	248	11 100	0·57

TABLE V

Summary of cables used for the auxiliaries at Ptolemais power station

Purpose	Length m	Type	Connections	Connected by
Power cables				
15 kV	950	Hochstädter multicore armoured and served	18 (each 3-core)	cable end-boxes
6 kV	2 400	Multicore armoured and served	34 (each 3-core)	cable end-boxes
0·4 kV	9 000 appr.	Plastic insulated and sheathed	700 appr. (each 4-core)	cable shoes
Control, metering, etc.				
Control and metering	40 000 appr.	Plastic insulated and sheathed	1 500 appr. (each 2 to 16-core)	—
Lighting, telephone, loudspeaker	43 000 appr.	Plastic ins. & sh. Plast. ins. & arm. Rubber covered	—	—

Also in the electrical control room is the gear for checking the frequency, comprising a secondary clock controlled by a master clock, showing the exact astronomical time, with a synchronous clock controlled by the mains frequency, and an adjustable differential clock which automatically indicates the positive or negative deviation from the desired frequency of 50 c/s. This system is combined with the general clock system, the master clock of which controls seven secondary clocks in the various parts of the station by impulses.

For the carrier-frequency telephony and telemetering special conditions had to be fulfilled: on the one hand the links over the 150-kV lines to Agra and Larissa had to be fitted into the existing system and the distance protection system installed at the time by Siemens, the latter firm being asked by Brown Boveri to supply the supplementary equipment; on the other hand, for Ptolemais power station a number of extra communication channels had to be provided, having particular regard to future extensions, and these could not be accommodated in the existing system. Consequently, in addition to the existing system, a Brown Boveri single-sideband carrier system was supplied for indication and cyclic telemetering, as shown in Fig. 14. In this manner a direct, extensible link, only passing through Lamia substation, could be established with Rouf substation near Athens, which will eventually be the system control and load dispatching centre for the whole network.

Transport of the Mechanical and Electrical Equipment

Having carried out comprehensive preliminary calculations regarding the transport facilities, the decision was made in favour of land transport. All material was handled by a single transport firm, thereby effecting a marked rationalization. The total transport volume for the mechanical and electrical equipment amounted to 615 railway wagon-loads, with a total weight of 7700 t.

Fig. 12. – Cable passage between bunker house and the switchgear bay

The cables are laid on prefabricated trays of galvanized iron. Sections are bolted together without any welding.

Erection of the Equipment

The mechanical and electrical equipment of the power station erected by the Company under the terms of the general contract, included items supplied by over 40 firms, the suppliers of all the items belonging to the boiler only being counted as one firm. In principle, the organization was so arranged that each supplier unloaded his own material from the railway wagons and erected it with his own personnel, according to a time schedule worked out by the general contractors. The necessary number of unskilled labourers was provided by the general contractors to meet the requirements of the particular supplier. The Chief Erector appointed by the Company was in charge of all erection work. At his

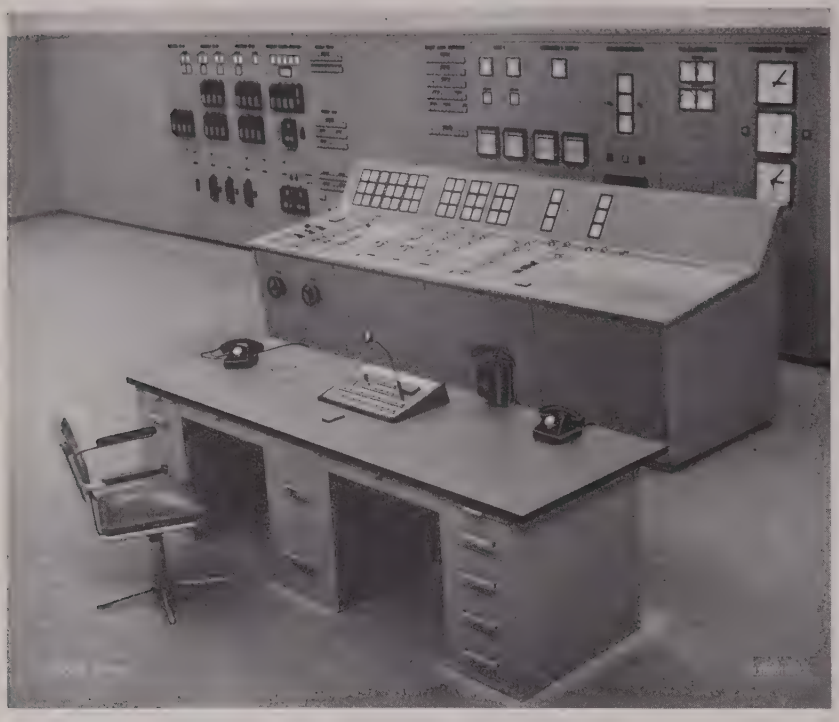

Fig. 13. – Electrical control room

Left, in the background, are the relays and the switchboard for the 15-kV equipment, then the signalling, metering and recording panels for 150 kV, with the synchronizer, telemetering equipment, clocks and frequency control set. In the middle is the control desk for the generator and the 150-kV equipment. In the foreground is the supervisor's desk with loudspeaker system.

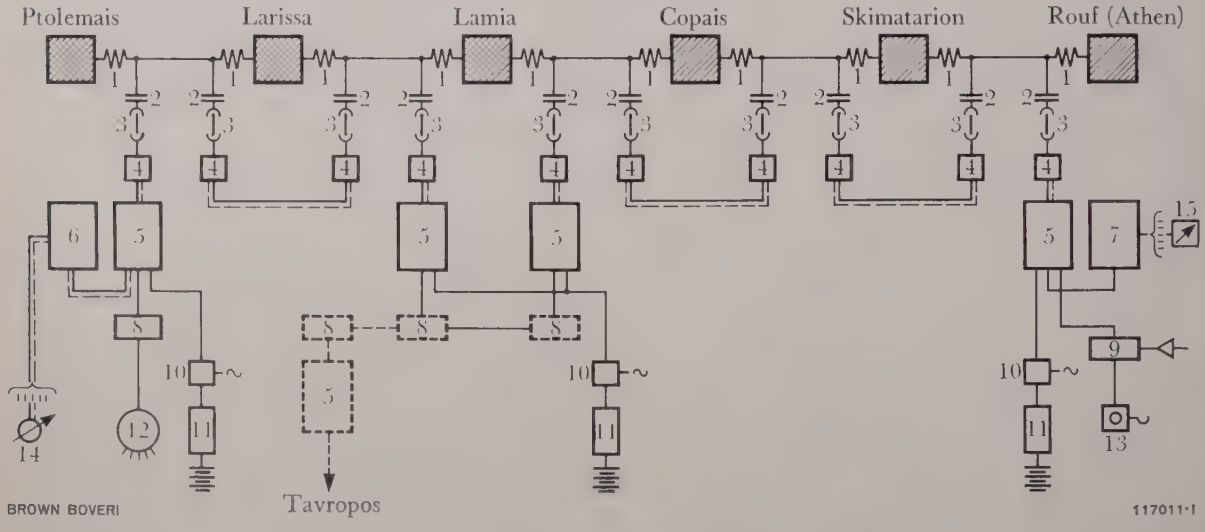

Fig. 14. – Telephony and telemetering using power line carrier equipment

1 = Frequency trap
2 = Coupling capacitor
3 = Protective gear
4 = Line-matching unit
5 = Single-sideband set
6 = Cyclic telemetering transmitter
7 = Cyclic telemetering receiver
8 = Coupling transformer with direct four-wire connection
9 = Subscriber's transformer
10 = Automatic changeover unit
11 = Emergency generator set
12 = Branch exchange
13 = Subscriber's phone
14 = Transmitting instrument
15 = Receiving instrument

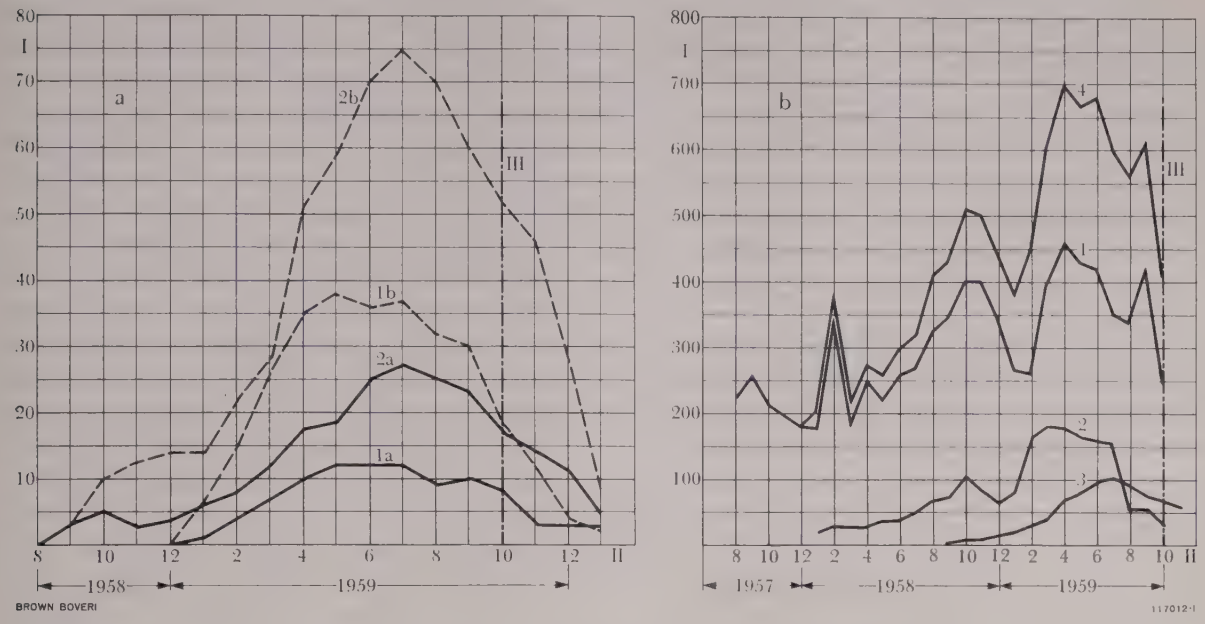

Fig. 15. – Number of persons engaged on building and erection work at Ptolemais power station

a: Ratio of unskilled workers to Brown Boveri erectors

I = Ordinates: Monthly average of the number of workers

II = Abscissae: Time in months of 1958 and 1959

III = Date of commissioning

1a = ——— = Brown Boveri erectors engaged on erecting the turboset, condensing plant and accessories

1b = - - - - - = Greek labourers engaged on erecting the turboset, condensing plant and accessories

2a = ——— = Brown Boveri erectors engaged on erecting the electrical equipment, including power and light distribution systems

2b = - - - - - = Greek labourers engaged on erecting the electrical equipment

b: Curve showing the total numbers of local and foreign workers on the site

I = Ordinates: Monthly average number of persons working

II = Abscissae: Building and erection time in the years 1957, 1958 and 1959

III = Date of commissioning

1 = Number of workers engaged on the building

2 = Number of workers engaged on the mechanical part: boiler, turboset, fuel handling plant, etc.

3 = Number of men engaged on erecting the electrical equipment

4 = 1 + 2 + 3 = Total number of men engaged on building and erection

disposal he had an office staff for the accounts and book-keeping, for wages, purchase of materials, and so on.

Fig. 15a shows the ratio of the number of Greek labourers to the number of Brown Boveri erectors for the two main categories—the turboset with accessories, and the electrical equipment. The total number of persons employed on the site is shown in Fig. 15b in the form of a graph. At its peak the curve shows 700 men, six months before commissioning took place. The heaviest power demand for building work (Fig. 16) occurred about eight months before commissioning and was then about 400 kW.

Commissioning Ptolemais Power Station

The station was finally commissioned 37 months after the date of ordering. This relatively long period was partly due to the severe winters, which stopped all work for several weeks (minimum temperature —17 °C), and the spring floods which rendered the site impassable for a time. On October 26th 1959

H.M. King Paul of the Hellenes officially opened the station, in the presence of the Greek Prime Minister and church dignitaries. The work on the dam and the staff village was still not complete at the time, but this did not affect the ordinary operation of the power station. When the power from Ptolemais became available, a number of small generating stations throughout Greece could be temporarily shut down for badly needed overhauls. This had not been possible before, owing to the extremely heavy load and the lack of any other reserve capacity.

C. KOCH
W. STAMM
(KME)

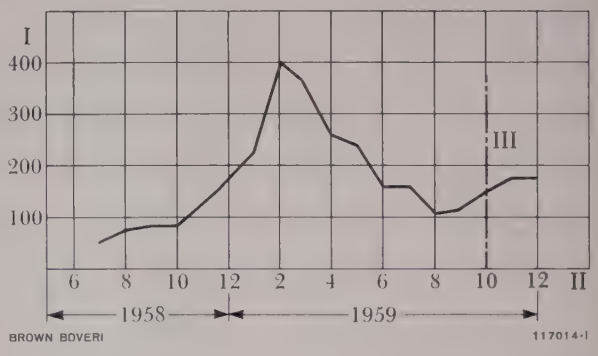

Fig. 16. – Electric power consumption during the period of building from June 1958 till the end of December 1959

I = Ordinates: Power in kW
II = Abscissae: Months during the building period
III = Date of commissioning the station

LOSSLESS CONTROL OF PUMP DRIVES BY SCHERBIUS SETS

621.65/.69–83

When the discharge of centrifugal pumps has to be controlled, the most economical method is to control the speed without loss; then the pump and its drive always operate at a good efficiency. For high powers the incorporation of a Scherbius set is to be recommended. Four installations are described as examples of the use of this system, three in water-works, the fourth being the coolant pumps in a steam power station. Stepwise speed control was chosen for the water-works pumps, thereby obtaining a good power factor for the drive motor over the whole of the control range, without any need for power factor regulation. The speed of the coolant pumps is steplessly controlled. It is interesting to note the different circuit combinations which can be obtained between the pump motors and the Scherbius machines in these installations.

FORMERLY the customary method of conveying liquids, particularly water, over long distances was to use reciprocating pumps driven by steam engines. Such pumps are noteworthy for their high efficiency. Nowadays it is more usual to employ centrifugal pumps which, although their losses are somewhat higher, are far less expensive. Driving by steam engines, however, is a thing of the past; nevertheless its easy control was very popular. Now electric motors are used for driving the pumps. When planning such installations account must be taken of the variation of the discharge with respect to time. In many cases, especially when severe fluctuation may be expected, the ability to control the speed, inherent in the reciprocating steam engine, leads to the most economical solution. But the normal three-phase motor's speed cannot be varied quite so easily; the addition of a Scherbius machine, however, renders it capable of variation [1].[1]

[1] The figures in brackets refer to the bibliography on p. 859.

First a comparison will be made with other well-known systems [2]. The one used most is the three-phase squirrel-cage motor, which is simple, cheap, robust and has a high efficiency. It is ideal when the discharge is constant or subject to only slight variation. A certain degree of adaptability to the fluctuation of the discharge is attained by switching the motor on and off, provided of course the frequent operation at the heavy making current involved is admissible.

The simplest method of controlling the discharge at constant speed is to control the pressure valve. The throttling effect resulting from this causes considerable losses, which reduce the efficiency of a pump. These conditions are illustrated in Fig. 1. The curve H is the pump characteristic. The total pressure head H has to overcome two resistance components, namely the static head and pressure difference H_s between the level of the pressure tank and that of the suction tank, and the dynamic head H_d of the pipeline, which is approximately proportional to the square of the discharge. The characteristic of the pipeline R is also shown, corresponding to this sum; it is a parabola of the form $H_d = f(Q)$ displaced by the distance H_s towards the vertical axis. At full power, i.e. at the point of intersection of the two characteristics, the pump operates with a good efficiency. At reduced discharge the resistance head $H_d + H_s$ is less than the total head H of the pump. The difference has to be dissipated in the valve (cross-hatched area); it appears in the power balance as a loss and it causes the efficiency of the pump to decrease. In the diagram η_p denotes the efficiency of the pump itself, η_D the efficiency when throttled. The vertically hatched area shows the deterioration,

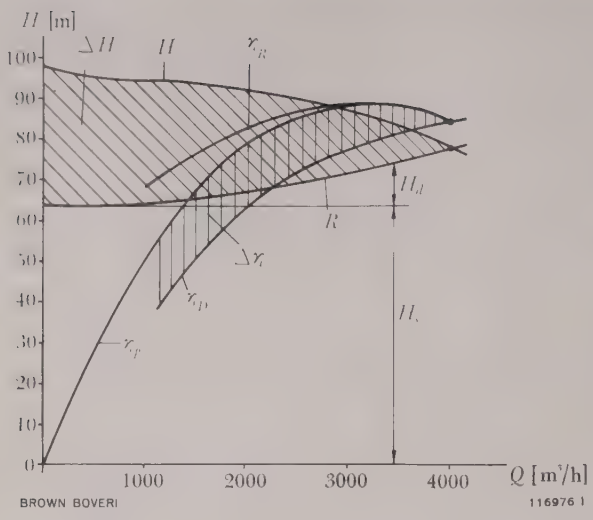

Fig. 1. – Pump diagram with throttle control

Pump data:

Discharge	4000 m³/h
Head	77 m
Speed	985 rev/min
Consumption	960 kW

Q = Discharge in m³/h
H = Characteristic of the pump showing the manometric head in terms of the discharge
H_s = Static difference in head and pressure between the level of the upper and lower reservoirs
H_d = Dynamic resistance head of the pipe-line
ΔH = Loss in head due to throttling
R = Characteristic of the pipe-line
η_P = Efficiency of the pump
η_R = Efficiency with speed control
η_D = Efficiency with throttle control
$\Delta\eta$ = Loss in efficiency

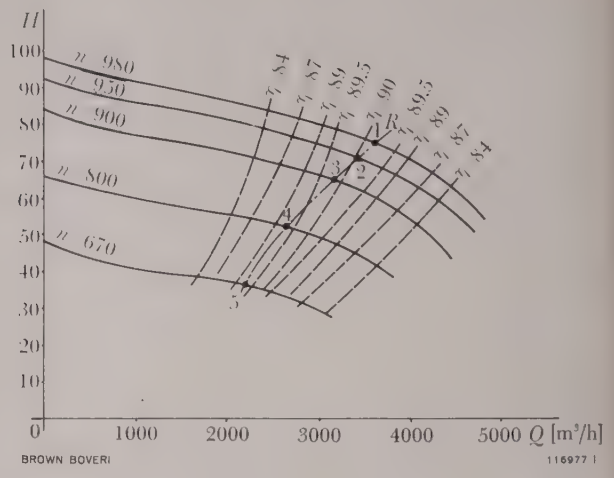

Fig. 2. – Pump diagram with speed control

——H = Pump characteristic: manometric pump head [m] in function of the discharge Q [m³/h] at different speeds n [rev/min]
–·–·– R = Characteristic of the pipe-line
– – – – η = Curves of equal pump efficiency

With speed control the pump can be designed to operate at its optimum point all the time. This method of control is far superior to the others.

it is quite appreciable. Moreover it must be remembered that a certain reserve must be allowed; that is to say, at full power the valve is not quite fully open, so that a slightly larger discharge can be obtained with certainty when the valve is fully opened, and a greater head attained. But then, at full power throttling losses must be taken into account, while at reduced power the pressure has to be throttled more than is essentially necessary. Hence additional throttling losses are always experienced.

If this appreciable deterioration of the pump efficiency is to be avoided, control should not take place at the valve, but should be effected in the pump by displacing the impeller blades. The constructional outlay for this is considerable, and simplicity is lost. Therefore this modification is only likely to be considered in special cases. The task of controlling the discharge of normal pumps, i.e. those with fixed impeller blades, is best performed by varying the speed to suit the requirements and leaving the valve full open. Conditions are illustrated by the diagram in Fig. 2, referring to the waterworks dealt with in greater detail later [3]. Again the characteristics of the pump and pipeline are plotted. The diagram also contains the curves for constant pump efficiency, which are almost parabolic—as will be well known. The pump can now be designed to operate in the vicinity of the optimum point all the time; the pipeline characteristic then almost coincides with the curve of optimum efficiency. But this condition can only be fulfilled by continuously adapting the speed. The deviation of the efficiency of the pump from its maximum value of 90 % is only small for all operating points coinciding with the pipeline characteristic. The favourable efficiency curve can be seen in Fig. 1, values being given in the Table below.

TABLE I

Pump speed rev/min	Point on curve in Fig. 2	Efficiency of pump in %
980	1	89·7
950	2	89·9
900	3	89·9
800	4	89·5
670	5	89·2

If a squirrel-cage motor is still used, the speed of the pump can be controlled by a hydraulic coupling. In this case power is transferred to the oil in the form of heat, corresponding to the speed reduction by the coupling. This, however, results in a similar deterioration of the efficiency as with throttling. The losses correspond to the slip between the motor and pump speeds. When the coupling is full, this amounts to about 2%; the efficiency drops by this amount at full power. It is also an awkward business to dissipate this heat and to devise a design which is absolutely oil-tight. But the three-phase motor can be freed from its synchronous speed, allowing an ordinary rigid coupling to be utilized. The motor is then equipped with slip rings, through which resistors are connected with the secondary circuit. This causes an additional slip, i.e. reduction in the speed. The resistors, which are mostly in the form of liquid resistors, absorb the slip power which has to be dissipated and cannot usually be utilized. The efficiency is therefore reduced as with the slip coupling. This is illustrated by Fig. 3, which refers to the same pump as Fig. 2. The speed, almost exactly proportional to the discharge, is plotted in this case as abscissa.

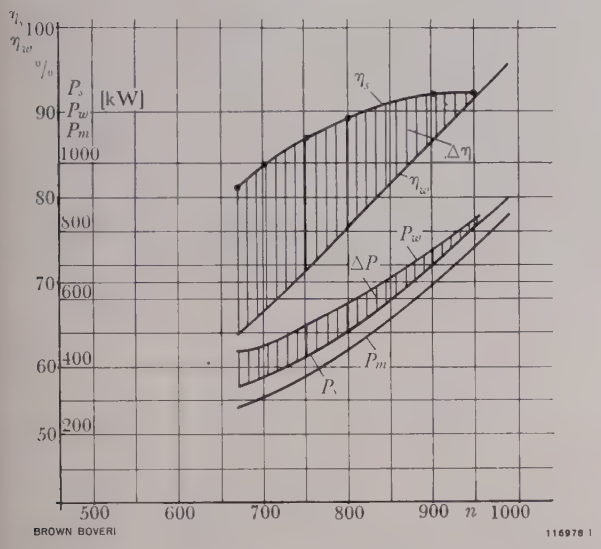

Fig. 3. – Power balance and overall efficiency of a pump drive with speed control by a Scherbius set, compared with control by resistors in the rotor circuit of a slip-ring motor

The following are plotted in terms of the speed n (rev/min):

P_m = Shaft output in kW

P_s = Total power input with lossless control by a Scherbius set (in kW)

P_w = Power consumption with control by a slip resistor (in kW)

ΔP = Additional consumption with resistor control compared with Scherbius control

η_s, η_w = Overall efficiencies with Scherbius and resistor control, respectively

$\Delta\eta$ = Difference in efficiency

• = Measurements taken during acceptance trials

The superiority of lossless control over the resistance method is very evident.

The improvement in the efficiency of the pump by slip control, either mechanically using a hydraulic coupling or electrically with a resistor, is counteracted by the high slip losses. This is intensified by the fact that, as with throttle control, a certain reserve has to be allowed at full capacity, in this case taking the form of additional slip. These methods cannot be considered satisfactory.

When the economics are taken into consideration, the only suitable motor in most cases proves to be one which permits the speed to be controlled without losses, thus enabling the pump to run at optimum efficiency. With a drive of this kind the previously mentioned reserve can be incorporated in the range of control without causing any adverse effect. Moreover, the number of units can be reduced; they are larger and, taken overall, cheaper than a number of small units. The cost of buildings is also lower. Finally, the variable-speed drive affords readier adaptation to such conditions as cannot be foreseen with accuracy in the planning stage. For example, in a waterworks, the resistance of a pipe-line can

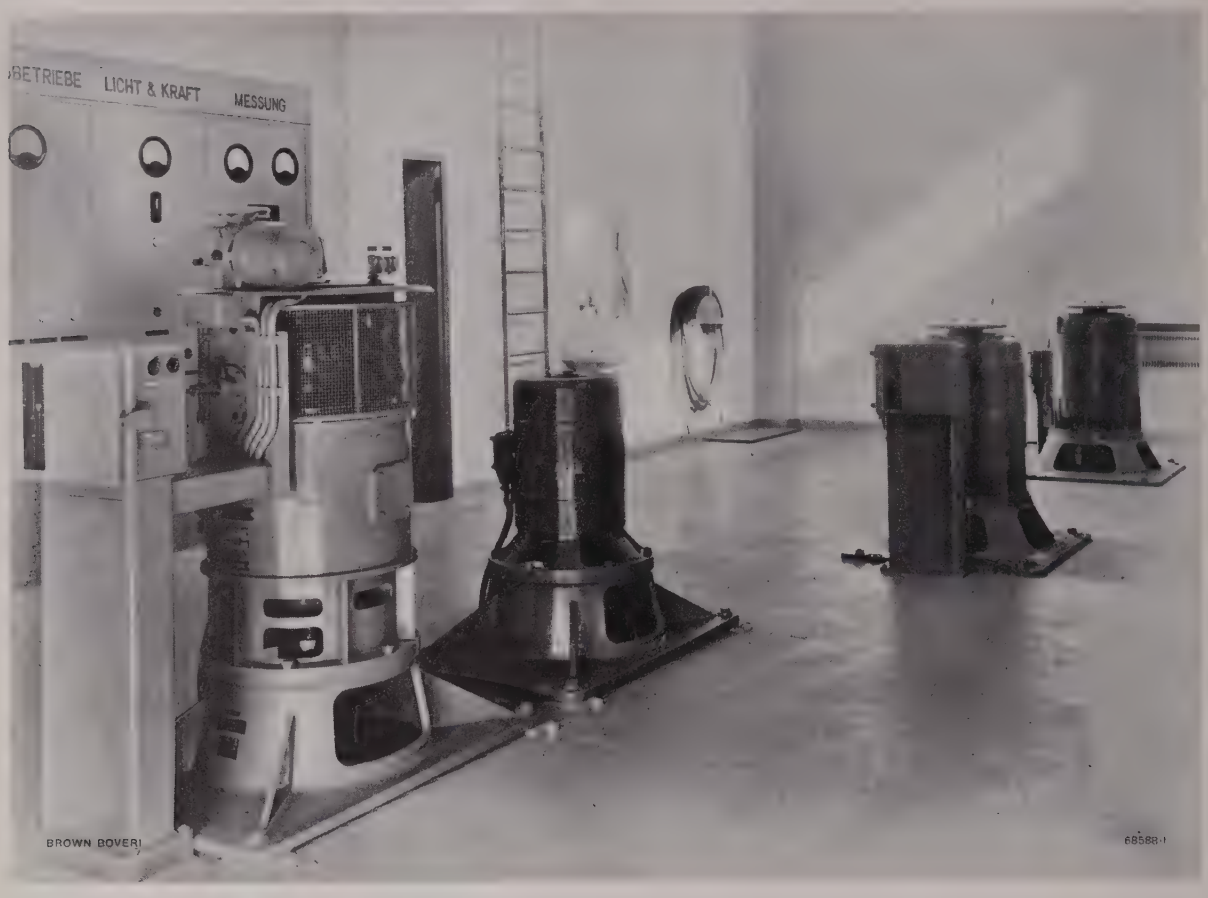

Fig. 4. – Commutator motor driving a pump in a station in Aarau, Switzerland

The motor, on the left, is automatically controlled by a float.

usually only be approximately calculated; sometimes the discharge can only be estimated. In such cases it is possible to cater for the actual conditions by adjusting the speed.

For small powers the commutator motor is an ideal variable-speed motor with no losses. An example of its use is shown in Fig. 4. For driving pumps of larger capacities an excellent method is to use a slip-ring motor with Scherbius control set. The latter, which is connected to the rotor of the motor, absorbs the slip power and transmits it almost without loss, either direct to the pump shaft if connected rigidly, or returns it to the supply system through an auxiliary machine. Hence the Scherbius machine performs the duties of the previously mentioned slip resistance, while avoiding its losses. It is therefore ideally suited to pump drives, for which the limits of speed control are not very widely separated, so that the slip is only small, and the rating of the Scherbius machine low in consequence. If the synchronous point of the pump motor is made somewhere about the middle of the specified speed range, this results in the smallest Scherbius machine and a better efficiency. The optimum efficiency is then obtained at a midway speed, i.e. at a discharge for which the demand is greatest as a rule. The Scherbius machine in no way affects the shunt characteristic of the drive motor. It therefore possesses excellent control properties. The speed follows the control command reliably and quickly since the torque provided by the induction motor for correction purposes is motive as well as generative. There is no need to go into the details of the theory of the Scherbius machine, as this is amply covered in the literature [4].

Four installations will now be described in which Scherbius sets are employed, three being pumping stations for municipal waterworks, the last being

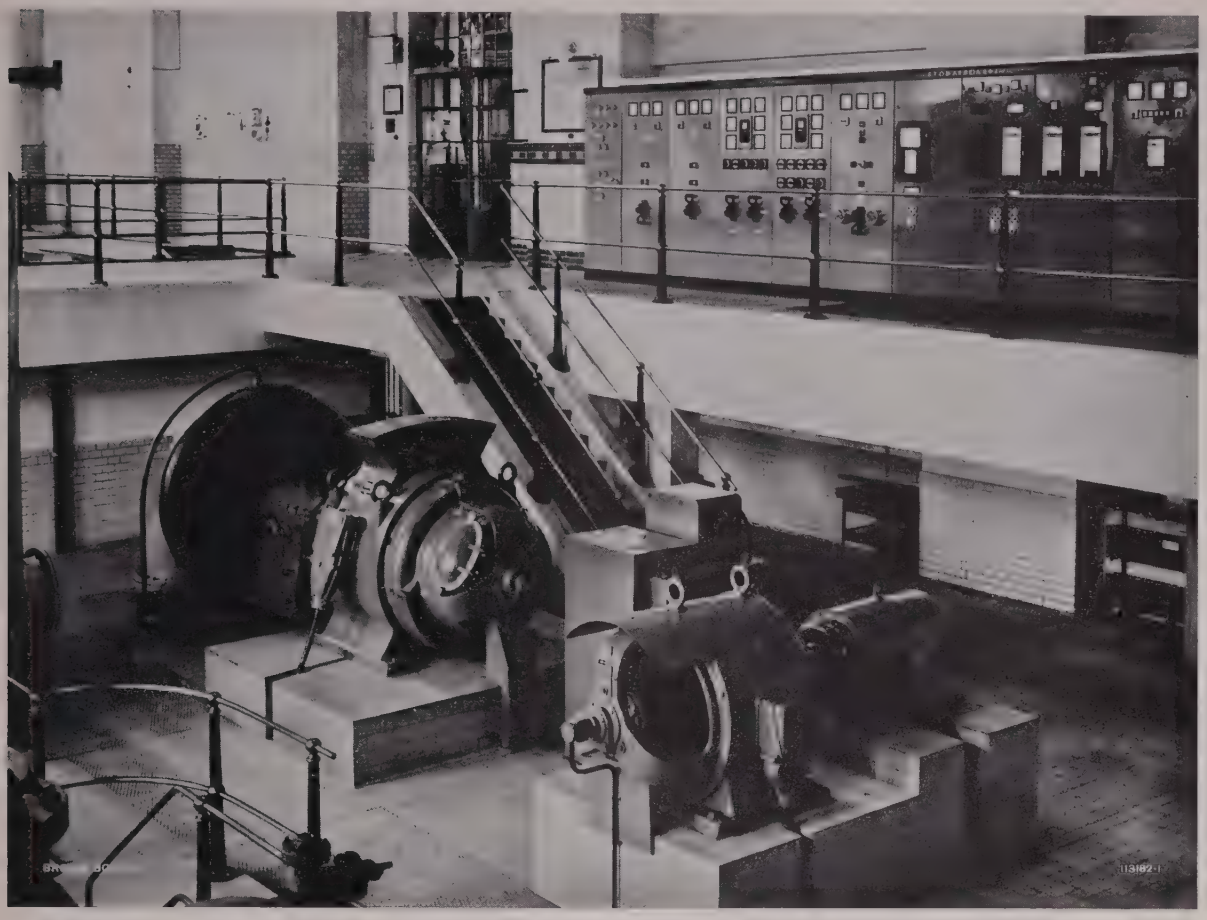

Fig. 5. – Scherbius control set in the Hattersheim pumping station of the Frankfurt-am-Main municipal water-works

At the rear, in the pit, is the centrifugal pump rated 800 kW, in front of it the Scherbius set. To set the speed between 960 and 830 rev/min, thereby varying the discharge, it is sufficient to displace the tap changer on the platform.

the pumps for the cooling water used in the condenser of a large thermal power station. The electrical equipment was built by Brown Boveri, Baden and Mannheim, in collaboration.

Extension to a Pumping Station

In this installation [5] there has been a reciprocating pump driven by a steam engine since 1928; depending on the speed, the discharge varies between 290 and 560 litres per second. In 1957 this station was extended by the addition of a centrifugal pump delivering 350 l/s (Fig. 5). This is driven by an induction motor rated 800 kW at 980 rev/min. The speed can be reduced to 830 rev/min in twelve steps with the aid of a Scherbius machine; this reduces the discharge roughly in proportion.

The circuit arrangement corresponds to the classical system, as shown in Fig. 6. Connected to the rotor of the induction motor *A* is the Scherbius machine *K*. The latter is a three-phase commutator machine with compensating winding, which is a mirror reflection of the armature winding, as in a d.c. machine. Thus, on the one hand, it cancels the effect of the armature on the field while, on the other, it destroys the transformatory voltage component of the armature winding, so that only the component which causes the rotation remains effective. Hence the Scherbius machine supplies a voltage proportional to the flux, like a d.c. machine, although the flux and current pulsate with the slip frequency. Corresponding to the rotor of the drive motor, the Scherbius machine has three phases, allotted to each of which is one pole and one brush rocker, over

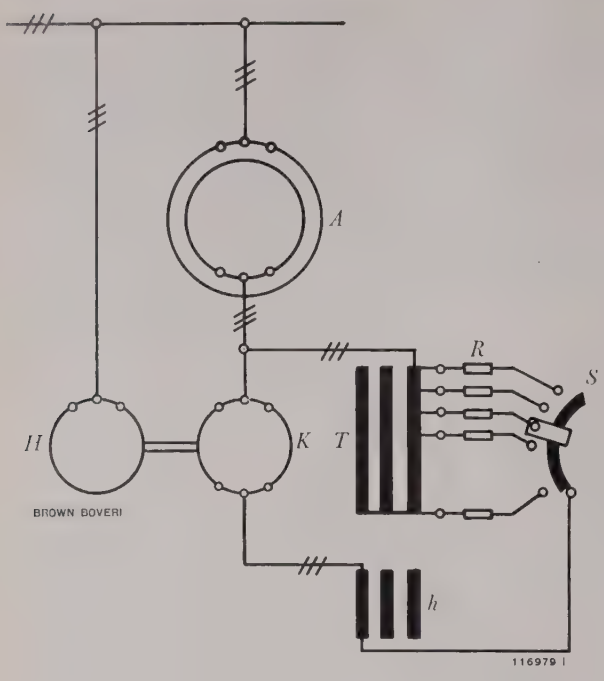

Fig. 6. – Schematic diagram of a normal sub-synchronous Scherbius set

The induction machine *A* transfers its slip power to the Scherbius machine *K*, which returns it to the mains via the auxiliary machine *H*. The Scherbius machine is shunt excited via transformer *T*. By selecting a suitable tapping on the transformer by tap changer *S*, it is possible to vary the speed of the main motor *A*. The power factor can be set permanently during commissioning, so that a correcting element is unnecessary.

R = Adjusting resistor
h = Auxiliary coil of transformer T

an arc of 360 electrical degrees. A three-phase voltage is taken from the brushes, which, as already mentioned, is proportional to the flux of the pole. The pole is excited in shunt via the auto-connected tapped transformer *T*.

Ignoring the voltage drops, the following three equations may be written

$$E_s = c_1 \Phi \quad (1)$$

$$E_e = c_2 s f \Phi \quad (2)$$

$$E_e = r E_s \quad (3)$$

From the above equations,

$$s = \frac{c_1}{c_2 f} r \quad (4)$$

in which

f = primary frequency of the motor A
s = slip of the motor A
$s \cdot f$ = secondary frequency of motor A
E_s = terminal voltage of the Scherbius machine
E_e = voltage of exciter winding of the Scherbius machine
Φ = flux of the Scherbius machine
r = transformation ratio of the transformer T

From the above it follows that the slip is proportional to the ratio of the transformer *T*. By selecting a suitable transformer tapping by means of the tap changer *S*, it is possible to set the speed of the motor *A* direct. A dephased auxiliary coil *h* of the transformer *T* and the adjusting resistor *R* make it possible for the voltage E_s of the Scherbius machine to be displaced in such a manner that the reactive power of the main motor *A* is balanced. This setting is carried out during commissioning; later the power factor is corrected on all tappings of the tap changer. In service it is merely necessary to select the desired speed with the tap changer. The auxiliary machine *H* returns the slip power to the mains. The calculated overall efficiency can be obtained from the following table:

TABLE II

Speed	rev/min	960	920	860	830
Output	kW	758	662	544	486
Overall efficiency	η%	93·83	93·15	91·92	90·86

Pumping Station for an Irrigation Plant

This station pumps water from a large high-head reservoir at the end of a long pipe-line. The same reservoir is also connected to other pumping stations, whose demand fluctuates, so that the water level in the reservoir is continually varying. The pumps in the present case pump the water up into another reservoir, whose level has to be kept constant because this head corresponds to the pressure in the supply network. The static head of the pumps is

equal to the varying difference in the levels of the reservoirs. Such difficult conditions are best fulfilled by means of speed control, as will easily be recognized from the pump characteristic. Fig. 2 applies in this case; for the pipe-line characteristics shown therein the efficiency of the pumps is in the region of maximum under all service conditions. If the water level changes in the lower reservoir—and with it the static head—this corresponds to a parallel shift of the pipe-line characteristic in the vertical direction. But this only results in a very slight change in the efficiency of the pumps.

The speed is controlled in the subsynchronous range, in the same manner as for the previously described installation. Three pumps were installed, two of which are for maintaining the water supply, the third as reserve. Their drive motors are rated 930 kW at 980 rev/min, and their speed can be reduced in 16 steps to 670 rev/min. Since, as stated, not more than two pumps are ever in operation at the same time, only two Scherbius sets were provided, either of which can be connected to any of the three pump motors. This underlines one of the main advantages of installing the Scherbius sets separately: it was possible to dispense with a third set. A favourable feature in this installation is that all motors are alike, and so are the two Scherbius machines. This, however, is not absolutely essential for arbitrary interconnection. At the moment, for instance, a Scherbius machine is being built for connection to four motors of different ratings.

Fig. 3 shows the curve of the overall efficiency, the measurements having been recorded during acceptance trials, based on the output P_m. Also plotted is the operating point without Scherbius machine, corresponding to 850 kW at 989 rev/min. With a Scherbius machine, however, the power factor is unity across the entire speed range.

The machines had to be installed in a narrow pit, so that the vertical design was selected for the pump sets as well as for the Scherbius machines and auxiliary drive (Fig. 7 and 8).

This pumping station is controlled automatically [3]. Floats keep a check on the water level in the two reservoirs. If the level in the upper reservoir drops to the minimum point while that in the lower reservoir is at a maximum, the pumps are switched on, the float contacts being adjustable for each pump, so that they are switched on gradually, and not all at once. They are started up with the valve closed; it is opened when the service speed has been attained. The throughput of the pumps can be controlled in two ways: The discharge is kept constant via a Venturi nozzle by two-step control, in that a contact in the measuring unit increases the speed as soon as a minimum level is attained, or vice versa, with a second contact. Alternatively it is possible to change over to programme control, a time-switch setting a predetermined speed according to the time of day.

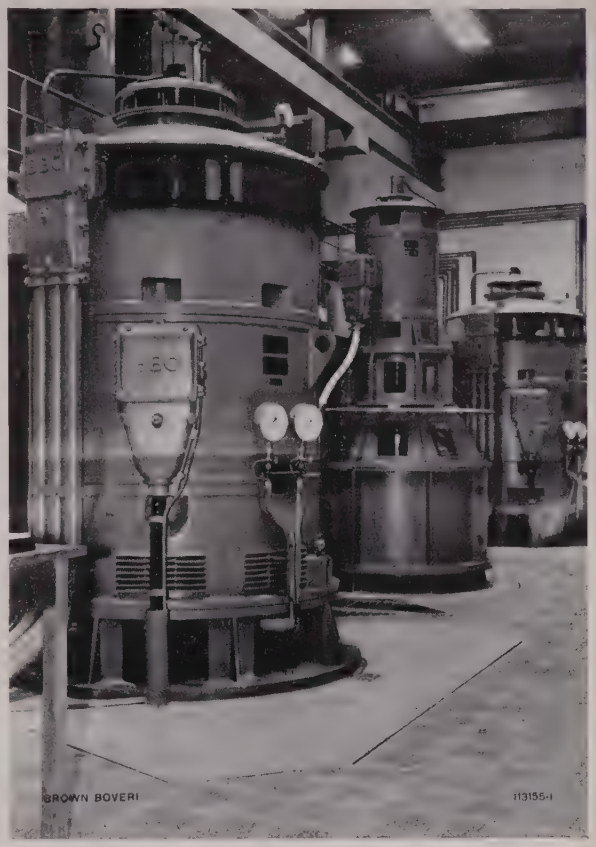

Fig. 7. – Pumping station of an irrigation system

Between the two pump motors can be seen the Scherbius machine with small built-on induction machine. This set is used for lossless speed control of the pump motors. The installation comprises three motors and two Scherbius machines, each of which can be connected to any one of the motors.

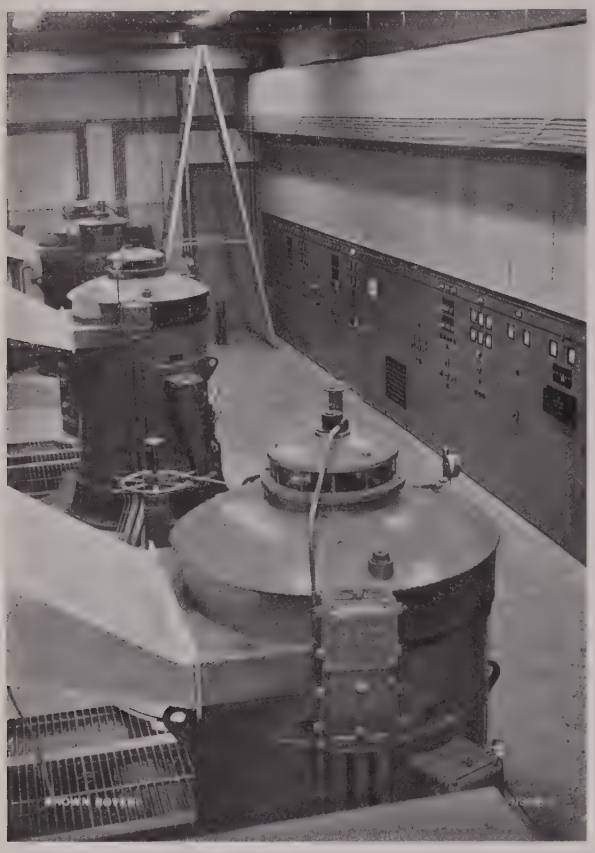

Fig. 8. – Switchgear of the irrigation pumping station

The simplicity of the switchboard gives an indication of how little equipment is needed with a Scherbius control set.

New Municipal Waterworks

As in many other cities, the consumption of drinking water in Hanover has increased considerably in recent years, in fact at a faster rate than the number of inhabitants. The municipal water supply authority therefore decided to counter this trend by erecting a new supply station near Fuhrberg. Planned on a liberal scale, this is a most up-to-date plant and commenced regular service in May 1959. The plant is situated some 25 km north of Hanover

Fig. 9. – Pump-house at Fuhrberg, Hanover city water-works

Three pumps extract the water from the reservoir and pump it through a pipeline to the main station in the city.

and utilizes ground-water from a depth of about 30 m. The water is extracted through a pair of wells with horizontal filters (Fig. 9), drawn off by three submerged pumps and conveyed to the main station 2·5 km away. Here it is treated in accelerators, to remove iron, manganese, H_2S and CO_2, and is enriched with oxygen. The resultant drinking water flows through filters into an underground reservoir holding 5000 m³. From there pumps extract the purified water and convey it through a 60 cm diameter pipeline 24 km long into the city distribution system. In view of the depth of the reservoir, the pumps are mounted in a pit excavated out of the ground. A pair of two-stage centrifugal pumps was selected. Since the floor space in the pit was limited, the vertical design was employed.

During the planning stage, the desire was expressed for the discharge to be variable in three stages. In addition, it was stipulated that these three stages should be variable slightly upwards or downwards. Since this long-distance supply system had not only to cope with fluctuation in the discharge, but also in the pressure, the variation in this case being quite considerable, it appeared advisable for the pumps to be provided with rather a wide control range. As a pump set equipped with a Scherbius control set had given excellent results in another pumping station of the same undertaking, where it was installed in 1930, it was an obvious solution for the same kind of system to be adopted for Fuhrberg. The final installation comprised the following sets of machines. Each pump is driven by an induction motor, the speed of which can be varied above or below the synchronous speed by a Scherbius machine. The two, separately driven Scherbius machines can be connected to either of the pump motors. For the transition through synchronism a commutator frequency converter is required.

The circuit diagram is shown in Fig. 10. This includes the elements of the sub-synchronous circuit (Fig. 6). The slip is proportional to the ratio of the transformer T, as given by equation (4). Each voltage tapping, selected by means of the tap changer S, corresponds to a definite value of the slip, but in this case a negative slip, i.e. super-synchronous speed, can be selected, for which the excitation winding is reversed (indicated schematically at the tap changer). For the transition through synchronism, the shunt excitation of the Scherbius machine is inadequate because the slip voltage collapses. This is where the small frequency converter F comes in. It runs in phase with the rotor of the main motor A and provides a fixed voltage at the slip frequency. Its phase angle is varied by the tap changer S via a suitable tapping on transformer P, which is energized from the mains and has a polygon secondary winding. The excitation of the Scherbius machine from the frequency converter by a voltage of appropriate phase angle allows the main motor to run at the synchronous speed and with a slight super-synchronous slip. Then for higher super-synchronous slip the transformer T takes over the excitation once more. As for the sub-synchronous connection, it is sufficient to set the

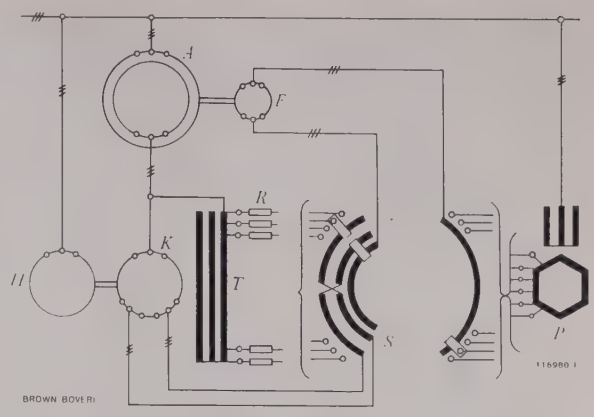

Fig. 10. – Schematic diagram of the normal super- and sub-synchronous Scherbius control set

The sub-synchronous circuit (Fig. 6) is now increased by a frequency converter F, fed from a tapping on the polygon-connected transformer P, connected to the mains; its task is to provide a fixed voltage for excitation of the Scherbius machine, allowing it to pass through the synchronous speed. The speed can be selected over the entire control range merely by means of the tap changer S, which affords power factor correction in all positions.

A = Main motor
T = Transformer
R = Adjusting resistor
K = Scherbius machine
H = Auxiliary machine

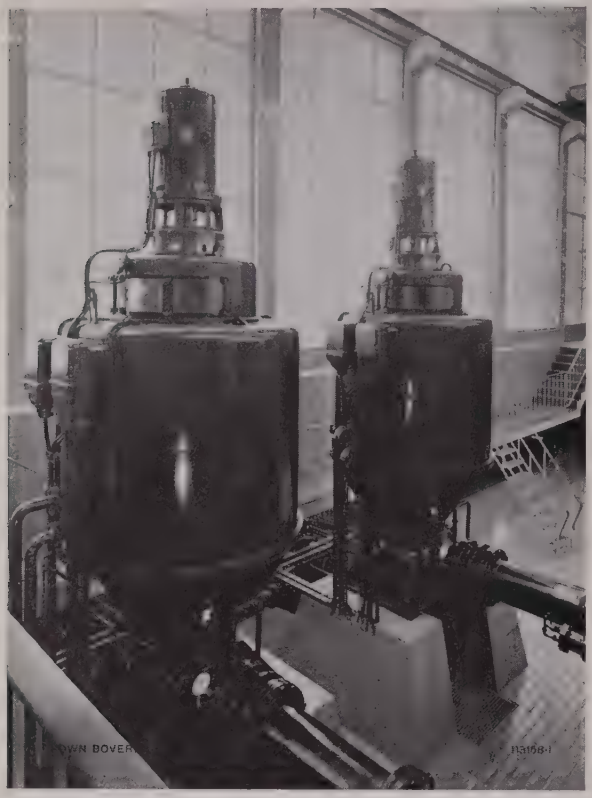

Fig. 11. – Fuhrberg pumping station, near Hanover

Motor rating: 830 kW at 1470 rev/min
Speed range: 1675–1181 rev/min

Each motor is attached to its pump by a mounting cage, the rigidly coupled frequency converter for super-synchronous speeds being fixed on the shaft extension of the motor. To ensure silent running, the motors are totally enclosed with closed-circuit cooling. The slip rings can be observed through a window.

tap changer to the appropriate tapping to select the desired speed. No further measures are necessary. Power factor correction is provided across the entire control range, once the resistor R has been set during commissioning.

Fig. 12. – Pump-room of the Fuhrberg station near Hanover

In the pit at the rear are the two pump sets, on the left an air-pressure vessel, and in the foreground the two Scherbius sets. Each of the latter can be connected to either of the pumps.

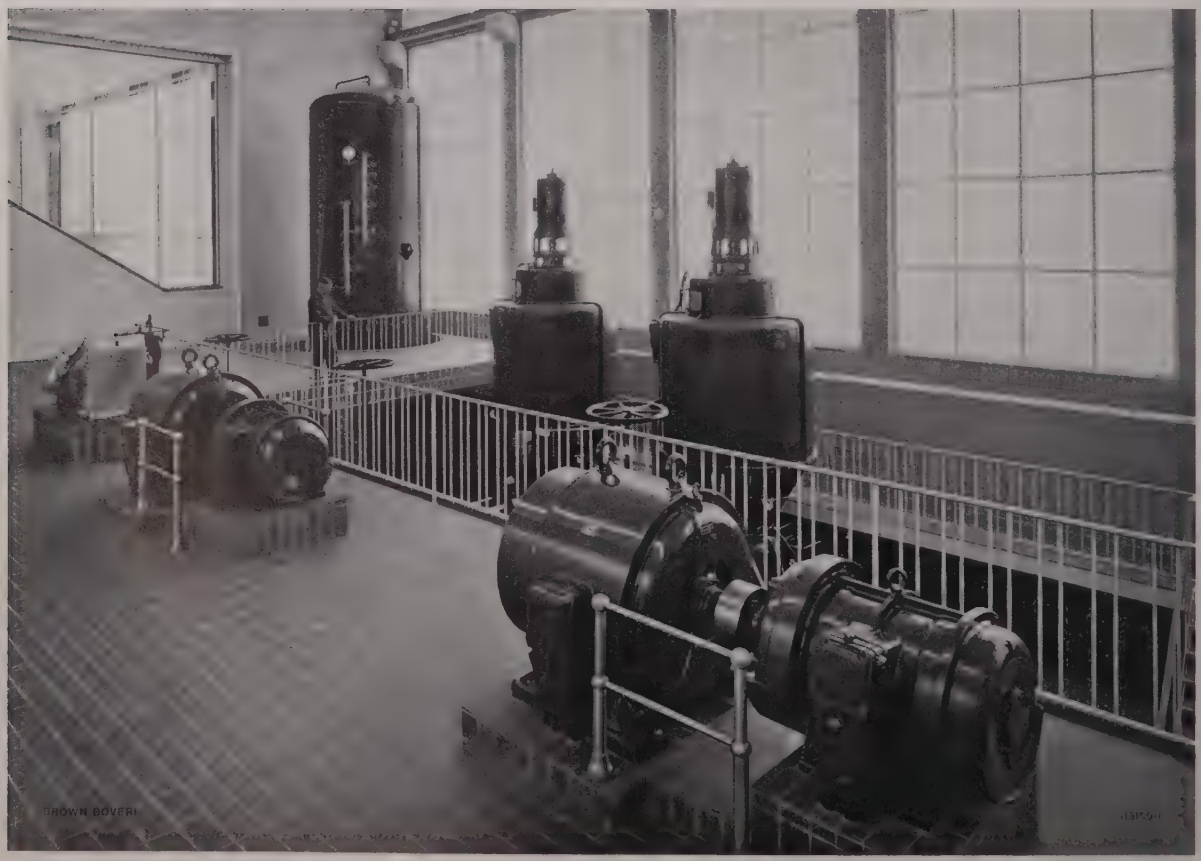

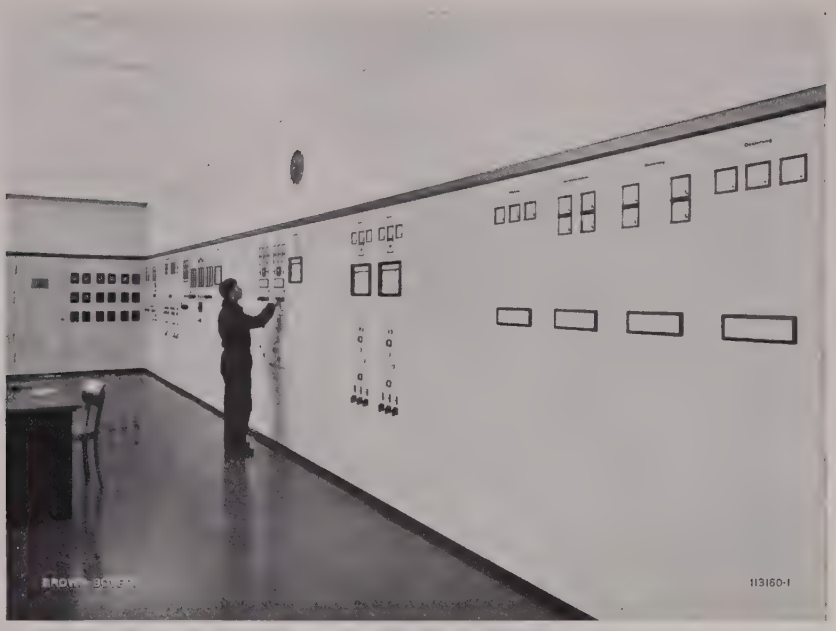

Fig. 13. – Fuhrberg control room

One switchgear cubicle is used to control each motor. To select the speed it is only necessary to operate a switch.

Fig. 11 shows a view of the two pump sets, while Fig. 12 is a view of the pump-room from the control room. Fig. 13 shows the control room, with the supervisor standing in front of the two cubicles from which the pumps are controlled. A glimpse inside the cubicle belonging to one of the Scherbius sets is afforded by Fig. 14.

During the acceptance trials the following performance figures were measured, the speed being 1680 rev/min:

Rate of flow, measured at Venturi nozzles	1805 m^3/h
Head, measured by manometers at the pump	14·15 kg/cm^2
Shaft output	916 kW
Overall efficiency, determined by the method of individual losses	94·25 %
Power factor over the entire control range	almost 1

Further measurements are shown in the form of a curve in Fig. 15. Both the drive and the pump operate at optimum efficiency over the entire range

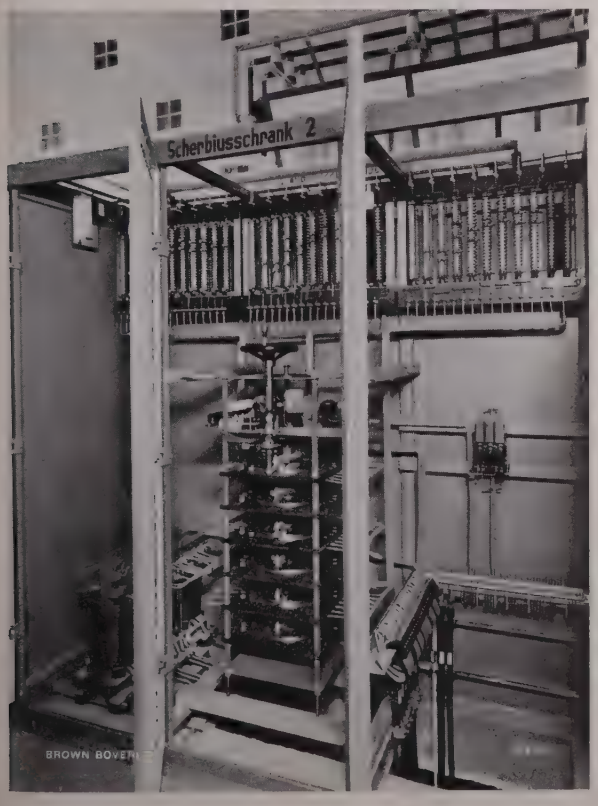

Fig. 14. – Control cubicle of a Scherbius set

In the middle is the tap changer, which is remote controlled from the control room; at the top the adjusting resistors, bottom left the tapped transformer. The cubicle only contains simple apparatus, which does not involve any difficult operation. The speed of the pump can be set in 18 steps.

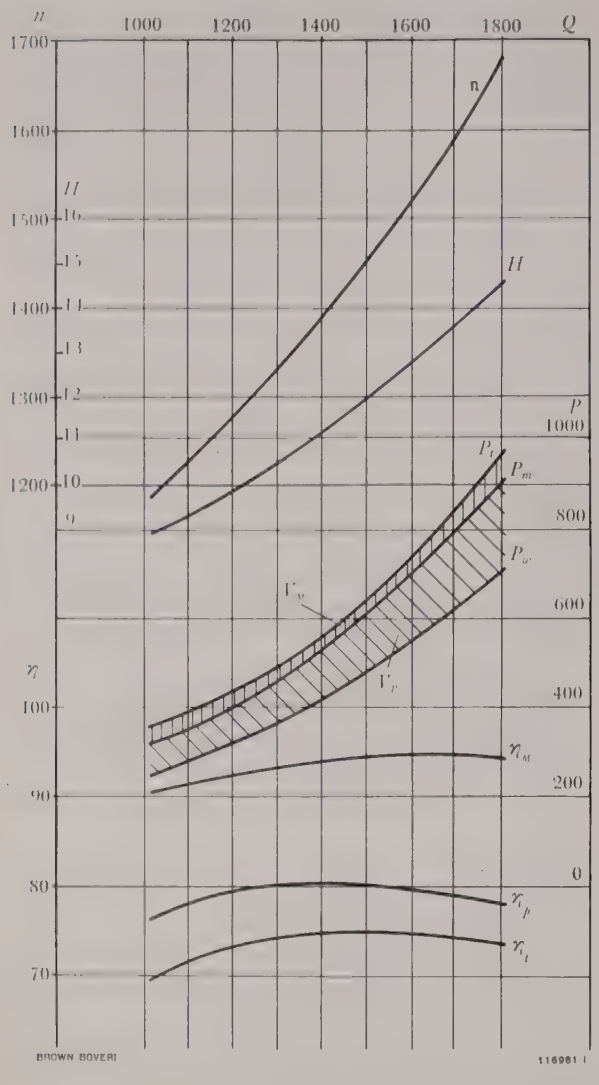

Fig. 15. – Power balance and efficiency of the pump drives at Fuhrberg

The following are plotted in terms of the discharge Q (m³/h):

n = Speed (rev/min)
H = Pump head (kg/cm²)
P_w = Discharge (kW)
P_m = Shaft power (kW)
P_t = Total power consumption of the drive (kW)
V_P = Pump losses (kW)
V_M = Motor losses (kW)
η_P = Efficiency of the pump (%)
$\eta_t = \eta_P \eta_M$ = Overall efficiency (%)
η_M = Overall efficiency of the drive (%)

At all discharges the pump and motor have a high efficiency.

of variation. When running above the synchronous speed, the Scherbius set draws the slip power from the mains, returning it at sub-synchronous speeds. The flow of power is illustrated in Fig. 16a and b.

Before a pump can be switched on, the suction valve must be opened by a solenoid valve. If, moreover, the water level in the pure-water reservoir is above the minimum and the pressure valve is closed, the motor can be switched on. When it has run up, the pressure valve will be opened automatically after about three minutes. Then the supervisor can set the desired discharge, i.e. the speed of the pump, to meet the requirements by throwing a switch. If one pump has to be stopped, the pressure valve must first be closed, then the motor shut down, as a result of which the suction valve automatically closes. This lasts about three minutes. If a motor fails in service, for any reason, the pressure valve is closed within nine seconds, so that water does not flow back and drive the pump as a turbine. The pressure of the reversed water column of the pumps is intercepted by the two air vessels (Fig. 12).

Pump Drives in a Thermal Power Station

For the extension to a thermal power station employed for district heating, to which a 100-MW condensing turbine was added, the plan visualized the condenser being cooled by water extracted from a neighbouring river. The water flows through an intake channel, passes trash-racks and screens to the machine house where it is cleaned. Two pumps then convey it to the condenser at higher level.

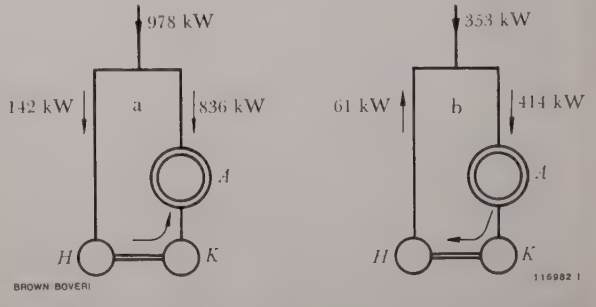

Fig. 16. – Flow of power with super- and sub-synchronous Scherbius control set

a: for super-synchronous speeds
b: for sub-synchronous speeds

The slip power of the main motor A is not dissipated, but flows in the indicated direction through the Scherbius machine K and the auxiliary machine H.

The input of condensate depends on the load on the turbine, the maximum rate being 185 and the minimum 59 t/h. Hence the demand for cooling water fluctuates accordingly, between about 4·2 and 1·5 m³/s. The task which the planning had to solve was to control the discharge of the pumps. After studying the economic aspect, the decision was taken to adopt the following solution. Two pumps were to be supplied, both of which could operate at the same time, or one pump acting solo, the speed being controlled without losses. At the maximum speed of 480 rev/min the two pumps together deliver 4·2 m³/s; at the minimum speed, the discharge of one pump is $\frac{1}{2} \cdot \frac{320}{480} \cdot 4{\cdot}2 = 1{\cdot}4$ m³/s, the discharge being considered proportional to the speed.

The selected drive employs induction motors with speed control by a single Scherbius machine. Each pump motor is rated 200 kW at 485 rev/min and 6 kV. The separately driven Scherbius machine can be connected to a single motor, or to both together, the motors then being in parallel on the primary and secondary sides. The speed is controlled below the synchronous value. For the accessories a new layout was selected, which is much simpler than that shown in Fig. 6. It is particularly advantageous for drives with a drooping speed-torque characteristic. The principle may be explained, first considering the simple case of operation with a single main motor.

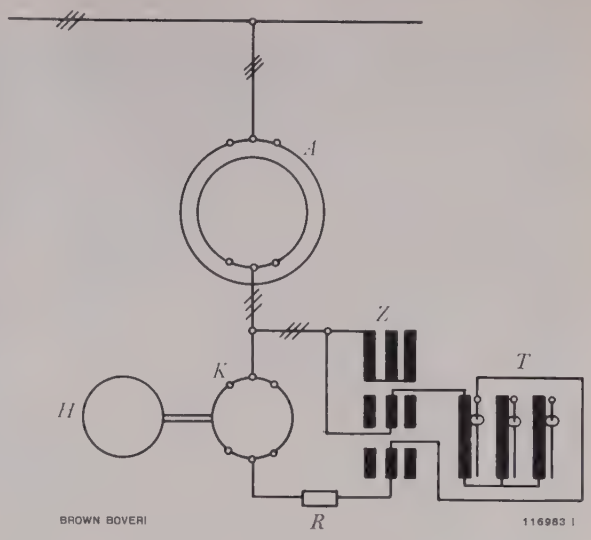

Fig. 17. – Schematic diagram of the stepless sub-synchronous control set

Compared with the normal circuit as shown in Fig. 6, the tap changer, tapped transformer and adjusting resistor are replaced by a setting transformer *T*, a single, small resistor *R* and a small supplementary transformer *Z*. The circuit has thus been simplified to a remarkable extent.

A = Main motor
K = Scherbius machine
H = Auxiliary machine

The tapped transformer of the normal circuit as in Fig. 6 has been changed for a setting transformer *T*, the secondary voltage of which is almost infinitely

Fig. 18. – Scherbius control set of the pump drive illustrated in Fig. 19

The control gear is accommodated in the switchboard, on the left of which are the starters for the two pump motors.

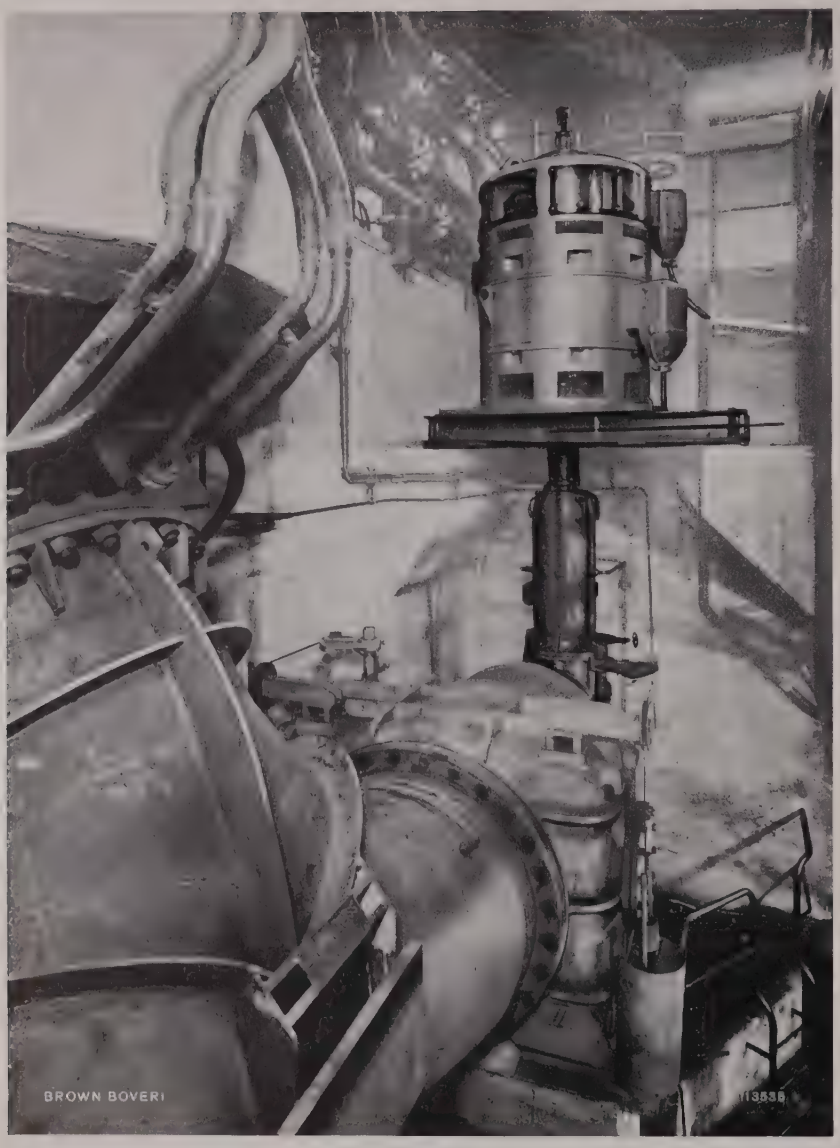

Fig. 19. – Pump drive in Gaisburg steam power station, Stuttgart, Germany

Showing the drive of one of two pumps supplying cooling water up to the condenser of a 100-MW steam turbine.

variable (Fig. 17). On the surface of its winding is a bare contact track. The phase angle of the excitation current is adjusted by a supplementary transformer Z with two secondary windings, which effect a displacement in the excitation voltage. One secondary voltage effects a constant displacement over the entire control range, while the second provides a dephased voltage component, after the fashion of the auxiliary coil h in Fig. 6. All windings of the supplementary transformer Z are tapped, permitting adjustment during commissioning. Furthermore, the adjusting resistor R is also available for balancing, and this is also tapped. All these settings are made once only, during commissioning. In service there is no need to interfere with the transformer Z or the resistor R. Compared with the conventional circuit (Fig. 6) the tap changer has been eliminated, while the large number of resistors have given way to a single resistor. Whereas in the former case the resistors allowed the power factor to be set to any desired value for every tapping, the new circuit does not permit the power factor to be varied over the entire control range, but it is nevertheless good. The circuit diagram (Fig. 17) could not possibly be simpler. The accessories for the Scherbius machine only comprise the setting transformer T,

with the small supplementary transformer Z and the small resistor R. Control is extraordinarily simple, the sole correcting element being the setting transformer T.

When both pump motors are running with the one Scherbius machine, the two main motors are connected in parallel on the primary and secondary sides, and are consequently automatically synchronized with each other. The prerequisite conditions for the motors remaining in step are favourable in this case, since the load is always equally shared by the two pumps. As has been proved in service, stability is quite adequate over the whole of the control range.

If both pumps are running and one has to be stopped, both motors are first brought up to top speed, then one is switched off. If the second motor is to be switched on to augment one running solo, the latter does not have to be switched off; it is merely run up to full speed, the second motor then being started and connected to the Scherbius machine on attaining full speed. Finally the two motors are jointly controlled to the desired speed.

The two vertical pump sets are installed at the lowest point in the boiler-house. The motors have closed-circuit air cooling with water coolers. The Scherbius machine with its accessories is mounted a short distance away where there is space to spare on the platform. The pump motors are remote controlled from the boiler control room by means of control and acknowledgement switches. The speed adjustment is effected by rotary switches which cause the servo-motor of the setting transformer to rotate in one direction or the other. Facilities are available for switching over the main motors to running with or without the Scherbius machine, without having to switch off the pumps. Alternatively, the machines can be controlled from the cubicle mounted next to the Scherbius machine. If the emergency stop valve of the turbine comes into action, the condenser has to cope with an abnormally large quantity of steam, necessitating an increase in the output of the pumps. In order that the pump speed may be increased rapidly, the transit time of the setting transformer was made 13 s. The automatic control gear of the emergency stop valve emits the following commands: The setting transformer is ordered into its uppermost position for maximum speed; if one of the pumps has been out of service, it is started up again. This installation has been operating successfully since May 1959.

(KME) P. RAUHUT

Bibliography

[1] F. BÜTTNER: Elektrische Antriebe drehzahlgeregelter Pumpen und ihre Anwendungen. BBC Nachr. 1955, Vol. 37, No. 3, p. 88–103.

[2] C. PFLEIDERER: Die Kreiselpumpen. Springer-Verlag 1949, edition.

[3] W. HÄNLEIN and E. SCHUPPAN: Planung der elektrischen Ausrüstung eines vollautomatischen Pumpwerkes mit verlustarmer Drehzahlregelung. Das Gas u. Wasserfach 1957, Vol. 98, No. 44, p. 1097–1101.

[4] P. RAUHUT: Scherbius machines for speed control, power factor correction and power regulation of induction machines. Brown Boveri Rev. 1951, No. 5/6, Vol. 38, p. 132–47.

P. RAUHUT: Factors governing the choice of Scherbius control equipment. Brown Boveri Rev. 1954, Vol. 41, No. 12, p. 456–72.

[5] K. STADAGER and W. ELLER: Die Wasserversorgung der Stadt Frankfurt am Main und deren Neubauten. Das Gas u. Wasserfach 1959, Vol. 100, No. 22, p. 545–49.

SCHERBIUS CONTROL SETS FOR BLOWER AND COMPRESSOR DRIVES

621.515.83
621.615-83

Lossless speed variation is the most economical method of adapting the performance of blowers and compressors to different operating conditions. For small drives with low powers the commutator motor may be used, while for larger capacities the Scherbius control set may be considered. Owing to the reduced power consumption when the driven machine runs at partial load for long periods, which is frequently the case with compressors, the increased capital outlay is quickly paid off. Examples are furnished of drives for fans, blast-furnace blowers and compressors.

THE following methods can be adopted for matching the performance of blowers and compressors to changing operating conditions.

When they are driven by constant-speed motors:

(a) Throttling the suction line

(b) Adjustable blades ahead of, or following the impeller (in the case of centrifugal compressors)

(c) Adjustable stator blades in axial compressors

(d) Blow-off points, with or without power recovery in a turbine

(e) Varying the speed by means of electric or hydraulic clutches between the motor and compressor.

When driven by variable-speed motors:

(f) Rheostat in the rotor circuit of the induction motor

(g) Commutator motors

(h) Scherbius control sets

(i) Ward-Leonard drives for compressors with a very wide speed range, as in the case of sub-sonic wind tunnels.

The methods (a) to (d) are in part subject to throttling losses and the economics of their operation differ accordingly. Preference for one or the other of these methods depends upon the resistance characteristic of the process with which the compressor is linked.

Speed variation by means of a clutch, either hydraulic or electric, is not accompanied by a change in the supply of energy to the motor terminals. The three last possibilities, (g) to (i), are the most economical; the commutator motor is only considered for low outputs. A number of theoretical references concerning fluids were made in the previous article dealing with Scherbius drives for centrifugal pumps. For the greater part, similar considerations apply to gaseous media, although an essential difference exists in the operational behaviour of the two machines. A centrifugal pump can be designed to have a completely stable characteristic throughout, i.e. the delivery head will decrease constantly with increasing fluid throughput. The characteristics of centrifugal and axial compressors for gaseous media, on the other hand, are always unstable when the throughput is reduced. Orderly operation is therefore only possible in the stable region, located on the other side of the line.

This article is concerned solely with the mechanical and electrical change of speed of the compressor set. Mechanically, the speed is regulated by varying the amount of oil in the hydraulic clutch, or the magnetic field of the electrical clutch. The difference in the speed of the two shafts is called the slip and is associated with considerable loss of power. Similar results are experienced with induction motors having resistors in the rotor circuit. In both cases, whether a regulating clutch or a rheostat is involved, the slip is associated with losses, whose magnitude can be determined by an approximate calculation:

The slip power

$$P_s = s \cdot P_1 \qquad (1)$$

s = Slip = relative speed reduction

P_1 = Energy taken from the mains

Since the slip power is not employed usefully, the power available at the shaft is

$$P_2 = P_1 - P_s = (1 - s)\, P_1 \qquad (2)$$

in which the motor losses are neglected. In the case of the torque associated with a fan (this is proportional to the square of the speed), the output at the shaft varies as the cube of the speed which, for its part, is proportional to $(1 - s)$. If P_m is the output available at the motor shaft at maximum speed, that is, at $s \approx 0$, then

$$P_2 = (1 - s)^3\, P_m \qquad (3)$$

The equation

$$P_1 = (1 - s)^2\, P_m \qquad (4)$$

is obtained from the equations (2) and (3) and with equation 1 inserted in equation (4).

$$P_s = s\,(1 - s)^2\, P_m \qquad (5)$$

In Fig. 1 P_1/P_m, P_2/P_m and P_s/P_m are plotted with respect to s. The maximum for the slip losses is 0·148 and is located at $s = 0{\cdot}333$. The rated motor output at this point coincides with P_m and is made equal to 1.

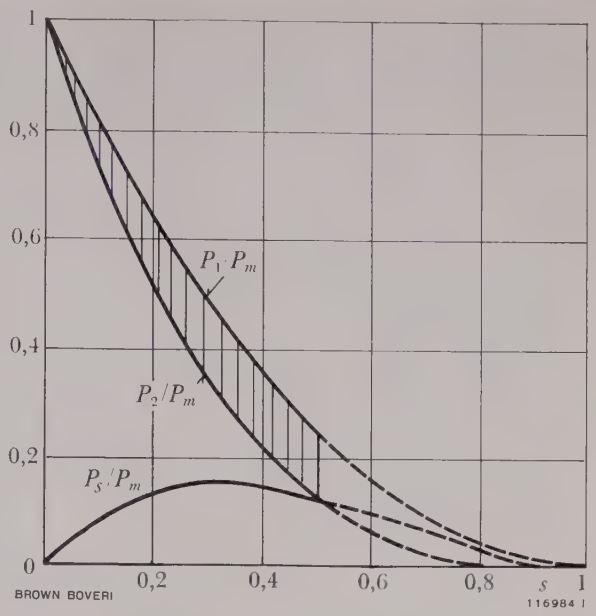

Fig. 1. – Power balance with fan torque and slip control

s = Slip
P_1 = Input
P_2 = Output
P_s = Slip power corresponding to the shaded difference between P_1 and P_2
P_m = Rated motor output = output at maximum speed

For the idealized curves the actual motor losses are neglected. The slip power is lost when control is by means of a clutch or resistors.

For a 420-kW blower running at 1500 rev/min, belonging to a large boiler plant, R. Modlinger[1] has prepared a comparison with the following kinds of drives: squirrel-cage motors with clutches, slip-ring motors with slip resistors, three-phase series-connected commutator motors. In the first case the power absorbed by the motor at 70% of full speed is 75 kW more than with the commutator motor; in the second case the difference is somewhat less. Taking the cost of current into consideration, the cost of the installation and interest on capital, Modlinger finds that even with an extremely low utilization factor, i.e. 1500 hours per annum, the commutator motor is more economical than the induction motor with a clutch.

Provided the drive losses are not increased in consequence, compressor regulation benefits most from speed variation. For such duty the three-phase shunt commutator motor is most suitable when small outputs are involved; the advantage of this motor is that the adjusting component, i.e. the movable brush rocker, is incorporated in the motor and no accessories are needed to change the speed. From the point of view of regulation, the shunt characteristic is desirable since the brush position corresponds to the speed. Fig. 2 shows two induced-draught blowers driven by commutator motors; these machines are attached to rotary kilns in a cement works. The efficiency and power factor characteristics are depicted in Fig. 3. The shunt commutator motor is also employed for driving other kinds of blowers, e.g. in boiler houses for primary and secondary air; for driving compressors for gas suction and delivery; fans in air-conditioning plants, etc.

Scherbius control sets may be used for high-output drives. Such systems are frequently employed for mine ventilation. The 1000-kW induction motor seen in Fig. 4 is controlled in the sub-synchronous range by a separately driven Scherbius machine. Adaptation to the conditions prevailing in the mine is possible with this arrangement. The circuit is the same as that illustrated in Fig. 6 of the previous

[1] R. MODLINGER: Über den Antrieb von Gebläsen für Grosskesselanlagen. Elektrizitätswirtsch. 1956, Vol. 55, No. 24, p. 896–900.

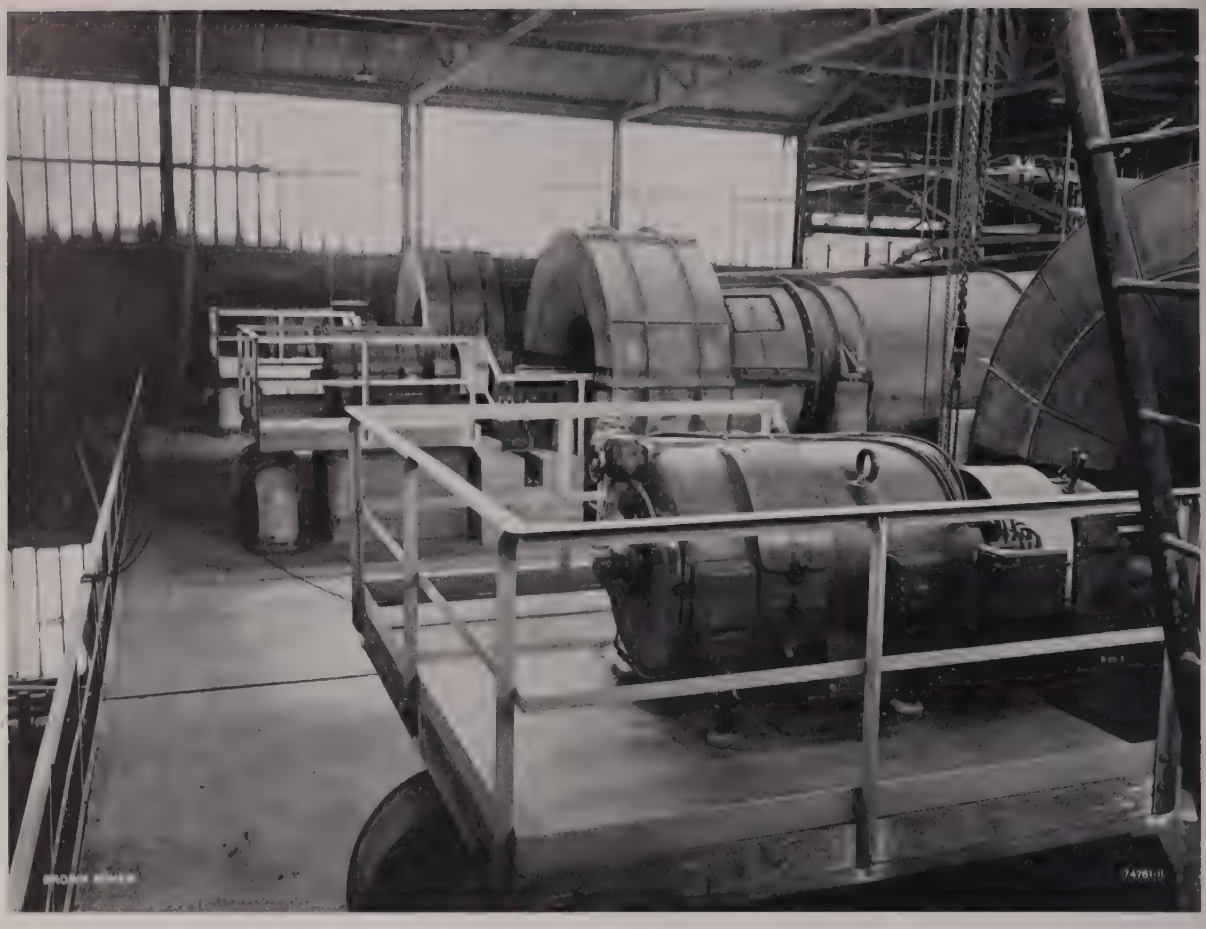

Fig. 2. Three induced-draught fans driven by shunt commutator motors, installed at the S.A. des Ciments d'Obourg, Obourg, Belgium

Output of each motor 220 h.p., 1300 rev/min, capable of lossless regulation up to 650 rev/min by remote control from the burner's platform at the other end of the rotary kiln.

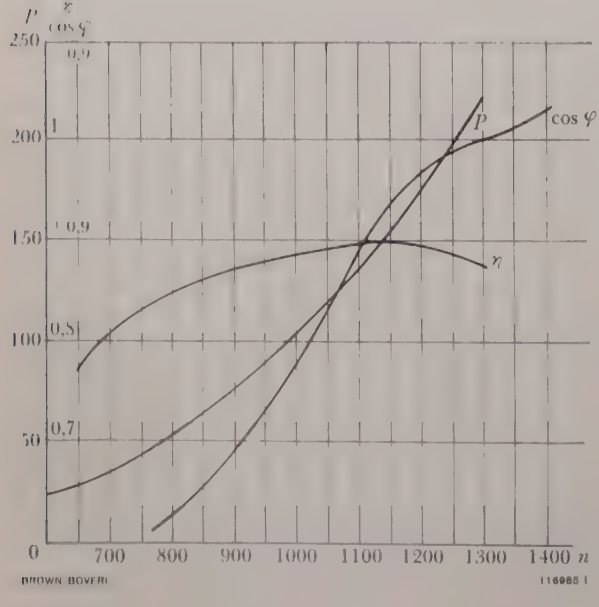

article. The advantage of sub-synchronous control here is that for full-speed operation the Scherbius machine is not needed. The latter can therefore be overhauled, i.e. the brushes or a bearing can be changed, without interfering with the ventilation of the mine. An arrangement requiring scarcely more

Fig. 3. – Efficiency and power-factor curves for the motors in Fig. 2

η = Efficiency [%]
$\cos\varphi$ = Power factor
n = Speed [rev/min]
P = Output [hp]

The curves are plotted from test-bed measurements. The fan torque is assumed.

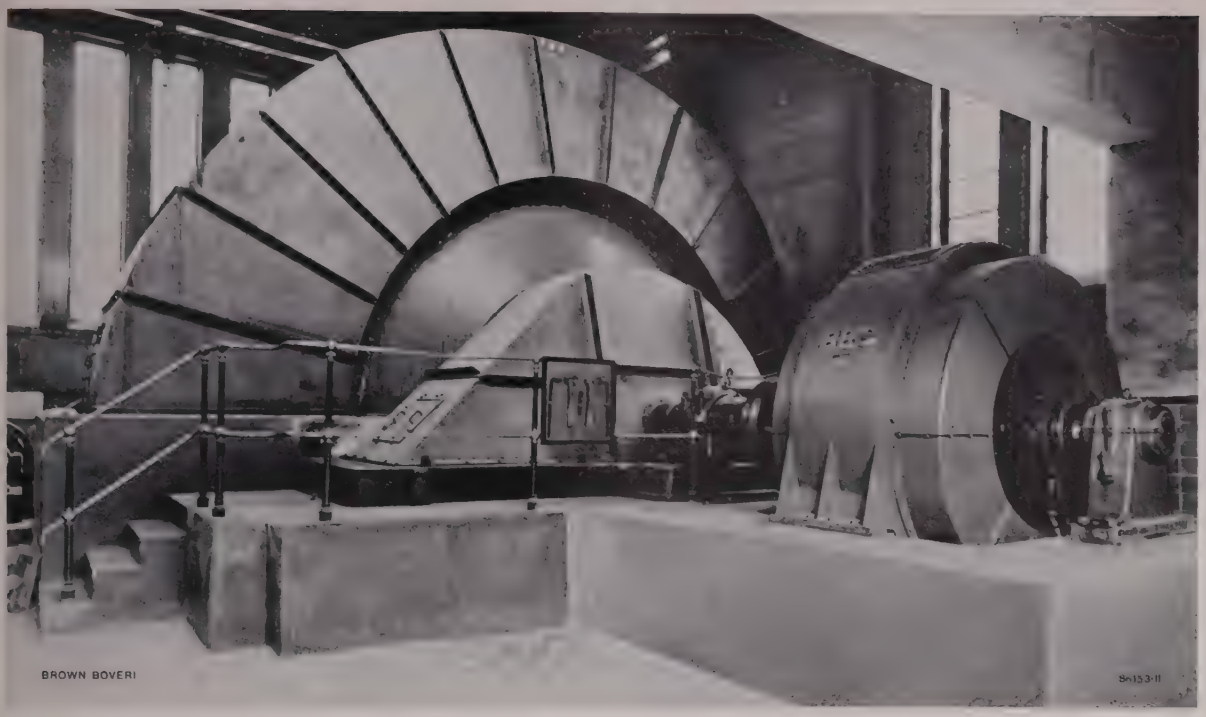

Fig. 4. – Mine fan

Driven by an induction motor controlled in the sub-synchronous range by a separate Scherbius machine. The ventilation is controlled according to the conditions underground.

equipment than a conventional drive enables the fan motors to be run with good efficiency at a particularly low speed, so that the output of the fans is reduced to correspond to the requirements on days of rest, when the miners are not in the pit.

For even larger outputs it is advantageous to control the induction motor partly in the super-synchronous and partly in the sub-synchronous range. The synchronous speed is then located approximately in the middle of the range of varia-

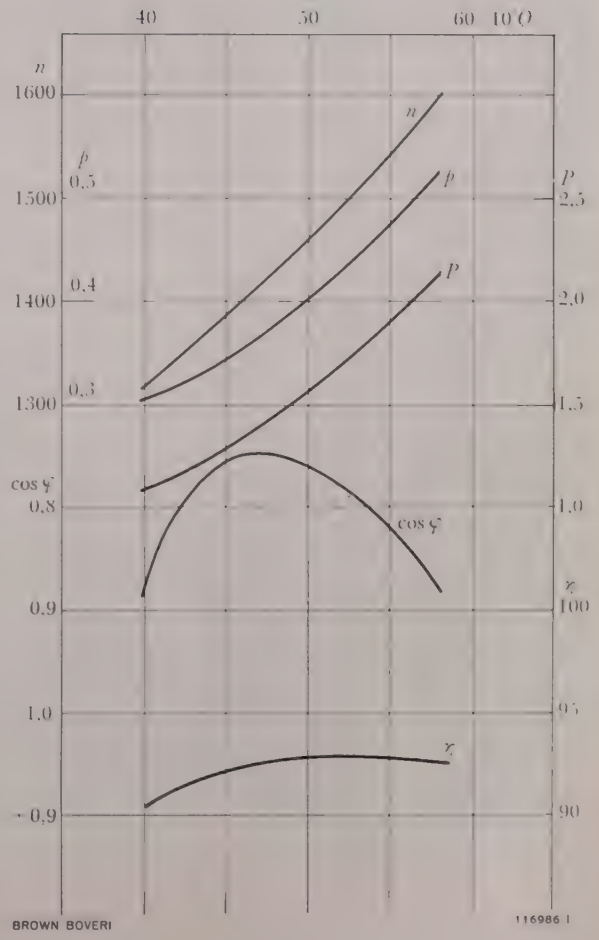

Fig. 5. – Efficiency and power factor of the blower drive at the Klöckner-Hütte AG., Bremen

The following are recorded with respect to the quantity Q (Nm³/h) being handled

n = Speed [rev/min]
p = Pressure [kg/cm²]
P = Output at the shaft [kW]
η = Overall efficiency of the drive [%]
$\cos \varphi$ = Power factor of the blower motor (+ = lagging, – = leading)

In spite of the low load, the efficiency is good over the entire range. The power factor is leading.

tion and the slip corresponds to only half of this. The slip power and accordingly the Scherbius machine with its accessories are then only half as large as with purely sub-synchronous control, and the efficiency is improved. Driving outputs of several thousand kilowatts are needed in the metallurgical industry, for instance for furnace blowers, for compressors in steelworks and for fans in sintering plants.

A drive of this nature was supplied to the Klöckner-Hütte AG., Bremen, where at the mouth of the Weser a new blast furnace has been built on to a new rolling mill. The blower built by Gutehoffnungshütte has the following rating: Capacity 100 000 m^3/h at normal temperature and pressure, 1·5 kg/cm^2, maximum speed 5640 rev/min. The induction motor, rated 3400 kW, 1485 rev/min, 6 kV, 50 c/s, drives the blower via a gear for transmitting 4070 hp, with a ratio of 5212/1668. The speed of this motor is variable in the range 1668 to 1296 rev/min by a separate Scherbius machine. The slip power of the main motor flows in the latter; in the *sub-synchronous* range this power blows back to the mains via the auxiliary motor coupled to the Scherbius machine, and in the *super-synchronous* range it is taken from the mains and supplied to the main motor. At maximum speed, therefore, the output of the Scherbius machine is available at the motor shaft in addition to the input from the mains; the output at the shaft of the main motor is accordingly greater than its rated output, i.e. 3650 kW. In principle, the circuit is the same as that shown in Fig. 10 of the preceding article. The speed is adjusted by means of a tap changer. The power factor is adjusted at the time the motor is taken into service and no provision is made for altering this; such adjustment is unnecessary in operation. At maximum speed the power factor is in the region of 1. For lower speeds, by utilizing the capacity of the rotor

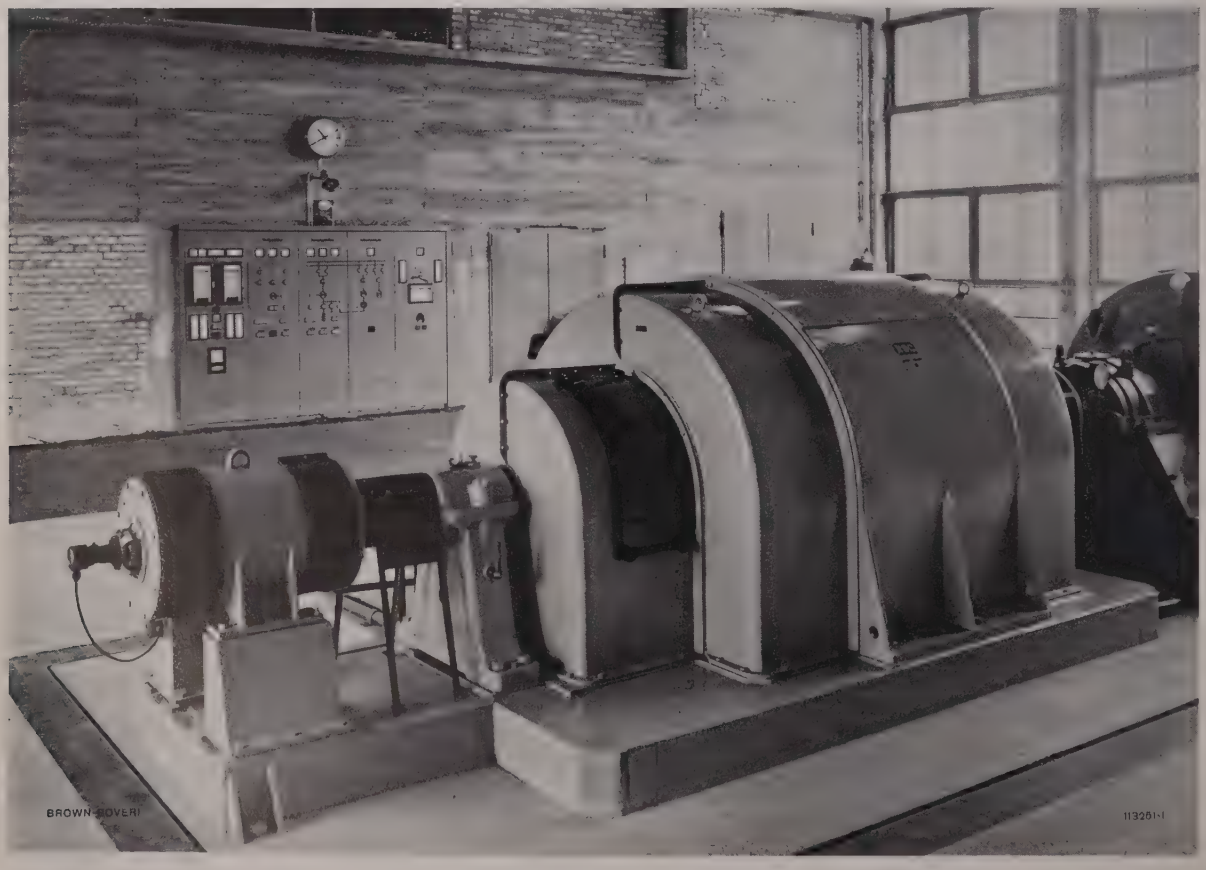

Fig. 6. – Furnace blower drive, in Bremen

From right to left: Blower (partly visible), drive motor and the small frequency converter of the Scherbius control set.

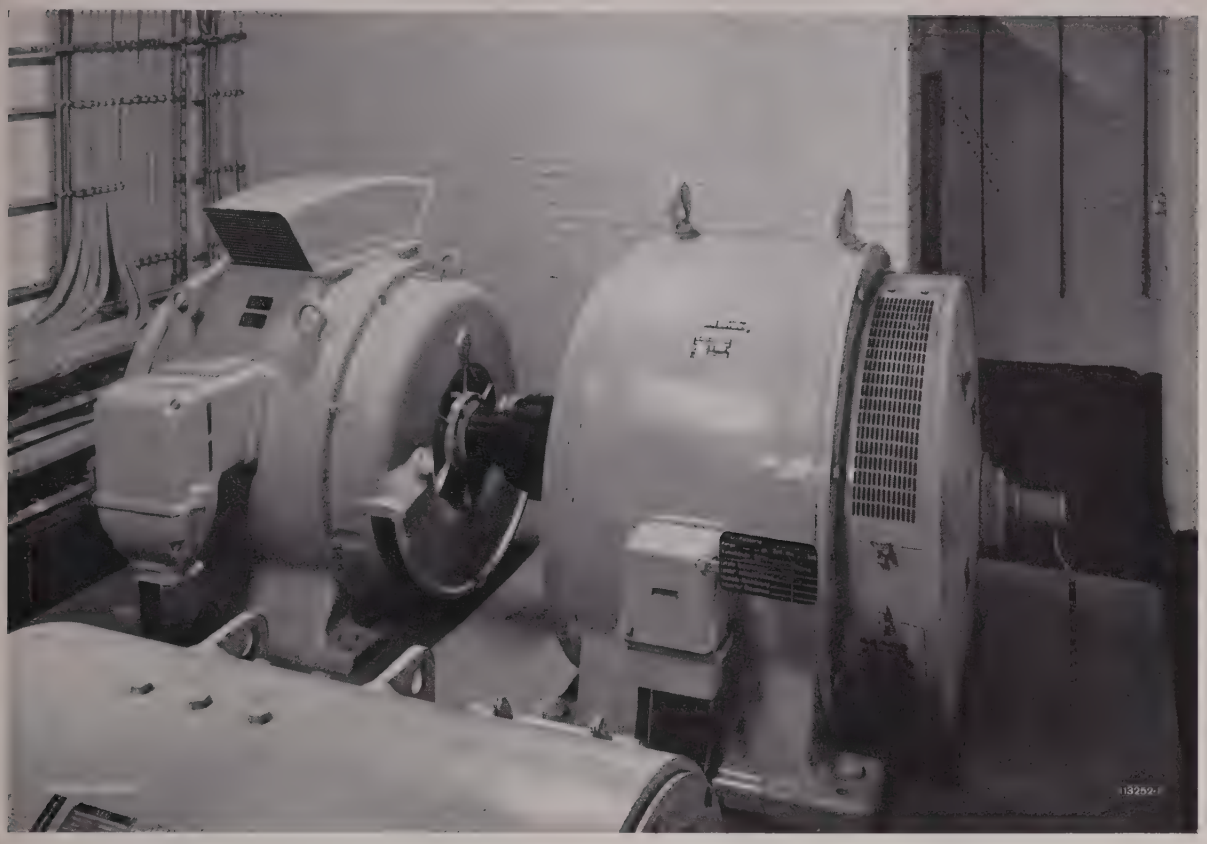

Fig. 7. – Scherbius control set of the machine in Fig. 6 on the ground floor of the installation

On the right, the Scherbius machine; on the left, the induction motor. These machines are installed in a vacant space, away from the machine hall.

circuit, it is even possible to employ the main motor for supplying reactive power to the supply system. In the neighbourhood of synchronism the Scherbius machine is excited by a small commutator frequency converter rigidly coupled to the main motor, and when the slip is greater, excitation is obtained principally from the slip rings of the main motor via a tap-changing transformer. Fig. 5 shows the characteristic of the overall efficiency of the drive, also the power factor at the blower motor. The readings were taken on site at approximately 63% of full load; at 100% load the efficiency is higher. It will be seen that over the entire range the drive operates with low losses, although the power factor is, in the main, leading. Fig. 6 shows the main motor of the installation on the right and the frequency converter on the left. The motor has closed-circuit ventilation; the air is cooled with water in a heat exchanger. The speed transmitter is visible on the left of the frequency converter. The Scherbius machine with its driving motor (Fig. 7) is housed on the ground floor of the building. Both machines are self-ventilated; since it is clean, the cooling air can be drawn direct from the room. The Scherbius machine accessories and the liquid starter belonging to the main motor are housed in a closed cubicle. The third and fourth panels from the left in the switchboard (Fig. 8, see also Fig. 6) accommodate the starting gear for the blower. It is possible to operate with or without the Scherbius machine, as desired. The recording instruments on the extreme right of the switchboard record the active and reactive power. On the left-hand side of the switchboard are the instruments for recording pressure and air quantity; the position indicator for the tap changer, also a rotary switch for controlling the latter manually are accommodated here. The air quantity is kept constant by an Askania regulator. Its desired value can be adjusted by remote control from the control desk of the blast furnace. The associated instrument

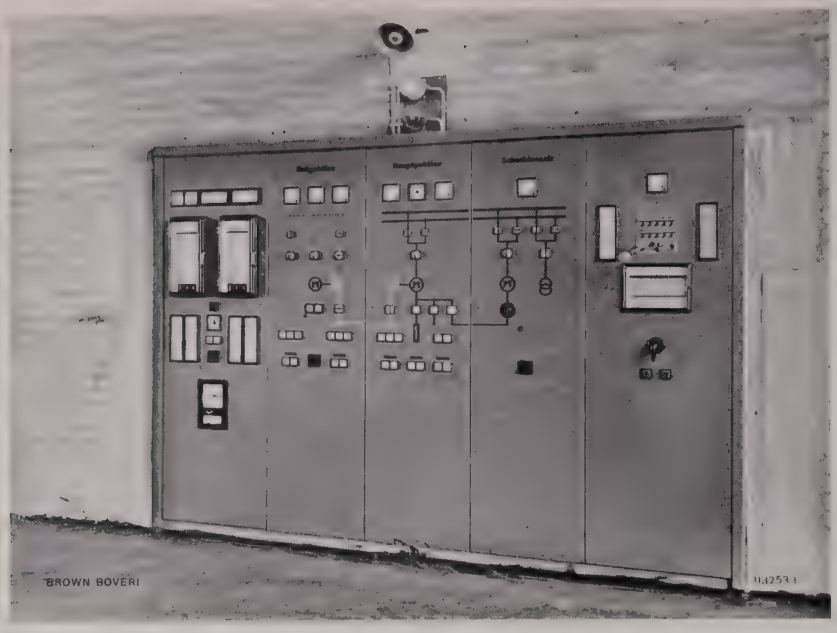

Fig. 8. – Switchboard belonging to the blower drive in Bremen

After the machine has been started, the blower is controlled with respect to constant air quantity by the Askania regulator at the bottom on the left-hand side. The desired value is imparted to the Askania regulator by the furnace control stand.

can be seen below, in the left-hand switchboard panel. The second panel from the left belongs to the emergency blower, which is started automatically in the event of the main blower failing.

Another interesting installation (Fig. 9) which was taken into service during the autumn of 1960, is the drive for a turbo-compressor, which Brown Boveri, Mannheim, supplied some time ago to the Essener Steinkohlenbergwerke AG., Essen, Germany:

Volume handled	800 m³/min
Inlet pressure	1 kg/cm² abs
Final pressure	6·6 kg/cm² abs
Maximum speed	5400 rev/min

Originally, the compressor was driven by a steam turbine; the conversion to an electric drive was carried out recently. The new drive is designed for the following outputs and speeds:

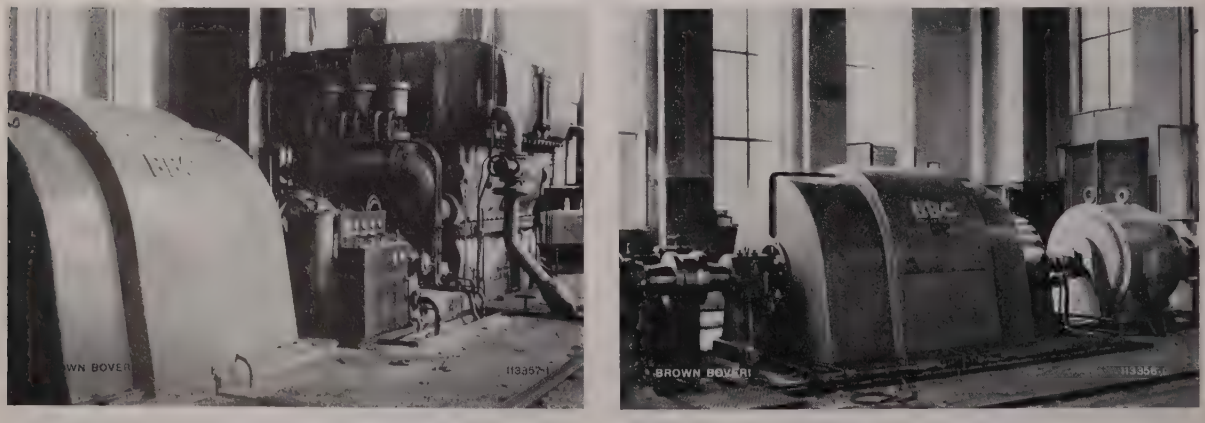

Fig. 9. – Electric drive for a Brown Boveri Isotherm compressor with Scherbius set in the installation at the Essener Steinkohlenbergwerke AG., Essen, Germany

a: Compressor with driving motor 4300/2200 kW, 5 kV, 50 c/s, gear ratio 1578/1414.

b: Scherbius control set: Left, induction motor; right, Scherbius machine and then (but not in picture) the frequency converter for control above and below synchronism.

4300 kW at 5800 rev/min (maximum speed)
2200 kW at 5200 rev/min (minimum speed)

A four-pole induction motor was provided, rated 4300 kW, 1490 rev/min, 5 kV, 50 c/s. It was possible to couple the Scherbius machine direct to the motor by means of a gear coupling. Having regard to the large output, the speed range is disposed on either side of synchronism, with the help of a frequency converter running in phase with the motor. The Scherbius machine and the frequency converter are also directly coupled by means of a gear coupling. The special Scherbius machine drive is not required here, so that the efficiency is very favourable. Otherwise, the circuit is the same as that illustrated in Fig. 10 of the previous article. When the plant was taken into service, the power factor was adjusted so that it is in the neighbourhood of unity over the entire range. The motor has closed-circuit cooling and this affords protection against dirt. The Scherbius machine is drip-proof and the frequency converter totally enclosed. The induction motor is built with a high stationary-rotor voltage, so that the rotor current is low. This has the following advantages:

Low brush losses on the slip rings of the motor and on the commutator of the Scherbius machine. It was still possible to build the Scherbius machine to run at 1500 rev/min and to couple it direct to the motor.

For starting the motor the stator voltage is reduced by an auto-transformer, so that during this period the rotor voltage is low. A liquid resistance is employed for starting. When the motor is running at approximately 80% of the synchronous speed, the stator voltage is increased without interruption to the full value and the motor is then run-up to full speed with the starter. The process of starting lasts about 37 s; during this time the power input reaches a peak of approximately 80% of the rated value. After run-up, it is only necessary to switch over to the Scherbius machine; the drive is then ready for automatic speed control, which ensures that the operating pressure is kept constant.

(FJH) P. RAUHUT

THE STATORLESS PHASE ADVANCER IN ITS PRESENT FORM

621.313.334

The principle of the statorless phase advancer is briefly described and the new vertical model compared with the former, conventional horizontal design. It is proved that this simple machine has retained its significance as a means of improving the power factor.

THE PRINCIPLE of the statorless phase advancer is not new, but there are many people who do not realize that this machine can be used to generate reactive power. It supplies reactive power to the rotor circuit of induction machines, thereby relieving the stator and the mains, which would otherwise have to provide this power. Since the induction machine is corrected from the rotor, it attains a higher pull-out torque, so that severe load surges cause only a slight fluctuation in the mains voltage in weak networks. There is no need to change any switchgear or control elements; the only accessories are ordinary commercial switches and line fittings. The advancer and its small drive motor are combined in a vertical unit, thus saving space, and can be installed where space is available—not necessarily close to the associated induction machine. If required, the induction machine can also be run without the phase advancer.

This article does not attempt to make any comparison with other methods of power factor correction, such as synchronous machines, synchronized induction machines, and static capacitors, but merely indicates that the statorless phase advancer may be superior to other methods in price and efficiency, particularly when a high overload capacity is stipulated. Hence, when studying such systems, a comparison with the statorless phase advancer must on no account be neglected.

Principle of the Statorless Phase Advancer

The phase advancer is a polyphase commutator machine which is connected to the slip rings of an induction motor. The armature of the advancer has a drum-type winding embedded in slots in the rotor iron and connected to the commutator. If a polyphase (rotor) current flows towards the brushes in contact with the commutator, the arrangement acts as a choke when at rest; an inductive voltage drop is caused, which in turn causes the current to lag. At a given current this drop in voltage is dependent solely on the frequency, i.e. the rate at which the rotating field produced in the advancer cuts the winding. If this cutting frequency is reduced by allowing the winding to rotate with the field, the reactance decreases, and with it the angle of lag, finally attaining the value zero at synchronism. When the speed is increased above synchronism, the reactance becomes negative and the advancer acts as a capacitance in the rotor circuit. This capacitance causes the rotor current to lead the slip-ring voltage of the induction motor.

The frequency of rotation is made sufficiently high for the leading rotor current to cater for some or all the magnetization of the induction motor. Hence the motor draws much less reactive power from the network. If the advancer and induction motor are appropriately dimensioned, it is even possible to return capacitive current to the mains.

Technical and Economic Advantages

All a.c. installations in which induction machines are employed require reactive power in addition to the active power. This lagging power covers the

excitation requirements. The reactive power is 90° out-of-phase with the active power. In the concrete case, as illustrated in Fig. 1, this implies that 600 kVar of reactive power are required for an induction motor with a terminal rating of 1000 kW, on which the diagram is based. To balance these 600 kVar the mains would have to supply 1155 kVA instead of only 1000 kW. Apart from this saving, which applies to all parts concerned with the supply, this also exerts a favourable influence on the characteristic of the induction machine.[1]

The advancer is always mounted separately from the induction machine; hence the latter can be augmented by an advancer at a later stage. On account of the compact arrangement and owing to the fact that the advancer is not bound to occupy a definite position, it is possible to save valuable production space. In certain circumstances it is even possible to increase the power, because the stator of the induction motor has to carry a lighter current when the power factor has been corrected. Since voltage drops are mainly caused by the reactive component—inductive reactive power—the phase advancer exerts a stabilizing effect on the voltage in weak networks.

The reduction of the total apparent power required is equivalent to a reduction of the stator current. Thus the total losses on the mains side are reduced, proportional to the square of the current. But a reduction in the losses, at constant power, implies better efficiency and lower running costs.

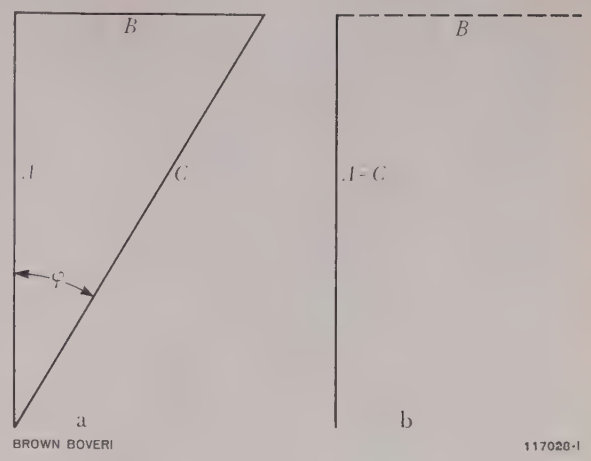

Fig. 1. – Vector diagrams in service

a: without phase advancer
- A = Active power drawn from network, 1000 kW
- B = Reactive power drawn from network, 600 kVar
- C = Total apparent power drawn from network, 1155 kVA

b: with phase advancer
- $A = C$ = Total power drawn from network, corresponding to the active power 1000 kW
- B = Reactive power generated by the phase advancer, 600 kVar

The statorless phase advancer keeps the reactive power component away from the network—transformer, switchgear and connecting leads—thus reducing the losses and lowering the running costs, while maintaining the same output.

Design of the Statorless Phase Advancer

The phase advancer which was brought out about 50 years ago (Fig. 2) was an open-type machine, in conformity with the requirements at that time. It was horizontal, with pedestal bearings, and was mounted with its drive motor on a common sole-plate. The enclosure merely covered the rotating stack of laminations and the winding, but not the commutator.

Nowadays the advancer is drip-proof, vertical, and built with flanged-on drive motor (Fig. 3 and 4). With this new design less space is required, the output is higher and the inherent losses lower. Special stress was laid on simplicity and robustness, and a minimum of constructional parts. The lightweight cage framework stands on three feet and carries the bearing of the non-driven end. The

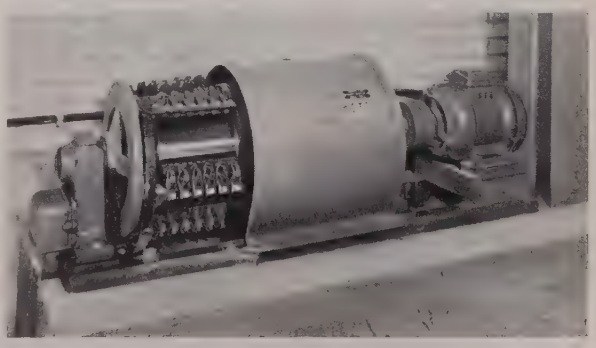

Fig. 2. – The former, well-known design of statorless phase advancer

This open-type, horizontal design with pedestal bearings, sole-plate and casing surrounding the rotor laminations and winding, has existed for about 50 years. Machines of this vintage are still in service today.

[1] See page 873.

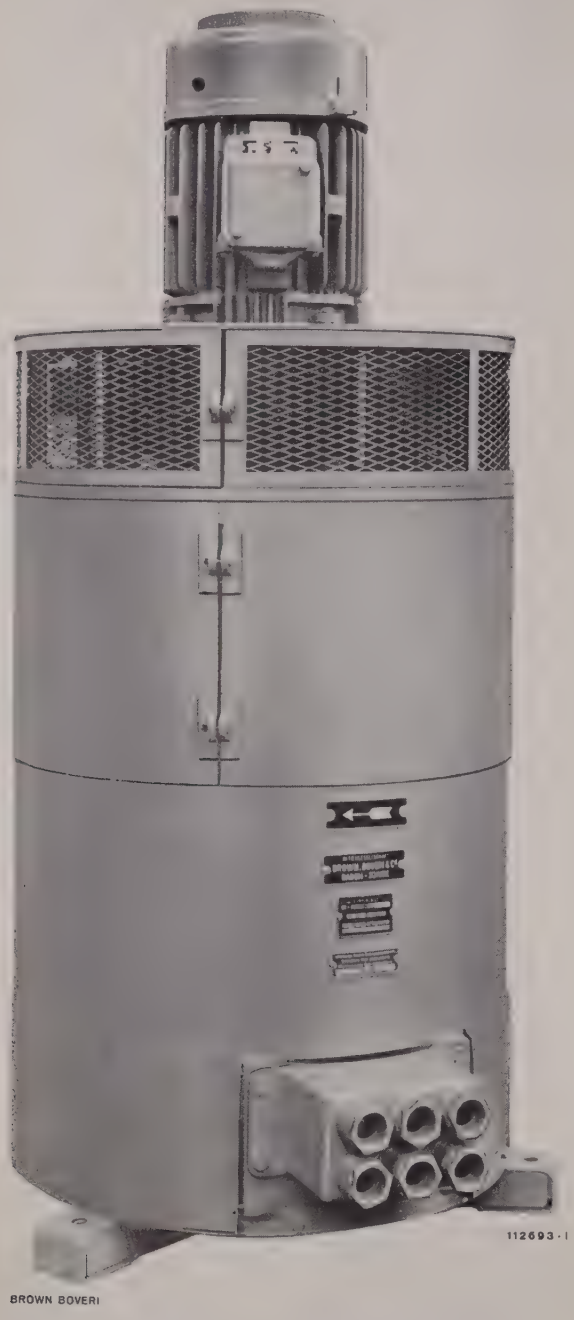

Fig. 3. – The modern design of statorless phase advancer

The advancer is drip-proof and vertical in design, thereby occupying a minimum of space. Removable enclosures afford easy access to the entire commutator space.

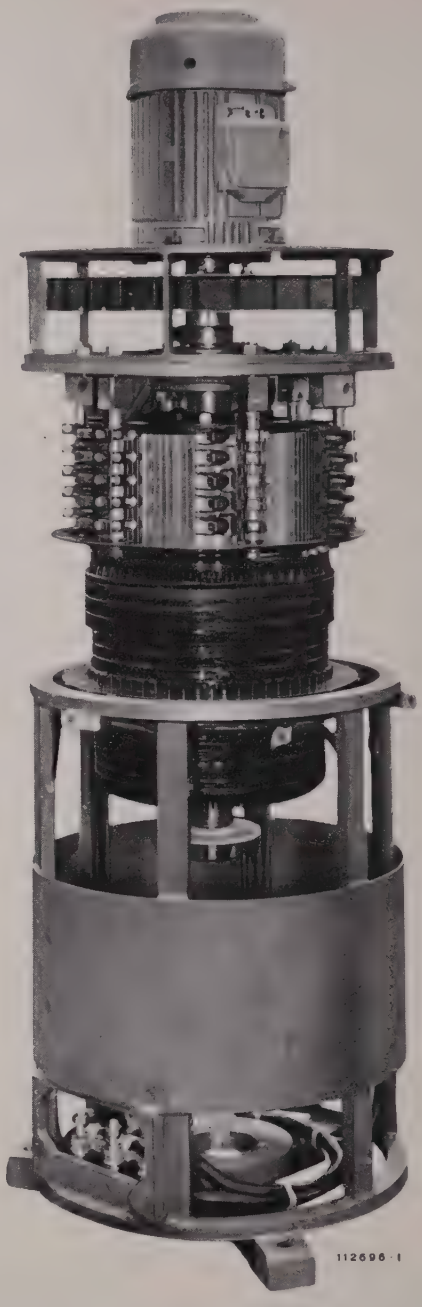

Fig. 4. – The rotor being inserted in the statorless phase advancer

From bottom to top: cage framework, rotor with commutator, end-shield to which the brush-holder rods are fixed, flexible bolted coupling with fan, cowling and drive motor. The simplicity of the machine and the small number of parts are evident from this illustration.

rotating parts are protected by a sheet-metal enclosure, which also stabilizes the body assembly. The lower opening provides access for assembly, the upper for maintenance of the carbon brushes. The thrust bearing is incorporated in the end-shield at the commutator end, which also carries the brush-holder rods. The cooling air is drawn through the end-shield by the fan, which is accommodated in

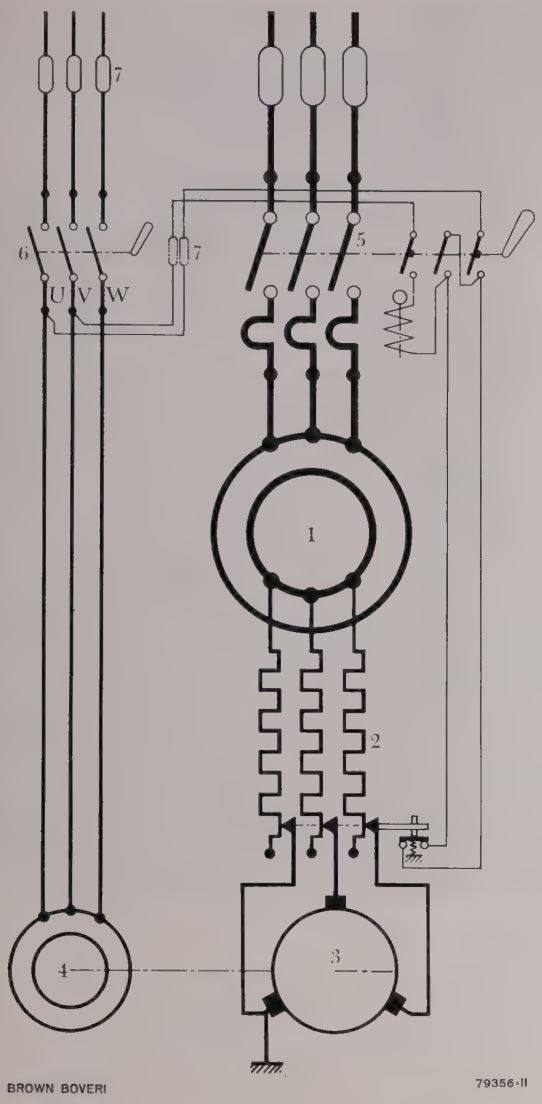

Fig. 5. – Circuit diagram of a statorless phase advancer with open-type starter

1 = Three-phase slip-ring motor
2 = Rotor starter
3 = Statorless phase advancer
4 = Motor driving the advancer
5 = Protecting switch for the slip-ring motor
6 = Switch for the advancer drive
7 = Fuses

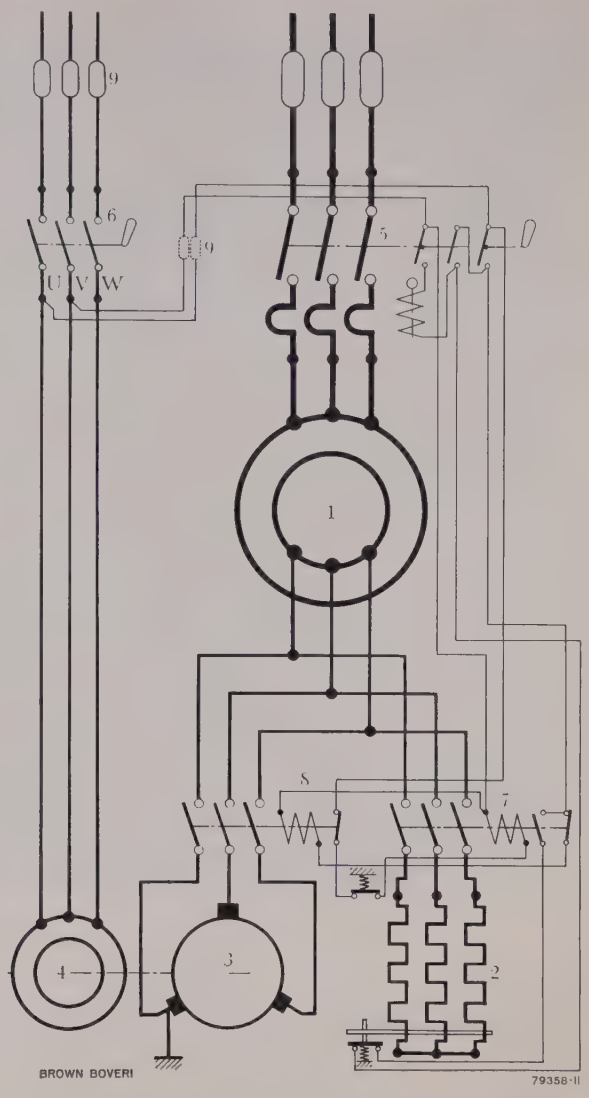

Fig. 6. – Circuit diagram of a statorless phase advancer with motor and separate starting resistor

This circuit is used when the motor driving the associated machine is equipped with a phase advancer after installation.

1 = Three-phase slip-ring motor
2 = Rotor starter
3 = Statorless phase advancer
4 = Three-phase motor driving the advancer
5 = Protecting switch for the slip-ring motor
6 = Switch for the advancer drive
7 = Starting contactor
8 = Contactor for the phase advancer
9 = Fuses

the supporting cowling above the end-shield at the commutator end and attached to the flexible bolted coupling between the advancer and its motor. The latter is flanged on to the advancer at the cowling. The cooling air flows upwards through the machine, entering between the three feet and emerging in all directions from the cowling. The connections of the heavy leads to the advancer are situated at the bottom end, so that the cable does not have to be bent.

Fig. 7. – Statorless phase advancer employed in a paper mill

Data of the advancer: 620 A, 17 V, $n = 980$ rev/min.

Right, behind the advancer is the motor driving the grinder, situated on the left of the picture. The induction motor is rated 1000 kW at 245 rev/min. Its power factor is improved from 0·78 to 0·99 lagging in service.

Circuitry for the Statorless Phase Advancer

As mentioned already, the statorless phase advancer is connected in the rotor circuit of an induction machine. There are two arrangements feasible in principle:

Starting resistors in open connection with the phase advancer as star-point. The motor is run-up with the phase advancer (Fig. 5)

Separate starting resistor. The phase advancer is not cut in until the motor has run-up to full speed (Fig. 6).

The simplicity of the circuit and the small number of elements enhances the reliability.

Applications

The primary application of the phase advancer is with medium-to-large induction motors which are kept running for long periods at a time, during the greater part of which the load is heavy. Hence this system may be encountered with wood grinders, cement mills, reciprocating compressors, pumps and motor-generator sets. The phase advancer can also be utilized with advantage for slow-running motors having a heavy magnetizing current and relatively low pull-out torque, because it exerts a beneficial influence on the properties of the motor. As intimated already, the advancer can be supplied for heavily loaded motors already in service. The extent to which the power factor of such motors can be

corrected depends on the thermal capacity of the motor. A statorless phase advancer can be seen in the foreground of Fig. 7; this unit has been running for some time in a paper-mill. The advancer is used to improve the power factor of the motor driving a magazine grinder.

Appendix

As mentioned in the paragraph dealing with the principle of the statorless phase advancer, the frequency of rotation is made high enough to allow the leading rotor current of the advancer to balance the magnetizing current of the induction motor partly or entirely. The frequency of the rotating field amounts to about 0·5 to 2 c/s in normal operation, while that of the phase advancer is between 25 and 50 c/s. Thus under normal circumstances frequency changes due to variation of the load on the induction motor have no effect on the voltage of the advancer. The magnitude of the latter depends solely on the magnitude of the current. If the machine being corrected changes from running as a motor to running as a generator, this reverses the rotating field. The fields of the motor and the advancer are thus rotating in opposite directions and a voltage with a lagging phase angle is induced. Consequently, when the load is reversed, the power factor deteriorates appreciably. A remedy is to exchange two phase leads.

Now how can a good power factor be obtained between relatively light load and full load? Supposing an imaginary capacitive resistance $X_c = E_K/I$ is introduced into the rotor circuit, which balances the inductive resistance of the rotor and stator at rated load, unity power factor would be attained for this point. If the resistance were to remain constant, a locus would be obtained corresponding approximately to the curve *a* in Fig. 8. Constant resistance, i.e. E_K/I = constant, for this case denotes the straight line *a* in Fig. 9. Now on the magnetic characteristic there is only one real point *A*, i.e. the point of intersection of the straight line *a* with the characteristic for this capacitive resistance. Consequently the current *I* is also known precisely for this particular case. If the current *I* (secondary current) thus obtained is plotted in Fig. 8 in the appropriate sense, the point *A* denotes the point actually attainable with power factor correction. A point on the locus was constructed. If, now, the same procedure is adopted for the lines *b*, *c* and *d* (Fig. 9), the associated currents are likewise obtained from the magnetic characteristic. These are plotted in the same manner as the current *A*, rendering the locus of the primary current. From this it will be evident that the high saturation of the phase advancer effects a correction to the power factor at quite low currents, and that optimum values are

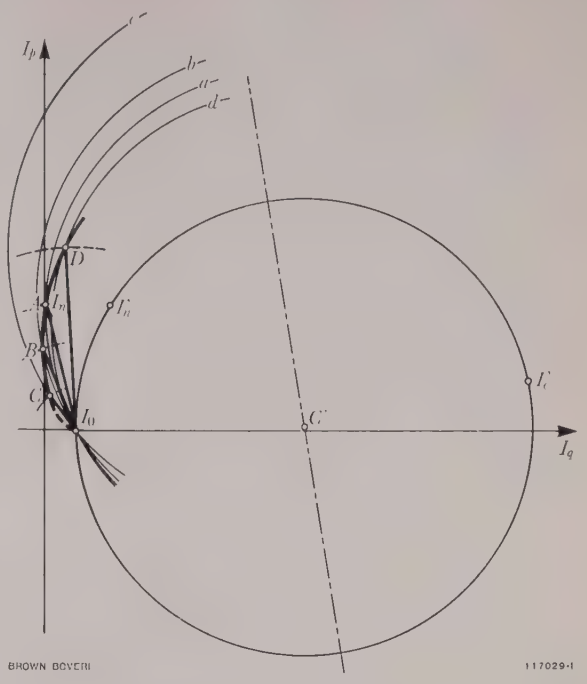

Fig. 8. – Construction of the locus for operation with phase advancer

Ordinates: I_p = active current (+ = as motor)
Abscissae: I_q = reactive current (+ = lagging)

The distances $\overline{I_0A}$, $\overline{I_0B}$, $\overline{I_0C}$ and $\overline{I_0D}$ are the secondary currents with which the portion of the curve is determined. The loci *a*, *b*, *c* and *d* represent constant values of E_K/I. These are plotted as the straight lines *a*, *b*, *c*, *d*. Since each straight line only intersects the magnetic characteristic at one point, only one point is valid on each of the loci *a*, *b*, *c* and *d*. The curve I_0–*C*–*B*–*A*–*D* gives the actual locus for operation with the phase advancer.

I_0 = No-load current
I'_c = Short-circuit current, uncorrected
I'_n = Rated current, uncorrected
I_n = Rated current, corrected

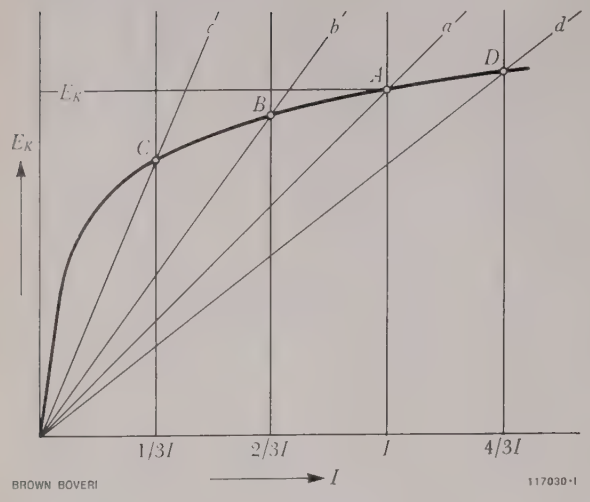

Fig. 9. – The magnetic characteristic of a statorless phase advancer

The working range of an advancer is above the saturation point. Since the machine is designed without any air-gap, this is easily attained. The straight lines *a*, *b*, *c* and *d* intersect the characteristic at the currents I, $^2/_3I$, $^1/_3I$ and $^4/_3I$, respectively. These values are plotted in Fig. 8 and yield the points *A*, *B*, *C* and *D*.

E_K = Voltage of phase advancer.

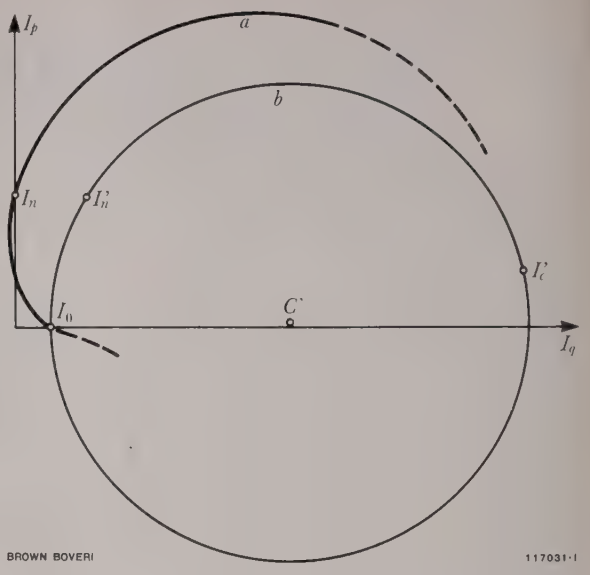

Fig. 10. – Locus of the primary current with motor load

a = Power factor corrected

b = Power factor uncorrected

For notation, see Fig. 8.

With a phase advancer a good power factor is obtained at only $^1/_3$ load; it remains in the vicinity of 1 until overload. The pull-out torque is considerably higher. The phase advancer needs no control element.

attainable for the power factor in normal operation, when the advancer is appropriately dimensioned. If the induction machine is able to withstand heavier secondary currents from the thermal aspect, the locus may also be in the capacitive region under normal operating conditions. From the comparison of the loci of the primary current with and without a statorless phase advancer (Fig. 10) the increase in the pull-out torque can be clearly recognized. At no-load, i.e. zero secondary current, the power factor cannot be corrected. But absolute no-load is hardly feasible with an induction motor driving a machine, so that at the low currents referred to there will still be a certain amount of power factor correction.

(KME) H. KOCH

TRANSFORMER NO-LOAD LOSSES WITH DISTORTED VOLTAGE WAVES

621.314.21.017.3

The effect of distorted voltage waves on the no-load loss measurements for transformers is investigated and the fundamental correctness of the method of correction laid down by the SEV[1] regulations confirmed up to very high voltage distortions. For an accurate reduction of the losses to sinusoidal voltage losses it is necessary to know the relationship between eddy-current and hysteresis losses. Experiments have confirmed the 50–50 ratio assumed by SEV for cold-rolled laminations with orientated grain, but yield a ratio of 30–70 for hot-rolled sheet, compared with the 20–80 ratio laid down by SEV.

WHEN measuring the no-load losses of large transformers, it is possible that, owing to the limited power available from the machines supplying the laboratory and the use of matching transformers between the generator and the test object, the voltage applied to the latter may deviate from its sinusoidal wave-form. The cause of the voltage distortion may be traced back to the voltage drop produced by the non-sinusoidal current of the test object across the short-circuit impedances of the generator and matching transformer.

Since the no-load losses have to be determined with a sinusoidal service voltage, which is always present in powerful networks with very small short-circuit impedances, it is necessary to make an appropriate correction to the losses measured with the distorted voltage. By ignoring the additional no-load losses in the transformer tank and other constructional parts of iron, and neglecting the copper losses of the excitation winding, which only form a very small part of the total no-load losses, we are left with the determination of the hysteresis and eddy-current losses of the transformer with sinusoidal voltage. Correction of the measured losses becomes simpler if the distorted no-load voltage is adjusted so that one portion of the no-load losses—i.e. the hysteresis losses—are made to equal the rated hysteresis losses with rated sinusoidal voltage. If we assume the distorted voltage only has simple zeros at $\omega t = 0$ and π—voltage waves with multiple zeros will rarely be experienced in practice— the flux density

$$B = K \int u(\omega t)\, \mathrm{d}\, \omega t \qquad (1)$$

in which K is a proportionality constant given by the dimensions of the iron frame, can only rise or can only fall during one quarter of a cycle. The hysteresis losses of the iron frame then only depend on the peak value of the flux density B_{max}

$$P_h = \Psi(B)_{max} \qquad (2)$$

By adjusting a distorted voltage $u(\omega t)$, which produces the same maximum flux density $B_{max} = B_{0max}$ as existing with the sinusoidal voltage U_0, the correct rated hysteresis losses can be measured. It will now be deduced that this distorted voltage should have the same mean value $U_m = U_{m0}$ as the sinusoidal rated voltage.

According to Fourier a skew-symmetrical no-load voltage $u(\omega t)$ can be expressed as follows:

$$u(\omega t) = U_{1max} \sin \omega t \pm U_{3max} \sin 3\omega t \pm \ldots \ldots U_{2n+1max} \sin[(2n+1)\,\omega t] \qquad (3)$$

According to equation (1) this voltage corresponds to a flux density of

$$B(\omega t) = K\left\{ - U_{1max} \cos \omega t \pm \frac{U_{3max}}{3} \cos 3\omega t \ldots \pm \frac{U_{2n+1max}}{2n+1} \cos[(2n+1)\omega t] \right\} = - B_1 \cdot \cos \omega t \mp \pm \frac{B_3}{3} \cos 3\omega t \ldots \pm \frac{B_{2n+1}}{2n+1} \cos[(2n+1)\,\omega t] \qquad (4)$$

To find the maximum value $B_{max}(\omega t)$, we substitute $\frac{\mathrm{d}B(\omega t)}{\mathrm{d}\omega t} = 0$, obtaining for $\omega t = \pi$

[1] SEV = Swiss Electrotechnical Association.

$$B_{max} = B_1 \pm \frac{B_3}{3} \pm \cdots \frac{B_{2n+1}}{2n+1} \qquad (5)$$

If the flux density B_{0max} is produced by a sinusoidal rated voltage $U_{0max} \cdot \sin \omega t$, and if the distorted voltage $u(\omega t)$ has the same mean value as the rated voltage

$$U_{0m} = \frac{2}{\pi} U_{0max} = \frac{1}{\pi} \int_0^{\pi} u(\omega t)\, \mathrm{d}\omega t =$$

$$= \frac{2}{\pi} \left[U_{1max} \pm \frac{U_{3max}}{3} \cdots \pm \frac{U_{2n+1max}}{2n+1} \right] \qquad (6)$$

If equation (6) is now multiplied by the proportionality factor K, we obtain

$$B_{0max} = B_1 \pm \frac{B_3}{3} \pm \cdots \frac{B_{2n+1}}{2n+1} \qquad (7)$$

From the comparison between equations (5) and (7) it is evident that the maximum flux density with sinusoidal voltage is equal to that with distorted voltage, i.e. $B_{0max} = B_{max}$. Thus on adjusting the voltage to the mean rated value, the hysteresis losses, which comprise the α_h-th part of the iron losses, are correctly determined.

To obtain the eddy-current losses P_{w0} present with sinusoidal voltage, the measured eddy-current losses P_w must be corrected. In an early publication by Rosenberg[2] it was proved that the eddy-current losses can be represented by a resistance R_b and that they vary with the square of the voltage, provided the depth of penetration a of the eddy current is greater than the thickness of the laminations δ. The depth of penetration is given by

$$a = 134{\cdot}0 \sqrt{\frac{\varrho \cdot H_{2n+1}}{f_{2n+1} \cdot B_{2n+1}}} \text{ [m]} \qquad (8)$$

in which

ϱ is the specific resistance of the lamination iron in Ωm,

H_{2n+1} is the r.m.s. value of the $(2n+1)$th harmonic of the magnetic field strength (in ampere-turns/metre),

f_{2n+1} is the $(2n+1)$th harmonic frequency (in c/s),

B_{2n+1} is the peak value of the $(2n+1)$th harmonic of the magnetic flux density (in Vs/m^2).

[2] E. ROSENBERG: Wirbelströme in massivem Eisen. Elektrotech. Z. 1923, No. 22, p. 513.

Exhaustive investigation of the curves, obtained with distorted voltages and analysed according to Fourier, of the no-load current I_0 and the flux density B proved that in the interesting region of the harmonic frequencies the condition

$$a_{2n+1} > \delta \qquad (9)$$

is always fulfilled. Hence the eddy-current losses measured with a distorted voltage $u(\omega t)$ are given by

$$P_w = \frac{1}{R_b} [U_1^2 + U_3^2 + \ldots U_{2n+1}^2] = \frac{U^2}{R_b} \qquad (10)$$

With sinusoidal rated voltage

$$P_{w_0} = \frac{1}{R_b} \cdot U_0^2 \qquad (11)$$

in which U and U_0 denote the r.m.s. values of the distorted and rated voltages. The eddy-current losses P_w at rated voltage U_0 can thus be determined from the losses P_w with distorted voltage U, namely

$$P_{w_0} = P_w \left(\frac{U_0}{U}\right)^2 = \alpha_w \cdot P \left(\frac{U_0}{U}\right)^2 \qquad (12)$$

in which α_w is the share of the eddy-current losses in the iron losses P. The corrected iron losses P_0 are then derived from the measured losses as follows

$$P_0 = P \left[\alpha_h + \alpha_w \left(\frac{U_0}{U}\right)^2\right] \qquad (13)$$

Thus, in principle, equation (13) conforms to the conversion formula given in the SEV regulations 0189.1956, with the fixed values $\alpha_h = 0{\cdot}8$, $\alpha_w = 0{\cdot}2$ for hot-rolled laminations, and $\alpha_h = \alpha_w = 0{\cdot}5$ for cold-rolled grain-orientated laminations.

According to American Standards, a slightly different form of this equation is given:

$$P_0 = \frac{P}{\alpha_h + \alpha_w \left(\frac{U}{U_0}\right)^2} \qquad (14)$$

in which the same coefficients $\alpha_h = 0{\cdot}8$ and $\alpha_w = 0{\cdot}2$ are stipulated. The difference between equation (13), which yields slightly higher values, and equation (14) is very small, even with severe distortion of the voltage wave (wave-form factors up to 1·3), and amounts to about 1 %.

According to equation (13) the rated iron losses of all transformers can be determined, with the exception of three-phase transformers without brought-out

neutral of the excitation winding and without any delta windings. In such transformers the third, ninth, etc. harmonic disappears from the phase-to-phase voltage, so that adjustment to the mean rated voltage does not lead to the desired object. Consequently, transformers of this kind should be measured with a voltage as nearly sinusoidal as possible. Nevertheless, the iron losses can be corrected by means of equation (13) in transformers with windings connected in star provided the star-point of the excitation winding is brought out and the voltage is set to the mean value of the rated phase voltage $U_{\lambda 0_m}$.

Experimental Investigations

To check the correction formula given by equation (13) exhaustive investigations were carried out with annular cores and on model transformers with hot- and cold-rolled laminations, as well as on single-phase radially laminated transformers of the well-known Brown Boveri design, fitted with hot-rolled laminations. The no-load losses were first determined with a sinusoidal voltage, or if this was not possible, with a voltage containing only slight distortion, and subsequently measured with artificially distorted waves up to quite severe distortions—the wave-form factor attained values up to 1·49—and were then corrected. The losses were determined for different values of the maximum flux density B_{max}, and for each of these values the coefficients α_h and α_w were calculated, using the well-known method of measuring losses at different frequencies.

The first experiments were carried out with two models of single-phase transformer frames. The weight of the frame made from hot-rolled sheet was 8·8 kg, while the one made of cold-rolled sheet weighed 12 kg. The experimental circuit is illustrated in Fig. 1.

To obtain the severely distorted voltage $u(\omega t)$, the voltage of the open secondary winding of a variable current transformer was employed. Distortion of the voltage by connecting resistors in series with the test object proved inadequate. By varying the excitation voltage and the ratio of the current transformer it was possible to vary the distortion in wide limits. To record the magnetic

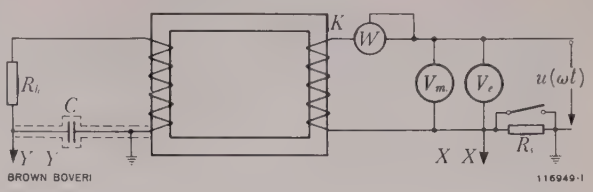

Fig. 1. – No-load measurement of losses, test set-up with model core

K = Model core
W = Wattmeter
R_s = Shunt
C = Capacitor
V_m = Voltmeter (mean value)
V_e = Voltmeter (r.m.s. value)
R_h = High resistance
$u(\omega t)$ = Applied alternating voltage
X–X, Y–Y = Horizontal and vertical deflector plates of oscillograph

flux density B, a special auxiliary winding with an integrator was used, comprising a high resistance R_h and a capacitance C. The voltage u_c picked off the capacitance, when $1/\omega C \ll R_h$, is a measure of the flux density B and is applied to the vertical deflector plates Y–Y of the oscillograph. The voltage drop picked off the shunt R_s was applied to the

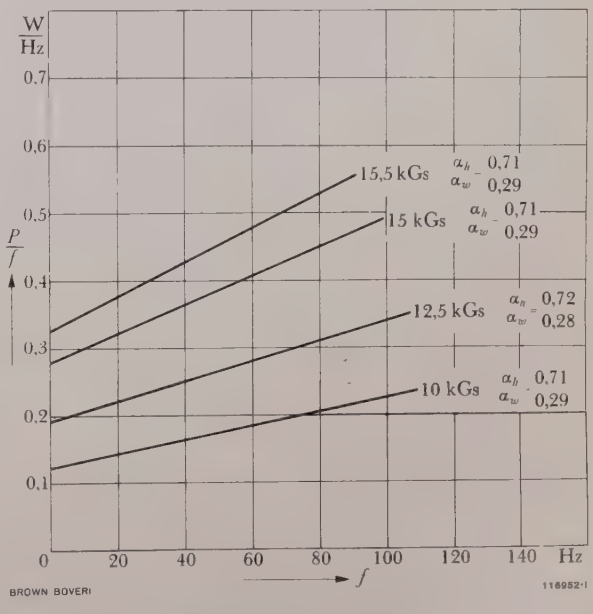

Fig. 2. – Measurement of separate losses on a model core with hot-rolled laminations

P = Losses
f = Frequency (in c/s)
α_h = Share of hysteresis losses
α_w = Share of eddy-current losses

horizontal plates X–X, thus giving the dynamic hysteresis loop on the oscillogram. From this we can obtain the particularly interesting value of the maximum flux density B_{max}, and compare the values for different degrees of distortion. For each frame the separate losses were plotted for flux densities between $B_{max} = 10$ and 16 kGs at frequencies of $16^2/_3$, 40, 50, 60 and 99 c/s, then the losses were determined with sinusoidal and distorted 50-c/s voltage.

The results of the measurements of the separate losses are shown in Fig. 2 for the frame with hot-rolled laminations, and in Fig. 3 for the cold-rolled frame. Whereas the coefficients for cold-rolled sheet agree quite closely with the values recommended by SEV, i.e. $\alpha_h = \alpha_w = 0{\cdot}5$, the proportions for hot-rolled sheet work out to $\alpha_h : \alpha_w = 0{\cdot}7 : 0{\cdot}3$. Tables I and II show the measured and corrected loss figures with sinusoidal and distorted voltage waves. The Tables also show the results obtained by correcting with the SEV coefficients, as well as the coefficients gained from Fig. 2 and 3.

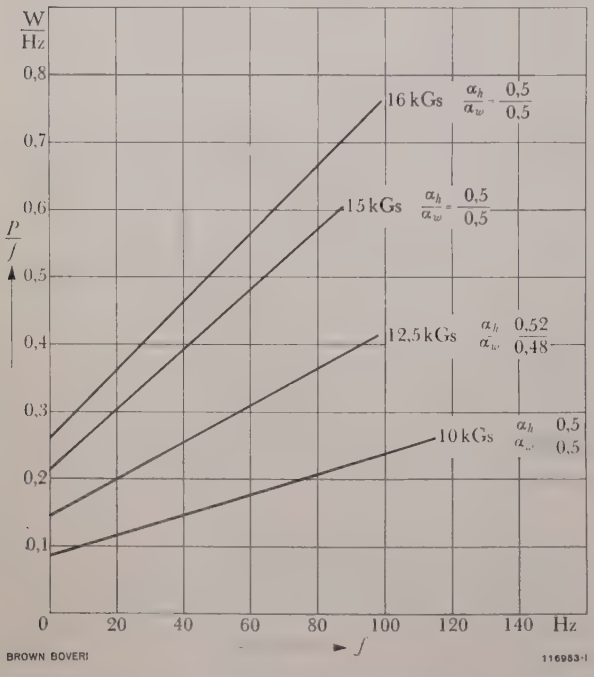

Fig. 3. – No-load measurements of separate losses on a model core with cold-rolled laminations

P = Losses
f = Frequency (in c/s)
α_h = Share of hysteresis losses
α_w = Share of eddy-current losses

TABLE I

Iron losses of the model frame of hot-rolled laminations with sinusoidal and distorted voltage waves

Inductance B_{max} kGs	Losses with approximately sinusoidal voltage wave		Losses with distorted voltage wave			
			Measured		Corrected	
	Form factor	Losses W	Form factor	Losses W	As per SEV W	With the coefficients in Fig. 2 W
10·0	1·11	8·71	1·13	8·75	8·56	8·67
12·5	1·11	13·30	1·17	13·65	13·40	13·25
15·0	1·11	19·50	1·26	21·10	20·20	19·75
16·0	1·12	22·90	1·49	26·50	24·20	23·20

TABLE II

Iron losses of the model frame of cold-rolled laminations with sinusoidal and distorted voltage waves

Inductance B_{max} kGs	Losses with approximately sinusoidal voltage wave		Losses with distorted voltage wave			
			Measured		Corrected	
	Form factor	Losses W	Form factor	Losses W	As per SEV W	With the coefficients in Fig. 3 W
10·0	1·11	8·68	1·137	8·85	8·64	8·75
12·5	1·11	14·25	1·17	15·07	14·30	14·35
15·0	1·115	21·9	1·23	24·30	22·0	22·0
16·0	1·12	25·7	1·37	31·50	26·0	26·0

Fig. 4a and 4b show the slightly distorted (factor 1·12) and severely distorted (factor 1·49) voltages recorded during the measurements on the hot-rolled frame, the same setting being used for the mean voltage. Fig. 4c and 4d show the corresponding dynamic hysteresis loops. Both these diagrams yield the same maximum flux density

$$B_{max} = 16 \text{ kGs} \triangleq 66 \text{ mm}$$

From the results in Tables I and II it may be seen that the losses measured with a corresponding setting of the mean value of the distorted voltage can be

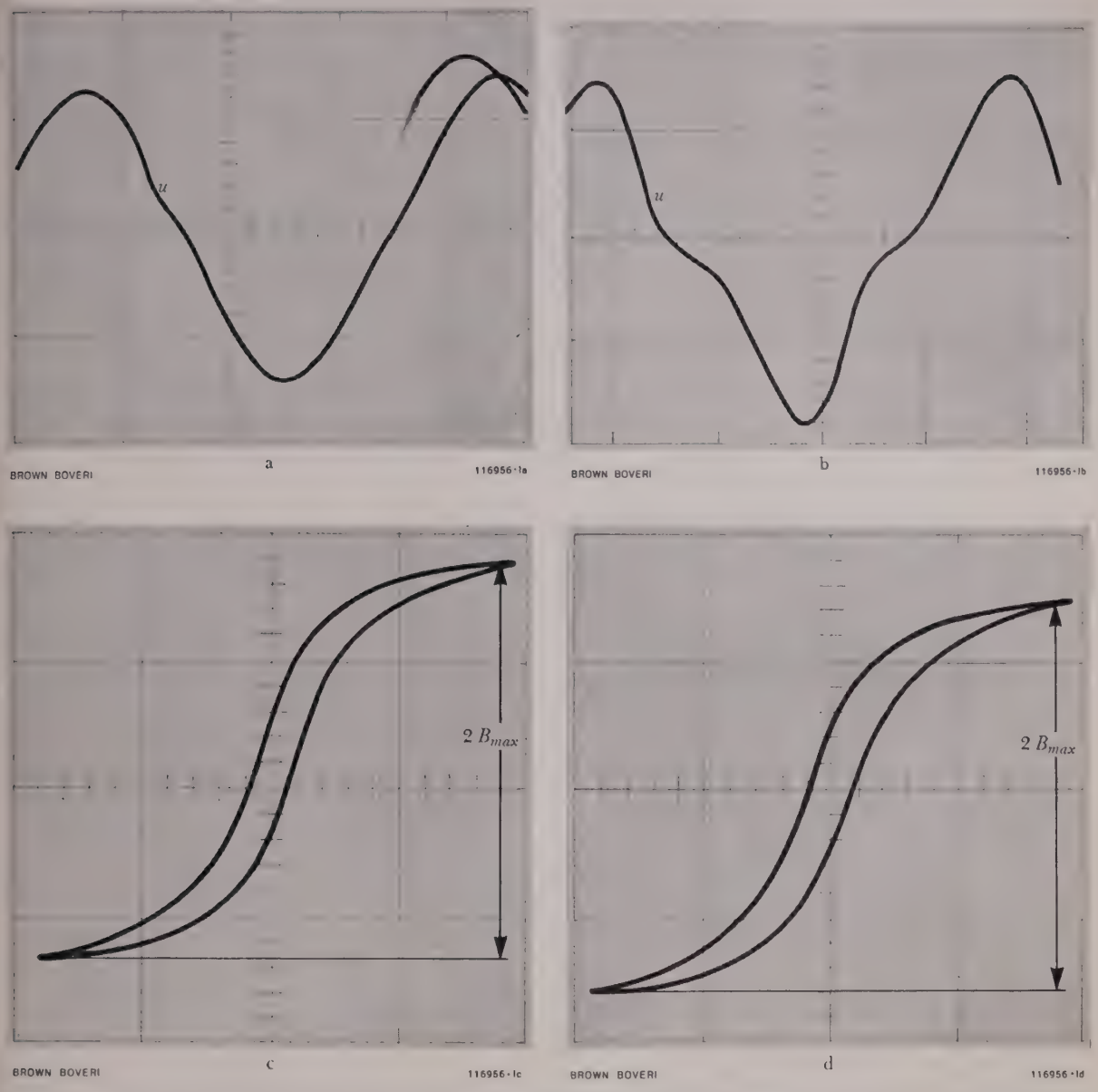

Fig. 4. – Voltage and flux density during no-load loss measurement on a model core of hot-rolled sheet with sinusoidal and severely distorted voltage waves

a: Practically sinusoidal voltage u

b: Severely distorted voltage (wave-form factor 1·49) with the same mean value as that in a

c: Hysteresis loop and maximum flux density B_{max} with almost sinusoidal voltage

d: Hysteresis loop and maximum flux density B_{max} with severely distorted voltage

corrected very accurately to the losses obtained with a sinusoidal voltage, provided the right coefficients α_h and α_w are inserted. Since the values specified by SEV for hot-rolled sheet were different, the resultant losses were too high, as may be seen from Table I. It therefore appeared desirable for further experiments to be performed with frames of hot-rolled sheet. Fig. 5 shows the dimensions of an annular core of continuous strip, the losses of which were determined, using the circuit in Fig. 1. The results of measuring the separate losses are given in Fig. 6, the losses measured with various distorted 50-c/s voltages, and the corrected values being shown in Table III.

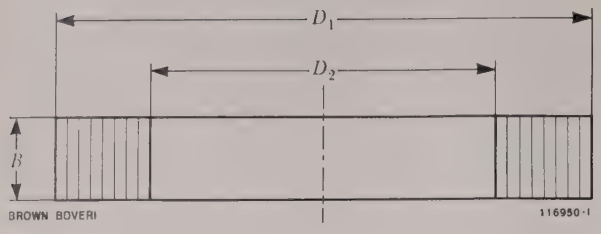

Fig. 5. – Annular wound-strip core of hot-rolled material

$D_1 = 260$ mm
$D_2 = 180$ mm
$B = 40$ mm

TABLE III

Iron losses of a wound annular core of hot-rolled strip, with sinusoidal and distorted voltage waves

Inductance B_{max} kGs	Losses with approximately sinusoidal voltage wave		Losses with distorted voltage wave			
			Measured		Corrected	
	Form factor	Losses W	Form factor	Losses W	As per SEV W	With the coefficients in Fig. 6 W
10·0	1·11	9·4	1·315	10·3	9·7	9·5
12·5	1·11	13·6	1·33	15·1	14·2	13·7
14·0	1·11	16·6	1·37	18·7	17·4	16·8
15·0	1·115	18·8	1·39	21·4	19·8	19·0
16·0	1·115	20·6	—	—	—	—

In this case, too, the losses with distorted voltage were corrected by inserting the measured values in the proportion $\alpha_h = 0{\cdot}7$ and $\alpha_w = 0{\cdot}3$.

Experiments on a 200-kV transformer pole with radially laminated core of hot-rolled sheet were finally carried out to clarify the position with regard to large transformers. The test set-up illustrated in Fig. 7 corresponds in principle to that in Fig. 1. The voltage was distorted by series resistors in the excitation circuit of the transformer and, as for the previous measurements, the dynamic hysteresis loop was oscillographed. Two series of tests, one with the active part removed from the tank and the other with it immersed, were performed and the influence on the method of correction of the additional losses at no-load thereby determined. Table IV lists the measured and corrected losses obtained with an

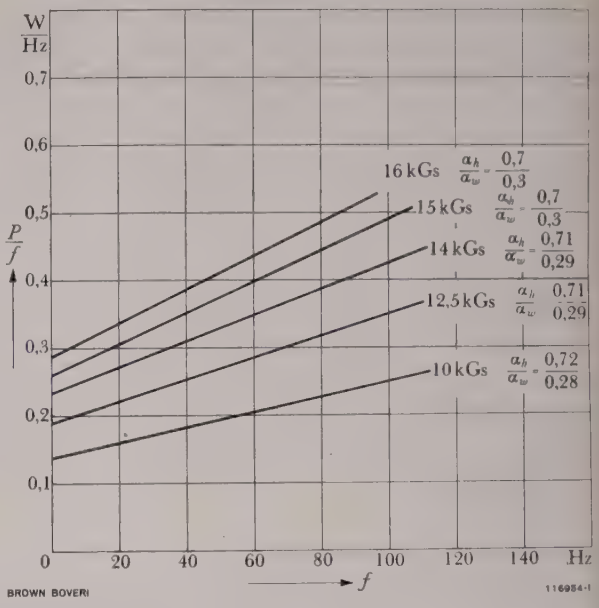

Fig. 6. – Separate measurements of no-load losses on the annular core of hot-rolled strip

P = Losses (in W / c/s)
f = Frequency (in c/s)
α_h = Share of hysteresis losses
α_w = Share of eddy-current losses

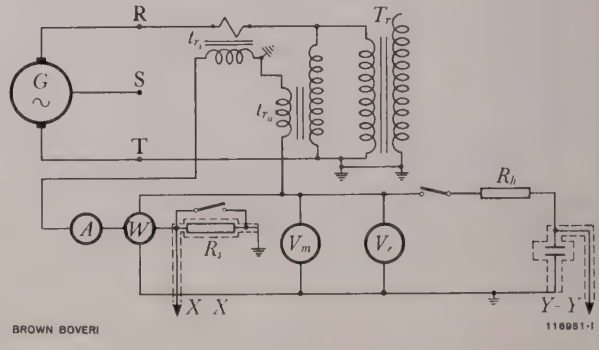

Fig. 7. – Test set-up for measuring no-load losses of a 200-kV single-phase transformer with hot-rolled laminations

G = Alternator
Tr = Transformer pole
tr_i = Current transformer
tr_u = Voltage transformer
A = Ammeter
W = Wattmeter
V_m = Voltmeter (mean value)
V_e = Voltmeter (r.m.s. value)
R_s = Shunt
R_h = High resistance
C = Capacitor
X–X, Y–Y = Horizontal and vertical deflector plates of oscillograph

TABLE IV

Iron losses of a 200-kV transformer with hot-rolled laminations, with sinusoidal and distorted voltage waves; active part removed from tank

Induc-tance B_{max} kGs	Losses with approximately sinusoidal voltage wave		Losses with distorted voltage wave			
			Measured		Corrected	
	Form factor	Losses kW	Form factor	Losses kW	As per SEV kW	With the co-efficients in Fig. 8 kW
10·0	1·11	15·2	1·167	15·6	15·3	15·2
12·5	1·115	23·0	1·17	23·6	23·2	23·0
14·0	1·12	29·4	1·23	31·5	30·4	29·7
15·0	1·125	34·1	1·286	37·3	35·4	34·5
15·5	1·125	36·3	1·335	40·4	38·0	36·7

TABLE V

Iron losses of a 200-kV transformer with hot-rolled laminations, with sinusoidal and distorted voltage waves; active part inserted in tank

Induc-tance B_{max} kGs	Losses with approximately sinusoidal voltage wave		Losses with distorted voltage wave			
			Measured		Corrected	
	Form factor	Losses kW	Form factor	Losses kW	As per SEV kW	With the co-efficients in Fig. 8 kW
10·0	1·11	15·25	1·145	15·45	15·25	15·2
12·5	1·115	23·15	1·17	24·0	23·55	23·3
14·0	1·12	29·90	1·24	32·2	30·9	30·3
15·0	1·125	35·10	1·295	38·40	36·4	35·4
15·5	1·125	38·20	1·336	42·50	39·9	38·6

almost sinusoidal or only slightly distorted 50-c/s voltage, and those yielded by a severely distorted voltage.

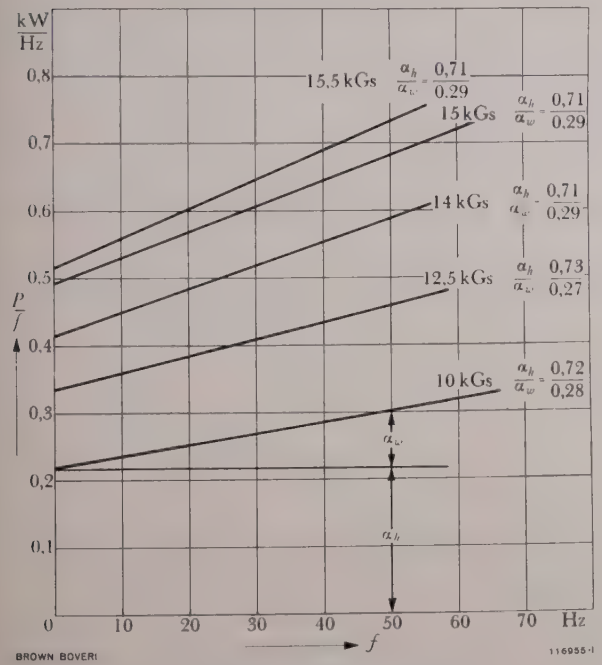

Fig. 8. – Separate measurement of no-load losses on a 200-kV transformer pole with hot-rolled laminations

P = Losses
f = Frequency
α_h = Share of hysteresis losses
α_w = Share of eddy-current losses

The measurement of the separate losses with the active part immersed in the tank yielded the same values for the coefficients α_h and α_w, as shown in Fig. 8.

Fig. 9a shows the oscillogram of the almost sinusoidal voltage and the dynamic hysteresis loop thereby obtained with $B_{max} = 14$ kGs. The traces in Fig. 9b and c depict the severely distorted voltage having the same mean value and the corresponding dynamic hysteresis loop. From Fig. 9a and c we obtain the same value for the maximum flux density:

$$2\,B_{max} \triangleq 30{\cdot}5 \text{ mm}$$

In conformity with the no-load measurements on the two model frames and on the annular strip core, the tests on the 200-kV pole with hot-rolled laminations also established that the iron losses measured with distorted voltage can be corrected with great accuracy—the error of measurement is only about 1 % with a wave-form factor of 1·3—to the losses obtained with a sinusoidal voltage, provided the values for the coefficients α_h and α_w obtained from the separate loss measurements are substituted in equation (13). Furthermore, from the results listed in Table V, it will be observed that, with the corresponding correction according to equation (13), the additional losses in the tank and constructive iron parts can be corrected to within the measuring

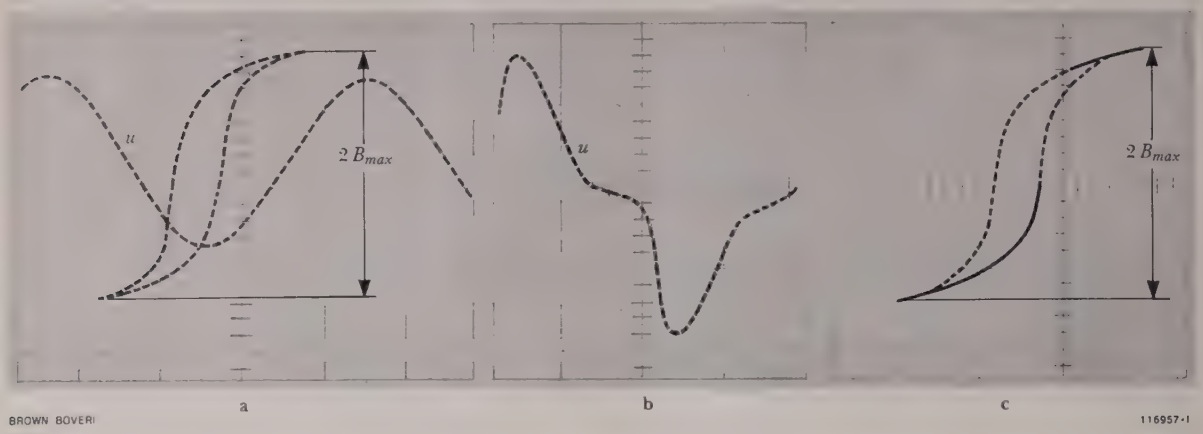

Fig. 9. – Voltage and flux density during no-load loss measurements on the 200-kV transformer pole with hot-rolled laminations

a: Slightly distorted voltage u and hysteresis loop b: Distorted voltage u (wave-form factor 1·24)

c: Hysteresis loop and maximum flux density B_{max} with distorted voltage.

accuracy to the losses obtained with the sinusoidal voltage. As a result of the measurements gained with the 200-kV transformer pole, it is now possible to firmly contradict the doubts which were occasionally expressed regarding the admissibility of correcting according to equation (13), also for the additional iron losses.

In conclusion it may be stated that the truth of the method of correcting the iron losses with severely distorted voltage waves was reliably confirmed by exhaustive tests up to very severe degrees of distortion. The measurements also confirmed the coefficients $\alpha_h = \alpha_w = 0{\cdot}5$, as laid down by SEV for cold-rolled laminations; on the other hand, the tests gave the ratio $\alpha_h : \alpha_w = 0{\cdot}7 : 0{\cdot}3$, whereas SEV regulations stipulate 0·8:0·2. By inserting the SEV coefficients, with voltage waves having wave-form factors up to 1·3, such as are feasible in practice, the losses obtained for the arrangements investigated were about 4% too high. It therefore appears justified for due regard to be paid to the improvement in the magnetic properties of hot-rolled sheet too, as characterized by a percentage reduction in the hysteresis losses—with cold-rolled laminations the hysteresis and eddy-current losses are equal, as shown—and for a discussion to be suggested with the purpose of checking the SEV coefficients for hot-rolled sheet, which are at present based on obsolete data.

(KME) A. AŠNER

ON THE THEORY OF BACKFIRES DUE TO COMMUTATION IN MERCURY-ARC RECTIFIERS

621.314.65.004.64

This journal has published a number of articles in the past dealing with the load capacity of mutators (mercury-arc rectifiers) under various operating conditions. In these the basis was an experimentally determined stress formula, whose validity is limited to low-voltage mutators. This theory, which hitherto was phenomenological in nature, is now given a physical interpretation and, in addition to the previous stress formula, a number of others are derived from the factors governing the process of arc extinction. Comparison with available measurements indicates a remarkable agreement between the theory and the experimental results, which is considered to give objective proof of the correctness of the basic physical hypothesis.

BY way of introduction to the present article, it should be explained that the commutation referred to in the title is the changeover by the arc from the currently conducting anode to the succeeding anode. The production of backfires when this change occurs has been thoroughly investigated and described by numerous authors, for example J. v. Issendorf (1929) [1],[1] Schenkel and Seeliger (1930) [2], Leblanc and Demontvignier (1931) [3], Slepian and Ludwig (1932) [4], Gaudenzi [5], Widmer (1938) [6], Maxfield and Fredendall (1938) [7], Kingdon and Lawton (1939) [8], Gabowitsch (1939) [9], Demontvignier (1941) [10], and others, without any conclusive explanation being found for this phenomenon peculiar to static current converters. The reason for the lack of this theory up to the present is to a certain extent due to the fact that the conditions under which an arc is produced must be defined, and that even for the steady arc there is still no conclusive theory.

In view of the fact that, according to Ecker [11], more than a thousand original papers have been published on the steady-state arc, without the interpretation of this phenomenon having been exhausted, it appears advisable to confine the present discussion to reasonable limits. Consequently the present article cannot be expected to afford a comprehensive, detailed physical analysis of the formation of an arc at the rectifier anode. An attempt will merely be made to interpret the known empirical factors from the physical aspect and to relate them to the measurable quantities in such a manner that the determining relationships may be recognized.

[1] The figures in brackets refer to the bibliography on p. 893.

Postulation of a Hypothesis

Considered physically, the commutation backfire represents the change from a post-arc current, incapable of supporting itself, to a self-supporting arc. Consequently it is produced by very powerful pre-ionization, for which reason theories, like that put forward by Townsend, for ignition from the uncharged state of space, cannot be adopted here.

With regard to the *genetics* of commutation backfires, only a small number of observation results are available, for two main reasons: firstly because ignition occurs statistically, and secondly because it happens very suddenly and lasts a very short time.[2] The two characteristic features which, at first sight only appear to hamper investigation, are so typical of this particular phenomenon that their evaluation provides two important hints regarding the physical nature of the process. The rapidity of the occurrence definitely excludes the thermionic emission—with its appreciable inertia—as the main effect giving rise to arcs, while from the statistical nature of the phenomenon it follows that it can only take place under quite definite circumstances, when certain significant quantities, under the influence of fluctuating factors,

[2] SLEPIAN and LUDWIG [4] found in their investigations that backfires could occur even when the necessary conditions are effective for less than 5×10^{-6} s.

attain or exceed certain critical numerical values. From this, though, the important conclusion must be drawn that a theoretical interpretation of the phenomenon must be based on those conditions under which the process of ignition takes place, not rarely but dependably. It is agreed that the basis for this shall be a probability of $W = 0{\cdot}5$ [12]. If an attempt is made to calculate the production of backfires from conventional discharge conditions at the instant of extinction, it would be sure to fail because it is exactly these "initial conditions" which normally do not lead to ignition, but require the assistance of the previously mentioned fluctuation conditions. Thus, when dealing with the process of ignition, it is common practice first to deal with those conditions of discharge which lead reliably to ignition —with the aid of the theory—and then to deal with the statistical fluctuations. This procedure is also adopted in subsequent considerations.

Useful information may be expected from experiments dealing with physically related phenomena, particularly the changeover from restricted and hampered glow discharges to arc discharges. Investigations carried out by Wehrli [13], Plesse [14], Becker and Seeliger [15], and Bauer and Schulz [16], among others, have proved that the transition from the glow to the arc discharge usually takes place when the current is raised above a certain value, which may be called the transition current. The last-mentioned authors found values of 0·13–0·17 A for this current in xenon. The conditions of similarity are, of course, best fulfilled by "dynamic" experiments. Höfert [17] performed such experiments, imparting brief, steep current impulses to a glow discharge, observing that the behaviour of the negative electrode differed according to the temperature. When the electrode was very hot, transition was regular and steady, with a transition time of about 10^{-4} s, producing an arc with obvious thermionic emission. When the temperature was not so high, the changeover took place statistically and unsteadily within about 5×10^{-8} s, with a suspicion of electron liberation by field emission. Since the lateral speed of propagation of the discharge amounted to only about 10^5 cm/s, it was possible to attain local current densities of the order of 10^2 A/cm^2, given sufficiently steep impulses. From the above observations it must be concluded that the reason for formation of an arc may be sought in a decided improvement in the process of electron emission, as was suspected by von Engel and Steenbeck [18]. It is well known that in the glow discharge the electrons are liberated as secondary emission on the arrival of ions, the yield normally being quite small. In an arc discharge, however, the electrons are liberated by much more effective mechanisms, i.e. thermionic or field emission, from which the tendency of the discharge to change to this more favourable form (as regards energy) is immediately comprehensible, as soon as the essential condition—minimum current—is fulfilled. However, this must be decisively supplemented if it can be utilized for the description of backfires, firstly by hypothetically establishing that the change from glow to arc, or backfire, must take place at a definite electron current. This additional stipulation is of fundamental importance because, in the course of the different discharges, the total current can be produced by electron and ion currents of different size and, furthermore, the formation of the arc is largely determined by the emission mechanism. With this hypothesis, according to which the formation of an arc commences at the critical electron current I_-, an attempt will now be made to interpret the commutation backfire. But before an approach can be made to this problem, it is essential for the discharge conditions at the moment of extinction to be enumerated more closely.

Post-Arc Current

It has been proved [19] that for *slow commutation* (duration $t_c \gg \tau$ [s], the life of the carriers), the carrier density at the beginning $N(0)$ [cm^{-3}] and at the end $N(t_c)$ is given by

$$N(t_c) = N(0)\,\frac{\pi}{2}\,\frac{\tau}{t_c} \qquad (1)$$

for which, at the beginning of commutation, the discharge current $i(0)$ [A] is related to the carrier density by

$$i(0) = e\,N(0)\,b_-\,G\,F \qquad (2)$$

in which b_- [cm^2/sV] = electron mobility, G [V/cm] = longitudinal field strength, e [As] = elementary charge and F [cm^2] = cross-section of discharge.

Supposing now, to simplify matters, we assume a current during commutation of

$$i(t) = i(0) \cos\left(\frac{\pi t}{2 t_c}\right) \tag{3}$$

then, at the moment of extinction ($t = t_c$)

$$\left(\frac{\mathrm{d}i}{\mathrm{d}t}\right)_{t_c} = i(0)\frac{\pi}{2 t_c} \tag{4}$$

With the aid of the ion velocity w_+ [cm/s] we obtain the following expression for the peak post-arc current at the moment of extinction

$$\hat{i}_+ = e\, N(t_c)\, \frac{w_+}{4} F \tag{5}$$

and, utilizing the preceding expressions (1), (2) and (4),

$$\hat{i}_+ = \frac{w_+}{4 b_- G} \tau \left(\frac{\mathrm{d}i}{\mathrm{d}t}\right)_{t_c} \tag{6}$$

according to which the post-arc current only depends on the change in current at the moment of extinction. From the theory of diffusion the time constant of the post-arc current is given by the following (with D [cm²/s] $= D_1/\sqrt{p}$ = ambipolar diffusion coefficient)

$$\tau = \frac{4 d^2}{\pi^2 D} = \frac{4}{\pi^2 D_1} \cdot d^2 \sqrt{p} \tag{7}$$

Results communicated by Ludwig [20] have shown that the life of charge carriers in rectifier tanks is in fact governed by the geometry of the space between the grid and anode d [cm] and the vapour pressure p [Torr]

$$\tau = 1{\cdot}7 \times 10^{-3}\, d^2 \sqrt{p} \tag{8}$$

From readings published by the same author it finally follows that

$$\hat{i}_+ = \left(\frac{w_+}{b_- G \pi^2 D_1}\right) d^2 \sqrt{p} \left(\frac{\mathrm{d}i}{\mathrm{d}t}\right)_{t_c} = $$

$$= 7 \times 10^{-7}\, d^2 \sqrt{p} \left(\frac{\mathrm{d}i}{\mathrm{d}t}\right)_{t_c} \tag{9}$$

thereby reliably confirming the derived relationships (6) and (7). In particular, convincing proof is obtained of the independence of the post-arc current from the active area of the anode or the cross-section of the discharge tube.

For *rapid commutation* (duration of commutation $t_c < \tau$ the life of the carriers) the following expression was obtained for the carrier density at the moment of extinction [19]

$$N(t_c) = N(0) \tag{10}$$

from which, utilizing the above equations (2) and (5), we obtain the following for the peak post-arc current

$$\hat{i}_+ = \frac{w_+}{4 b_- G}\, i(0) = 4{\cdot}1 \times 10^{-4}\, i(0) \tag{11}$$

This relationship should be employed at very small currents $i(0)$ and, in conformity with experience, proves that $\hat{i}_+ = 0$ at no-load.

Theory of Backfires in Low-Voltage Rectifiers

Starting with the observation that the transition from the glow to the arc discharge commences when a characteristic electron current is reached, let us postulate a characteristic electron current I_z at which a commutation backfire occurs:

$$(i_-)_z = I_z \tag{12}$$

The magnitude of this current may be assumed to be of the order of 0·1 A. Under the influence of the ion current i_+ impinging on the anode an electron current i_- is emitted

$$i_- = \gamma\, i_+ \tag{13}$$

and, assuming that the secondary emission coefficient γ and the acceleration voltage of the ions u_s are proportional ($\gamma = \gamma_0 u_s$) [21]

$$i_- = \gamma_0\, u_s\, i_+ \tag{14}$$

In mercury-arc rectifiers the initial inverse voltage Δu_s is experienced at the moment of extinction. Allowing for the fact that, with slow commutation, the peak value of the post-arc current i_+ is defined by

$$\hat{i}_+ = K_1 \tau\, \mathrm{d}i/\mathrm{d}t \tag{15}$$

according to (6), it follows that, with $K_1 = 4{\cdot}1 \times 10^{-4}$, and from the foregoing equations

$$I_z = \gamma_0 (\Delta u_s \cdot \hat{i}_+) = \gamma_0 K_1 \tau\, (\Delta u_s \cdot \mathrm{d}i/\mathrm{d}t) \tag{16}$$

which can also be written as follows, by introducing the blocking duty B_1

$$B_1 = (\Delta u_s \cdot \mathrm{d}i/\mathrm{d}t) \tag{17}$$

$$\frac{\gamma_0 K_1 \tau}{I_z} \cdot B_1 = 1 \tag{18}$$

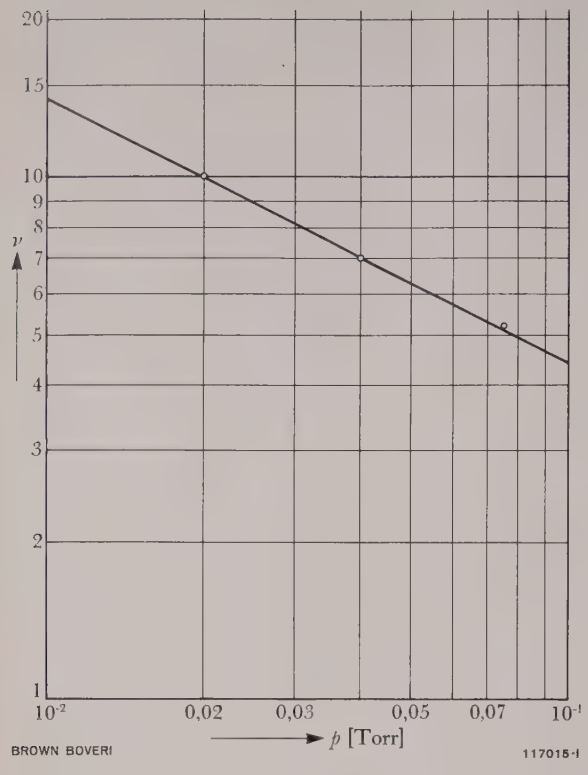

Fig. 1. – Variation of the valve quality ν with the pressure p of the mercury vapour

It has already been explained that, when considering the process of ignition, it is only permissible to employ the region of very high probability as a basis, for which a figure of $W = 0{\cdot}5$ has been agreed. Then, for ignition processes of greater probability, Poisson's equation [24] is valid

$$W(\nu) = e^{-\mu} \sum_{\nu}^{\infty} \frac{\mu^n}{n!} \tag{19}$$

which can be evaluated with the aid of

$$e^{-\mu} \sum_{\nu}^{\infty} \frac{\mu^n}{n!} = e^{-\mu} \left[\sum_{0}^{\infty} \frac{\mu^n}{n!} - \sum_{0}^{\nu-1} \frac{\mu^n}{n!} \right] = 1 - e^{-\mu} \sum_{0}^{\nu-1} \frac{\mu^n}{n!} \tag{20}$$

Thus we obtain

$$\text{for } W = 0{\cdot}5 \qquad \mu \approx \nu - 0{\cdot}3 \tag{21}$$

or, when $\mu > 1$

$$\text{for } W = 0{\cdot}5 \qquad \frac{\mu}{\nu} \approx 1 \tag{22}$$

Previously [22], the equation

$$\mu = 4 \times 10^{-11} \cdot B_1 \tag{23}$$

was obtained as an experimental result which, in conjunction with equations (22) and (18) allows the quality ν of the valve to be calculated.

$$\nu = \frac{4 \times 10^{-11} \cdot I_z}{K_1 \gamma_0 \tau} \tag{24}$$

Thus the quality of the valve is expressed in terms of the material property of the anode γ_0 and the time constant τ of the post-arc current. The latter time constant, according to (8), is itself dependent on the geometry of the tank and the vapour pressure, so that we may write

$$\nu \sim \frac{1}{d^2 \sqrt{p}} \tag{25}$$

for the quality of the valve.

The relationship expressed by (25) was also established experimentally, Fig. 1 showing the effect of the vapour pressure. The corresponding measurements were published in 1955 [22]. Admittedly in that publication (see Fig. 7 on page 141) the blocking capacity A was given in terms of the temperature t of the saturated vapour; however, these two quantities can easily be converted into the variables plotted in Fig. 1. It will be evident that the $\sqrt{p}$ law is well fulfilled. Measurements not reproduced in this case also clearly confirmed the variation with d^2.

Thus the former empirical characterization of the blocking capacity of mutators by means of μ and ν has been augmented by a theoretical interpretation and proof brought that, in fact, μ is merely determined by the electrical load on the mutator and n or ν by the physical characteristics of the mutator tank. On account of (19) the valve quality for $W = 0{\cdot}5$ is denoted by ν; when $W \ll 1$ by n, in conformity with [22]. The derivation also confirms the knowledge formerly obtained experimentally, that the blocking capacity of a mutator is independent of the size of its anode. It also proves that it is possible to explain the phenomena only by means of the current, and not by the current density. It can also be recognized that formation of an arc is not only determined by the power of the post-arc current, otherwise the graphite property γ_0 would be pointless, which is obviously not true. Indeed, it is quite easy to discover that this property, which varies with the temperature of the anode, the preliminary treatment and, to a certain extent, with ageing, is responsible

for the greatest uncertainty in the above definition [21].

With *very rapid commutation* the post-arc current is defined by (11), from which

$$I_z = \gamma_0 \Delta u_s \hat{i}_+ = \gamma_0 K_2 \Delta u_s i(0) \qquad (26)$$

is obtained, whence we may derive

$$B_2 = \Delta u_s i(0) \qquad (27)$$

for the blocking duty and

$$\nu \sim \frac{I_z}{\gamma_0 K_2} \qquad (28)$$

for the valve quality. These relationships should be employed in the region of no-load. By means of

$$B_2 = B_1 \cdot \frac{2}{\pi} \cdot \frac{t_c}{\tau} \qquad (29)$$

we can inter-relate the two stresses.

Discussion and Augmentation of the Theory

So far no attempt was made to take into account the fact that the post-arc current varies with respect to time, as given by

$$i_+ = \hat{i}_+ \, e^{-t/\tau} \qquad (30)$$

all operations being carried out with the peak value $\hat{i}_+$. In doing so it was tacitly assumed—and this is now pointed out deliberately—that it is essentially the maximum value of the product $u_s i_+$ which is important, and this is sure to occur at the instant of extinction, with the value $\Delta u_s \hat{i}_+$, under the previously assumed conditions. Particular proof of this conclusion is unnecessary, since equation (14) shows directly that the value I_z is preferentially attained when the product $u_s(t) i_+(t)$ attains its maximum with respect to time. Later the case will be discussed in which u_s does not immediately assume the value of the initial inverse voltage Δu_s, but passes through an oscillatory transient phase.

The range of validity of the above theory, as far as expressing it by means of formulae is concerned, is limited by the fact that equation (9), giving the relationship between the post-arc current and vapour pressure, as postulated by Ludwig [20], is only valid for the range of application of the theory of diffusion. In practice this implies that it can be applied to

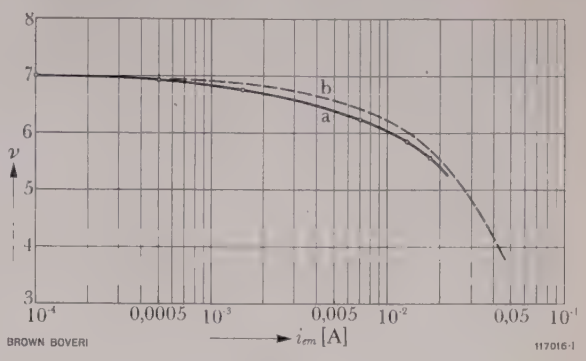

Fig. 2. – Influence of the thermal emission current i_{em} on the valve quality ν

a: Measured b: Calculated

all low-voltage mutators, as was fully explained on an earlier occasion. With high-voltage mutators it is common practice to operate with saturated-vapour temperatures below 50 °C, which explains why the above formulae cannot be applied without a certain amount of criticism. This point will be dealt with later.

An attempt will now be made to estimate the influence of the *thermionic emission* of the anode on its ability to block. If we also assume here that the occurrence of a backfire is associated with a critical electron current I_z, equation (16) can obviously be modified to

$$I_z = \gamma_0 \Delta u_s i_+ + i_{em} \qquad (31)$$

when the thermionic emission current is denoted by i_{em}. Utilizing (22) and (23) it follows that

$$\nu = \frac{4 \times 10^{-11}}{K_1} \frac{I_z - i_{em}}{\gamma_0 \tau} \qquad (32)$$

If, for example, we assume that, at $i_{em} = 0$, the other factors would yield $\nu = 7$, which represents an average normal value for the valve quality, ν would decrease in the manner illustrated in Fig. 2 with increasing i_{em}. This theoretical result is very well confirmed by measurements obtained with a mutator anode. Here it is underlined that such measurements are extremely laborious to obtain and at high emission currents are restricted by the thermal properties of the experimental tank. From the foregoing results we may draw the conclusion that thermionic emission currents below 10 mA do not give rise to any catastrophic deterioration in medium-quality mutators. This agrees well with the experimental results pub-

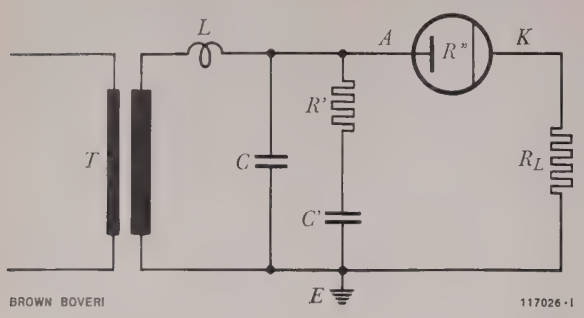

Fig. 3. – Single-phase circuit diagram to explain the transient oscillations

A = Anode
K = Cathode
L = Transformer inductance
C = Capacitance
R_L = Load resistance
C' = Capacitor
R' = Resistor
R'' = Resistance to post-arc current
T = Transformer

lished by Kobel [23]. He discovered that small emission currents do not greatly affect the blocking capacity, but that at $i_{em} = 0{\cdot}2$ A the change to an arc discharge occurs at once (i.e. corresponding to $W = 1$). Here it is also noteworthy that the deciding quantity is not the current density, but the actual current. The consequence of this is that the thermionic emission severely limits the current, particularly with large anodes, demanding appropriate constructional measures.

Once again it has been proved that the blocking capacity is independent of the size of the anode, although practical application would indicate that a proportional relationship is especially desirable. This physical fact also explains why glass-bulb rectifiers possess such an astonishing blocking capacity, although the construction of their valve is quite simple and, with small units, the rated current with retarded firing point does not have to be reduced.

The foregoing remarks may be concluded by comparison with the observations of Schmalenberg [24]. Assuming that $I_z = 0{\cdot}15$ A and $\gamma_0 = 10^{-5}$, it follows from (16) that the power of the post-arc current which is certain to result in a backfire is given by

$$(\hat{i}_+ \Delta u_s)_z = \frac{I_z}{\gamma_0} = 1{\cdot}5 \times 10^4 \text{ [W]} \qquad (33)$$

Schmalenberg found a power density of about 10^3 W/cm² for $W = 0{\cdot}5$ and $n = 7$, from which a post-arc power of 70 kW is obtained for an anode with a surface area of 70 cm² exposed to ionic bombardment. When comparing this numerical value with (33) it must be borne in mind that the above figures for I_z and γ_0 originate from other measurements and that closer agreement cannot be expected. That the same order of magnitude was found may be considered a remarkable achievement in itself.

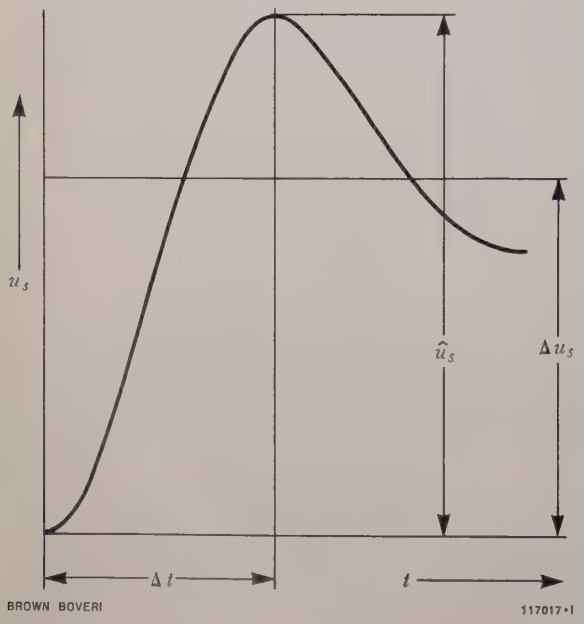

Fig. 4. – Variation of the inverse voltage with damped transient oscillation

u_s = Inverse voltage
Δu_s = Initial inverse voltage
$\hat{u}_s$ = Maximum value of inverse voltage during transient oscillation

The Effect of Transient Oscillations

Previously it was assumed that the inverse voltage jumped to a value of Δu_s at the moment of extinction, corresponding to the momentary difference between the commutating phase voltages of the transformer. This representation is quite sufficient when the problem is discussed to a first approximation. However, a more detailed analysis shows that the inverse voltage at the moment of extinction does not immediately jump to the initial inverse voltage, but effects this change in the form of a damped oscillation. The occurrence of such oscillations has been repeatedly observed and described

in the literature [25, 26]. The reason for these oscillations is that the energy stored in the earth capacitances and stray inductances at the moment of changing from one anode to the next must be balanced; the problem has been given considerable attention with respect to high-voltage rectifiers. Recent investigations, however, have also brought to light such transient oscillations with low-voltage rectifiers and considerably retarded firing point. It was also established that the probability of backfire was greatly increased by these transient oscillations or, in contrast, greatly diminished by the insertion of damping elements. These brief remarks should suffice to indicate the importance of such oscillations on the blocking action and to justify subsequent, more detailed considerations.

Gerecke [26] discovered that, in general, the frequency of the transient oscillations do not exceed 2×10^5 c/s. Damping due to the production of eddy currents rapidly increases with the frequency. According to Rüdenberg [27], the following natural transformer frequencies were observed. At high voltages: $1{\cdot}5 \times 10^4$ c/s, at medium voltages 5×10^4 c/s and at low voltages $1{\cdot}5 \times 10^5$ c/s.

Fig. 3 shows a simplified single-phase circuit diagram. Assuming the neutral of the transformer to be earthed, the cathode K of the mutator is then at a potential determined by the load resistance R_L, while the anode A can oscillate at the natural frequency of the transformer ω_0. Here the inductance L of the transformer and the capacitance C form a resonant circuit. But since, during the oscillation by C to the initial inverse voltage Δu_s, the post-arc current i_+ flows from K to A, the oscillation is damped more when the resistance $R'' = u_s/i_+$ is smaller. Without going into the details of the calculation it is evident that this voltage-dependent damping is the reason for the well-known fact that the transient oscillations become more pronounced, the larger the initial inverse voltage Δu_s. Therefore, with high-voltage mutators it is usual to fit damping elements consisting of a resistor R' and capacitor C', thereby compulsorily obtaining the frequency ω and the damping δ.

If we now substitute a series resonant circuit with the resultant damping resistance R for the anode circuit in Fig. 3, the transient oscillations, as illustrated in Fig. 4, obey the equation

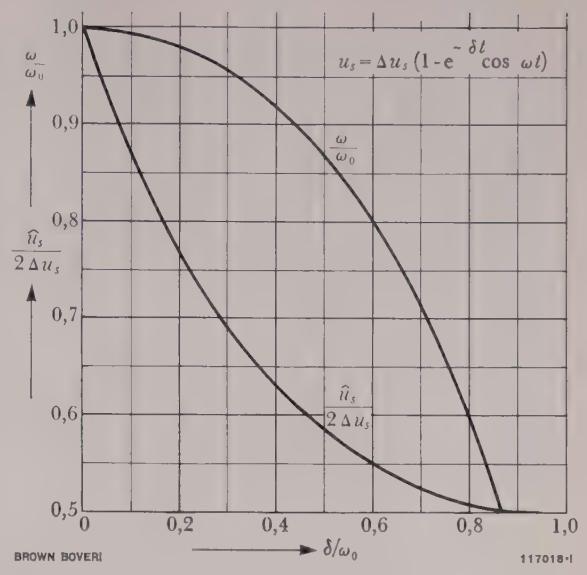

Fig. 5. – Dependence of the maximum inverse voltage $\hat{u}_s$ and the frequency ω on the damping δ of the transient oscillation

ω_0 = Angular frequency of the undamped oscillation
Δu_s = Initial inverse voltage

$$u_s = \Delta u_s \left[1 - e^{-\delta t}\left(\cos \omega t + \frac{\delta}{\omega} \sin \omega t\right)\right] \quad (34)$$

or, when the damping δ is small, approximately

$$u_s = \Delta u_s (1 - e^{-\delta t} \cos \omega t) \quad (35)$$

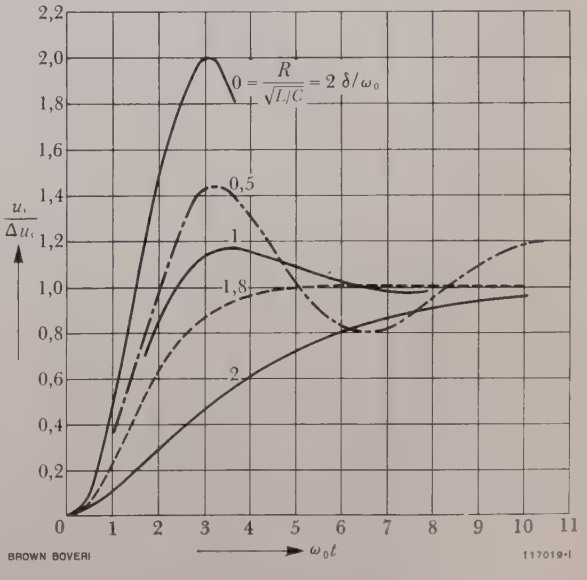

Fig. 6. – Variation of the inverse voltage u_s with respect to time, for various values of the damping δ

Δu_s = Initial inverse voltage
ω_0 = Angular frequency of the undamped oscillation

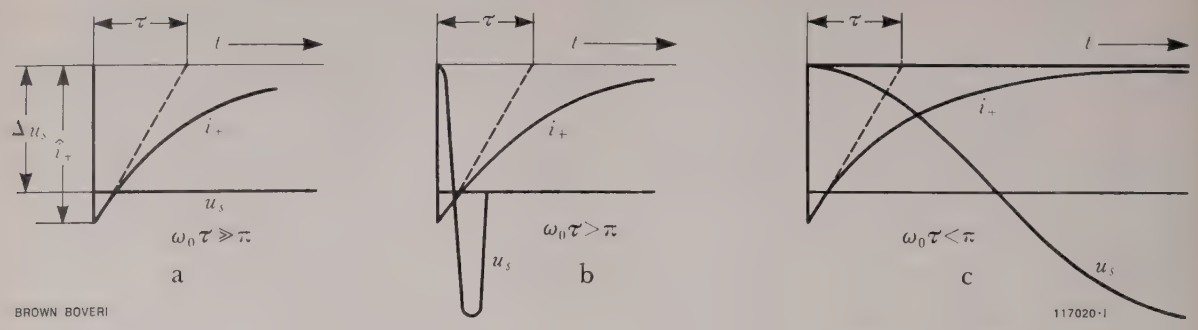

Fig. 7. – Variation of the inverse voltage u_s and post-arc current i_+ with respect to time

a: Momentary abrupt change in voltage Δu_s, without any overswing
b: Undamped overswing with high frequency
c: Undamped overswing with very low frequency.

where $\delta = R/2L$, $\omega = \sqrt{\omega_0^2 - \delta^2}$ and $\omega_0^2 = (LC)^{-1}$. By measuring the time and amplitude intervals between zero and the first maximum voltage in an available oscillogram (Fig. 4), we obtain, with $\omega t = \pi/u_s = \Delta u_s[1 + e^{-\delta\pi/\omega}]$ the desired data according to the following relationships:

$$\text{Frequency:} \quad f = \frac{1}{T} = \frac{0{\cdot}5}{\Delta t}\,; \quad \omega = \pi/\Delta t \tag{36}$$

$$\text{Damping:} \quad \delta = \frac{R}{2L} = \frac{1}{\Delta t}\log_e\left[\frac{\hat{u}_s}{\Delta u_s} - 1\right] \tag{37}$$

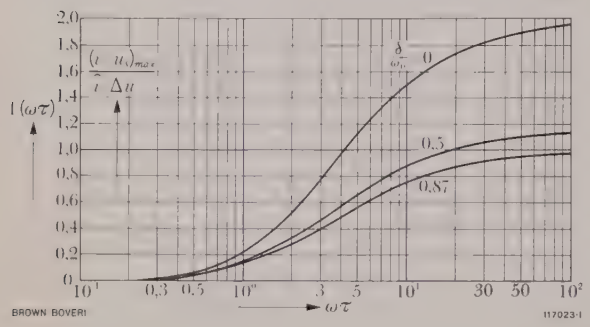

Fig. 8. – Maximum value of the power in the post-arc current $(i_+ u_s)_{max}$ plotted in terms of the angular frequency of the transient oscillation ω and the time constant τ of the post-arc current, for different values of the damping

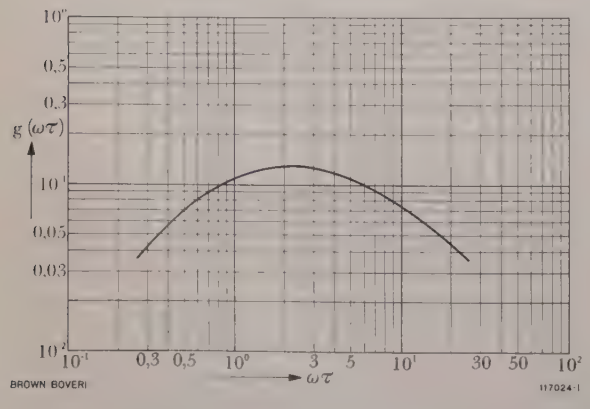

Fig. 9. – Dependence of the function $g(\omega\tau)$ on the angular frequency ω and the time constant τ of the post-arc current

In Fig. 5 ω/ω_0 and $\hat{u}_s/\Delta u_s$ are evaluated in terms of δ/ω_0. The shape of the oscillation for a series connection of L, C and R is shown graphically in Fig. 6 for some noteworthy values of the damping ($R/\sqrt{L/C} = 0$, undamped, $R/\sqrt{L/C} = 2$, aperiodic oscillation). According to this, it is not necessary to raise the damping as far as the aperiodic oscillation, but it will usually be sufficient to allow $R/\sqrt{L/C} \approx 1$, because at this value there is no longer any appreciable overswing. The necessary damping elements should always be provided in installations where the firing point can be considerably retarded, because they greatly reduce the blocking duty and their price is low.

From equation (14) it follows that the electrical duty is proportional to the maximum value of the product of post-arc current and inverse voltage. Provided the variation of the inverse voltage can be taken mathematically to be an exact step change (Fig. 7a), the above maximum is defined by

$$(i_+ u_s)_{max} = \hat{i}_+ \Delta u_s \tag{38}$$

When the inverse voltage is oscillatory, the curves of the above quantities are as illustrated in Fig. 7b and 7c. It can be seen that the maximum of the product

$$i_+ u_s = \hat{i}_+ \Delta u_s \, e^{-t/\tau} (1 - e^{-\delta t} \cos \omega t) \qquad (39)$$

noticeably deviates from the approximate value $\hat{i}_+ u_s$. This deviation becomes larger, the greater the relationship between the duration of a period of the transient frequency T and the time constant τ of the deionization process.

In order to obtain the clearest possible conditions, let us first consider an undamped oscillation:

$$2u_s = \hat{u}_s (1 - \cos \omega t) \qquad (40)$$

In this case the maximum of the product of the post-arc current and the inverse voltage occurs at the instant ωt^*, as determined by the equation

$$\omega \tau = (1 - \cos \omega t^*) / \sin \omega t^* \qquad (41)$$

Thus, for the magnitude of these maxima we obtain

$$\frac{(i_+ u_s)_{max}}{\hat{i}_+ \hat{u}_s} = \frac{e^{-t^*/\tau}}{2} (1 - \cos \omega t^*) = \frac{e^{-t^*/\tau}}{2} \omega \tau \sin \omega t^* \qquad (42)$$

as illustrated graphically in Fig. 8. The result is that at very high transient frequencies ($\omega \tau > 10^2$) and with due allowance for overswing (by means of the factor 2), the previous formula is quite a good approximation, but with decreasing transient frequency ($\omega \tau < 1$) the actual duty drops appreciably below the value given by the approximation equation. Substituting (42) in the equation for I_z, we obtain

$$I_z = \gamma_0 K_1 \tau \frac{\hat{u}_s}{\Delta u_s} \left(\Delta u_s \frac{di}{dt} \right) \cdot f(\omega \tau) \qquad (43)$$

with $2f(\omega \tau) = e^{-t^*/\tau} (1 - \cos \omega t^*)$, for the terms on the right-hand side of which it is necessary to distinguish between circuit and tank data, if we are to utilize Poisson's summation equation (19). Unfortunately, such procedure is obstructed by the term $f(\omega \tau)$, which correlates the characteristic data of both kinds.

Refinement of the theory of backfires by allowing for the transient oscillation of the inverse voltage consequently does not produce any formula which can immediately be adopted easily and, at the same time, universally. It is only feasible to represent two limiting cases in the desired manner, one of which has already been described for $u_s = \Delta u_s$, while the second will now be dealt with.

Theory of Backfires in High-Voltage Mutators

Starting from the universally valid formula (43), an approximate formula will now be derived, permitting evaluation by means of Poisson's equation. But (43) must first be modified with the aid of (42)

$$I_z = \gamma_0 K_1 \tau \frac{di}{dt} \hat{u}_s \left[\frac{e^{-t^*/\tau}}{2} \omega \tau \sin \omega t^* \right] \qquad (44)$$

From the simplified equation for the inverse voltage (40) we obtain the following expression for its steepest gradient at the instant $\omega t = \pi/2$

$$\left(\frac{du_s}{dt} \right)_{max} = \hat{u}_s \omega \qquad (45)$$

Substituting this in (44) and rearranging the factors

$$I_z = \gamma_0 K_1 \tau^2 g(\omega \tau) \cdot \left(\frac{di}{dt} \right) \left(\frac{du_s}{dt} \right) \qquad (46)$$

there still remains the common function illustrated in Fig. 9

$$g(\omega \tau) = \frac{e^{-t^*/\tau}}{2} \sin \omega t^* \qquad (47)$$

between the quantities belonging to the tank and those of the circuit, but, without introducing an unduly large error, this can be assumed to be constant, in the range $0{\cdot}6 < \omega \tau < 10$. Incidentally, this error is always present when the transient oscillation of the inverse voltage is characterized by its gradient. Hence, if g, with the average of approximately 0·1 in the above range, is substituted for the function $g(\omega \tau)$, we obtain

$$I_z = \gamma_0 K_1 \tau^2 g \cdot \left(\frac{di}{dt} \right) \left(\frac{du_s}{dt} \right) \qquad (48)$$

from which we can immediately effect the distinction between the characteristic data of the circuit

$$B_3 = \left(\frac{di}{dt} \right) \left(\frac{du_s}{dt} \right) \qquad (49)$$

and those belonging to the tank

$$\nu \sim \frac{1}{\gamma_0 \tau^2} \qquad (50)$$

This relationship was in fact established experimentally for high-voltage tanks by Keller [28].[3] This

[3] Fig. 6 of this publication shows load curves for two check temperatures, characterized by $(di/dt)\,(du_s/dt) = \text{constant}$.

agreement with practical experience can be taken as a further important proof of the correctness of the physical views. Similar conditions ought also to be encountered with certain thyratrons, the blocking properties of which have been expressed by various authors, e.g. [29] and [30] and also by (49). It may be mentioned that this quantity was found quite empirically for the thyratrons, because the respective publications do not contain any physical interpretation.

For low-voltage rectifiers $B_1 = 666\ P_0$ was found for hexapulse operation at a mains frequency of 50 c/s [22]. Taking (45) into account, we can immediately deduce a relationship between the power of an uncontrolled rectifier for very high voltage $P_0 = U_0 I_0$ and its blocking duty B_3

$$B_3 = P_0 \cdot 666\ \omega \qquad (51)$$

in which the influence of the transient frequency ω is obvious at a glance. When the firing point is retarded, the blocking duty increases in the same manner as previously shown for low-voltage rectifiers. Since the latter operate in the region of power limitation, a corresponding reduction must be made in the current at partial load, if the probability of backfiring is to be kept constant.

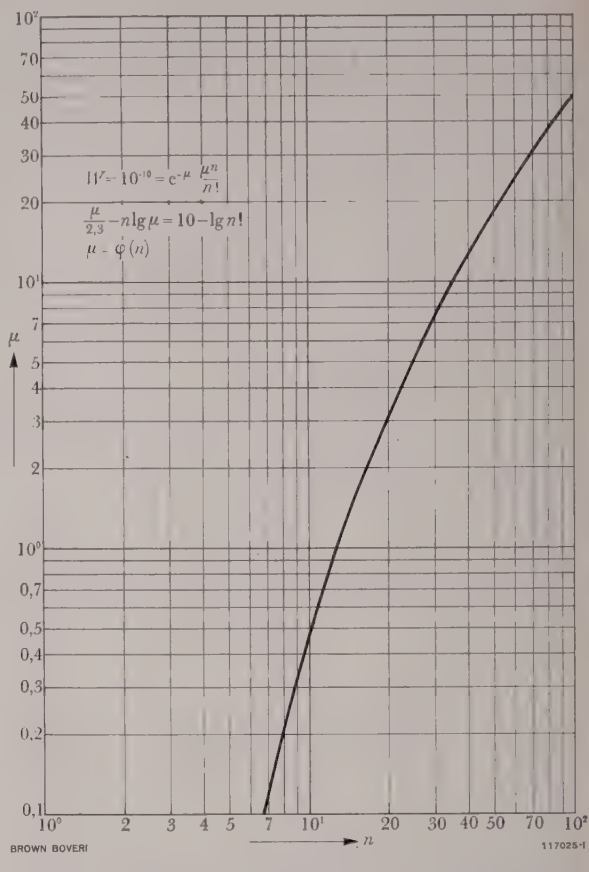

Fig. 10. – Dependence of the variable μ on the parameter n of Poisson's equation

$$W = e^{-\mu}\ \frac{\mu^n}{n!}$$

when W is made constant $= 10^{-10}$

Probability of Backfire

Up to now the remarks were related to the conditions for discharge with a probability of $W = 0{\cdot}5$, which can only be produced experimentally with very high post-arc power ($u_s\, i_+ > 10$ kW) [24]. Operation in practice, on the other hand, takes place under quite different conditions, because backfires have to be avoided at all costs. But since the probability of backfire across the entire range is described by Poisson's equation, it is possible to use it to determine the load capacity when the probability of backfiring is very small (e.g. when $W = 10^{-10}$) from the results obtained when $W = 0{\cdot}5$, as will now be done.

For low-voltage mutators with *slow* commutation, let us first examine the experimentally obtained factor 4×10^{-11} contained in equation (23). As will be agreed, a theory is expected to be able to help us understand constants of this kind. Equations (18) and (22) yield

$$\frac{\mu}{\nu} = \frac{B_1}{I_z (\gamma_0 K_1 \tau)^{-1}} \qquad (52)$$

If the above numerical values are substituted for I_z, γ_0 and K_1, the denominator of the right-hand side becomes $2{\cdot}5 \times 10^7/\tau$, and with $\tau = 10^{-4}$ s this works out to $2{\cdot}5 \times 10^{11}$, i.e. a very large number, while ν is supposed to possess a value between 1 and 10. This discrepancy can only be eliminated when the denominator is multiplied by a constant C_1 and, so as not to alter the equation, the numerator as well. For the two denominators we may write

$$\nu = C_1\ \frac{I_z}{\gamma_0 K_1 \tau} \qquad (53)$$

from which C_1 may be calculated at once because all other quantities are known, according to the assump-

tions. If, for example we choose $\nu = 7$, $d = 1$ cm and $p = 10^{-2}$ Torr, we obtain $\tau = 1{\cdot}7 \times 10^{-4}$ s from (8) and $C_1 = 4{\cdot}8 \times 10^{-11}$. The agreement with the measured value is again very gratifying, considering that very inaccurate figures were introduced for I_z and γ_0.

For the probability of backfire the value of $W = 10^{-10}$ [22] was formerly suggested. Between this region of very rare and the above region of very frequent backfires, equation (19) at $W \ll 1$ yields the simple Poisson's equation

$$W = e^{-\mu} \frac{\mu^n}{n!} \tag{54}$$

If we now substitute $W =$ constant $= 10^{-10}$ in this equation, we can calculate μ at once in terms of n. Since $\log_{10}(n!)$ is obtainable from tables, we may take logs of (54), i.e.

$$\mu = 2{\cdot}3\,[n \log \mu + 10 - \log(n!)] = \varphi(n) \tag{55}$$

The result is plotted graphically in Fig. 10. As may be seen from a comparison of (19) and (54), the two equations give the same numerical value for W when $n = \nu$ (with $W \ll 1$), because the contributions from $n > \nu$ can be ignored in practice.

Thus the rated power P_0 of an uncontrolled hexapulse mutator can be expressed in terms of the valve quality n, as follows

$$P_0 = \frac{A}{666} = 3{\cdot}75 \times 10^7\, \mu = 3{\cdot}75 \times 10^7\, \varphi(n) \tag{56}$$

the factor $\varphi(n)$ being taken from Fig. 10, since an approximation by means of a simple exponential expression would only be true for a very small range of n. If we now take into account the definite dependency on pressure of n, as expressed by (53) or (8), we arrive at the expression for the rated power P_0 and blocking capacity A which was published in 1955 [22].

Adopting the same procedure for high-voltage mutators, and substituting

$$\frac{\mu}{\nu} = \frac{C_3 B_3}{C_3 I_z (K_1 \gamma_0 g \tau^2)^{-1}} \tag{57}$$

it follows from (45) that

$$\mu = C_3 B_3 = C_1 B_1 = \frac{C_1}{\omega} B_3 \tag{58}$$

and

$$\nu = \frac{C_3 I_z}{K_1 \gamma_0 g \tau^2} = \frac{C_1 I_z}{\omega K_1 \gamma_0 g \tau^2} \tag{59}$$

and we are again faced by the same dilemma as in (43) because the quantity ω from the circuit recurs. Here we can obviously only make use of the representation by means of Poisson's equation for the probability by imposing further restrictions and keeping the transient frequency ω constant while investigating the blocking properties during commutation by a high-voltage mutator.

The explanation of the blocking capacity may be undertaken, taking the Russian high-voltage rectifier VR–9 as an example. Butaev and his co-authors [31] published the following operating data:

$$\frac{du_s}{dt} = 7{\cdot}5 \times 10^8 \text{ V/s and } \frac{di}{dt} = 10^6 \text{ A/s}$$

These give $B_3 = (du_s/dt)\,(di/dt) = 7{\cdot}5 \times 10^{14}$ VA/s^2 and with $\omega = 3 \times 10^4$ s^{-1} as in (58) $\mu = 1$.

The probability of backfire observed with this duty amounted to 1 per day, i.e. $W = 2{\cdot}3 \times 10^{-7}$. Substituting μ and W in a graphical representation of Poisson's equation (see [22] Fig. 5), we may read off $n \approx 10$, which is quite a reasonable value for the check temperature given, $\Theta = 25$ °C. From this it follows, with equation (59), that the time constant of the post-arc current $\tau = 1{\cdot}3 \times 10^{-4}$ s and $\omega\tau \approx 4$. These figures are also quite plausible. When dealing with tanks for very high voltage, having regard to the maximum admissible field strength, the distance between the anode and the adjoining grid must be made much larger than for low-voltage mutators: $d \approx 5 - 9$ cm. From this we may conclude that τ cannot possibly decrease so far as might be expected from the low check temperature.

(KME) T. WASSERRAB

Bibliography

[1] J. v. ISSENDORF: Neuere Untersuchungen über das betriebsmässige Verhalten von Quecksilberdampf-Gleichrichtern. Elektrotech. Z. 1929, Vol. 50, No. 30, p. 1079–86.

[2] J. v. ISSENDORF, M. SCHENKEL, R. SEELIGER: Die Entstehung und Bekämpfung der Rückzündungen in Grossgleichrichtern. Wiss. Veröff. Siemens 1930, Vol. 9, No. 1, p. 73–114.

[3] M. LEBLANC, M. DEMONTVIGNIER: L'état actuel de nos connaissances sur l'arc à mercure à basse pression. Rev. gén. Elect. 1931, Vol. 29, No. 23, p. 891–904 and No. 24, p. 935–50.

[4] J. SLEPIAN, L. R. LUDWIG: Backfires in mercury-arc rectifiers. Trans. amer. Inst. elect. Engrs 1932, Vol. 51, March, p. 92–104.

[5] A. GAUDENZI: Some causes of backfires and their suppression. Brown Boveri Rev. 1938, Vol. 25, No. 5/6, p. 97–8.

[6] S. WIDMER: The importance of uncontrolled and of controlled grids in mutators. Brown Boveri Rev. 1938, Vol. 25, No. 5/6, p. 99–102.

[7] F. A. MAXFIELD, G. L. FREDENDALL: Characteristics of the glow to arc transition in mercury vapour. J. appl. Phys. 1938, Vol. 9, p. 600–10.

[8] K. H. KINGDON, E. J. LAWTON: The relation of residual ionization to arc-back in thyratrons. Gen. elect. Rev. 1939, Vol. 42, No. 11, p. 474–8.

[9] M. D. GABOWITSCH: Rückzündungen in Quecksilberdampf-Gleichrichtern. J. tech. Phys. (in Russian) 1939, Vol. 9, p. 2104–19.

[10] M. DEMONTVIGNIER: Essai d'une théorie de l'ionisation résiduelle dans l'arc à mercure. Conséquences pratiques sur le fonctionnement des redresseurs. Rev. gén. Elect. 1941, Vol. 50, No. 4, p. 239–55.

[11] G. ECKER: Current transition gas-metal. Tech. Report FTR 1 1959, Inst. Theor. Phys., Bonn University.

[12] T. WASSERRAB: Die statistischen Gesetzmässigkeiten der Mutator-Rückzündungen. Scientica Electrica 1954, Vol. 1, No. 3, p. 112–26.

[13] M. WEHRLI: Die Vorgänge an der Kathode beim Übergang von der Glimm- in die Bogenentladung. Helv. phys. Acta 1928, Vol. 1, p. 247–323.

[14] H. PLESSE: Untersuchungen am elektrischen Lichtbogen. Ann. d. Phys. 1935, Vol. 22, p. 473.

[15] O. BECKEN, R. SEELIGER: Über den Mechanismus der Bogenentladung. Ann. d. Phys. 1935, Vol. 24, p. 619–35.

[16] A. BAUER, P. SCHULZ: Elektrodenfälle und Bogengradienten in Hochdruckentladungen, insbesondere bei Xenon. Z. Phys. 1954, Vol. 139, No. 2, p. 197–211.

[17] H. J. HÖFERT: Der Übergang von der Glimmentladung in die Bogenentladung, hervorgerufen durch kurzzeitige Stösse. Ann. d. Phys. 1939, Vol. 35, p. 547–76.

[18] A. v. ENGEL, M. STEENBECK: Elektrische Gasentladungen II. Springer, Berlin 1934.

[19] T. WASSERRAB: Die positive Säule bei veränderlichem Entladungsstrom. Z. angew. Phys. 1955, Vol. 7, No. 4, p. 176–9.

[20] E. H. LUDWIG: Gesetzmässigkeiten für den Rückstrom in Quecksilberdampf-Stromrichtern. Z. angew. Phys. 1955, Vol. 7, No. 1, p. 17–27.

[21] T. WASSERRAB: Die Zündspannung von Quecksilberdampf-Entladungsgefässen. Z. angew. Phys. 1961, Vol. 13, p. 194–201.

[22] T. WASSERRAB: The load capacity of mutators. Brown Boveri Rev. 1955, Vol. 42, No. 4/5, p. 133–43.

[23] E. KOBEL: Untersuchungen über den Einfluss der Elektronenemission an den Anoden auf die Entstehung von Rückzündungen im Quecksilberdampf-Gleichrichter. Bull. schweiz. elektrotech. Ver. 1932, Vol. 23, No. 14, p. 344–8.

[24] W. SCHMALENBERG: Über die Kathodenfleck-Entstehung auf elektrisch beanspruchten Flächen. VDE-Fachber. 1956, Vol. 19, p. I/8–I/13.

[25] H. v. BERTELE, T. WASSERRAB: Umschaltschwingungen in Stromrichteranlagen. Elektrotech. u. Maschinenb. 1942, Vol. 60, No. 31/32, p. 332–8.

[26] E. GERECKE: Origin and propagation in high-current system of high-frequency oscillations produced by grid-controlled ionic converters. CIGRE Report No. 314/1952.

[27] R. RÜDENBERG: Transient performance of electric power systems. McGraw-Hill, New York, Toronto, London 1950.

[28] H. KELLER: Latest developments bring first direct-current high-voltage transmission system with mutators in sight. Brown Boveri Rev. 1945, Vol. 32, No. 9, p. 310–18.

[29] A. W. COOLIDGE JR.: A new line of thyratrons. Trans. amer. Inst. elect. Engrs. 1948, Vol. 67, Part 1, p. 723–7.

[30] W. M. BROOKER, D. G. WARE: Cheater circuits for testing thyratrons. Philips tech. Rev. 1954, Vol. 16, No. 4/5, p. 141–7.

[31] F. I. BUTAEV, N. S. KLIMOV, M. F. KOSTROV, A. A. SAKOVICH: The high-power, high-voltage rectifier. Electric Technology (original in Russian) 1959, Vol. 2, 209–23.

BRIEF BUT INTERESTING

160 000 Hours Service by a Brown Boveri Steam Turbine

621.165.004.5

THIS photograph was taken when the 8000-hp steam turbine driving the blast-furnace blower in an Australian steelworks was overhauled recently. This turbine has been running for 20 years with an average service of 8000 hours per year. Owing to the appropriate design of the blades and the excellent steam separators, the blades are still in very good condition.

The operators of this machine purchased their first blower driven by a Brown Boveri turbine in 1926. The set had a capacity of 60 000 ft^3/min. Ten years later they ordered a set with a throughput of 80 000 ft^3/min, the turbine of which is shown here.

After the war a larger set delivering 105 000 ft^3/min was installed in 1949, and in 1957 the Company was entrusted with the supply of two further sets, each rated 125 000 ft^3/m with a total power of 16 000 hp. These two machines, which are of the axial type, were taken into service during the spring of 1959 and will help to effect a considerable increase in the output of this large Australian steelworks.

C. DE RHAM

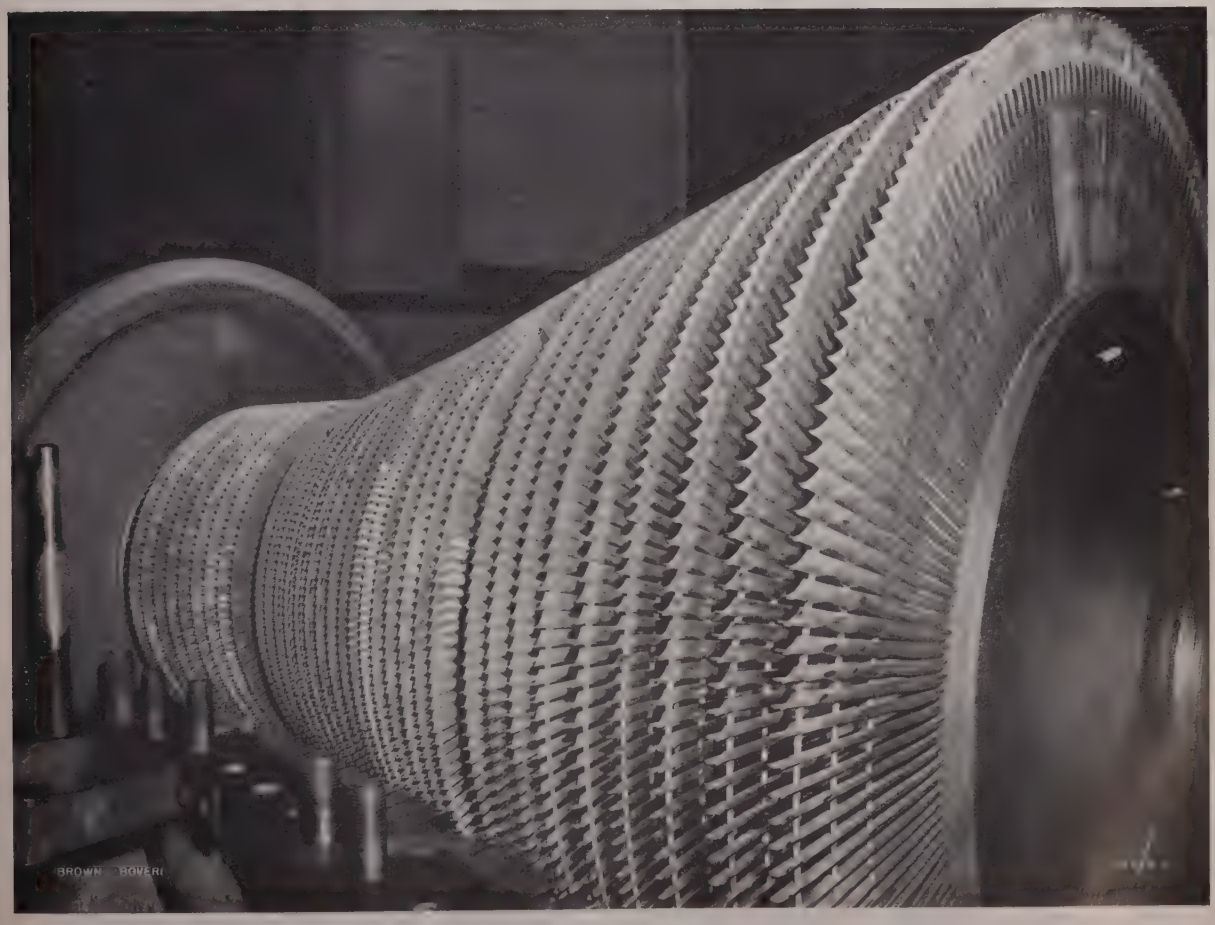

Brown Boveri Magnetic Circuit-Breakers Render Excellent Service with Electric Furnaces

621.316.57.064.44

THE operation of electric furnaces, either induction or arc furnaces, imposes very severe demands on the associated circuit-breakers. In furnace installations of this kind the main breaker also has to perform the duties of the control breaker, which means that it must perform 50 to 60 switching operations every day. This imposes a tremendous strain on the mechanical part of the breaker. With arc furnaces, moreover, the furnace transformer also has to be disconnected at no-load, for which, though the currents are low, the natural frequency of the restriking voltage is relatively high.

The special physical properties of the new magnetic circuit-breakers, and the fact that this unit was developed to conform to practical requirements, make it ideal for use with furnaces. When disconnecting transformers at no-load, the Brown Boveri magnetic circuit-breakers do not produce any overvoltages. The contact wear is extremely small because the breaking arc is immediately blown away from the contacts as soon as they begin to open. In addition, the contacts are easily inspected after simply removing the arc chutes. Thus it only takes a few minutes to overhaul the breaker.

A Brown Boveri type T circuit-breaker is employed as furnace breaker in a large Swiss steelworks, in conjunction with a 12-t arc furnace. Up to the present, the breaker has performed 8000 operations. The contacts have not had to be renewed yet, in fact they show hardly any signs of wear. The arc chutes too are as good as new and have not been overhauled either. The customer particularly appreciates the easy maintenance of the breaker, which can be carried out in a remarkably short space of time, for instance between two charges or during the weekly inspection, thus avoiding interruption of the melting schedule.

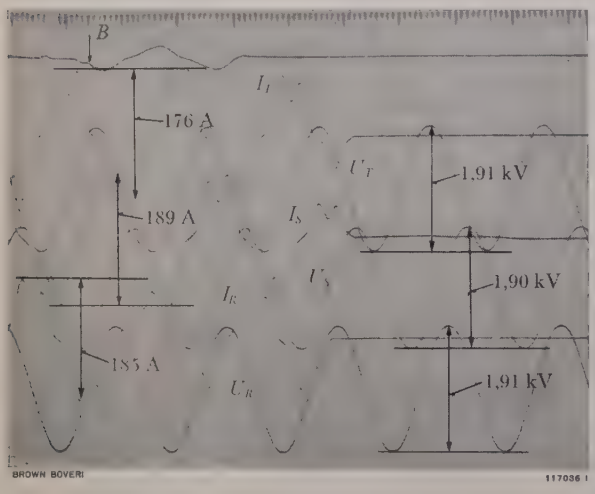

Fig. 1. – Oscillogram showing the disconnection at no-load of the transformer supplying a 5-t arc melting furnace, by means of a magnetic circuit-breaker

U_R, U_S, U_T = Phase voltages on the input side
I_R, I_S, I_T = No-load currents of the transformer
B = Command impulse to break

The currents and voltages shown are r.m.s. values.

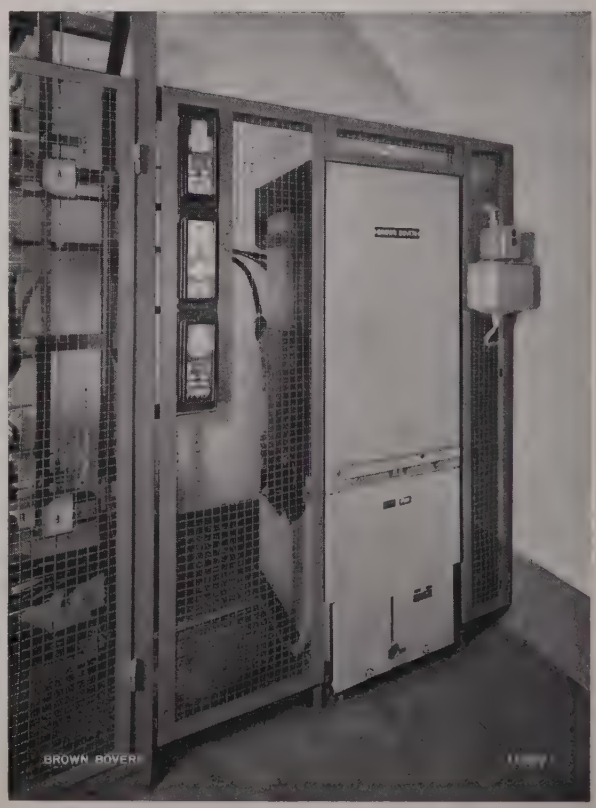

Fig. 2. – Magnetic circuit-breaker in an open-type cell, used for controlling an 8-t arc melting furnace

After this breaker had been in regular service for about a year, oscillograms were recorded of interruptions under different service conditions. The furnace transformer was also disconnected several times at no-load without any overvoltages being indicated on the oscillograms. The total break time was only 47 ms. One of these oscillograms is reproduced in Fig. 1. At a normal service current of about 700 A the break time amounted to 70–85 ms, and with short-circuited electrodes, i.e. on entering the melt, 47 ms. In no case were overvoltages experienced. A further breaker of the same kind is in service in another steelworks, controlling an 8-t arc furnace for grey cast iron (Fig. 2). Up to the present, this breaker has carried out 8200 operations without the least trouble. Magnetic circuit-breakers of the Brown Boveri design have therefore proved their ideal suitability for use with electric furnaces.

(KME) A. MAYER

Publications by Brown Boveri Authors in Other Journals

016

BALTENSPERGER P.: Schnellwiedereinschaltung bei Höchstspannungsübertragung. Bulletin des Schweizerischen Elektrotechnischen Vereins 1960, No. 21, p. 1106–12.

BELDI F.: Krankheiten der Transformatoren. Chapter II (except for the section "Unbrennbare Isolierflüssigkeiten") from the book by Spieser R. and Grütter F.: Krankheiten elektrischer Maschinen, Transformatoren und Apparate. Published by Springer, Berlin, Göttingen, Heidelberg, 1960.

DICK M.: Übertragungseigenschaften anodenmodulierter Telephoniesender mit hochselektiven Antennen. Bulletin des Schweizerischen Elektrotechnischen Vereins 1960, No. 20, p. 963–71.

GERSPACHER F.: Grundlagen der elektrischen Widerstandsschweissung. Schweisstechnik, 1960, No. 5, p. 49–56.

HÜBNER R.: Schaltungen mit Kaltkathodenröhren. Elektrotechnische Zeitschrift, Edition B, 1960, No. 18, p. 438–44.

HÜBNER R.: Neue Erkenntnisse über biologische Wirkungen durch Hochfrequenz. Elektronische Rundschau 1960, No. 6, p. 229–30.

HÜBNER R.: Ferroelektrische Energiegewinnung. Neue Zürcher Zeitung, Technical Supplement of Sept. 7th, 1960.

KUPPER K., STALDER H. and KAESER F.: Krankheiten elektrischer Apparate. Chapter III (except for the section "Ölarme Schalter und Expansionsschalter") from the book by Spieser R. and Grütter F.: Krankheiten elektrischer Maschinen, Transformatoren und Apparate. Published by Springer, Berlin, Göttingen, Heidelberg, 1960.

LÜTHY A.: Die Anwendung der Schweisstechnik bei dem Bau von Gasturbinen. Zeitschrift für Schweisstechnik 1960, No. 8, p. 230–7 and No. 9, p. 273–7.

MANZ O.: Die Luftseilbahn Gornergrat-Stockhorn. Internationale Berg- und Seilbahn-Rundschau 1960, No. 3, p. 26-8.

PFENNINGER H.: Verschmutzung und Korrosion der Strömungsmaschinen von Gasturbinenanlagen im Hüttenwerk. Stahl und Eisen 1960, No. 12, p. 796–801.

RISCH R.: Trennung der Ummagnetisierungsverluste auf Grund der Wirbelstromellipse. Scientia Electrica 1960, No. 2, p. 75–9.

SEIPPEL C.: Brown Boveri Turbogruppe für 500 MW. Schweizerische Bauzeitung 1960, No. 26, p. 421–4.

SONTHEIM R.: Forschung als langfristige Investition. Industrielle Organisation 1960, No. 7, p. 285–90.

STARKERMANN R.: Die n-fach-Regelung einschleifiger, m-fach gekoppelter Systeme. Regelungstechnik 1960, No. 8, p. 257–61.

WIDERÖE R.: Physikalische Grundlagen der Strahlentherapie. Physikalische Blätter 1960, Nr. 10, p. 528–33.

ZWAHLEN R.: Einführung in die Technik der Laplace-Transformation. Technische Rundschau, issue of Oct. 14th, 1960.

INDEX TO VOLUME 47 (1960)

General

Atomic Energy

Mechanical Engineering

Compressors, Gears, Turbochargers

Gas Turbines

Steam Turbines

Electrical Engineering

Generators

Power Transmission

Rectifiers

Transformers

Switchgear

Control Engineering

Industrial Drives

Traction

BROWN BOVERI
AT FAIRS AND EXHIBITIONS 1960

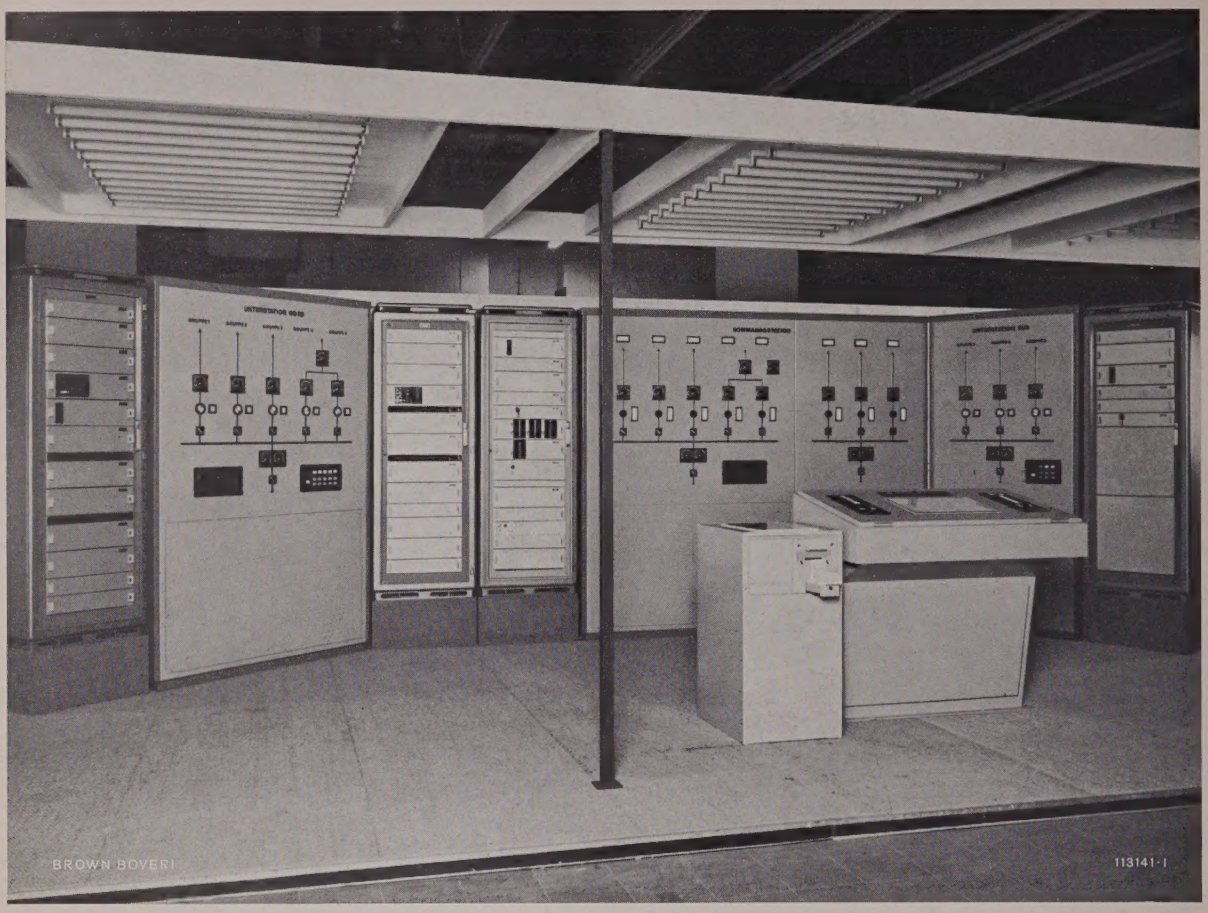

International Congress and Exhibition for Instrumentation and Automation (Interkama) held in Düsseldorf 1960. View of part of the Brown Boveri stand (above and below).

Combined electronic remote-control installation with pulse-code remote-control equipment employing digital, rapid-cyclic transmission of telemetered measurands, comprising:

Control station with master desk (front right) and its associated mimic diagram (behind the desk) for the remote control of two power stations, one substation (left) and another substation (right)

◀ *Contactless control of a planing machine drive demonstrated by a model machine (left in the background), with constant reversal regardless of the table speed and load, combined with digital punched-tape control of the tool feed*

Left in the foreground is the control desk for the cutting and feed drives with selector and indicator of the table travel.

Above: ▶

The Brown Boveri stand at the Comptoir Suisse 1960, held in Lausanne

Below:

The Swiss Television, Radio, Phono, Electronic Show held in Zurich in 1960

Brown Boveri exhibited some of the latest electron tubes from their wide range.


BROWN BOVERI
Schindler
PHOTO MAXIM
MAISON DE LA BIBLE
10, avenue de la Gare, Lausanne

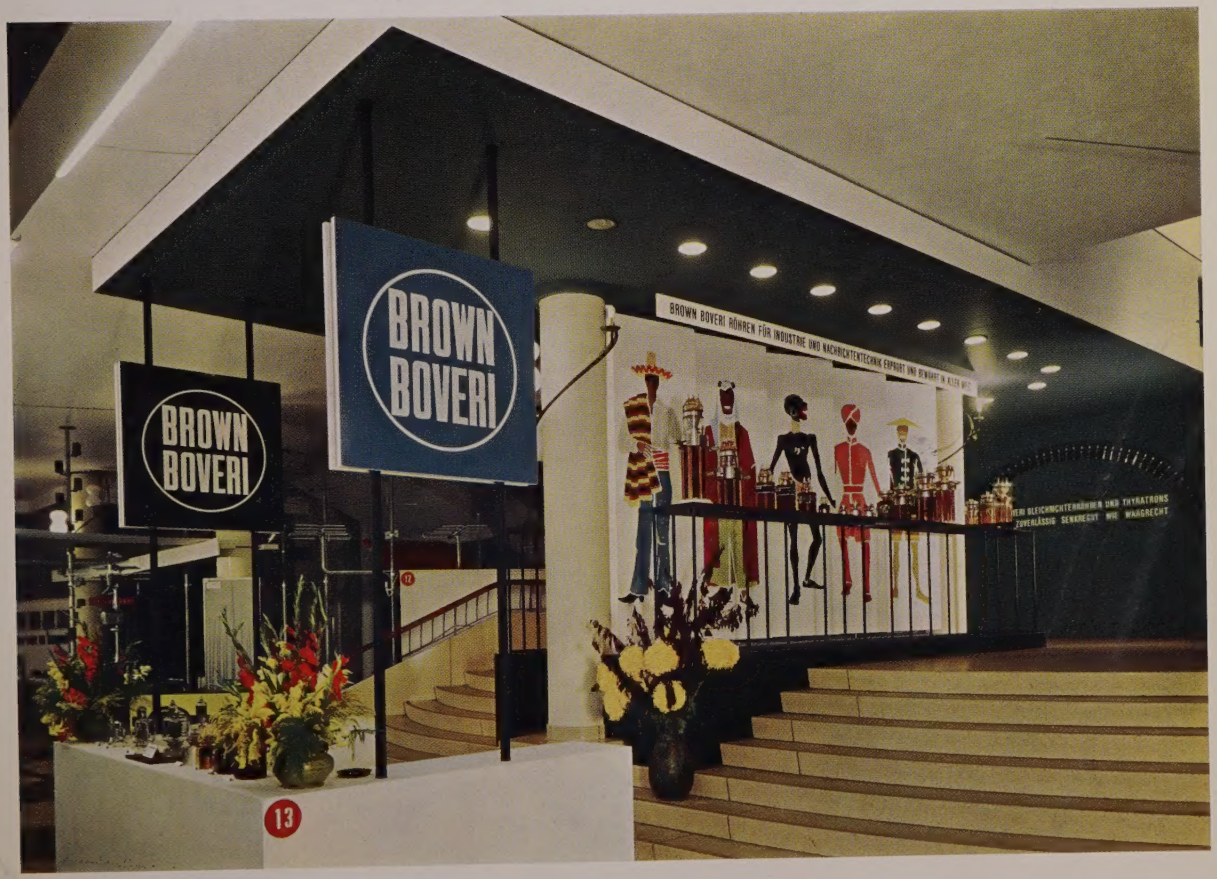
BROWN BOVERI
BROWN BOVERI
BROWN BOVERI RÖHREN FÜR INDUSTRIE UND NACHRICHTENTECHNIK EXPORT UND INLAND
13

Published by Brown, Boveri & Company, Limited, Baden, Switzerland. Printed by Kreis & Co. AG., Basle, Switzerland.
Obtainable direct from the publishers.